SQT

OCTOBER 1977

RELIABILITY STUDY OF OPTO-COUPLED SEMICONDUCTOR DEVICES AND LIGHT EMITTING DIODES (LED)

FINAL TECHNICAL REPORT

OCTOBER 1974 — OCTOBER 1977

R. C. MAURER
V. A. WEISSFLUG
E. V. SISUL

PREPARED FOR THE GEORGE C. MARSHALL SPACE FLIGHT CENTER,
MARSHALL SPACE FLIGHT CENTER, ALABAMA 35812

MCDONNELL DOUGLAS ASTRONAUTICS COMPANY • EAST

MCDONNELL DOUGLAS CORPORATION

UNCLASSIFIED

SECURITY CLASSIFICATION OF THIS PAGE (When Data Entered)

REPORT DOCUMENTATION PAGE		READ INSTRUCTIONS BEFORE COMPLETING FORM
1. REPORT NUMBER	2. GOVT ACCESSION NO.	3. RECIPIENT'S CATALOG NUMBER
4. TITLE (and Subtitle) Reliability Study of Opto-Coupled Semiconductor Devices and Light Emitting Diodes (LED)		5. TYPE OF REPORT & PERIOD COVERED Final Technical Report October 1974-October 1977 6. PERFORMING ORG. REPORT NUMBER
7. AUTHOR(s) R. C. Maurer V. A. Weissflug E. V. Sisul		8. CONTRACT OR GRANT NUMBER(s) NAS8-30777
9. PERFORMING ORGANIZATION NAME AND ADDRESS McDonnell Douglas Astronautics Company-St. Louis		10. PROGRAM ELEMENT, PROJECT, TASK AREA & WORK UNIT NUMBERS
11. CONTROLLING OFFICE NAME AND ADDRESS National Aeronautics and Space Administration George C. Marshall Space Flight Center Marshall Space Flight Center, Alabama 35812		12. REPORT DATE October 1977 13. NUMBER OF PAGES
14. MONITORING AGENCY NAME & ADDRESS(if different from Controlling Office)		15. SECURITY CLASS. (of this report) Unclassified 15a. DECLASSIFICATION/DOWNGRADING SCHEDULE

16. DISTRIBUTION STATEMENT (of this Report)

17. DISTRIBUTION STATEMENT (of the abstract entered in Block 20, if different from Report)

18. SUPPLEMENTARY NOTES

NASA MSFC Contracting officer's representative
Mr. F. Villella
Area Code 205-453-2864

19. KEY WORDS (Continue on reverse side if necessary and identify by block number)

Accelerated Testing
Opto-Electronics
Reliability

20. ABSTRACT (Continue on reverse side if necessary and identify by block number)

Opto-coupler and LED failure mechanisms and associated activation energies were determined from the results of environmental and accelerated life tests of over 2,400 devices. The evaluation program included LED/phototransistor opto-couplers from three sources, LED/photoamplifier opto-couplers from a single source, and discrete infrared emitting LEDs from two sources. Environmental tests to evaluate device mechanical integrity included power cycling (10,000 cycles), temperature cycling (500 cycles) and a sequence of monitored

DD FORM 1 JAN 73 1473 EDITION OF 1 NOV 65 IS OBSOLETE

UNCLASSIFIED

SECURITY CLASSIFICATION OF THIS PAGE (When Data Entered)

PREFACE

The work described in this report was performed by the Parts Evaluation Laboratory section of McDonnell Douglas Astronautics Company-St. Louis (MDAC-St. Louis) Engineering Reliability Department during the period between October 1974 and October 1977. The work was performed for the National Aeronautics and Space Administration (NASA), George C. Marshall Space Flight Center under Con act Number NAS8-30777. In-house related effort, beyond the contract Statement of Work, was also performed to fully define the physical basis for observed LED output power degradation.

The work conducted under NAS8-30777 was directed by Mr. F. Villella who acted as the NASA Contracting Officer's Representative. Significant technical contributions were made by Messrs. Gordon Johnson, Michael Roberts, Bruce Kirk, Karl Pommer, and Larry Conaway of the MDAC-St. Louis Engineering Reliability Department.

TABLE OF CONTENTS

LIST OF FIGURES

LIST OF TABLES

LIST OF TABLES (Continued)

LIST OF PAGES

1.0 INTRODUCTION

Semiconductor reliability characterization is an essential prerequisite for high reliability space and military applications. Failure mechanisms related to the assembly, materials and processes must be identified, and aging characteristics must be related to applied electrical and environmental stresses. This is especially important for newer device types, such as optically coupled isolators, fabricated with a diversity of different materials and processes. Typical opto-couplers include GaAs light emitting diodes, silicon photodectors, and a light transmission/dielectric isolation medium. A single device type comprised of these different elements could be expected to exhibit a variety of different failure mechanisms, and possibly pose a serious reliability risk.

The objectives of the study described in this report were to: a) identify the failure mechanisms related to the materials and processes used in the fabrication of opto-couplers and light emitting diodes (LEDs) when subjected to space environments, and b) describe device aging characteristics for the identified failure mechanisms as a function of applied electrical and thermal stresses.

2.0 PROGRAM DESCRIPTION

The program for identifying failure mechanisms of opto-coupled isolators and light emitting diodes included two major groups of tests (Group I and Group II). Group I consisted of environmental tests designed to evaluate the mechanical integrity of devices, and included power cycling, temperature cycling, vibration, shock and acceleration. Group II consisted of multiple temperature life tests designed to evaluate device aging characteristics. Two types of opto-couplers (A and B) were subjected to the Group I and Group II tests. Opto-coupler Type A is a diode-phototransistor opto-coupler, initially procured from three sources. However, one of the three sources was unable to provide sufficient good devices for both the Group I and Group II tests, and only the Group I tests were accomplished with this manufacturer's opto-couplers. The Type B opto-coupler is a dual channel diode-photoamplifier device. A single type of infrared emitting LED from two sources was also included in the program. All device types were procured as commercial grade devices with no additional screening or preconditioning.

The evaluation programs for the Type A opto-couplers, Type B opto-couplers, and the LEDs are similar, but have been tailored to most effectively evaluate each specific device type. A general program description for each device type is provided in the following paragraphs. Specific details related to test methods and procedures are provided with the test results.

2.1 TYPE A AND TYPE B OPTO-COUPLER PROGRAMS

The test programs for the Type A and Type B opto-couplers are illustrated in Figures 1 and 2 respectively. The primary differences between the Type A and Type B Opto-coupler programs are the quantities of devices in the various tests and the addition of one Type A extended high temperature reverse bias (HTRB) test.

Initially, all devices were serialized and subjected to fine and gross leak tests. With the exception of a small sample of each manufacturer's devices that was allocated for construction analyses (2 devices) and life test bias circuit evaluations (5 devices), all devices surviving the seal leak tests were subjected to a sequence of screening and preconditioning tests. The screening and preconditioning test sequence was performed in accordance with the NASA 85M03638 specification, using the electrical end-point limits of MIL-S-19500/436 as the pass/fail criteria for Type A devices and the manufacturer's specified limits for

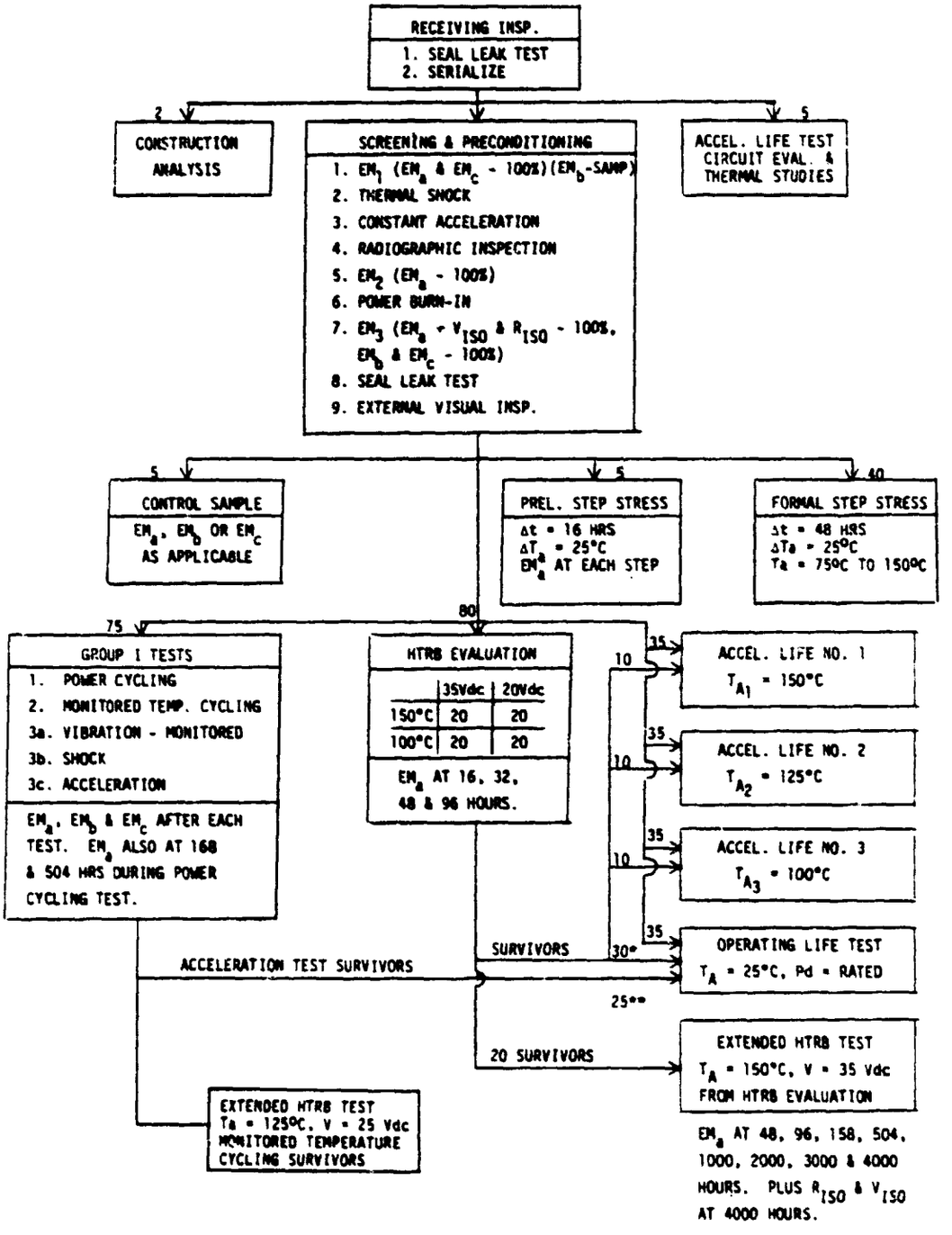

* ONLY 23 T.I. HTRB SURVIVORS AVAILABLE FOR OPERATING LIFE TEST
** ONLY 14 OPTRON ACCEL. TEST SURVIVORS

FIGURE 1. TYPE A OPTO-COUPLER TEST PROGRAM FLOW

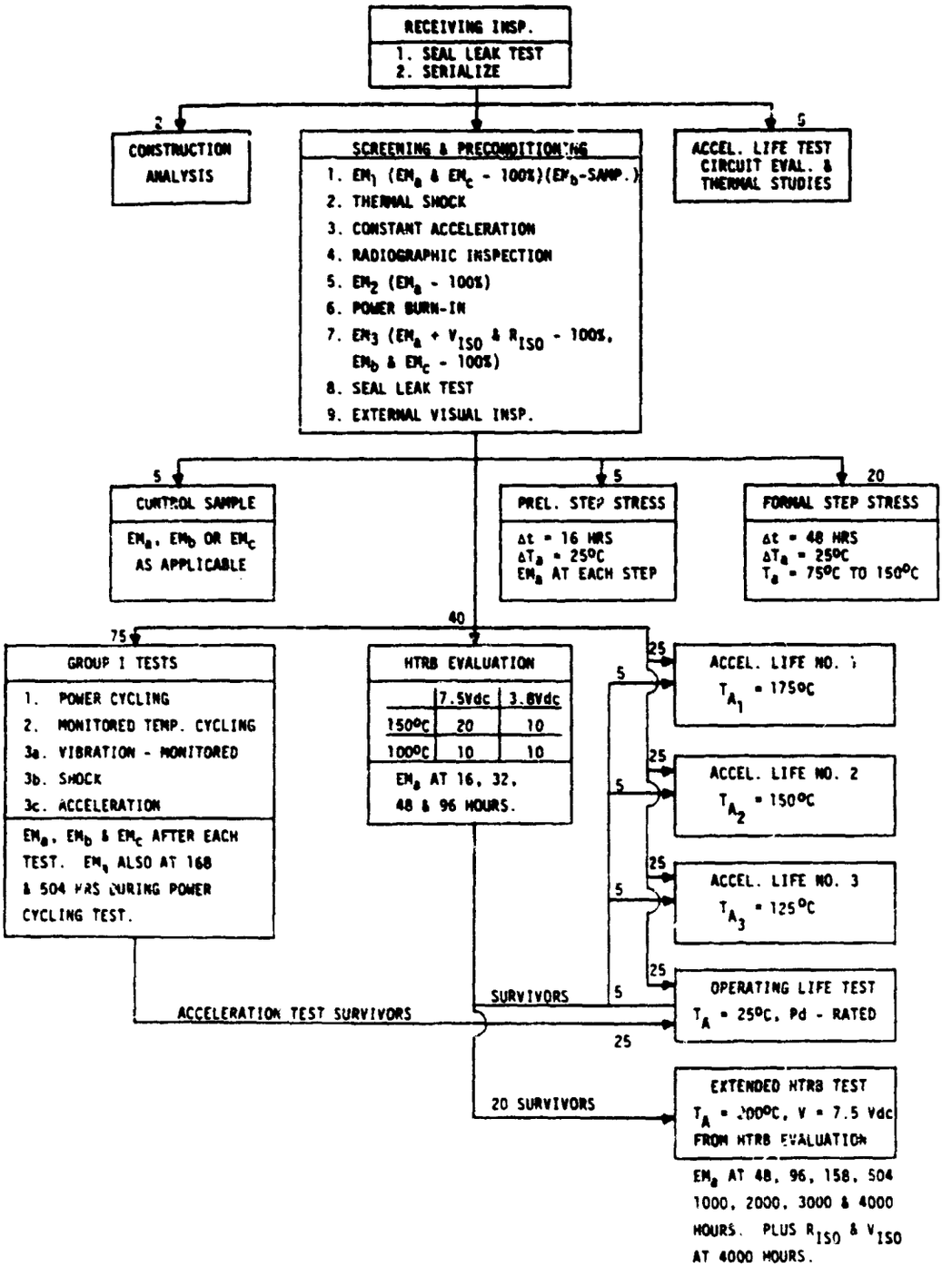

FIGURE 2. TYPE B OPTO-COUPLER TEST PROGRAM FLOW

Type B devices. However, the high temperature reverse bias test (HTRB) was omitted from the screening sequence due to an anticipated high failure percentage. All candidate manufacturers of Type A opto-couplers indicated their devices were incapable of passing a 96 hour HTRB test at 125°C and 28 Vdc. Consequently, a special HTRB test matrix was implemented to evaluate the effectiveness of HTRB screening, and to determine the optimum HTRB time-temperature voltage combination.

2.1.1 Opto-Coupler Group I Tests

Group I tests were comprised of three subgroups of 25 of each manufacturer's opto-couplers that survived the screening and preconditioning tests. The three subgroups were: (a) 10,000 power on/off cycles with each cycle comprised of 3 minutes of power "on" followed by 3 minutes of power "off" at room ambient conditions (~25°C), (b) 500 cycles of monitored operation between -55°C and 125°C, and (c) a sequence of monitored vibration (50 g's, 20 to 2,000 Hz), monitored shock (5,000 g's, 0.3 milliseconds) and constant acceleration (30,000 g's).

2.1.2 Opto-Coupler Group II Tests

Group II tests consisted of: (a) operating life tests at room ambient conditions (~25°C), (b) three operating accelerated life tests at ambient temperatures between 100°C and 175°C, and (c) long term life tests at HTRB conditions. Devices subjected to the operating and accelerated life tests were primarily those that had only been subjected to, and survived, the screening and preconditioning tests. However, survivors of the 96 hour HTRB evaluation matrix and acceleration test survivors were also included in the life tests to evaluate the effects of these prior stresses on device aging characteristics. The extended HTRB tests were primarily comprised of survivors from the HTRB evaluation matrix. However, the 125°C extended HTRB test of Type A opto-couplers was comprised of temperature cycling test survivors due to device availability. This test was performed subsequent to the other HTRB tests to determine if the same failure mechanisms would be observed at lower stress levels, and, if possible, determine activation energies for HTRB failure mechanisms.

Prior to performing the life tests, bias circuit evaluations, thermal characterization, and step-stress tests were performed to establish life test conditions.

2.2 LED PROGRAM

The test program for the LEDs is illustrated in Figure 3. Initially, both manufacturers' devices were optically examined and subjected to parametric testing. Survivors of these tests were then subjected to construction analyses (2 devices), Group I tests, and Group II tests. Preliminary and Formal Step-Stress tests were also performed to establish the Group II accelerated life test conditions.

2.2.1 LED Group I Tests

The Group I tests for LEDs were the same as the Group I opto-coupler tests. Twenty-five of each manufacturer's devices were included in each of the three subgroups: (a) power cycling for 10,000 cycles, (b) monitored temperature cycling for 500 cycles, and (c) vibration/shock/acceleration.

2.2.2 LED Group II Tests

The LED Group II tests consisted of three accelerated life tests at ambient temperatures of 150°C, 200°C and 225°C. Thirty-five of each manufacturer's LEDs were included in each of three life tests. Life test conditions were established from the results of step-stress testing.

2.3 ELECTRICAL TESTING

Three groups of electrical measurements, designated as EM_a, EM_b and EM_c, were used in the program. The EM_a electrical tests include the dc parametric tests performed at 25°C. The EM_b electrical tests are generally the same as the EM_a tests, but are performed at 125°C and -55°C. The EM_c electrical tests are dynamic tests performed at 25°C.

The EM_a tests were used as the primary criteria for device failure, and were performed on all devices initially and at the prescribed points during Group I and Group II tests. The EM_b and EM_c tests were initially performed on a sample basis and, with one exception, were also performed at the completion of Group I tests. EM_b and EM_c tests of LED's were not performed at the completion of the Group I vibration/shock/acceleration sequence.

The specific EM_a, EM_b and EM_c test parameters and test conditions for the various opto-coupler and LED devices are provided in detail in Appendix B, Tables B4, B5 and B6.

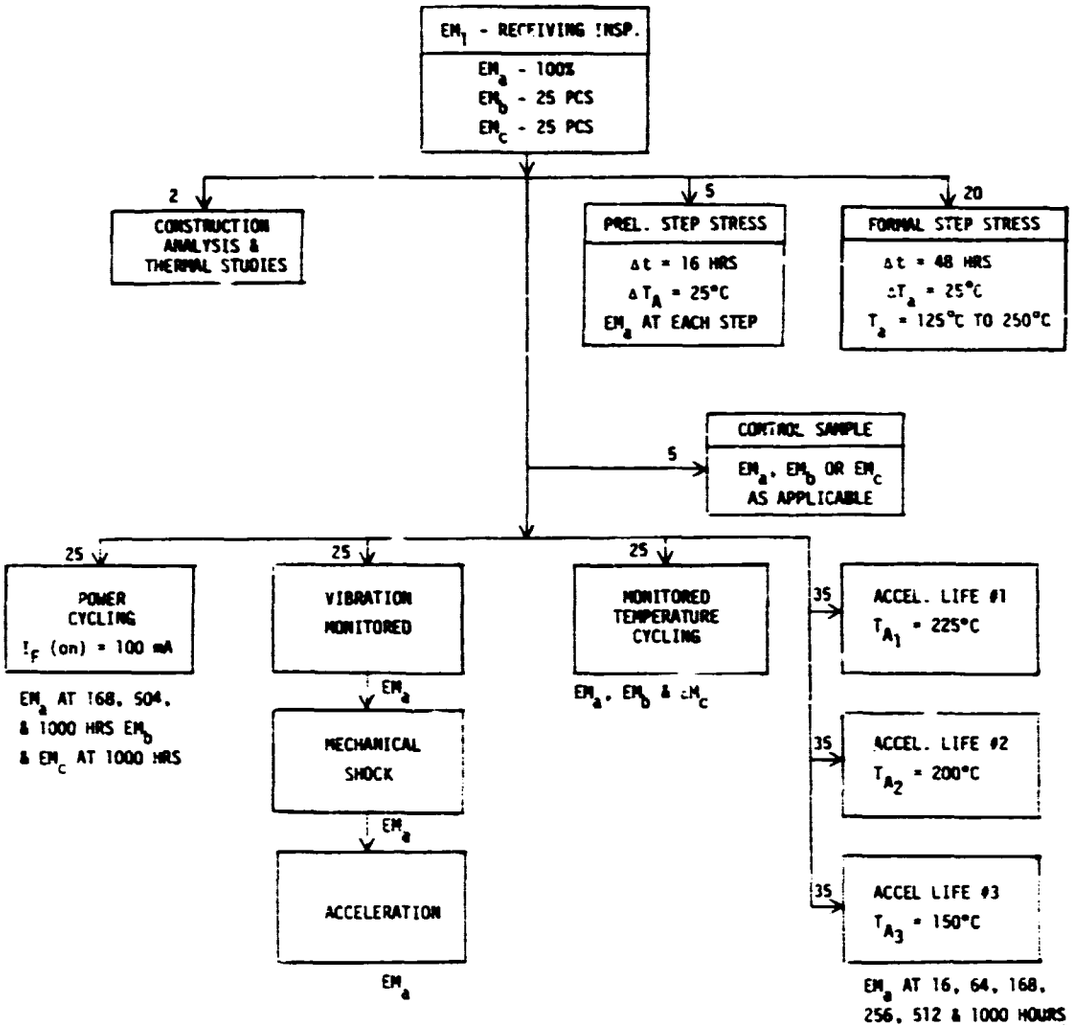

FIGURE 3. LED TEST PROGRAM FLOW

A control sample of each manufacturer's devices was also subjected to electrical testing each time devices from environmental or life tests were electrically tested. These control sample device measurements provided a check on the long term stability of the automated test equipment used for performing electrical measurements.

2.4 FAILURE ANALYSIS

All devices that failed an interim or final electrical measurement during Step-Stress, HTRB Evaluation, Group I, or Group II tests were subjected to a detailed failure analysis to determine the failure mode, mechanism and probable cause.

3.0 TEST DEVICE DESCRIPTIONS AND ELECTRICAL CHARACTERISTICS

3.1 DEVICE DESCRIPTIONS

The devices included in the program are shown in Table 1. Initially, the Texas Instruments, Optron and Spectronics Type A opto-couplers were the only opto-couplers included in the program. However, when a sufficient quantity of Spectronics devices could not be successfully processed through the screening and preconditioning test sequence, they were deleted, and the Hewlett Packard Type B opto-couplers were added to the study. The Texas Instruments, Optron and Spectronics Type A opto-couplers utilize LEDs and phototransistors. The Hewlett Packard, Type B opto-coupler, is a dual channel isolator and utilizes LEDs and high gain photodetectors. The Type A opto-couplers were supplied in modified TO-5 cans, while the Type B opto-coupler was supplied in a hermetic, 16 pin, dual in-line ceramic package. The discrete LEDs are the infrared emitting, gallium-arsenide type supplied in modified TO-18 type cans.

Detailed physical analyses, including external and internal optical and SEM evaluations, resulted in the summary of major construction features shown in Table 2. Complete details of the construction analyses are contained in Appendix A. These analyses revealed no construction features or anomalies that limited subsequent testing, however, it was noted that all of the opto-couplers were overcoated with silastic, Dow Corning R6104, which later caused open bond problems.

3.2 ELECTRICAL CHARACTERISTICS

Complete electrical characterization data for all devices meeting the specified limits is contained in Appendix C. The characterization data includes initial and post screening values of the mean and standard deviation of each measured parameter at room, high and low temperatures. Baseline pre Group I and Group II EM_a test data is summarized in Table 3 for Type A opto-couplers, Table 4 for Type B opto-couplers and Table 5 for LEDs.

Examination of the Type A opto-coupler data for the three manufacturers reveals a marked difference in several critical parameter values. The Optron devices exhibit the highest average value of transfer ratio (TR), the lowest h_{FE} and the highest dark current (I_D) of the three manufacturers' devices. In contrast, the Spectronics devices exhibit the lowest TR and the highest h_{FE}. Since TR is a

TABLE 1. DEVICE SELECTIONS

DEVICE TYPE	DESCRIPTION	MANUFACTURER	PART NUMBER
TYPE A OPTO-COUPLER	GaAs LED/PHOTOTRANSISTOR	TEXAS INSTRUMENTS	4N22
		OPTRON	OPI 1123
		SPECTRONICS	SPX 1830 (1)
TYPE B OPTO-COUPLER	DUAL CHANNEL GaAs LED/ PHOTOAMPLIFIER	HEWLETT PACKARD	5082-4365
LED	GaAs INFRARED EMITTING DIODE	TEXAS INSTRUMENTS	SL1466
		RCA	SG1009A

(1) THIS DEVICE LATER DELETED DUE TO INSUFFICIENT NUMBER OF ACCEPTABLE DEVICES

TABLE 2. MAJOR CONSTRUCTION DETAILS

	OPTO-COUPLERS				LEDs	
PART NO.	4N22	SPX-1830	OPI-1123	5082-4365	SG1009A	SL3466
MANUFACTURER	TEXAS INSTRUMENTS	SPECTRONICS	OPTRON	HEWLETT PACKARD	RCA	TEXAS INSTRUMENTS
PACKAGE TYPE	MODIFIED (6 PIN) TO-5 TYPE CAN	MODIFIED (6 PIN) TO-5 TYPE CAN	MODIFIED (6 PIN) TO-5 TYPE CAN	16 PIN DUAL IN-LINE CERAMIC	TO-18 W/WINDOW	TO-18 W/WINDOW
LEAD MATERIALS:						
EXTERNAL	Au PLATED KOVAR	Au PLATED KOVAR	Au PLATED KOVAR	Au PLATED KOVAR	Au PLATED KOVAR	Au PLATED KOVAR
INTERNAL	Au	Au	Au	Au	Au	Au
FRAME	Au PLATED KOVAR	Au PLATED KOVAR	Au PLATED KOVAR	Au PLATED REFRACTORY METAL	Au PLATED KOVAR	Au PLATED KOVAR
LED						
TYPE	GaAs PLANER	GaAs, LIQUID PHASE EPITAXY	GaAs, LIQUID PHASE EPITAXY	GaAs, PLANAR	GaAs, LIQUID PHASE EPITAXY	GaAs, LIQUID PHASE EPITAXY
CHIP CHARACTERISTICS:						
ATTACH	⚠1	Ag EPOXY	Au EUTECTIC	Au EUTECTIC	Ag EPOXY	Au EUTECTIC
METALLIZATION	AuGe	Al	Au ALLOY	Al	Au	AuSn
SCRIBE	LASER	MECHANICAL	MECHANICAL	MECHANICAL	MECHANICAL	MECHANICAL
WIRE BONDS:						
CHIP	Au/AuGe THERMOCOMPRESSION	Au/Al THERMOCOMPRESSION	Au/Au THERMOCOMPRESSION	Au/Al THERMOCOMPRESSION	Au/Au THERMOCOMPRESSION	Au/Au THERMOCOMPRESSION
FRAME	Au/Au THERMOCOMPRESSION	Au/Au THERMOCOMPRESSION	Au/Au THERMOCOMPRESSION	Au/Au THERMOCOMPRESSION	Au/Au THERMOCOMPRESSION	Au/Au THERMOCOMPRESSION
TRANSISTOR						
CHIP CHARACTERISTICS:						
ATTACH	Au EUTECTIC	Ag EPOXY	Ag EPOXY	Au EUTECTIC	---	---
METALLIZATION	Al	Al	Al	Al	---	---
SCRIBE	LASER	MECHANICAL	MECHANICAL	LASER	---	---
WIRE BONDS:						
CHIP	Au/Al THERMOCOMPRESSION	Au/Al THERMOCOMPRESSION	Au/Al THERMOCOMPRESSION	Au/Al THERMOCOMPRESSION	---	---
FRAME	Au/Au THERMOCOMPRESSION	Au/Au THERMOCOMPRESSION	Au/Au THERMOCOMPRESSION	Au/Au THERMOCOMPRESSION	---	---
COUPLING MEDIUM/LENS MATERIAL	3 MIL GLASS/R6104 ADHESIVE AND OVERCOAT	DOW CORNING R6104 SILICONE RESIN	DOW CORNING R6104 SILICONE RESIN	DOW CORNING R6104 SILICONE RESIN	DOW CORNING 7052 GLASS LENS	DOW CORNING 7052 GLASS LENS

⚠1 LED ATTACHED ATOP TRANSISTOR VIA A COUPLING MEDIUM.

TABLE 3. TYPE A OPTO-COUPLER EM_a PARAMETER CHARACTERIZATION

PARAMETER	MIL-STD LIMITS		NASA LIMITS		TEXAS INSTRUMENTS		SPECTRONICS		OPTRON		UNITS
	MIN	MAX	MIN	MAX	MEAN	SIGMA	MEAN	SIGMA	MEAN	SIGMA	
V_F	0.8	1.3	---	1.3	1.161	0.014	1.095	0.015	1.152	0.014	Vdc
R_D	---	---	---	5.0	2.853	0.993	3.447	0.761	3.790	0.895	Ω
I_R	---	100	---	10.0	0.016	0.274	14.399	24.463	0.296	4.243	μAdc
BV_{CBO} ⚠	35	---	35	---	62.834	5.707	61.740	5.527	63.043	1.995	Vdc
BV_{CEO} ⚠	35	---	35	---	57.243	10.713	57.700	7.086	61.498	4.675	Vdc
BV_{EBO}	4	---	4	---	10.337	1.806	8.083	2.641	7.355	0.217	Vdc
I_D	---	100	---	100	0.463	3.850	0.191	1.775	4.807	9.384	nAdc
HFE	---	---	100	500	1067	1127	14,710	71,901	499.900	142.700	---
TR	.25	---	.25	1.0	0.731	0.229	0.513	0.197	0.834	0.615	---
V_{CES}	---	0.3	---	0.3	0.104	0.020	0.317	0.036	0.146	0.023	Vdc

⚠ MAXIMUM LIMIT OF ~63.0 Vdc IMPOSED BY TEST HARDWARE CONSTRAINTS.

TABLE 4. TYPE B OPTO-COUPLER EM_a PARAMETER CHARACTERIZATION

PARAMETER	LIMITS		MEAN	SIGMA	UNITS
	MIN	MAX			
I_{OH}	---	250	5.089	5.509	μAdc
V_{OL}	---	0.6	0.377	0.048	Vdc
I_{CCH}	---	20	15.934	1.321	mAdc
I_{CCL}	---	36	25.736	3.109	mAdc
V_F	---	1.75	1.536	0.015	Vdc
BV_R	5.0	---	9.873	1.697	Vdc

TABLE 5. LED EM_a PARAMETER CHARACTERIZATION

PARAMETER *	LIMITS		RCA		T.I.		UNITS
	MIN	MAX	MEAN	SIGMA	MEAN	SIGMA	
I_R	---	0.050	0.016	0.013	0.002	0.005	μAdc
BV_R	5.0	---	31.410	2.742	26.620	8.832	Vdc
$V_F(2)$	---	1.10	1.060	0.007	1.057	0.009	Vdc
$V_F(20)$	---	1.30	1.193	0.013	1.165	0.017	↓
$V_F(50)$	---	1.40	1.299	0.028	1.234	0.029	↓
$V_F(100)$	---	1.60	1.432	0.051	1.314	0.040	↓
$P_0(2)$	0.005	---	0.044	0.008	0.024	0.009	mW
$P_0(20)$	0.200	---	0.807	0.143	0.522	0.146	↓
$P_0(50)$	0.700	---	2.162	0.378	1.495	0.411	↓
$P_0(100)$	1.600	---	4.187	0.676	3.039	0.661	↓

* NUMBERS IN PARENTHESES INDICATE THE VALUE OF MEASUREMENT CURRENT IN mA.

function of LED output power and phototransistor gain (related to h_{FE}), it may be inferred that the Optron LEDs have the highest output power, and that the Spectronics LEDs have the lowest output power. This suggests that the NASA 85M03638 specification limits for h_{FE} may be useful as a means for controlling LED output power. However, h_{FE} is not the best method for controlling LED output power, since the h_{FE} and TR measurements are not performed at the same transistor current conditions. A measurement of the transistor photocurrent is a better method, and was later incorporated as a measurement parameter during life testing.

The parametric data for the Type B opto-coupler is for only one manufacturer's devices, and the specification limits are either the manufacturer's limits or were derived from initial electrical test results. None of the parameters appear to be too tightly or too loosely specified. Device instability was observed during the initial electrical tests which necessitated the incorporation of by-pass capacitors mounted as close to the devices as possible. Further investigation revealed that in most cases these capacitors had to be within ½ inch of the device, causing difficulties when the devices were tested with automatic test equipment and when they were mounted in the Group I and Group II test fixtures. This problem will also require attention during printed circuit board layout for operational equipment utilizing these devices.

The LED parametric data indicates that the RCA and TI device are similar, although the RCA LED does have a slightly higher output power than the TI LED. Specification limits for the LEDs were derived almost entirely from the initial electrical measurements, since the manufacturer's catalog sheets included end-point limits for only a few parameters.

4.0 INITIAL EVALUATIONS AND TESTS

4.1 ELECTRICAL BIAS CONFIGURATIONS

Suitable electrical biasing configurations were required for operating devices during the various burn-in, HTRB evaluation matrix, Group I and Group II tests. The biasing requirements for each test were generally different, and individual circuits were selected to meet these requirements. Operating a sample of each manufacturer's device at the anticipated test conditions verified the suitability of each circuit. Bias configuration requirements for each test and the selected bias circuit are presented in the following paragraphs. Results of circuit suitability evaluation tests are contained in Appendix D.

4.1.1 Opto-Coupler Burn-In Circuits

During burn-in testing, opto-couplers are required to dissipate maximum rated power in the photodetector, and the LEDs are required to conduct maximum rated forward current. These conditions are satisfied with the circuits shown in Figure 4. The Type A opto-coupler circuit places the phototransistor in a constant current configuration, and this current source is used to bias the LED at the maximum rated current of 40 mA. Maximum rated power dissipation is achieved by adjusting the positive supply voltage. The LED is placed in the collector circuit to provide a positive voltage across the coupling medium. This polarity of voltage stress will drift any mobile cations that may be present in the coupling medium toward the base region of the transistor. A build-up of positive charge at the p-type base will tend to invert the underlying silicon and cause excessive leakage currents. This was a suspected failure mechanism with the sandwich type construction (LED, coupling glass and photo-transistor) used in the Texas Instruments opto-coupler.

The Type B opto-coupler offered little flexibility in bias circuit design due to the nature of the photodetector. Consequently, it was biased in a conventional manner with maximum rated current in the LEDs and output transistors.

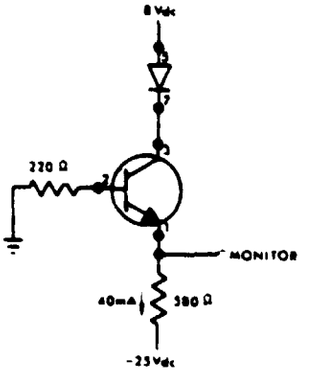

TYPE A OPTO-COUPLER

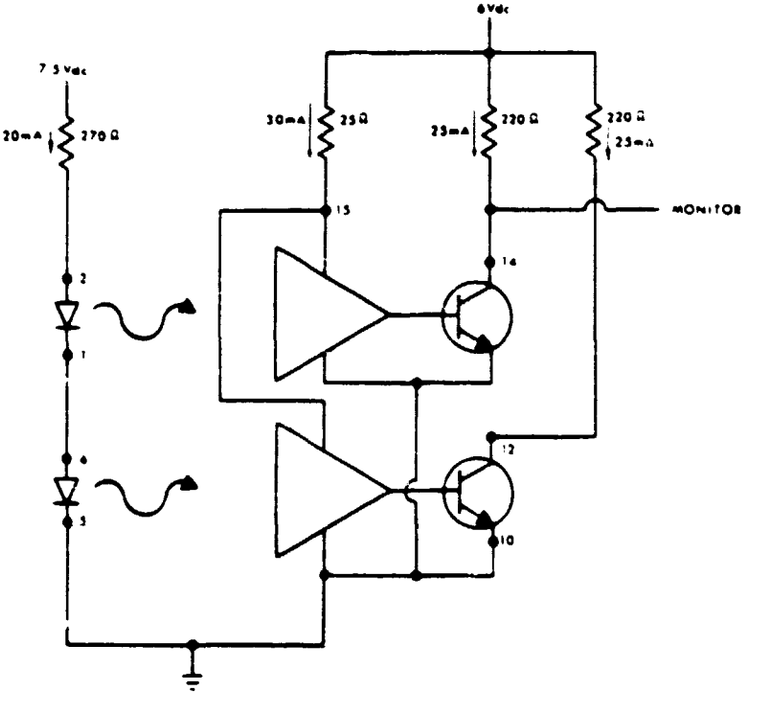

TYPE B OPTO-COUPLER

FIGURE 4. OPTO-COUPLER BURN-IN CIRCUITS

4.1.2 Opto-Coupler Power Cycling Circuits

The primary requirement for power cycling was to cause a 100°C rise in the junction temperature of the phototransistor or photoamplifier. This was accomplished for the Type A opto-coupler by utilizing the burn-in circuit, and adjusting the power dissipation to provide a 100°C rise in junction temperature. Due to the nature of the Type B opto-coupler, power dissipation could not be adjusted in the photoamplifier or its output transistor. Consequently the burn-in circuit was used to cycle the Type B devices between an "off" condition and the maximum rated current condition in the output transistor. Power cycling circuits for both the Type A and B opto-couplers are shown in Figure 5.

4.1.3 Opto-Coupler Monitored Vibration, Shock and Temperature Cycling Circuits

During the vibration, shock and temperature cycling tests, it was required that open and shorted conditions within each device be readily detectable. This requirement was satisfied with the bias circuits shown in Figure 6. The monitor point voltage at pin 3 of the Type A opto-coupler and pin 10 of the Type B opto-coupler are typically 2 Vdc, and any single open wire, or short between adjacent wires will cause a change in the monitor point voltage of at least 0.25 Vdc and in most cases a greater than 1 Vdc change.

4.1.4 Opto-Coupler HTRB Bias Circuits

During the HTRB evaluation matrix and the extended HTRB tests, it was required that the opto-couplers be operated in the "off" state (LED current = 0) with a specified voltage across the photodetector. This was accomplished with the bias circuits shown in Figure 7.

4.1.5 Opto-Coupler Operating and Accelerated Life Test Circuits

Biasing requirements during operating and accelerated life tests of the Type A opto-coupler were the same as those established for burn-in tests. However, for the Type B dual channel opto-coupler, it was required that one channel be operated in the burn-in configuration, and that the other channel be operated in the HTRB configuration. This "on"/"off" configuration within each device during life testing would permit the assessment of activation energies for each operating state. Life test configurations for the Type A and Type B opto-couplers are shown in Figure 8.

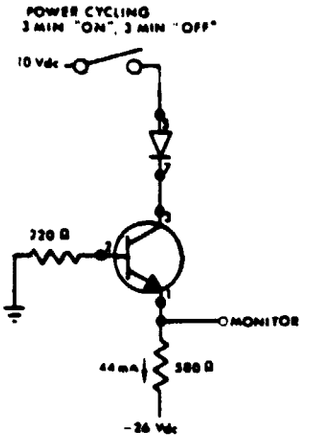

TYPE A OPTO-COUPLER

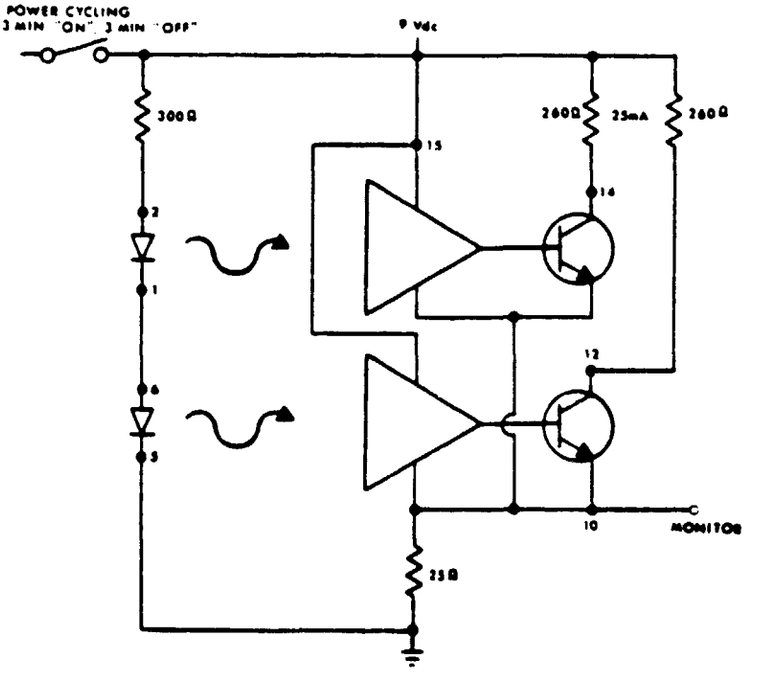

TYPE B OPTO-COUPLER

FIGURE 5. OPTO-COUPLER POWER CYCLING BIAS CIRCUITS

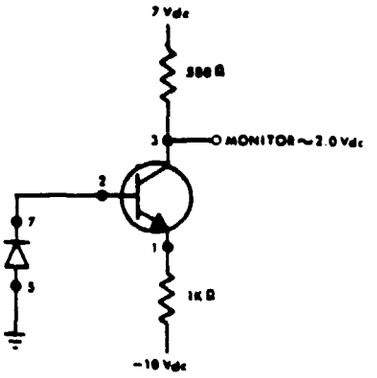

TYPE A OPTO-COUPLER

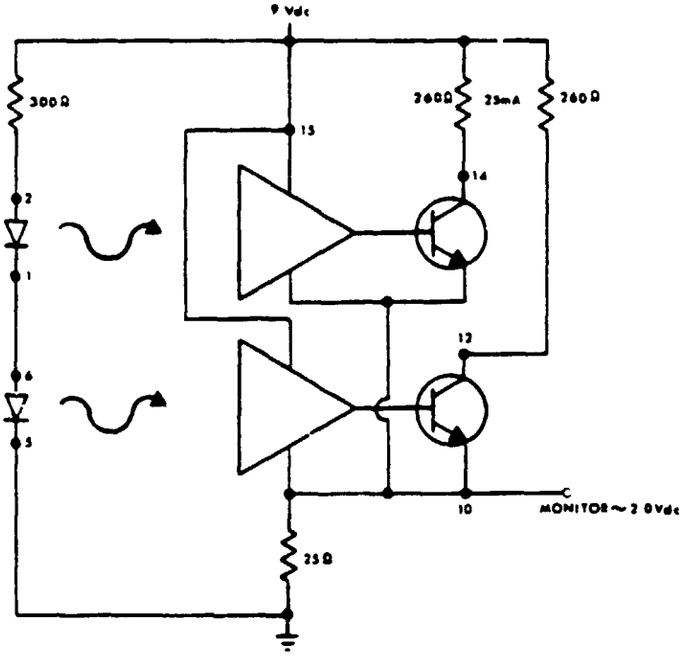

TYPE B OPTO-COUPLER

FIGURE 6. OPTO-COUPLER MONITORED VIBRATION, SHOCK AND TEMPERATURE CYCLING TEST CIRCUITS

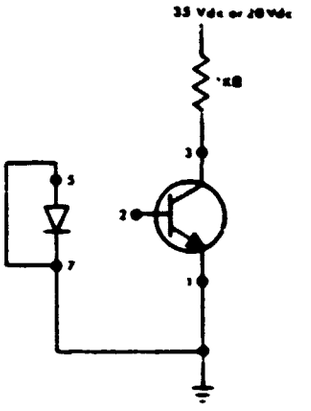

TYPE A OPTO-COUPLER

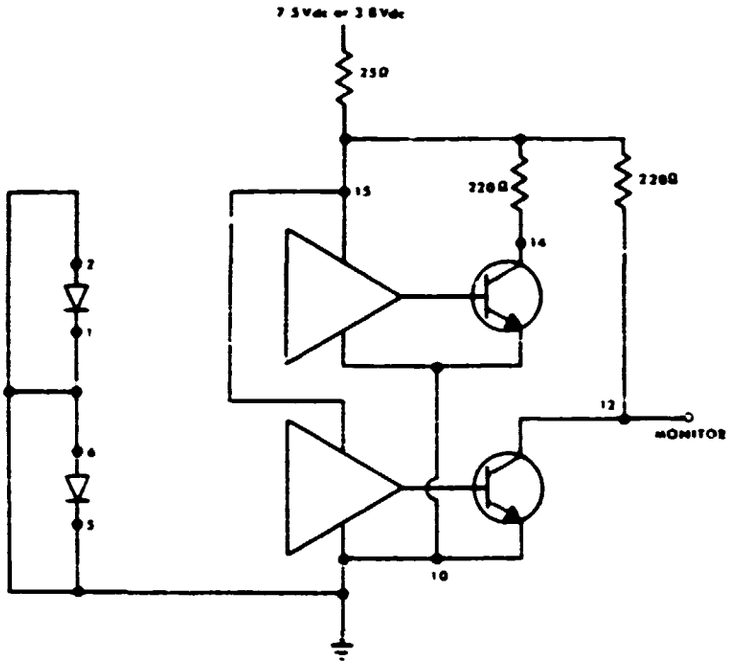

TYPE B OPTO-COUPLER

FIGURE 7. OPTO-COUPLER HTRB BIAS CIRCUITS

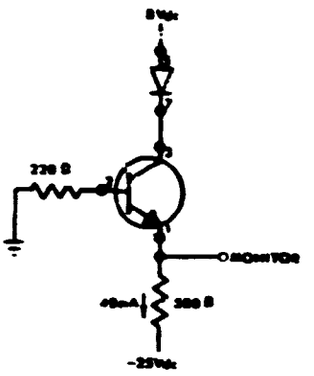

TYPE A OPTO-COUPLER

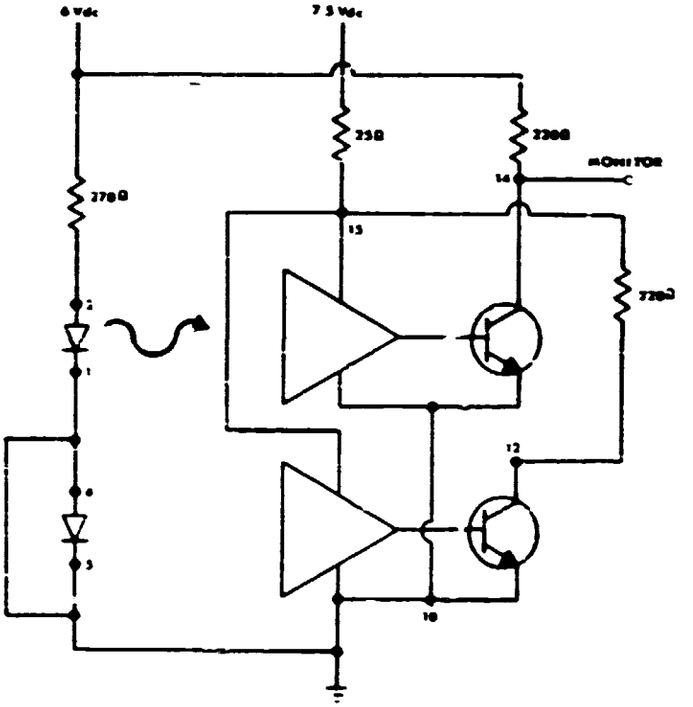

TYPE B OPTO-COUPLER

FIGURE 8. OPTO-COUPLER OPERATING AND ACCELERATED LIFE TEST CIRCUITS

4.1.6 LED Bias Circuits

All operating tests of LEDs were performed with the devices forward biased at the maximum rated current of 100 mA. This configuration, shown in Figure 9, satisfies all of the previously discussed requirements for those tests applicable to LEDs. Since HTRB tests of LEDs are not included in the program, a reverse bias configuration was not required.

4.2 DEVICE THERMAL CHARACTERISTICS

Subsequent to verifying the suitability of each bias circuit, device junction temperatures were established at anticipated power cycling, operating life, and accelerated life test conditions. Junction temperatures were determined from electrical measurements of device temperature sensitive parameters using a technique similar to MIL-STD-883, Method 1012. The LED forward voltage was used as the temperature sensitive parameter for measurements of LED junction temperature, the base-emitter voltage was used to determine Type A opto-coupler phototransistor junction temperatures, and a substrate diode was used for determining Type B opto-coupler photoamplifier junction temperatures. Results of these studies are presented later in the discussions of Group I and Group II tests.

4.3 STEP-STRESS TESTS

Following the selection of accelerated life test bias circuits, step-stress tests were performed to: (a) validate the nondestructive nature of the bias circuits, and (b) obtain sufficient failure data on a reasonable quantity of devices to make a final determination of the accelerated life test conditions. A preliminary step-stress test using a sample of 5 parts was first performed to aid in the selection of conditions used in the subsequent formal step-stress tests. The formal step-stress test, using a 40 piece sample of Type A opto-couplers and 20 piece samples of LEDs and Type B opto-couplers, was performed to obtain failure data on a reasonable quantity of devices to permit a determination of accelerated life test conditions. During both types of step-stress tests, devices were monitored, in situ, at the test temperature to ascertain application of bias and to detect open bonds. At the completion of each step, devices were cooled to room temperature with bias applied, and subjected to 25°C electrical measurements (EM_a). Devices failing an EM_a measurement were generally removed from test and subjected

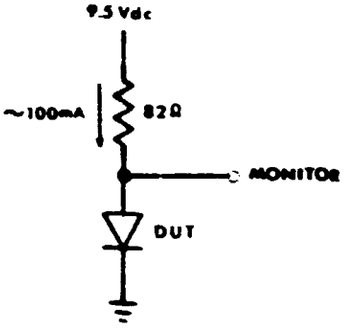

FIGURE 9. LED BIAS CONDITION - ALL TESTS

to failure analysis. However, degraded LEDs, and opto-couplers with only slightly out-of-tolerance parameter values were left on test. Devices exhibiting an open bond at the step-stress test temperature, but passing the EM_a tests, were subjected to the next temperature step of the sequence.

4.3.1 Type A Opto-Coupler Step-Stress Test Results

The Type A opto-coupler preliminary step-stress test consisted of five, 16 hour steps in 25°C increments from 25°C to 150°C, plus an additional 48 hours at 150°C. The results of these tests are summarized in Table 6. Since there was no evidence that the selected bias circuit (previous Figure 8) was responsible for the observed failures, formal step-stress testing was initiated with T.I. and Optron devices (Spectronics now deleted from the program). The formal step-stress tests were initiated at 75°C, and continued to 150°C in 25°C, 48 hour increments. The 150°C step was subsequently extended an additional 168 hours in an attempt to observe additional parametric degradation. Results of these tests are shown in Table 7.

A total of nine T.I. device failures were observed during the formal step-stress tests; five due to open circuits at the 125°C and 150°C test temperatures, and four that failed the 25°C electrical tests. The four 25°C parametric failures were: a) 2 devices with excessive dark current, b) 1 device with low transfer ratio, and c) one device with multiple failed parameters resulting from an inadvertently fused open emitter metallization. The cause of the open circuits at elevated temperatures was attributed to weak wire bonds being broken by expansion of the Dow Corning R6104 overcoat. All of the Optron device failures were attributed to weak bonds aggravated to failure by expansion of the R6104 overcoat.

Based on these test results, accelerated life test temperatures of 100°C, 125°C, and 150°C were selected. It was recognized that a substantial number of open bonds would be encountered during life testing at these temperatures. However, on the basis of observed parameter degradation, primarily transfer ratio, it was felt that these temperatures were required to generate sufficient parametric failure data for aging characteristic analysis.

TABLE 6. TYPE A OPTO-COUPLER PRELIMINARY STEP STRESS TEST RESULTS

MANUFACTURER	QTY. IN TEST	CUMULATIVE NUMBER OF FAILURES						
		50°C 16 HRS.	75°C 32 HRS.	100°C 48 HRS.	125°C 64 HRS.	150°C 80 HRS.	150°C 104 HRS.	150°C 128 HRS.
Texas Instruments:	5							
25°C Elect. Test Failures		0	0	0	0	0	0	0
Open Lead at Temp.		0	0	0	0	0	0	0
Total		0	0	0	0	0	0	0
Spectronics:	5							
25°C Elect. Test Failures		0	0	1	2	2	4	-
Open Lead at Temp.		0	0	0	0	0	0	-
Total		0	0	1	2	2	4	-
Optron:	5							
25°C Elect. Test Failures		0	0	0	0	0	0	-
Open Lead at Temp.		0	1	1	2	3	4	-
Total		0	1	1	2	3	4	-

TABLE 7. TYPE A OPTO-COUPLER FORMAL STEP STRESS TEST RESULTS

MANUFACTURER	QTY. IN TEST	CUMULATIVE NUMBER OF FAILURES				
		75°C 48 HRS.	100°C 96 HRS.	125°C 144 HRS.	150°C 192 HRS.	150°C 360 HRS.
Texas Instruments:	40					
25°C Elect. Test Failures		0	0	0	1	4
Open Lead at Temp.		0	0	5	5	5
Total		0	0	5	6	9
Optron:	40					
25°C Elect. Test Failures		1	1	1	2	2
Open Lead at Temp.		1	3	9	14	19
Total ⚠		1	3	9	14	19

⚠ Because some devices failed the 25°C electrical test and exhibited an open at the elevated temperature, the total is not the sum of the two categories.

4.3.2 Type B Opto-Coupler Step-Stress Test Results

The Type B opto-coupler preliminary step-stress test consisted of eight, 16 hour steps in 25°C increments from 100°C to 275°C. The results of these tests are summarized in Table 8. Four of the five devices on test failed due to open leads at ambient temperatures above 200°C. No other device failures were observed and the selected bias circuit (previous Figure 8) was considered acceptable. Formal step-stress testing was initiated at 125°C and continued to 250°C in 25°C, 48 hour increments. Results of this test are summarized in Table 9. Only one parametric failure was observed, and this was due to an LED exhibiting low reverse breakdown voltage following the 225°C step. The remaining failures (20) were due to open bonds either at elevated temperatures above 175°C (17 failures) or at 25°C following temperature steps of 225°C and 250°C. All of the open bonds were attributed to open wires caused by expansion of the R6104 overcoat.

Based on the step-stress test results, accelerated life test temperatures of 125°C, 150°C and 175°C were selected. The maximum temperature of 175°C was selected to avoid an excessive number of open wire failures. Life tests of Type A opto-couplers conducted prior to this time had indicated that test temperatures should be kept below those resulting in open wires/bonds due to expansion of the R6104, even though fewer parameter degradation failures would be observed.

4.3.3 LED Step-Stress Test Results

The preliminary LED step-stress test consisted of six 25°C, 16 hour steps from 125°C to 250°C, plus a 16 hour step at 270°C. Since LED end-point limits were not established prior to the preliminary step-stress test, all devices were continued on test through the 270°C step. No catastrophic failures were observed during this test, but output power degradation (50% to 75% following the 270°C step) was evident in all devices.

Formal step-stress testing of twenty of each manufacturer's LED was performed from 125°C to 250°C in 25°C, 48 hour increments. The LEDs were biased as shown in the previous Figure 9 with 100 mA of forward current. Test results, based on the now established Appendix B end-point limits, are shown in Table 10. A total of 30 LEDs failed during these tests (14 T.I. and 16 RCA). Seven of the failures

TABLE 8. TYPE B OPTO-COUPLER PRELIMINARY STEP STRESS TEST RESULTS

MANUFACTURER	QTY. IN TEST	CUMULATIVE NUMBER OF FAILURES							
		100°C 16 HRS.	125°C 32 HRS.	150°C 48 HRS.	175°C 64 HRS.	200°C 80 HRS.	225°C 96 HRS.	250°C 112 HRS.	275°C 128 HRS.
Hewlett Packard:	5								
25°C Elect. Test Failures		0	0	0	0	0	1	1	2
Open Lead at Temp		0	0	1	2	2	2	2	2
Total ⚠		0	0	1	2	2	2	2	2

⚠ Because some devices failed the 25°C electrical test and exhibited an open at the elevated temperature, the total is not the sum of the two categories.

TABLE 9. TYPE B OPTO-COUPLER FORMAL STEP STRESS TEST RESULTS

MANUFACTURER	QTY. IN TEST	CUMULATIVE NUMBER OF FAILURES					
		125°C 48 HRS.	150°C 96 HRS.	175°C 144 HRS.	200°C 192 HRS.	225°C 240 HRS.	250°C 288 HRS.
Hewlett Packard	20						
25°C Elect. Test Failures		0	0	1	1	3	4
Open Leads at Temp.		0	0	0	1	8	17
Total ⚠		0	0	1	2	8	17

⚠ Because some devices failed 25°C electrical test and exhibited an open at the elevated temperature, the total is not the sum of the categories.

TABLE 10. LED FORMAL STEP STRESS TEST RESULTS

MANUFACTURER	QTY. IN TEST	CUMULATIVE NUMBER OF FAILURES					
		125°C 48 HRS.	150°C 96 HRS.	175°C 144 HRS.	200°C 192 HRS.	225°C 240 HRS.	250°C 288 HRS.
RCA	20	2	2	8	14	15	16
Texas Instruments	20	2	4	5	11	13	14

were due to low output power, fifteen were due to high reverse current, and eight were catastrophic. Seven of the eight catastrophic failures were due to an electrical overstress of unknown origin, and which never reoccurred during life testing. The remaining catastrophic failure was a shorted LED due to migration of silver at 250°C from the RCA epoxy die attach. The silver migration failure mechanism limited life test temperatures to below 250°C, and accelerated life test temperatures of 150°C, 200°C and 225°C were selected.

5.0 OPTO-COUPLER SCREENING AND PRECONDITIONING TEST RESULTS

The results of subjecting all manufacturers' Type A and Type B opto-couplers to the sequence of tests shown in Table 11 are summarized in Table 12. As previously noted, insufficient Spectronics devices successfully completed the screening tests and testing of these devices was terminated. The Spectronics optically-coupled devices exhibited: a) a high percentage (37%) of initial (Lot A) seal leak test failures, b) a 47% fall-out during post burn-in electrical tests, and c) a 45% rejection of the Lot B devices (replacements for Lot A seal leak test failures) during initial electrical testing. It is estimated that if the Lot B device screening had not been terminated, only 20% of the 683 devices tested would have been available for Group I and Group II tests. In contrast, 70% to 85% of the other manufacturers' devices successfully completed the screening sequence. Thus, the screening sequence is quite effective for eliminating grossly defective devices. However, as will be seen later from the life test results, devices successfully completing the sequence are not necessarily defect-free.

TABLE 11. OPTO-COUPLER SCREENING/PRECONDITIONING TESTS

TEST	MIL-STD-883 METHOD	CONDITIONS
SEAL LEAK FINE GROSS	 1014 1014	 CONDITION A1 CONDITION C2
SERIALIZATION		NUMERICAL; NO TWO PARTS SHALL HAVE THE SAME SERIAL NUMBER.
INITIAL ELECTRICAL MEASUREMENTS		(EM_a & EM_c - 100%)(EM_b - 50 PIECE SAMPLE MIN.)
THERMAL SHOCK	1011	CONDITION B; -55°C TO +125°C, 10 CYCLES
CONSTANT ACCELERATION	2001	20,000g; 1 MINUTE MINIMUM IN ORIENTATION Y_1 AND X_1.
RADIOGRAPHIC INSPECTION		MSFC-STD-355
PRE BURN-IN ELECTRICAL MEASUREMENTS		(EM_a - 100%)
POWER BURN-IN		240 HOURS OF OPERATION IN THE APPLICABLE FIGURE 8 CIRCUIT AT T_A=25°C
POST BURN-IN ELECTRICAL MEASUREMENTS		(EM_a, EM_b & EM_c - 100%)
SEAL LEAK FINE GROSS	 1014 1014	 CONDITION A1 CONDITION C2
VISUAL EXAMINATION (EXTERNAL)		QUALITY OF WORKMANSHIP, MECHANICAL SOUNDNESS AND MARKING AT 7X MIN.

TABLE 12. OPTO-COUPLER SCREENING/PRECONDITIONING RESULTS

	TEXAS INSTRUMENTS		OPTRON		SPECTRONICS-LOT A		SPECTRONICS-LOT B		HEWLETT PACKARD	
	NO. TESTED	NO. FAILED	NO. TESTED	NO. FAILED	NO. TESTED	NO. FAILED	NO. TESTED	NO. FAILED	NO. TESTED	NO. FAILED
SEAL LEAK TEST	500	7	495	5	500	183	181	26	300	0
INITIAL ELECTRICAL MEASUREMENTS	493	7	490	16	310	24	155	71	300	6
THERMAL SHOCK	472	---	460	---	273	---	84	---	294	---
CONSTANT ACCELERATION	472	---	460	---	273	---	84	---	286	---
RADIOGRAPHIC INSPECTION	471	29	460	42	273	17	72	0	285	---
PRE BURN-IN ELECTRICAL MEASUREMENTS	471	11	460	63	273	31	31	13	285	9
POWER BURN-IN	460	---	397	---	240	---	(1)		276	---
POST BURN-IN ELECTRICAL MEASUREMENTS	460	31	397	50	240	113			275	13
SEAL LEAK TESTS	429	2	347	5	127	5			262	0
VISUAL EXAMINATION	427	0	342	0	122	0			262	8
TOTAL PARTS AVAILABLE FOR GROUP I AND GROUP II TESTS	427		342		122				254	

NOTES: (1) SPECTRONICS DEVICES WERE DELETED FROM THE PROGRAM.

2 PERIODICALLY, DEVICES WERE REMOVED FROM SCREENING/PRECONDITIONING TO INITIATE CONSTRUCTION ANALYSIS, BIAS CIRCUIT EVALUATION, ETC.

6.0 GROUP I TEST RESULTS

Group I tests were environmental tests designed to evaluate the mechanical integrity of the opto-couplers and LEDs. Three subgroups of tests were included in Group I: a) power cycling, b) monitored temperature cycling and c) a sequence of monitored vibration, monitored shock and constant acceleration with survivors of each test being subjected to the subsequent test. Twenty-five of each manufacturer's device types were included in each subgroup. Spectronics opto-couplers were also included in two of the subgroups. The specific conditions and test methods for performing each Group I test are shown in Table 13. EM_a, EM_b and EM_c electrical measurements were performed at the completion of each test except the LED vibration/shock/acceleration sequence. However, LED end-point limits for EM_b and EM_c tests were not established, and the number of EM_b and EM_c failures is indeterminate.

6.1 POWER CYCLING RESULTS

The results of cycling 25 of each manufacturer's opto-couplers and LEDs for 10,000 3 minute "on"/3 minute "off" cycles at room ambient conditions are shown in Table 14. Junction temperature rises between the "off" and "on" conditions during the test were as shown in Table 15. Three basic failure modes were observed: a) excessive LED reverse current (13 Spectronics opto-couplers and 3 T.I. LEDs), b) degraded transfer ratio (2 Optron opto-couplers) and c) open bonds (6 Optron and 2 Spectronics opto-couplers). Spectronics device failures were not subjected to formal failure analysis, but the cause of the high number of LED reverse current failures is believed to be due to an excessive build-up of the LED epoxy die attach. The analysis and cause of the remaining failures is presented in Appendix E. However, it is apparent that only the Optron and Spectronics devices are susceptible to bond failures during power cycling, which was the expected predominant failure mode in this test.

An indication of average LED parameter changes resulting from exposure to the power cycling test is presented in Table 16. The only important parameter change noted was LED output power, and the percentage change appears to be greater at the 125°C measurement condition than at the 25°C and -55°C condition. Little change was observed at the -55°C measurement temperature. The reason for the different percent changes at each measurement temperature is not well understood, but with properly established EM_b and EM_c parameter limits, no additional power cycling failures would be expected.

TABLE 13. GROUP I TESTS

SUBGROUP	MIL-STD-883 METHOD	CONDITIONS
A. Power Cycling - 25 devices each Manufacturer	N/A	10,000 cycles, 3 min on - 3 min off, T_A = 25°C, EM_a at 1,680 and 5,040 cycles. EM_a, EM_b and EM_c at 10,000 cycles, Figures 5 and 9 bias circuits.
B. Monitored Temperature Cycling - 25 devices each Manufacturer	1010 Cond. B	500 cycles from -55°C to 125°C, Continuous monitoring for opens and shorts, Figures 6 and 9 bias circuits. EM_a, EM_b and EM_c after 500 cycles.
C1. Monitored Vibration - 25 devices each Manufacturer	2007 Cond. B	50g, 20 to 2,000 Hz, 4 sweeps in each of X , Y and Z axis, Continuous monitoring, Figures 6 and 9 bias circuits. EM_a EM_b and EM_c after completion of test.
C2. Monitored Shock - Vibration Test Survivors	2002 Cond. D	5,000g, 0.3 millisecond, 5 blows in each of X_1, X_2, Y_1, Y_2, Z_1 and Z_2 axis, Continuous monitoring, Figures 6 and 9 bias circuits. EM_a, EM_b and EM_c after completion of test.
C3. Acceleration - Shock Test Survivors	2001 Cond. E	30,000g, 3 minutes in each of X_1, Y_1, Y_2 and Z_1 axis. EM_a, EM_b and EM_c after completion of test.

TABLE 14. POWER CYCLING TEST RESULTS

MANUFACTURER	QTY. IN TEST	CUMULATIVE NUMBER OF FAILURES						TOTAL
		1680 CYCLES	5040 CYCLES	10,000 CYCLES				
		EM_a	EM_a	EM_a	EM_b (1)		EM_c	
		25°C	25°C	25°C	+100°C	-55°C	25°C	
OPTO-COUPLERS:								
TEXAS INSTRUMENTS	25	0	0	0	0	0	0	0
SPECTRONICS	25	14	14	15	15	15	15	15
OPTRON	25	3	6	8	8	8	8	8
HEWLETT PACKARD	25	0	0	0	0	0	0	0
LEDs:								
TEXAS INSTRUMENTS	25	0	0	3	(2)	(2)	(2)	3
RCA	25	0	0	0	(2)	(2)	(2)	0

(1) HIGH TEMPERATURE EM_b ELECTRICAL TESTS PERFORMED AT 125°C FOR HEWLETT PACKARD OPTO-COUPLERS AND BOTH LEDs.

(2) ELECTRICAL TEST PERFORMED WITH NO FAILURE LIMITS.

TABLE 15. DEVICE TEMPERATURE RISE DURING POWER CYCLING

DEVICE TYPE	TEMPERATURE RISE - °C	
	PHOTODETECTOR	LED
Opto Couplers		
Texas Instruments	97	99
Spectronics	99	86
Optron	105	85
Hewlett Packard	25	39
LEDs		
Texas Instruments	--	20
RCA	--	30

TABLE 16. AVERAGE LED PARAMETERS, PRE AND POST POWER CYCLING

TEXAS INSTRUMENTS

PARAMETER	25°C		125°C		-55°C		UNITS
	PRE	POST	PRE	POST	PRE	POST	
I_R	0.002	0.002	0.272	0.140	0.054	0.015	μAdc
$V_F(2)$	1.057	1.053	0.888	0.876	1.180	1.174	Vdc
$V_F(20)$	1.165	1.146	1.030	1.019	1.254	1.264	Vdc
$V_F(50)$	1.234	1.216	1.115	1.105	1.323	1.333	Vdc
$V_F(100)$	1.314	1.295	1.213	1.207	1.408	1.419	Vdc
$P_O(2)$	0.024	0.017	0.007	0.216	0.027	0.033	mW
$P_O(20)$	0.522	0.379	0.199	0.270	0.420	0.386	mW
$P_O(50)$	1.495	1.150	0.610	0.395	1.117	1.031	mW
$P_O(100)$	3.039	2.500	1.299	0.616	2.207	2.101	mW
λ_P	938.2	934.0	---	---	---	---	nm
B	48.92	49.12	---	---	---	---	nm

RCA

PARAMETER	25°C		125°C		-55°C		UNITS
	PRE	POST	PRE	POST	PRE	POST	
I_R	0.016	0.011	0.425	0.630	0.003	0.000	μAdc
$V_F(2)$	1.060	1.064	0.904	0.898	1.162	1.128	Vdc
$V_F(20)$	1.193	1.199	1.055	1.061	1.282	1.273	Vdc
$V_F(50)$	1.299	1.309	1.154	1.174	1.388	1.418	Vdc
$V_F(100)$	1.432	1.451	1.272	1.317	1.481	1.594	Vdc
$P_O(2)$	0.044	0.042	0.003	0.136	0.061	0.060	mW
$P_O(20)$	0.807	0.792	0.287	0.275	0.820	0.798	mW
$P_O(50)$	2.162	2.138	0.814	0.532	2.214	2.001	mW
$P_O(100)$	4.187	4.249	1.583	0.901	4.264	3.809	mW
λ_P	944.6	947.4	---	---	---	---	nm
B	42.60	43.80	---	---	---	---	nm

6.2 MONITORED TEMPERATURE CYCLING RESULTS

The results of continuously monitoring opto-couplers during 500, -55°C to 125°C, temperature cycles are summarized in Tables 17 through 20. These tables show the cumulative number of devices that had exhibited one or more intermittent faults at the indicated number of temperature cycles. There were no intermittent faults detected during temperature cycling of LEDs. Table 21 shows the results of EM_a, EM_b and EM_c testing of opto-couplers and LEDs at the completion of 500 temperature cycles. With the exception of one Optron device with excessive dark current, all of the failures were due to broken wires caused by expansion and contraction of the Dow Corning R6104 overcoat.

The average values of LED parameter changes after exposure to 500 temperature cycles is shown in Table 22. As was previously noted from similar power cycling data, the maximum percentage change was noted at the 125°C measurement condition. At the -55°C measurement temperature, increased output power was noted, and this effect is not well understood. However, these effects are not indicative of temperature cycling related problems, and no additional failures would be expected with properly established EM_b and EM_c parameter limits.

6.3 VIBRATION/SHOCK/ACCELERATION TEST RESULTS

The results of the vibration/shock/acceleration test sequence are summarized in Table 23. With the exception of the eleven Optron opto-couplers that failed the post acceleration test as a result of broken internal lead wires, most devices passed this sequence of tests with no indication of intermittency or electrical failure. In addition to the Optron device failures, there were only three devices (1 opto-coupler and 2 LEDs) exhibiting intermittencies, and three other devices (all LEDs) that failed the post acceleration test. Two of the LEDs failing the post acceleration electrical test were RCA devices with open bonds. The third LED failure exhibited low output power due to an inadvertent fracture of the lens during acceleration.

TABLE 17. TEXAS INSTRUMENTS OPTO-COUPLER TEMPERATURE CYCLING CUMULATIVE FREQUENCY DISTRIBUTION

CYCLES	CUM. FAILURES	CUM. % FAILURES
2	1	4
5	4	16
17	5	20
45	6	24
145	7	28
221	8	32
374	9	36
389	10	40
479	11	44

TABLE 18. SPECTRONICS OPTO-COUPLER TEMPERATURE CYCLING CUMULATIVE FREQUENCY DISTRIBUTION

CYCLES	CUM. FAILURES	CUM. % FAILURES
153	1	4
432	2	8
464	3	12

TABLE 19. OPTRON OPTO-COUPLER TEMPERATURE CYCLING CUMULATIVE FREQUENCY DISTRIBUTION

CYCLES	CUM. FAILURES	CUM. % FAILURES
2	1	4
3	2	8
47	3	12
290	5	20
311	6	24

TABLE 20. HEWLETT PACKARD OPTO-COUPLER TEMPERATURE CYCLING CUMULATIVE FREQUENCY DISTRIBUTION

CYCLES	CUM. FAILURES	CUM. % FAILURES
1	1	4
2	2	8
10	7	28
61	21	84
183	22	88
201	23	92
331	24	96

TABLE 21. POST TEMPERATURE CYCLING ELECTRICAL TEST RESULTS

MANUFACTURER	QTY. IN TEST	NUMBER OF FAILURES				
		EM_a(25°C)	EM_b(125°C) (1)	EM_b(-55°C)	EM_c(25°C)	TOTAL
OPTO-COUPLERS:						
TEXAS INSTRUMENTS	25	3	1	0	0	4
SPECTRONICS	25	0	0	0	0	0
OPTRON	25	1	1	1	0	3
HEWLETT PACKARD	25	20	4 (2)	0	0	24
LEDs:						
TEXAS INSTRUMENTS	25	0	(3)	(3)	(3)	0
RCA	25	0	(3)	(3)	(3)	0

(1) HIGH TEMPERATURE EM_b ELECTRICAL TESTS PERFORMED AT 125°C FOR HEWLETT PACKARD OPTO-COUPLERS AND BOTH LEDs.

(2) ONLY THE FIVE DEVICES THAT PASSED THE 25°C EM_a ELECTRICAL TEST WERE SUBMITTED TO ADDITIONAL TESTING.

(3) ELECTRICAL TEST PERFORMED WITH NO FAILURE LIMITS.

TABLE 22. AVERAGE LED PARAMETERS, PRE AND POST TEMPERATURE CYCLING

TEXAS INSTRUMENTS

PARAMETER	25°C		125°C		-55°C		UNITS
	PRE	POST	PRE	POST	PRE	POST	
I_R	0.002	0.001	0.272	0.137	0.054	0.000	μAdc
$V_F(2)$	1.057	1.056	0.888	0.847	1.180	1.175	Vdc
$V_F(20)$	1.165	1.163	1.030	0.999	1.254	1.265	Vdc
$V_F(50)$	1.234	1.232	1.115	1.090	1.323	1.334	Vdc
$V_F(100)$	1.314	1.316	1.213	1.199	1.408	1.423	Vdc
$P_O(2)$	0.024	0.018	0.007	0.022	0.027	0.055	mW
$P_O(20)$	0.522	0.395	0.199	0.080	0.420	0.575	mW
$P_O(50)$	1.495	1.184	0.610	0.219	1.117	1.530	mW
$P_O(100)$	3.039	2.557	1.299	0.470	2.207	3.108	mW
λ_P	938.2	934.2	---	---	---	---	nm
B	48.92	48.68	---	---	---	---	nm

RCA

PARAMETER	25°C		125°C		-55°C		UNITS
	PRE	POST	PRE	POST	PRE	POST	
I_R	0.016	0.003	0.425	0.408	0.003	0.000	μAdc
$V_F(2)$	1.060	1.064	0.904	0.865	1.162	1.171	Vdc
$V_F(20)$	1.193	1.190	1.055	1.027	1.282	1.293	Vdc
$V_F(50)$	1.299	1.241	1.154	1.129	1.388	1.402	Vdc
$V_F(100)$	1.432	1.406	1.272	1.254	1.481	1.545	Vdc
$P_O(2)$	0.044	0.034	0.003	0.018	0.061	0.076	mW
$P_O(20)$	0.807	0.651	0.287	0.186	0.820	0.881	mW
$P_O(50)$	2.162	1.781	0.814	0.512	2.214	2.242	mW
$P_O(100)$	4.187	3.580	1.583	1.010	4.264	4.358	mW
λ_P	944.6	942.0	---	---	---	---	nm
B	42.60	41.64	---	---	---	---	nm

TABLE 23. VIBRATION/SHOCK/ACCELERATION TEST RESULTS

MANUFACTURER	QTY. IN TEST	NUMBER OF FAILURES				
		MONITORED VIBRATION		MONITORED SHOCK		CONSTANT ACCELERATION
		INTERMITTENT	ELECTRICAL	INTERMITTENT	ELECTRICAL	ELECTRICAL
OPTO-COUPLERS:						
TEXAS INSTRUMENTS	25	0	0	0	0	0
OPTRON	25	0	0	3 (1)	0	11 (2)
HEWLETT PACKARD	25	0	0	1 (3)	0	0
LEDs:						
TEXAS INSTRUMENTS	25	0	0	1 (4)	0	1 (5)
RCA	25	0	0	1 (4)	0	2

(1) TWO INTERMITTENT FAULTS IN THE Y_1 AXIS AND ONE IN THE Z_2 AXIS. TWO OF THE THREE INTERMITTENT DEVICES SUBSEQUENTLY FAILED AFTER CONSTANT ACCELERATION. THE INTERMITTENT IN THE REMAINING DEVICE COULD NOT BE VERIFIED.

(2) ALL FAILURES WERE DUE TO OPEN BONDS.

(3) INTERMITTENT FAULT IN THE X_2 AXIS, 3RD SHOCK ONLY. DEVICES PASSED POST SHOCK ELECTRICAL TESTS.

(4) THIS FAILURE EXHIBITED A SINGLE FAULT AND PASSED THE SUBSEQUENT ELECTRICAL TEST. FAILURE ANALYSIS DISCLOSED NO CAUSE FOR THE INTERMITTENCY.

(5) THIS DEVICE FAILED THE OUTPUT POWER TEST AFTER THE LENS WAS INADVERTENTLY SHATTERED DURING THE ACCELERATION TEST.

7.0 HTRB EVALUATION TEST MATRIX RESULTS

The special HTRB evaluation of opto-couplers consisted of a two temperature, two voltage square matrix of tests. Twenty of each manufacturer's Type A and ten of the Hewlett Packard Type B opto-couplers were included in each of the four cells in the matrix. An additional cell of ten Hewlett Packard Type B opto-couplers was subsequently added to the matrix in an attempt to produce additional failure data. Devices in each cell were operated for 96 hours in the previously described bias circuits. EM_a electrical measurements were performed, after cool-down to room temperature with bias applied, at 16, 32, 48 and 96 hours. The temperature/voltage combinations comprising the matrix and the number of device failures noted at each measurement time are shown in Table 24. Failures were only observed with the Texas Instruments opto-coupler in the highest temperature cells (150°C). Four failures were observed in the 35 Vdc, 150°C cell, and 3 failures were observed in the 20 Vdc, 150°C cell. Five of the seven total failures were due to excessive dark current, and two were due to low transfer ratio. This low number of failures indicates that the initial concern over excessive HTRB test failures during screening and preconditioning was not warranted.

TABLE 24. OPTO-COUPLER HTRB EVALUATION TEST RESULTS

MANUFACTURER	QTY. IN TEST	CELL TEMP.	CELL VOLTAGE	CUMULATIVE FAILURES			
				16 HRS	32 HRS.	48 HRS.	96 HRS.
TEXAS INSTRUMENTS	20	150°C	35 Vdc	0	0	3	4
	20	150°C	20 Vdc	0	1	1	3
	20	100°C	35 Vdc	0	0	0	0
	20	100°C	20 Vdc	0	0	0	0
OPTRON	20	150°C	35 Vdc	0	0	0	0
	20	150°C	20 Vdc	0	0	0	0
	20	100°C	35 Vdc	0	0	0	0
	20	100°C	20 Vdc	0	0	0	0
HEWLETT PACKARD	10	150°C	7.5 Vdc	0	0	0	0
	10	150°C	3.8 Vdc	0	0	0	0
	10	100°C	7.5 Vdc	0	0	0	0
	10	100°C	3.8 Vdc	0	0	0	0
	10	200°C	7.5 Vdc	0	0	0	0

8.0 GROUP II TEST RESULTS

Group II Tests of opto-couplers consisted of 25°C operating life tests, accelerated life tests, and HTRB life tests. The LED Group II tests consisted of only accelerated life tests. The duration of each opto-coupler life test was 4,000 hours, and the duration of each LED life test was 1,000 hours. EM_a electrical tests were performed after cool-down to room temperature with bias applied at the following times:

Opto-couplers - 48, 96, 168, 1,000, 2,000, 3,000 & 4,000 hours
LEDs - 16, 64, 168, 256, 512 & 1,000 hours

During the life tests, devices were operated in the previously described bias circuits at the selected ambient test temperatures. Device electrical conditions and junction temperatures at each test temperature are summarized in Table 25 for Type A opto-couplers, Table 26 for Type B opto-couplers, and Table 27 for LEDs.

The results of the Group II life tests are summarized in Tables 28, 29, 30 and 31. These tables show the cumulative number of devices failing an EM_a test at each measurement point. The cumulative number of opto-coupler failures are further subdivided to show the failure history of devices previously subjected to other Group I and HTRB evaluation tests as compared to the failure history of devices subjected to only the screening and preconditioning sequence. Comparative evaluations of the failure histories revealed no important differences due to prior stressing during Group I and HTRB evaluation tests.

TABLE 25. TEXAS INSTRUMENTS AND OPTRON OPTO-COUPLER ACCELERATED LIFE TEST, OPERATING LIFE TEST AND EXTENDED HTRB CONDITIONS

VENDOR	AMBIENT TEMPERATURE	TEST	V_{CE} Vdc	V_{LED} Vdc	I mAdc	$P_{d(TRANS.)}$ mW	$P_{d(LED)}$ mW	JUNCTION TEMPERATURE	
								TRANSISTOR	LED
TEXAS INSTRUMENTS	25°C	OPERATING LIFE	7.15	1.44	39.4	282	56	92°C	111°C
	100°C	ACCEL. LIFE	7.07	1.38	39.6	280	55	130°C	150°C
	125°C	ACCEL. LIFE	7.02	1.36	40.2	282	55	154°C	174°C
	150°C	ACCEL. LIFE	6.98	1.24	40.4	282	50	178°C	193°C
	125°C	HTRB	24.96	----	0.12	3.0	--	125°C	-----
	150°C	HTRB	34.76	----	0.51	17.7	--	152°C	-----
OPTRON	25°C	OPERATING LIFE	7.07	1.47	40.5	286	60	97°C	101°C
	100°C	ACCEL. LIFE	7.09	1.42	40.7	289	58	129°C	139°C
	125°C	ACCEL. LIFE	7.40	1.37	41.8	310	57	155°C	165°C
	150°C	ACCEL. LIFE	7.22	1.32	40.5	292	54	180°C	193°C
	125°C	HTRB	24.95	----	0.37	3.2	--	125°C	----
	150°C	HTRB	34.63	----	0.13	12.8	--	151°C	----

TABLE 26. HEWLETT PACKARD OPTO-COUPLER ACCELERATED LIFE TEST, OPERATING LIFE TEST AND EXTENDED HTRB TEST CONDITIONS

TEST	T_A °C	V_{15} Vdc	V_F Vdc	V_{14} Vdc	V_{12} Vdc	P_{TOTAL} mW	JUNCTION TEMPERATURE	
							PHOTO AMP. (BOTH) °C	LED (ON) °C
OPERATING LIFE	25	6.89	1.49	0.45	6.89	201	47	43
ACCEL. LIFE	125	6.91	1.40	0.45	6.91	204	143	138
ACCEL. LIFE	150	6.91	1.37	0.45	6.91	203	168	163
ACCEL. LIFE	175	6.91	1.30	0.46	6.91	202	193	188
HTRB	200	7.00	0	7.00	7.00	140	212	200

TABLE 27. LED ACCELERATED LIFE TEST CONDITIONS

VENDOR	T_a °C	V_F Vdc	I mAdc	P_d MW	T_j °C
TI	225	1.18	101.4	119.7	241.9
↓	200	1.24	100.7	124.9	217.6
↓	150	1.31	99.9	130.9	168.5
RCA	225	1.31	99.9	130.9	249.7
↓	200	1.33	99.6	132.5	225.0
↓	150	1.40	98.8	138.3	176.1

TABLE 28. TEXAS INSTRUMENTS OPTO-COUPLER ACCELERATED LIFE TEST, OPERATING LIFE TEST AND EXTENDED HTRB TEST RESULTS

TEST	QTY. IN TEST	AMBIENT TEMP.	CUMULATIVE NO. OF FAILURES AT HOURS OF TEST								FINAL
			48	96	168	504	1000	2000	3000	4000	
ACCELERATED LIFE #1:		150°C									
SCREENED DEVICES	35		2	2	3	10	22	31	32	32	32
150°C/35 Vdc HTRB	10		0	0	2	5	5	7	8	9	9
TOTAL	45		2	2	5	15	27	38	40	41	41
ACCELERATED LIFE #2:		125°C									
SCREENED DEVICES	35		2	4	4	9	16	24	28	31	31
150°C/20 Vdc HTRB	10		0	0	0	1	2	4	5	6	6
TOTAL	45		2	4	4	10	18	28	33	37	37
ACCELERATED LIFE #3:		100°C									
SCREENED DEVICES	35		0	1	3	5	8	17	19	21	21
100°C/20 Vdc HTRB	10		0	0	0	1	1	3	6	6	6
TOTAL	45		0	1	3	6	9	20	25	27	27
OPERATING LIFE:		25°C									
SCREENED DEVICES	35		0	0	0	0	1	2	5	13	13
150°C/35 Vdc HTRB	6		0	0	0	0	0	0	2	3	3
150°C/20 Vdc HTRB	7		0	0	0	0	0	0	0	1	1
100°C/20 Vdc HTRB	10		0	0	0	0	0	0	1	2	2
VIB./SHOCK/ACCEL.	25		0	0	0	0	1	3	3	9	9
TOTAL	83		0	0	0	0	2	5	11	28	28
EXTENDED HTRB:		150°C									
100°C/35 Vdc HTRB	20		1	2	2	6	8	14	15	15	15
EXTENDED HTRB:		125°C									
TEMP. CYCLING	20		0	0	0	0	3	5	7	8	8

TABLE 29. OPTRON OPTO-COUPLER ACCELERATED LIFE TEST, OPERATING LIFE TEST AND EXTENDED HTRB TEST RESULTS

TEST	QTY. IN TEST	AMBIENT TEMP.	CUMULATIVE NO. OF FAILURES AT HOURS OF TEST								FINAL
			48	96	168	504	1000	2000	3000	4000	
ACCELERATED LIFE #1:		150°C									
SCREENED DEVICES	35		5	7	10	14	18	21	24	30	30
150°C/35 Vdc HTRB	10		1	1	2	5	8	9	9	9	9
TOTAL	45		6	8	12	19	26	30	33	39	39
ACCELERATED LIFE #2:		125 C									
SCREENED DEVICES	35		5	7	10	19	22	28	29	32	32
150°C/20 Vdc HTRB	10		0	0	0	4	6	7	8	9	9
TOTAL	45		5	7	10	23	28	35	37	41	41
ACCELERATED LIFE #3:		100°C									
SCREENED DEVICES	35		3	5	5	6	6	10	18	21	21
100°C/20 Vdc HTRB	10		0	0	0	0	2	2	5	7	7
TOTAL	45		3	5	5	6	8	12	23	28	28
OPERATING LIFE:		25°C									
SCREENED DEIVCES	35		0	0	0	1	3	6	8	13	13
150°C/35 Vdc HTRB	10		0	0	0	1	2	4	4	4	4
150°C/20 Vdc HTRB	10		0	1	2	4	4	4	4	4	4
100°C/20 Vdc HTRB	10		0	0	0	0	2	3	4	5	5
VIB./SHOCK/ACCEL.	14		2	2	2	3	3	4	4	5	5
TOTAL	79		2	3	4	9	14	21	24	31	31
EXTENDED HTRB:		150°C									
100°C/35 Vdc HTRB	20		0	0	1	2	3	5	9	10	10
EXTENDED HTRB:		125°C									
TEMP. CYCLING	20		0	0	0	0	1	1	1	1	1

TABLE 30. HEWLETT PACKARD OPTO-COUPLER ACCELERATED LIFE TEST, OPERATING LIFE TEST AND EXTENDED HTRB TEST RESULTS

TEST	QTY. IN TEST	AMBIENT TEMP.	CUMULATIVE NO. OF FAILURES AT HOURS OF TEST								FINAL
			48	96	168	504	1000	2000	3000	4000	
ACCELERATED LIFE #1:		175°C									
SCREENED DEVICES	25		0	0	1	2	2	2	2	2	2
100°C/3.8 Vdc HTRB	5		0	0	0	0	0	0	0	0	0
TOTAL	30		0	0	1	2	2	2	2	2	2
ACCELERATED LIFE #2:		150°C									
SCREENED DEVICES	25		0	0	0	0	0	0	1	1	1
100°C/7.5 Vdc HTRB	5		0	0	0	0	0	0	0	0	0
TOTAL	30		0	0	0	0	0	0	1	1	1
ACCELERATED LIFE #3:		125°C									
SCREENED DEVICES	25		0	0	0	1	1	1	1	1	1
100°C/3.8 Vdc HTRB	5		0	0	0	1	1	1	2	2	2
TOTAL	30		0	0	0	2	2	2	3	3	3
OPERATING LIFE:		25°C									
SCREENED DEVICES	25		1	1	1	1	1	1	1	1	1
100°C/7.5 HTRB	5		0	0	0	0	0	0	0	0	0
VIB./SHOCK/ACCEL.	25		0	0	0	0	0	0	0	0	0
TOTAL	55		1	1	1	1	1	1	1	1	1
EXTENDED HTRB:		200°C									
150°C/7.5 Vdc HTRB	10		0	0	0	2	2	3	5	6	6
150°C/3.8 Vdc HTRB	10		0	0	0	1	1	3	4	6	6
TOTAL	20		0	0	0	3	3	6	9	12	12

TABLE 31. LED ACCELERATED LIFE TEST RESULTS

MANUFACTURER	TEST	QTY. ON TEST	TEMP.	CUMULATIVE NO. OF FAILURES AT HOURS OF TEST					
				16	64	168	256	512	1000
RCA	ACCEL. LIFE #1	35	225°C	12	14	25	26	33	35
	ACCEL. LIFE #2	35	200°C	2	10	12	12	21	28
	ACCEL. LIFE #3	35	150°C	0	1	4	6	11	14
TEXAS INSTRUMENTS	ACCEL. LIFE #1	35	225°C	10	21	27	27	34	35
	ACCEL. LIFE #2	35	200°C	4	18	22	22	27	34
	ACCEL. LIFE #3	35	150°C	1	1	6	8	17	29

9.0 FAILURE ANALYSIS

With two exceptions, all devices failing an electrical test were subjected to analyses to determine the failure mode, mechanism and probable cause. The two exceptions were: a) Spectronics opto-couplers failing any test were not analyzed, and b) all manufacturers' opto-couplers failing an electrical test during screening and preconditioning were not analyzed. Summaries of the failure analysis findings for each manufacturer's devices are contained in Tables 32 through 35. Complete details of the failure analysis procedures and findings are contained in Appendix E.

TABLE 32. TEXAS INSTRUMENTS OPTO-COUPLER FAILURE ANALYSIS SUMMARY

	A. FAILURE SYMPTOMS B. FAILURE MODE C. FAILURE MECHANISM OR CAUSE	QUANTITY OF FAILURES AND TIME OF FAILURE (HOURS OR CYCLES) BY TEST CELL									
		FORMAL	HYRB		EXT HYRB		ACCELERATED LIFE			OPER LIFE	TEMP CYCLE
		STEP STRESS	20V/150°C	35V/150°C	150°C	125°C	#1 (150°C)	#2 (125°C)	#3 (100°C)	25°C	500 CYCLES
SURFACE INSTABILITY FAILURES	A. HIGH DARK CURRENT B. DEGRADED C-B OR C-E C. INVERSION OF THE BASE	10192H/150°C 10360H/150°C	1032 1096	3048	1048 30504	301000 102000 203000 104000	40504 101000	1048 1096 101000	10168	101000 104000	
	A. LOW TRANSFER RATIO B. DEGRADED B-E JUNCTION C. INVERSION OF THE BASE		1096	1096	1096 10504 302000		301000 202000	1096 10504 10200 103000 104000	104000		
	A. BOTH HIGH ID AND LOW TR B. DEGRADED JUNCTION C. INVERSION OF THE BASE				201000 30[illegible] 103000	102000	401000	201000 502000 103000	102000		
BULK-RELATED FAILURES	A. LOW TRANSFER RATIO B. DEGRADED LED C. BULK DEFECTS	10360H/150*					1048 20168 70504 * 301000 802000 203000	1048 40504 501000 302000 303000 304000	1096 10168 30504 301000 902000 403000 104000	101000 102000 603000 1604000	
WIRE AND BOND FAILURES	A. OPEN EMITTER B. LIFTED Au-Al BALL BOND C. EXPANSION OF THE R6104 AND KIRKENDALL VOIDING						101000 102000 104000	102000			
	A. OPEN LED B. LIFTED Au-Au BALL BOND C. EXPANSION OF THE R6104 AND UNDERBONDED BALL	50144H/125*					1048 10168	10504	103000	202000	
	A. OPEN EMITTER OR LED B. BROKEN WIRE C. FATIGUE OR CREEP RUPTURE DUE TO R6104 EXPANSION										40500
TEST ERROR	A. OPEN EMITTER B. MELTED OPEN STRIPE C. ELECTRICAL OVERSTRESS	10360H/150									
	A. NONE B. NONE C. INADVERTENTLY REMOVED FROM TEST								102000		
	TOTAL NUMBER OF FAILED PARTS	9	3	4	15	8	41	37	27	28	4

*ONE PART ALSO FAILED DUE TO HIGH I_D AND IS TABULATED UNDER THAT CATEGORY ALSO.

TABLE 33. OPTRON OPTO-COUPLER FAILURE ANALYSIS SUMMARY

			QUANTITY OF FAILURES AND TIME OF FAILURE (HOURS OR CYCLES) BY TEST CELL								
		FORMAL	EXT HTRB		ACCELERATED LIFE			OPER. LIFE	ACCELERATION	TEMP CYCLE	POWER
		STEP STRESS	150°C	125°C	#1 (150°C)	#2 (125°C)	#3 (100°C)	25°C	30,000 G'S	500 CYCLES	CYCLING
SURFACE INSTABILITY FAILURES	A. HIGH DARK CURRENT		1@3000	1@1000	1@4000	3@48				1@500	
	B. DEGRADED C-B OR C-E		1@4000			1@1000					
	C. INVERSION OF THE BASE										
	A. LOW TRANSFER RATIO		1@1000								
	B. DEGRADED B-E JUNCTION		1@3000								
	C. INVERSION OF THE BASE										
BULK-RELATED FAILURES	A. LOW TR & BV_{EBO}/HIGH ID		1@3000		2@48	1@96	1@504	1@1000			1@5040
	B. DEGRADED LED				1@3000	1@50*		3@2000			1@10,000
	C. BULK DEFECTS					1@1000		3@4000			
						1@2000					
	A. LOW TR & BV_{EBO}/HIGH ID				1@1000						
	B. DEGRADED E-B JUNCTION				1@2000						
	C. METAL PENETRATION				1@3000						
					2@4000						
WIRE AND BOND FAILURES	A. OPEN EMITTER OR BASE	1@48HR/75°	1@168		4@48	2@48	1@48	1@48			3@1680
	B. LIFTED Au-Al BALL BOND	2@96H/100°	1@504		2@96	1@96	2@96	1@168			2@5040
	C. EXPANSION OF THE R6104	6@144H/125°	2@2000		4@168	3@168	2@1000	5@504			1@10,000
	AND WEAK BONDS	4@192H/150°	1@3000		7@504	12@504	4@2000	4@1000			
		6@360H/150°			6@1000	3@1000	11@3000	3@2000			
					3@2000	6@2000	5@4000	3@3000			
					1@3000	2@3000		4@4000			
					3@4000	4@4000					
	A. OPEN LED							1@48			
	B. LIFTED Au-Au BALL BOND										
	C. EXPANSION OF THE R6104										
	AND UNDERBONDED BALL										
	A. OPEN COLLECTOR									1@5000	
	B. BROKEN BOND										
	C. FAULTY BOND										
	A. OPEN LED									1@5000	
	B. BROKEN WIRE										
	C. CREEP RUPTURE DUE										
	TO EXPANSION OF										
	THE R6104										
	A. OPEN LED OR COLLECTOR									2@5000	
	B. BROKEN WIRE										
	C. FATIGUE DUE TO R6104										
	A. MULTIPLE OPENS								11		
	B. BROKEN WIRES										
	C. R6104 EXPANSION UNDER ACC.										
TEST ERRORS	A. OPEN EMITTER						2@48				
	B. MELTED WIRE										
	C. ELECTRICAL OVER STRESS										
	A. SHORTED LED							1@96			
	B. BULK SHORT										
	C. PROBABLY ELECT. OVERSTRESS										
	A & B. NONE										
	C. INADVERTENTLY							1@2000			
	REMOVED FROM TEST										
TOTAL NUMBER OF FAILED PARTS		19	10	1	39	41	28	31	11	3	8

TABLE 34. HEWLETT PACKARD OPTO-COUPLER FAILURE ANALYSIS SUMMARY

	A. FAILURE SYMPTOM B. FAILURE MODE C. FAILURE MECHANISM OR CAUSE	QUANTITY OF FAILURES AND TIME OF FAILURE (HOURS OR CYCLES) BY TEST CELL							
		STEP STRESS		EXT HTRB	ACCELERATED LIFE			OPERATING LIFE	TEMP
		PRELIMINARY	FORMAL	200°C	#1-175°C	#2-150°C	#3-125°C	25°C	CYCLE
WIRE AND BOND FAILURES	A. OPEN PIN B. BROKEN GOLD WIRE C. CREEP RUPTURE AND/OR FATIGUE DUE TO EXPANSION OF THE R6104	1@96H/225° 1@128H/275°	2@240H/225° 1@288H/250°	1@504 1@2000 1@3000 3@4000					24
	A. OPEN LED B. LIFTED Au/Al BALL BOND C. KIRKENDALL VOIDING AND EXPANSION OF THE R6104			1@504 2@2000 1@3000	1@168 1@504	1@3000	1@3000		
BULK RELATED FAILURES	A. SHORTED PIN 14 B. SHORTED JUNCTION C. JUNCTION FLAW AND AN ELECTRICAL TRANSIENT			1@504					
	A. LOW BVR (LED) B. DEGRADED JUNCTION C. NOT DETERMINED		1@240H/225°					1@48	
SURFACE-RELATED FAILURES	A. HIGH V_{OL} B. SURFACE INSTABILITY C. CONTAMINANT IONS OR CHARGES						2@504		
	A. HIGH I_{OH} B. SURFACE INSTABILITY C. CONTAMINANT IONS OR CHARGES			1@3000					
	TOTAL NUMBER OF FAILED PARTS	2	4	12	2	1	3	1	24

TABLE 35. TEXAS INSTRUMENTS AND RCA LED FAILURE ANALYSIS SUMMARIES

	A. FAILURE SYMPTOM B. FAILURE MODE C. FAILURE MECHANISM OR CAUSE	QUANTITY OF FAILURES AND TIME OF FAILURE BY TEST CELL									
		TEXAS INSTRUMENTS					RCA				
		STEP STRESS	ACCELERATED LIFE			POWER CYCLING	STEP STRESS	ACCELERATED LIFE			ACCELERATION
			#1(225°C)	#2(200°C)	#3(150°C)			#1(225°C)	#2(200°C)	#3(150°C)	
BULK RELATED FAILURES	A. LOW OUTPUT POWER B. DEGRADED LED C. DISLOCATION CLIMB	1@125°C 1@150°C 2@200°C 2@225°C 1@250°C	10@16 11@64 6@168 7@512 1@1000	4@16 11@64 4@168 5@512 3@1000 (1)	5@168 1@256 7@512 7@1000 (2)			1@64 6@168 7@512 2@1000	1@168 4@512 5@1000		
	A. HIGH REVERSE CURRENT B. DEGRADED JUNCTION C. NOT DETERMINED	1@125°C 1@150°C 1@175°C		3@64 5@1000	1@16 1@256 2@512 8@1000	3					
EPOXY-RELATED FAILURES	A. SHORT-CIRCUIT B. BRIDGING SILVER EPOXY C. SILVER MIGRATION						1@250°C	5@168 1@256	4@512		
	A. HIGH REVERSE CURRENT B. INTERNAL MOISTURE C. OUTGASSING OF SILVER EPOXY						6@175°C 5@200°C 1@225°C	11@16 1@64	2@16 6@64	3@168 1@256 2@512 1@1000	
	A. HIGH FORWARD VOLTAGE B. RESISTIVE SILVER EPOXY C. PROBABLY OUTGASSING OF THE EPOXY							2@16 (1)	2@64 (1) 1@168 1@512 2@1000	1@64 1@256 3@512 2@1000	
BOND FAILURES	A. OPEN-CIRCUIT B. BROKEN GOLD BOND C. DEFECTIVE BOND										2
TEST ERRORS	A. OPEN-CIRCUIT B. MELTED WIRE C. ELECTRICAL OVERSTRESS	4@200°C					2@125°C 1@200°C		1@64		
	TOTAL NUMBER OF FAILED PARTS	14	35	34	29	3	16	35	28	14	2

(1) ONE DEVICE ALSO EXHIBITED HIGH IR AND IS TABULATED UNDER THAT CATEGORY ALSO.

(2) THREE DEVICES ALSO EXHIBITED HIGH IR AND ARE TABULATED UNDER THAT CATEGORY ALSO.

10.0 DATA EVALUATIONS AND CORRELATIONS

Evaluations and correlations of the data generated during the program were performed to determine: a) the roles of applied stresses, materials and processes in generating the observed failure modes, b) device aging characteristics, and c) effectiveness of actual or potential defect screens. This was accomplished through comparisons of the types of failure modes observed in each type of test, plots of failure distributions, Arrhenius model evaluations, and calculations of use-temperature failure rates. The determinations of failure distributions, Arrhenius model parameters, and use-temperature failure rates generally followed published techniques [1], [2], and [3]. However, certain refinements of these techniques, primarily in the area of device failure time determinations, were employed. Detailed descriptions of the techniques used in the analysis of life test failure data are contained in Appendix F.

10.1 FAILURE MODE/MECHANISM COMPARISONS

A composite summary of the number and percentage of each manufacturer's device type that failed during each of the Group I and Group II tests is shown in Table 36. Examination of this data shows that each manufacturer's device type was susceptible to a different Group I test. No single Group I test consistently produced failures in all device types. Temperature cycling appeared to be the most effective test for opto-couplers, but produced no LED failures. This is due to the R6104 overcoat used in all the opto-couplers. The Group II operating and accelerated life tests produced, with the exception of Type B opto-couplers, a high percentage of failures in each manufacturer's device type.

The types of failure modes/mechanisms generated in each of the Group I and Group II tests is summarized in Table 37. The predominant failure mode of opto-couplers was open circuits, and was observed in each of the Group I and II tests. Use of the Dow Corning R6104 overcoat in all of the opto-couplers was the primary factor responsible for the open circuits. However, multiple contributory factors were also present, and these factors varied between manufacturers and test environments. Broken internal lead wires due to a combination of fatigue and creep rupture caused by expansion and contraction of the R6104 was the observed failure mechanism during temperature cycling. The Hewlett Packard Type B opto-couplers were especially susceptible to this failure mechanism, and, as described in Appendix G,

TABLE 36. COMPOSITE FAILURE SUMMARY

TYPE OF TEST	FAILED DEVICES*											
	OPTO-COUPLERS								LEDs			
	TYPE A						TYPE B					
	SPECTRONICS		OPTRON		T.I.		HP		RCA		T.I.	
	NO.	%	NO.	%	NO.	%	NO.	%	NO.	%	NO.	%
POWER CYCLING	15	60	8	32	0	0	0	0	0	3	3	12
TEMPERATURE CYCLING	0	0	3	12	4	16	24	96	0	0	0	0
VIB./SHOCK/ACCEL.	--		11	44	0	0	0	0	2	8	1	4
"ON" LIFE TESTS	--		139	65	133	61	7	5	77	73	98	93
"OFF" LIFE TESTS	--		11	28	23	58	12	60	--		--	
TOTAL	15	30%	172	57%	160	43%	43	18%	79	44%	102	57%

*Percent failures are based on the number of devices placed in each type of test

TABLE 37. FAILURE MODE/MECHANISM SUMMARY

FAILURE MODE/MECHANISM	FAILED DEVICES									
	POWER CYCLING		TEMP. CYCLING		VIB/SHOCK/ ACCEL.		"ON" LIFE		"OFF" LIFE	
	NO.	%	NO.	%	NO.	%	NO.	%	NO.	%
OPTO-COUPLERS										
PHOTODETECTOR SURFACE INSTABILITY			1	3			42	16	29	65
LED OUTPUT POWER DEGRADATION	2	25					102	37	1	2
DEGRADED JUNCTIONS							6	2		
OPENS (R6104 RELATED)	6	75	30	97	11	100	124	45	15	33
MISC.							2		1	
ELECT. OVERSTRESS (TEST ERROR)							3			
TOTAL OPTO- JUPLERS (EXCLUDES SPECTRONICS)	8	100%	31	100%	11	100%	279	100%	46	100%
LEDs										
OUTPUT POWER DEGRADATION					1	33	108	62	--	
DEGRADED JUNCTION	3	100					16	9	--	
Ag EPOXY DIE ATTACH RELATED							50	28.5	--	
OPENS (WIRE BONDS)					2	67			--	
ELECT. OVERSTRESS (TEST ERRORS)							1	0.5	--	
TOTAL LEDs	3	100%	0	0	3	100%	175	100%		

Hewlett Packard has taken corrective action to minimize the occurrence of this type of failure. Broken wires in the Optron Type A opto-coupler due to stretching of the R6104 was the primary failure mechanism during the constant acceleration portion of the vibration/shock/acceleration test sequence. During power cycling and life testing, the primary mechanism leading to open circuits was lifted marginal bonds (underbonded or overbonded) due to expansion of the R6104. The Optron device failures were due almost exclusively to this type mechanism, and, as will be shown later, the times to failure were temperature and possibly current density dependent.

The second most frequently observed opto-coupler failure mode was parameter degradation due to LED output power degradation or phototransistor surface effects. Output power degradation was also the primary cause of the discrete LED failures. However, many of the discrete RCA LED failures were related to outgassing of moisture or migration of silver from the epoxy die attach. Failure symptoms were high reverse leakage currents, shorts and high resistive contacts. These ty[illegible] failures were only observed at the accelerated life test conditions, and [illegible] is unknown if the failures would be observed at temperatures below the manufac[illegible]s 125°C maximum rating. Similar failure symptoms (excessive reverse current and shorted LEDs) were also observed during power cycling of the Spectronics opto-couplers. However, the Spectronics failures were due to an excessive build-up of epoxy die attach material around the LED, and is a workmanship problem.

A summary of the types of defects observed during Group I and II testing and the suspected causes is shown in Table 38 for each manufacturer's device type. Since many of the failures were attributed to multiple problems or the absolute cause of the failure could not be determined, the assigned causes are somewhat arbitrary. In addition, defects attributed to process related problems may be better eliminated by a design change rather than a tightening of process controls.

TABLE 38. DEFECT/CAUSE SUMMARY - GROUP I & GROUP II

PRIMARY DEFECT/CAUSE CATEGORY	NUMBER OF FAILED DEVICES					
	OPTO-COUPLERS				LEDs	
	TYPE A			TYPE B		
	SPECTRONICS*	OPTRON	T.I.	HP	RCA	T.I.
DEFECT CATEGORY						
PHOTODETECTOR SURFACE INSTABILITY	0	11	58	3	--	--
LED OUTPUT POWER DEGRADATION	0	18	87	0	26	83
DEGRADED JUNCTIONS	0	5	0	1	0	19
OPENS (WIRE BOND RELATED)	0	0	0	0	2	0
OPENS (R6104/WIRE/BOND RELATED)	0	134	14	38	--	--
Ag EPOXY DIE BOND RELATED	15	--	--	--	50	--
ELECTRICAL OVERSTRESS	0	3	0	0	1	0
MISC.	0	1	1	1	0	0
CAUSE CATEGORY**						
PROCESS	--	34	145	4	26	83
DESIGN	--	12	4	30	--	--
MATERIAL	--	--	--	--	50	--
PROCESS AND DESIGN	--	120	10	8	--	--
WORKMANSHIP	15	2	--	--	2	--
TEST	--	4	1	--	1	--
UNDETERMINED	--	--	--	1	--	19
TOTAL NUMBER OF FAILED DEVICES	15	172	160	43	79	102

*Spectronics only subjected to power & temp. cycling tests
**Cause category definitions are contained in Appendix E, page E6

10.2 FAILURE DISTRIBUTIONS

Distributions of the times, or cycles, to failure were determined for each manufacturer's device type in each of the Group I and II tests whenever sufficient failure data was available. In all cases, the failure time distributions were assumed to be either single lognormal distributions, or bimodal distributions that could be represented by two lognormal distributions. Other distributions, such as the Weibull, could have also been assumed, but the lognormal distributions appeared to provide a good representation of the observed data. When a bimodal distribution was apparent, it was represented by two lognormal distributions; an early distribution of failures (Freak), and a distribution of failures occurring later in time (Main).

10.2.1 Group I Failure Distributions

Power Cycling - During power cycling, only the Spectronics and Optron Type A opto-couplers exhibited sufficient failure data for failure distribution analysis. Since the failure modes for these opto-couplers (excessive LED reverse current for the Spectronics devices, and lifted bonds for the Optron devices) appeared to be time-temperature rather than cyclic related, the failure data was plotted as a function of total "on" time during power cycling. The resulting plots are shown in Figure 10. The Optron data for open bonds appeared to be a single lognormal distribution with a median lifetime of 4700 hours. This value of median lifetime, as will be seen later, correlates reasonably well with accelerated life test failure data for open bonds at a similar junction temperature (125°C).

The Spectronics failure data for excessive LED reverse current appeared to be a bimodal distribution, but there was only sufficient data to evaluate the Freak population. The Freak population of devices was estimated to be approximately 50% of the total test population, and exhibited a median life of 44 hours. This is believed to be a good representation of failure times for devices previously subjected to 240 hours of burn-in at a junction temperature of approximately 125°C. However, approximately 50% of the initial population also failed due to excessive LED reverse current during the prior burn-in. Thus, a better representation of the actual failure distribution may be a single distribution with a median life of 240 hours. Accelerated life test results would have provided a more accurate estimate of the actual nature of the failure distribution, but insufficient devices were available for life testing. Thus, accurate estimates of the failure distribution

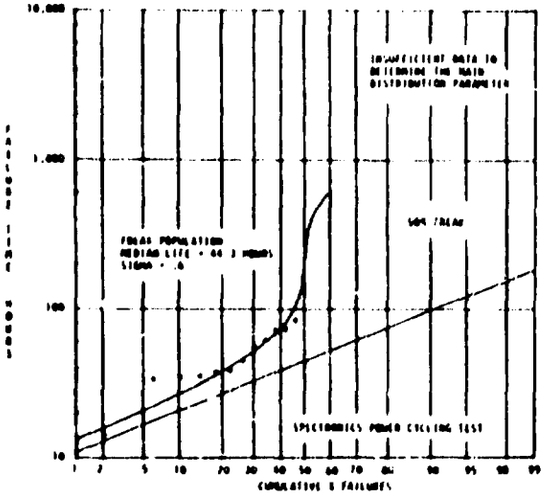

SPECTRONICS
FAILURE MODE - EXCESSIVE I_R

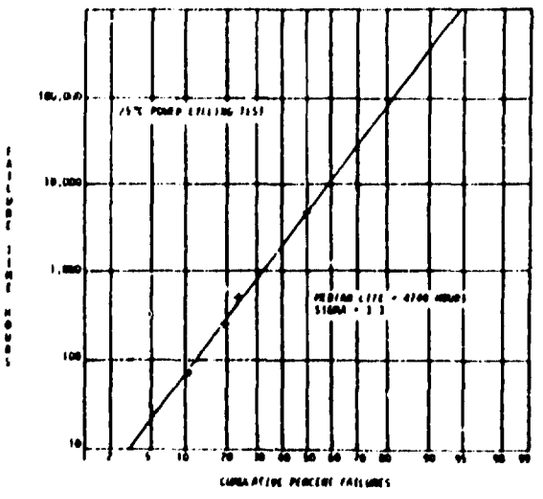

OPTRON
FAILURE MODE - OPEN BONDS

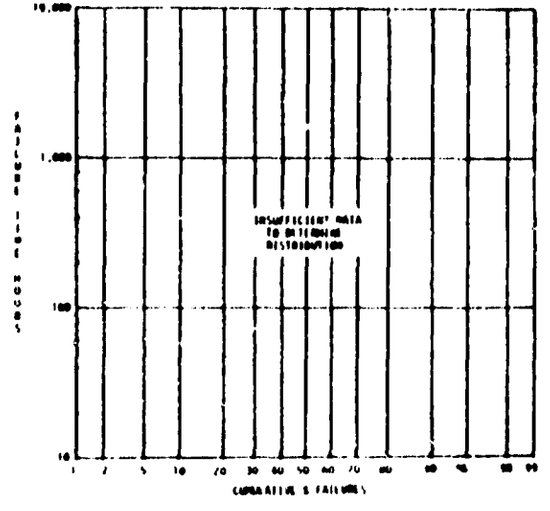

TEXAS INSTRUMENTS

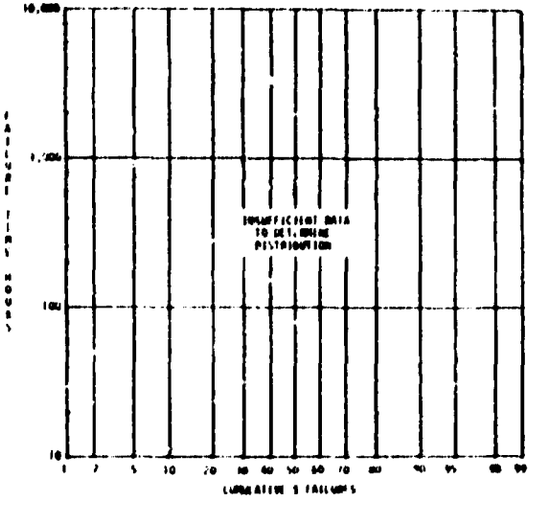

HEWLETT PACKARD

FIGURE 10. OPTO-COUPLER FAILURE DISTRIBUTIONS - POWER CYCLING

could not be obtained. However, the combined burn-in and power cycling test results indicate a serious workmanship/processing problem with the entire lot of delivered devices. Consequently, a lot acceptance test would probably have been a better defect screening technique than the 240 hour burn-in conducted during screening and preconditioning.

Temperature Cycling - During temperature cycling, devices were monitored for intermittent opens and shorts. None of the discrete LEDs exhibited intermittent opens or shorts, but a certain percentage of each manufacturer's opto-couplers exhibited intermittent opens. The distributions of opto-coupler intermittent opens are shown in Figure 11. Also shown are the number of devices exhibiting intermittent opens that were subsequently detected as opens during ambient, low or high temperature testing. Not all of the intermittent opens were confirmed by the electrical testing, and if the intermittent open could not be confirmed, the device was not analyzed further. Thus, it can not be stated with certainty if all of the indicated intermittent opens during temperature cycling were device malfunctions, or if the indicated opens were due to false triggering of the monitoring circuit. Temperature cycling tests conducted by Hewlett Packard (Appendix G) suggest that false triggering during the McDonnell Douglas tests may have indicated a lower number of cycles to failure for their device than was actually realized. (All Hewlett Packard device opens were confirmed.) However, the Hewlett Packard test results and the results shown in this report were obtained under somewhat different conditions. Transfer time between the -55°C and 125°C ambient temperatures was 10 minutes during the Hewlett Packard tests and only several seconds during the McDonnell Douglas tests. In addition, the monitoring point triggering levels may have been different for the two tests. Consequently, the Hewlett Packard test results cannot be used as conclusive evidence of false triggering. Similar tests of opto-couplers during monitored shock and vibration, and monitored temperature cycling tests of LEDs resulted in a total of only three intermittent faults, suggesting that false triggering was not being experienced during the monitored temperature cycling tests of opto-couplers.

Examination of the failure distributions shown in the previous Figure 11 shows that the Hewlett Packard and Spectronics devices could be represented by single lognormal distributions, and that the Optron and Texas Instruments devices could be represented by bimodal distributions. The occurrence of bimodal distributions

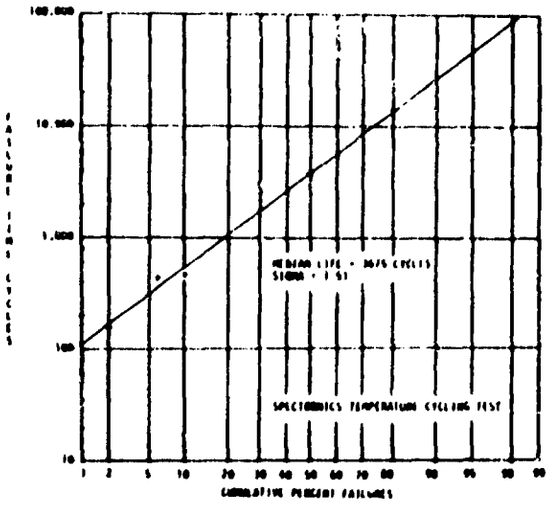

SPECTRONICS

INTERMITTENT OPENS - 0 POST TEST ELECTRICAL FAILURES

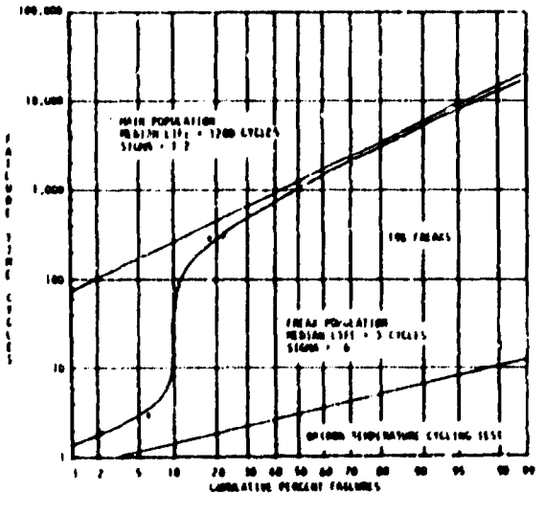

OPTRON

INTERMITTENT OPENS - 3 POST TEST ELECTRICAL FAILURES

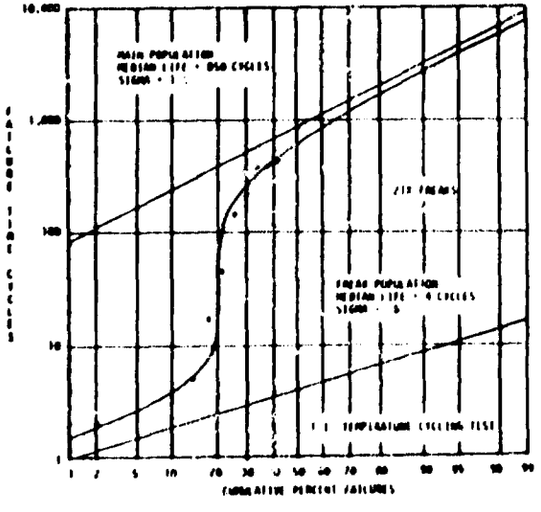

TEXAS INSTRUMENTS

INTERMITTENT OPENS - 4 POST TEST ELECTRICAL FAILURES

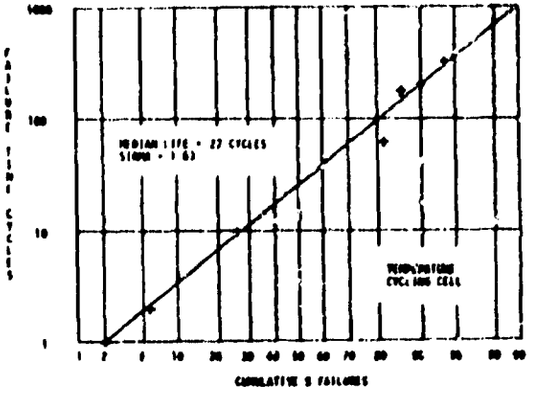

HEWLETT PACKARD

INTERMITTENT OPENS - 24 POST TEST ELECTRICAL FAILURES

FIGURE 11. OPTO-COUPLER FAILURE DISTRIBUTIONS - TEMPERATURE CYCLING

with widely separated Freak and Main population suggests that a monitored temperature cycling test may be a useful defect screening test. The Freak population represented 10% to 20% of the total test population and exhibited median cycles to failure of 3 to 4 cycles. However, all devices were previously subjected to ten cycles of thermal shock during screening and preconditioning. Thus, the median number of cycles to failure for the Freak population is probably closer to 13 or 14. A screening test of approximately 40 cycles should be sufficient to eliminate the Freak population and result in a greatly improved number of cycles to failure.

Monitored Vibration/Shock and Acceleration - Failure data from the vibration/shock/acceleration test sequence does not lend itself to failure distribution analysis. The bulk of the observed failures were open bonds induced by the constant acceleration test.

10.2.2 Group II Failure Distributions

Sufficient failure data was generated in the Group II life tests for most manufacturer's device types to evaluate failure distributions for the predominant failure modes/mechanisms.

HTRB Tests - During extended HTRB the predominant failure modes were: a) parameter degradation due to phototransistor surface effects in the Texas Instruments opto-coupler, b) open bonds in the Optron devices, and c) broken wires in the Hewlett Packard devices. Distributions of failure times during HTRB for each device type are shown in Figure 12. As can be noted later, the median lifetimes for the Texas Instruments devices correlate well with the median lifetimes observed during accelerated life testing at similar junction temperatures. However, the median lifetime for the Optron devices during HTRB was much higher than the median lifetime during accelerated life testing. This suggests that device current plays a role in the mechanism leading to the observed open phototransistor bonds. During accelerated life testing, phototransistor current is approximately two orders of magnitude higher than the phototransistor current during HTRB. Thus, it is believed that localized bond heating due to I^2R losses and electromigration further accelerated device failures during accelerated life testing.

Comparisons of the Hewlett Packard opto-coupler HTRB results with the temperature cycling results suggests two different failure mechanisms for these devices.

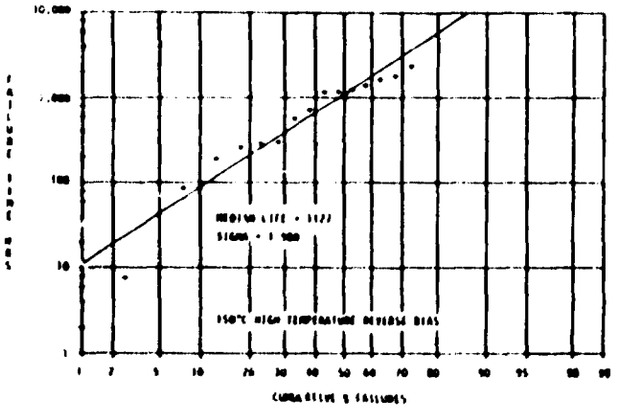

TEXAS INSTRUMENTS 150°C
PHOTOTRANSISTOR SURFACE INSTABILITY

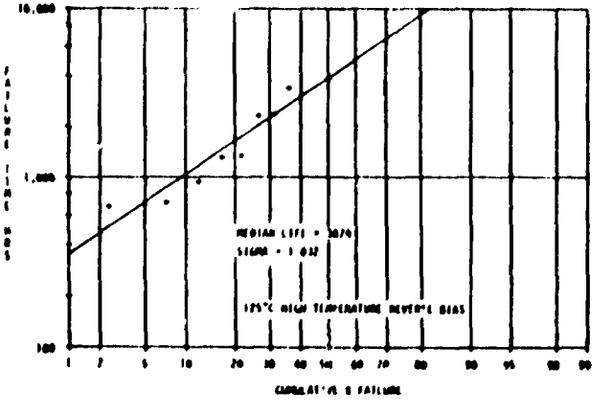

TEXAS INSTRUMENTS 125°C
PHOTOTRANSISTOR SURFACE INSTABILITY

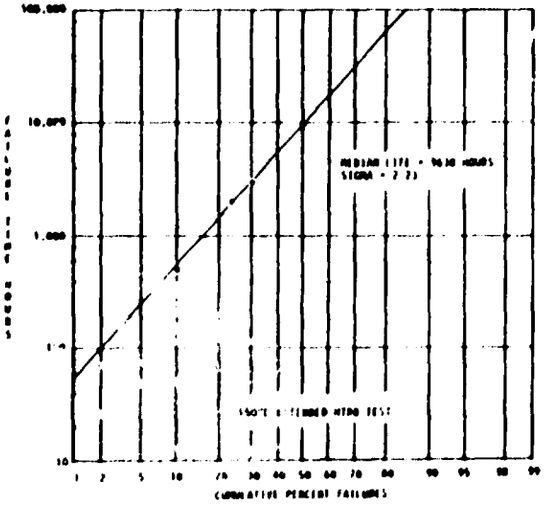

OPTRON - 150°C
OPEN BONDS

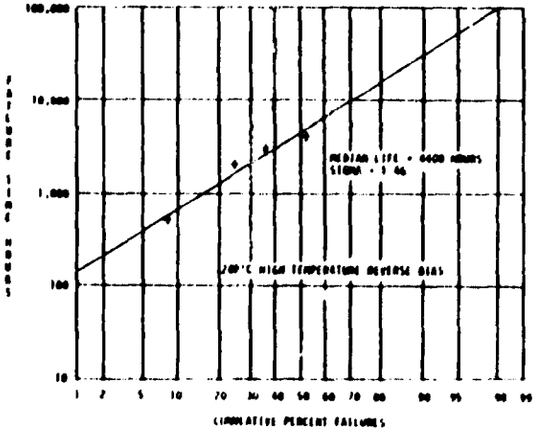

HEWLETT PACKARD
OPEN WIRES

FIGURE 12. OPTO-COUPLER FAILURE DISTRIBUTIONS - HTRB

During 4000 hours of HTRB testing at an ambient temperature of 200°C, 50% of the devices failed due to open wires. SEM and optical examinations of the wires established that the opens were the result of creep rupture, a time-temperature dependent mechanism. During temperature cycling, 96% of the devices failed due to open wires and examination of the wires revealed no marked physical difference between these failures and those encountered during HTRB. However, the temperature cycle failures could not have been due to creep rupture alone. In terms of time/temperature, the temperature cycle devices experienced less stress (125°C for 168 hours) than did the HTRB devices (200°C for 4000 hours), yet exhibited a much higher percentage of opens. Thus, it is suspected that the wire breaks during temperature cycling were due primarily to the cyclic dependent mechanism - fatigue.

Operating and Accelerated Life Tests - During the 25°C operating and high temperature accelerated life tests of opto-couplers and discrete LEDs, a variety of failure mechanisms were observed. The predominant failure mechanisms responsible for Texas Instruments opto-coupler failures were phototransistor surface effects and LED output power degradation. Failure distributions for these mechanisms are shown in Figures 13 and 14. The determination of failure distributions for both mechanisms required that the test sample size be adjusted for each mechanism. This was accomplished by assuming that the LED failures were from a test population comprised of all devices initially placed on test, minus phototransistor and all other non LED output power related failures. The test sample size for the phototransistor failures was then assumed to be the total number of phototransistor failures. Sample sizes for all other manufacturer's devices were also adjusted to exclude failures that were not related to the predominant failure mechanism.

The predominant failure mode in the Optron opto-coupler was open bonds due to Kirkendall voiding, which is a time-temperature dependent mechanism. Plots of the failure distributions for open bonds in the Optron devices are shown in Figure 15.

Insufficient failure data was generated in the accelerated life tests of the Hewlett Packard opto-couplers to permit evaluation of failure distributions. It is believed that wire break failures, similar to those observed during HTRB were not experienced during accelerated life testing due to the lower temperatures during accelerated life testing.

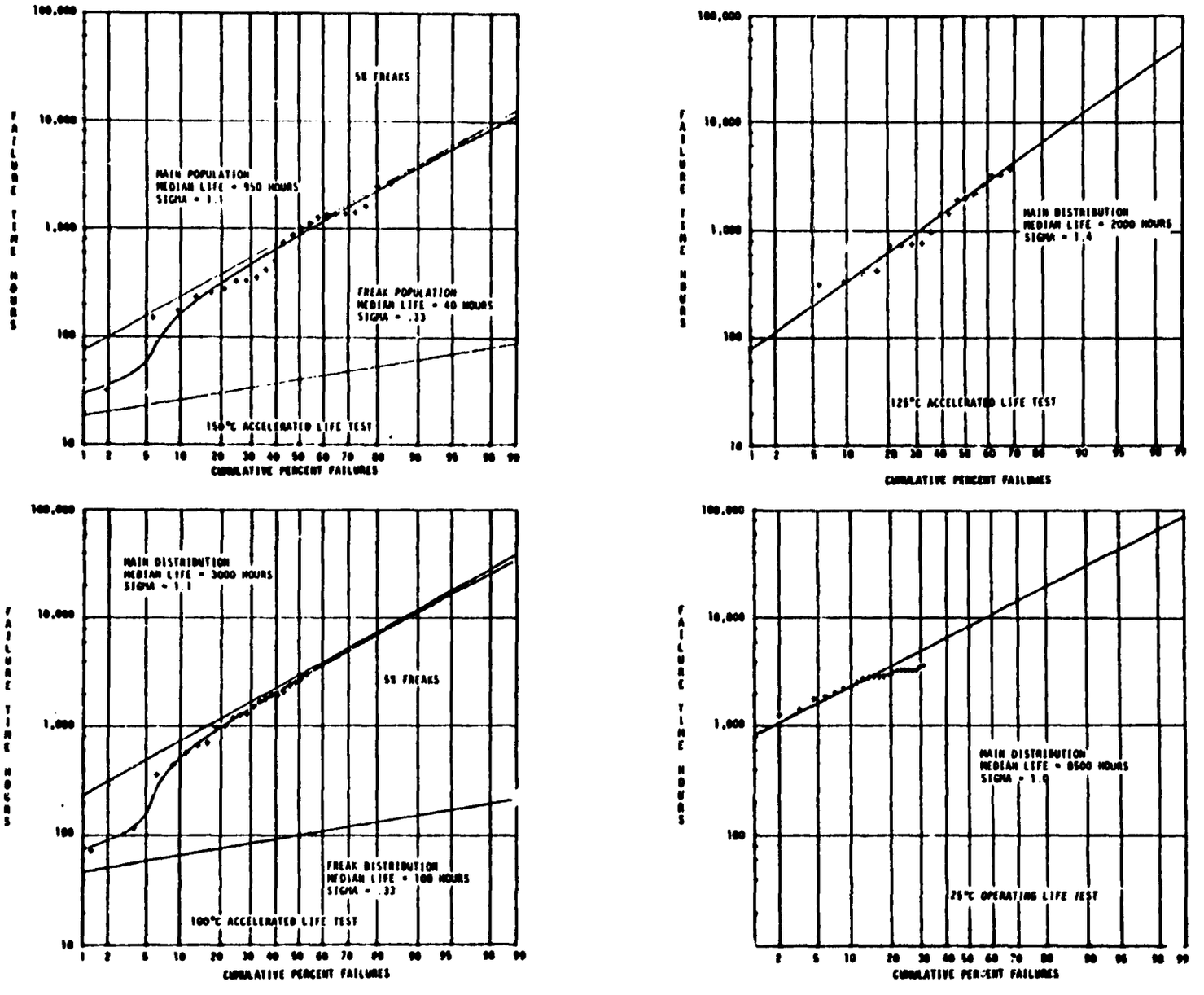

FIGURE 13. TEXAS INSTRUMENTS OPTO-COUPLER LED FAILURE DISTRIBUTIONS - LIFE TEST

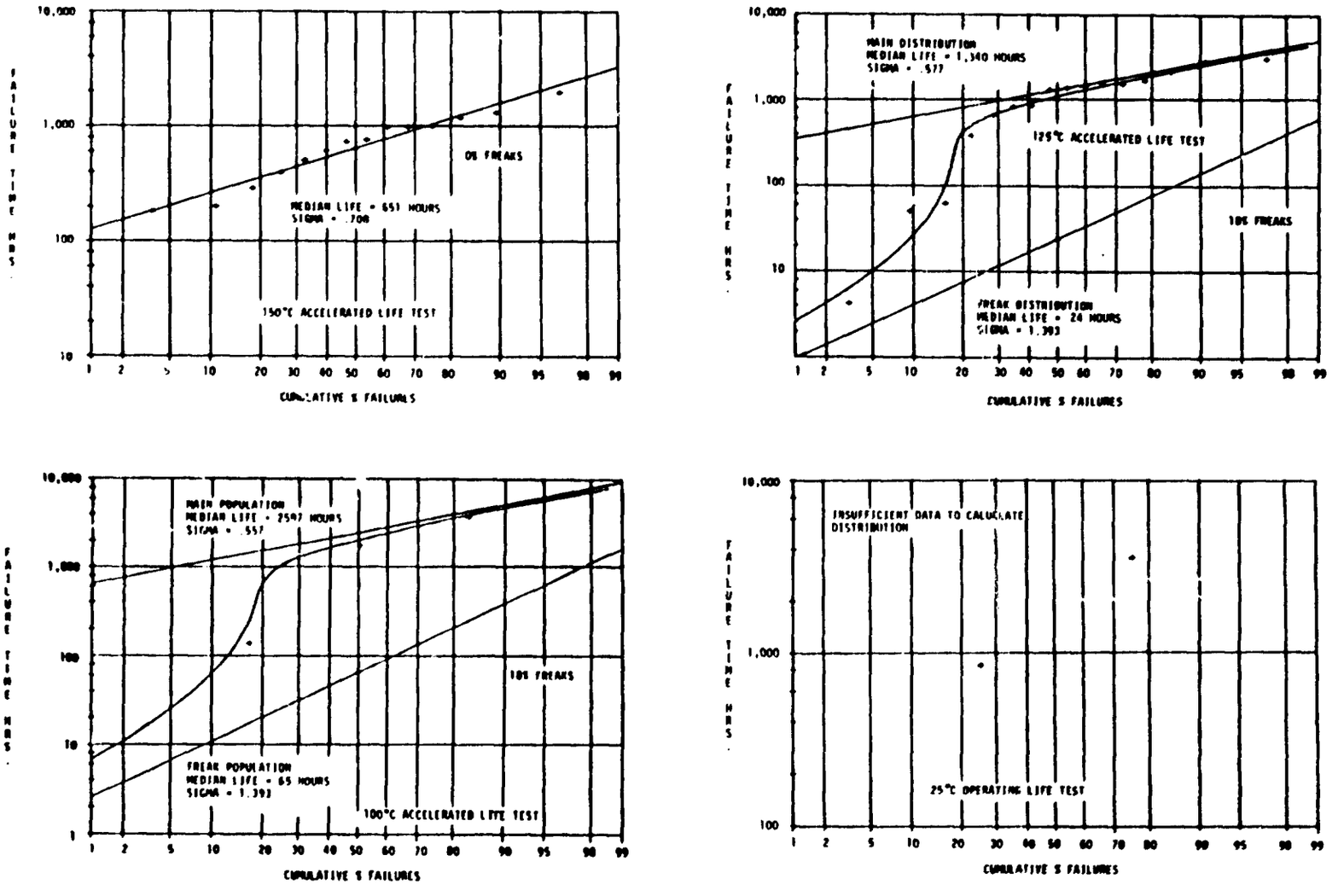

FIGURE 14. TEXAS INSTRUMENTS OPTO-COUPLER PHOTOTRANSISTOR FAILURE DISTRIBUTIONS - LIFE TEST

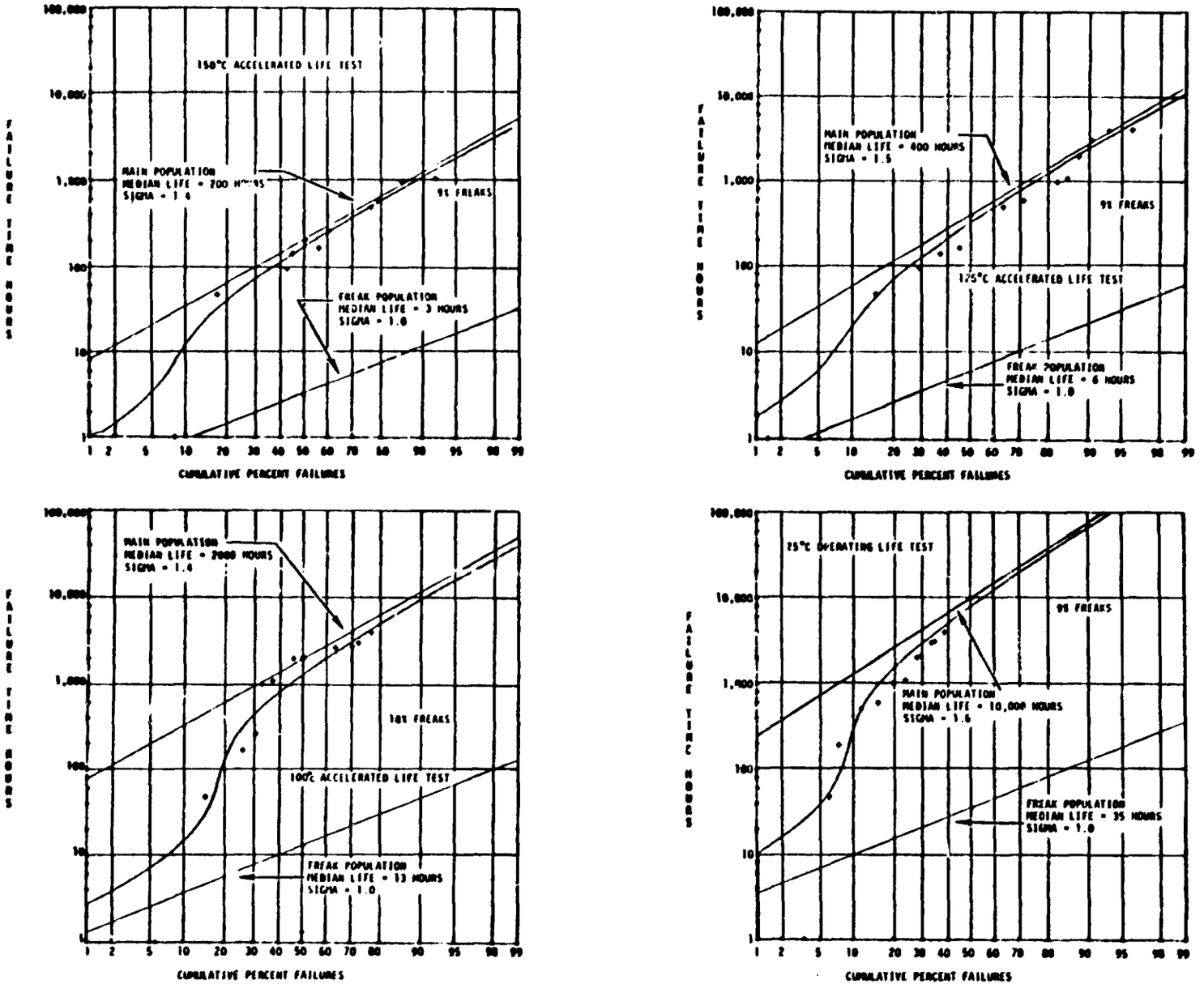

FIGURE 15. OPTRON OPTO-COUPLER OPEN BOND FAILURE DISTRIBUTIONS - LIFE TEST

Output power degradation was the primary failure mode of both the RCA and T.I. discrete LEDs, and failure distributions for these devices are presented in Figures 16 and 17. Failure times in excess of 1,000 hours shown in these plots are extrapolated values based on a linear relationship between output power and the logarithm of time.

10.3 AGING CHARACTERISTICS

Sufficient multiple temperature failure data was generated during the operating and accelerated life tests to evaluate aging characteristics for the predominant failure modes observed in each manufacturer's device type. The Arrhenius reaction rate model [4] was found to provide a good representation of the aging characteristics for the Freak and Main device populations, and was used to relate median lifetimes and junction temperatures as follows:

$$t_{50\%} = A \exp\left(\frac{E_A}{kT}\right)$$

where:

$t_{50\%}$ = Freak or Main population median lifetime at a given junction temperature

A = a constant

E_A = experimental activation energy - eV

k = Boltzman's constant - 8.617×10^{-5} eV/K

T = absolute junction temperature - K

Texas Instruments Type A Opto-Coupler - Arrhenius plots for the Texas Instruments opto-couplers are shown in Figure 18. Both Freak and Main distributions of phototransistor and LED failures were observed. Activation energy estimates for the surface instability mechanism(s) responsible for phototransistor degradation indicate a 0.64 eV activation energy for the Freak population and a 0.45 eV activation energy for the Main population. This suggests two different mechanisms are responsible for the Freak and Main failure populations. However, due to the small number of Freak population failures, there is a large uncertainty in the estimate of Freak population median lifetimes. Therefore, the activation energy of the Freak population may actually be lower than the estimated 0.64 eV, and approach the 0.45 eV activation energy computed for the Main population. The small percentage of Freak population devices in the total test sample may also explain the absence of both phototransistor and LED Freak failures in some of the individual life test samples.

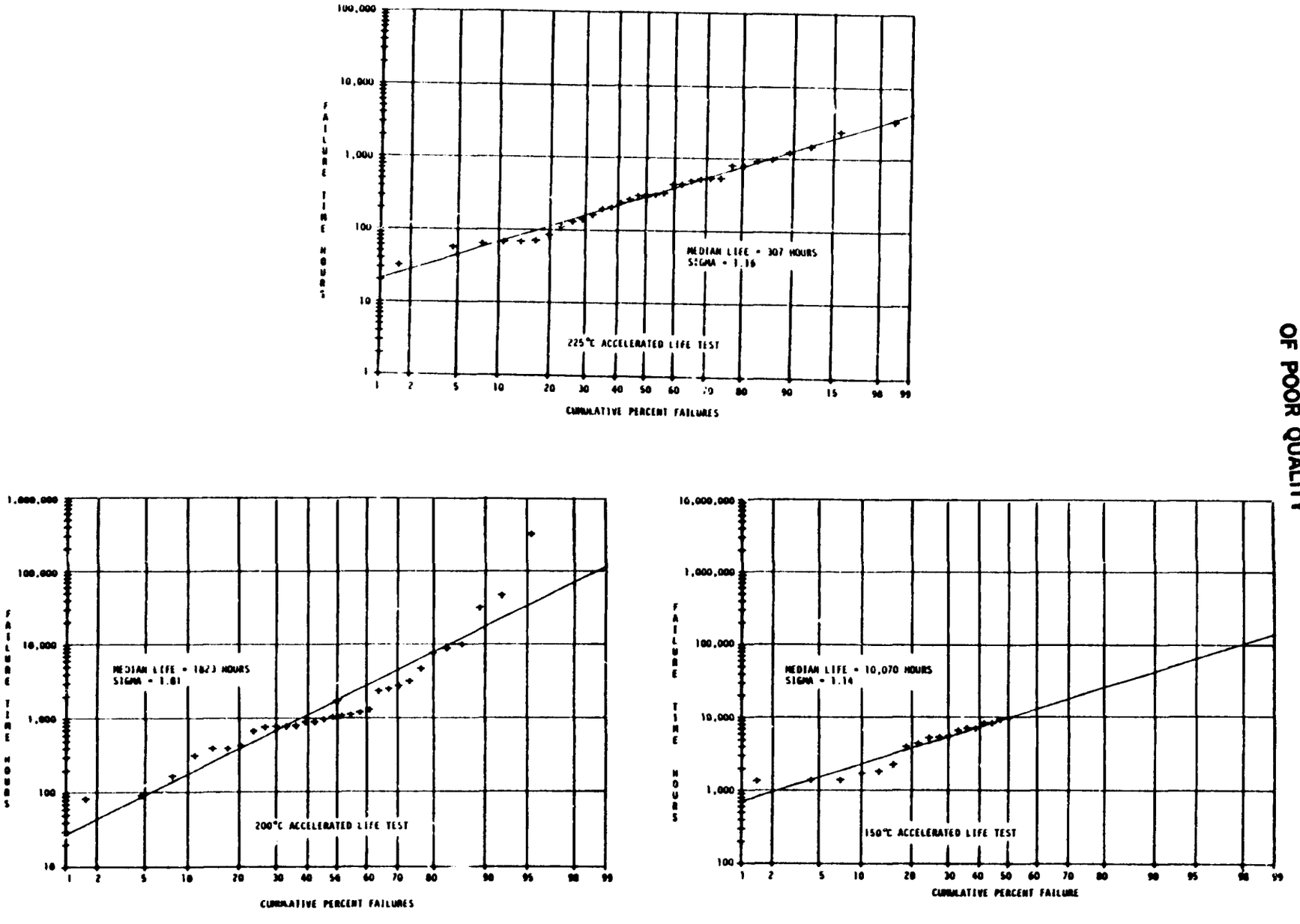

FIGURE 16. RCA LED OUTPUT POWER FAILURE DISTRIBUTIONS - LIFE TEST

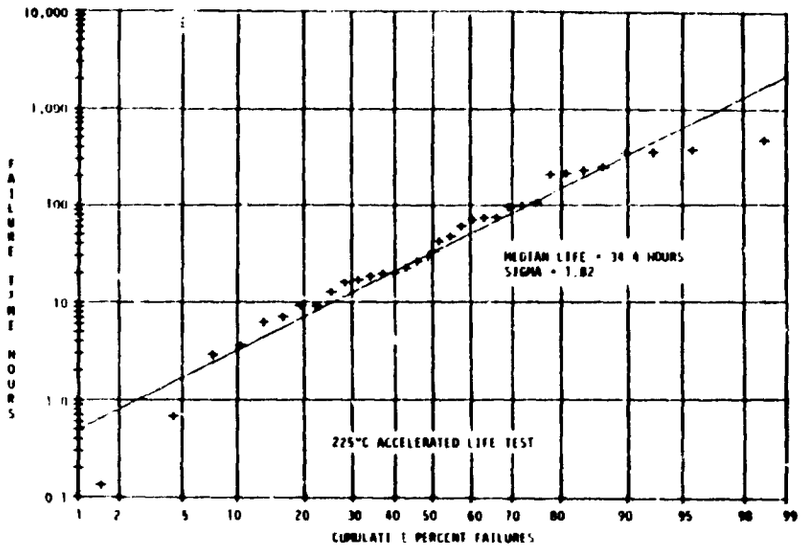

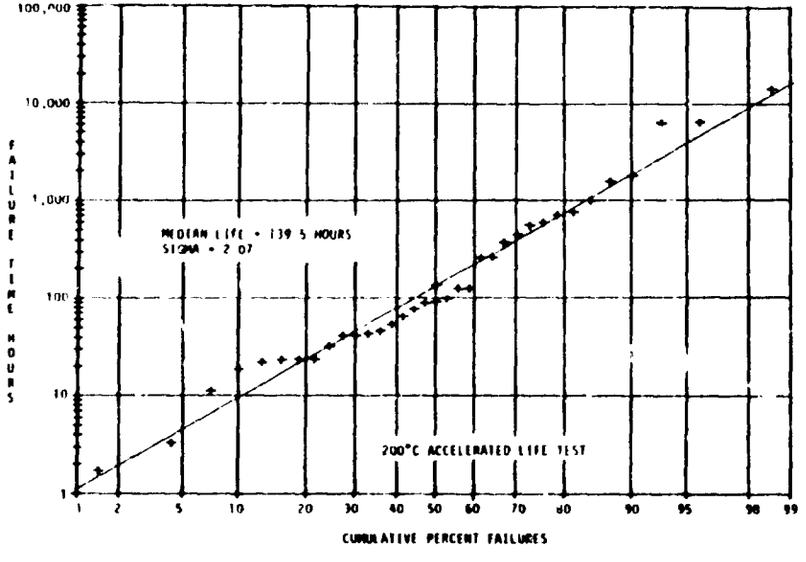

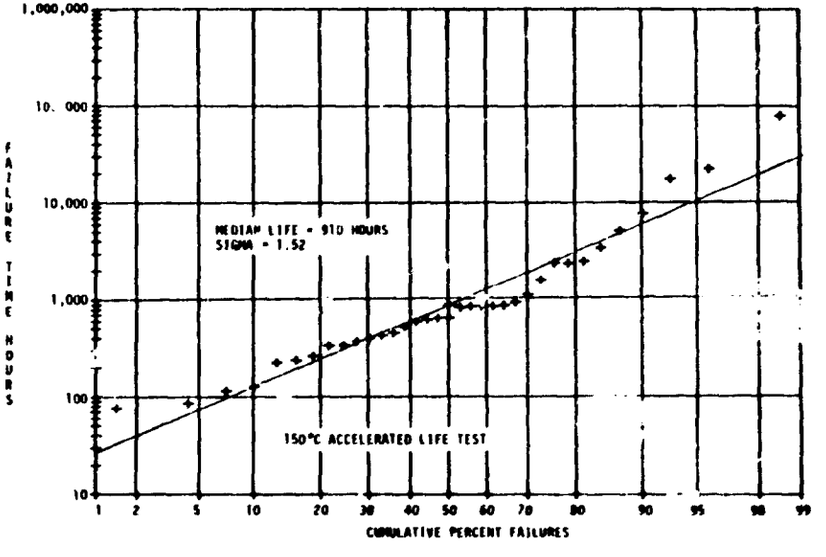

FIGURE 17. TEXAS INSTRUMENTS LED OUTPUT POWER FAILURE DISTRIBUTIONS - LIFE TEST

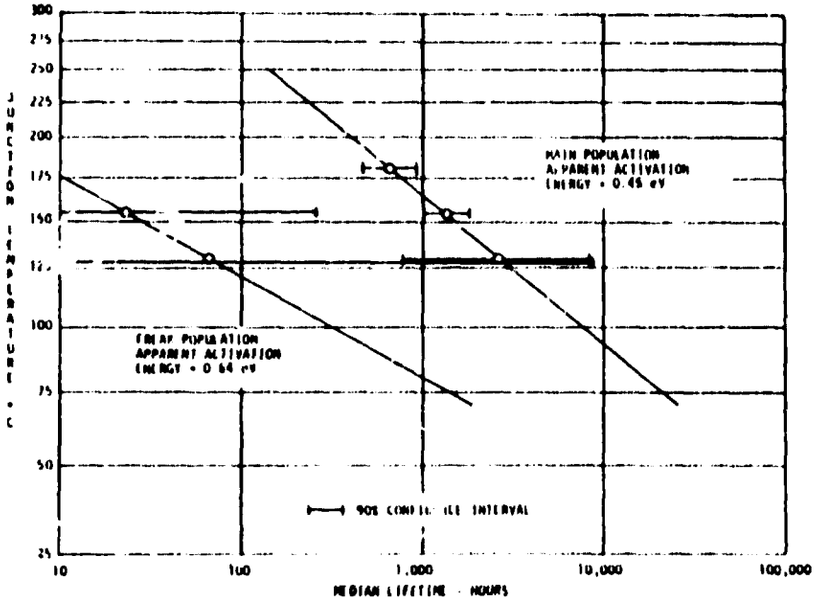

PHOTOTRANSISTOR SURFACE INSTABILITY

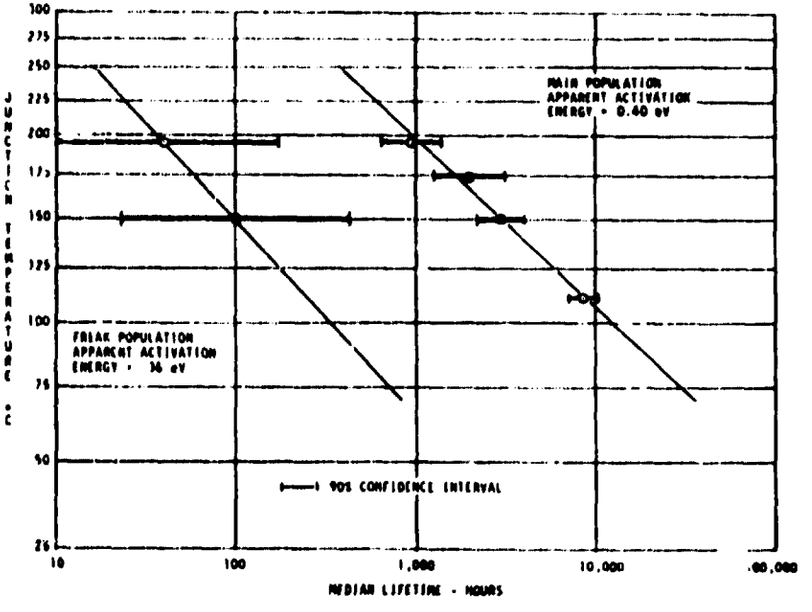

LED OUTPUT POWER DEGRADATION

FIGURE 18. ARRHENIUS PLOTS, TEXAS INSTRUMENTS TYPE A OPTO-COUPLER

Activation energy estimates for LED output power degradation resulted in values of 0.36 eV and 0.40 eV for the Freak and Main populations. Thus, values are quite similar and indicate there is no difference in the failure mechanisms responsible for Freak and Main failures.

A composite of the Arrhenius plots for phototransistor and LED median lifetimes is provided in Figure 19. Also shown on the plots are the median lifetimes of devices under HTRB conditions. Note that the HTRB median lifetimes are based on phototransistor failures and correlate well with the phototransistor median lifetimes observed during accelerated life testing. Since the applied voltage stresses across the phototransistor are considerably different during HTRB and accelerated life, these results indicate that phototransistor lifetimes are not strongly dependent upon the value of applied voltage.

The percentage figures shown for each of the Freak and Main populations on the composite Arrhenius plot are based on the total percentage of each type of device failure experienced during all of the 25°C and accelerated life tests. Failures due to other than the predominant failure mechanisms, such as open bonds, were excluded from the total sample size when computing the percentage values.

Optron Type A Opto-Couplers - Arrhenius plots for the open bond failure mode noted in the Optron opto-coupler are shown in Figure 20. Also shown are median lifetimes for open bond failures calculated from the power cycling and HTRB test results. Note that power cycling test results correlate reasonably well with the accelerated life test results, but that the HTRB results do not correlate. The high value of median lifetime observed during HTRB is, as previously discussed, attributed to lower values of phototransistor current during HTRB testing.

Estimated activation energies for the Freak and Main population are 0.43 eV and 0.70 eV, respectively. Since all of the failures were the result of open bonds and since some of the bonds were obviously underbonded and some obviously overbonded, it is suspected that the Freak population failures are primarily due to open bonds that were underbonded, whereas the Main population failures were due to open bonds that were overbonded. This would explain the presence of the two distributions, but not the differences in activation energies. Bonds that were initially weak due to underbonding would fail early in time due to expansion of the R6104 and

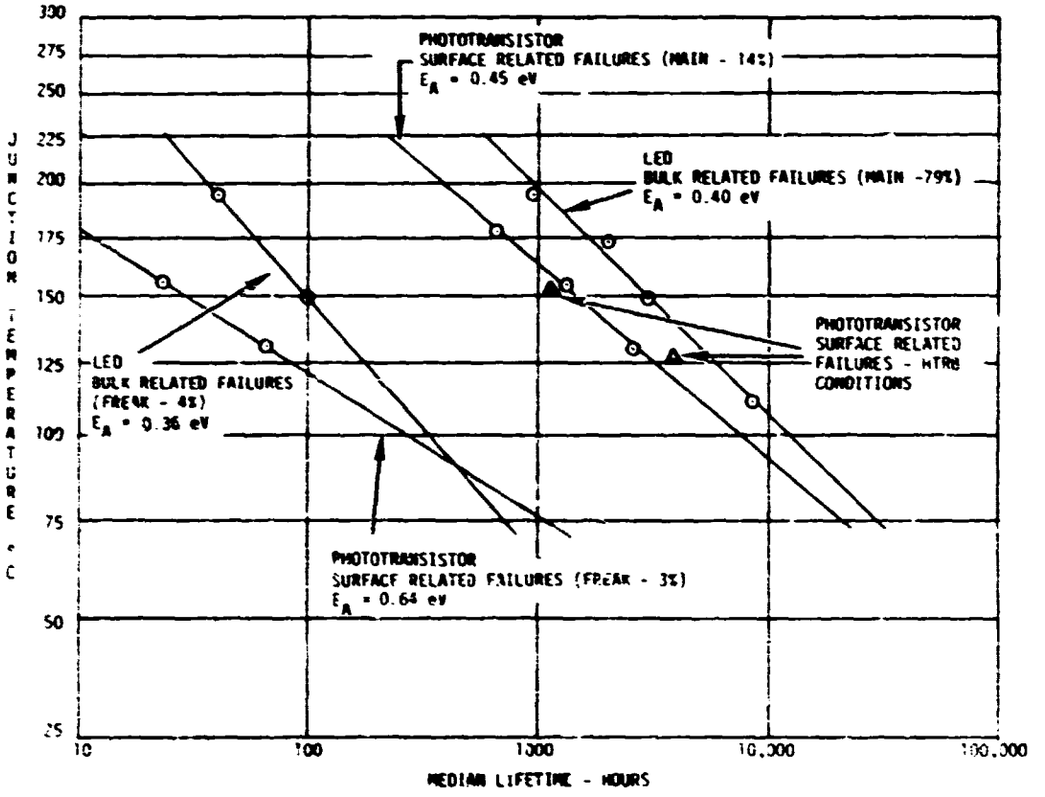

FIGURE 19. COMPOSITE ARRHENIUS PLOTS, TEXAS INSTRUMENTS TYPE A OPTO-COUPLER, PHOTOTRANSISTOR & LED

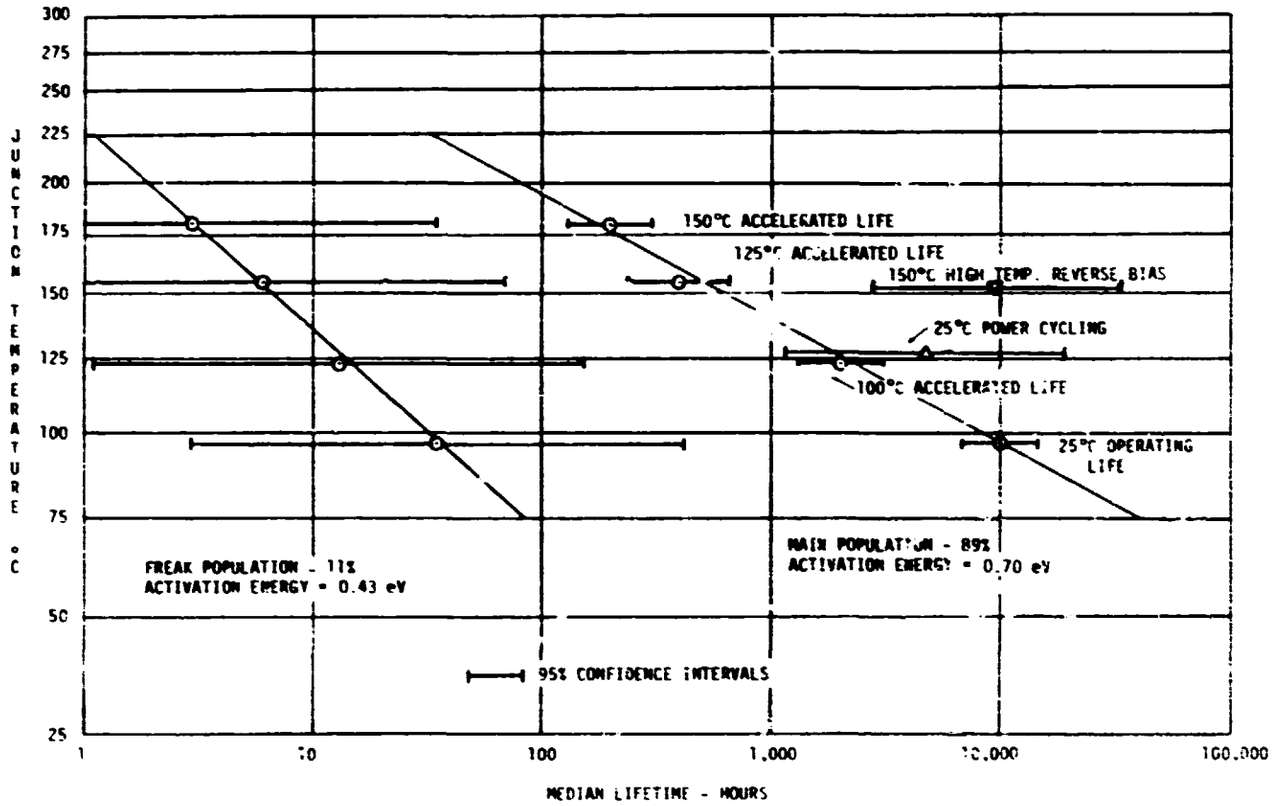

FIGURE 20. ARRHENIUS PLOTS OPTRON TYPE A OPTO-COUPLER - OPEN BONDS

Kirkendall voiding. Bonds that were initially good, but had experienced excessive intermetallic formation due to overbonding, would weaken later in time due to time-temperature dependent Kirkendall voiding and electromigration. Forces exerted on the weakened bonds due to expansion of the R6104 would then be sufficient to produce open circuits. Since both the Freak and Main failures appear to be due to the same mechanism (Kirkendall voiding and expansion of the R6104), the activation energies for the Freak and Main populations should be similar. Thus, the activation energy of the Freak population may actually be closer to the 0.7 eV estimate for the Main population. This is not unreasonable since a large uncertainty exists in the Freak population median lifetimes due to the small number of Freak failures.

Hewlett Packard Type B Opto-Couplers - Insufficient failure data was observed during life testing to evaluate the aging characteristics of the Hewlett Packard opto-coupler. This lack of failure data in 4,000 hours of accelerated life testing suggests these devices should exhibit long life and high reliability if the open wire failure mode observed during temperature cycling is eliminated. The Hewlett Packard report contained in Appendix G indicates that design changes have been made to minimize the severity of the open wire failure mode.

RCA and TI Discrete LEDs - Arrhenius plots for the RCA and TI discrete LED failures due to output power degradation are shown in Figure 21. A Freak population of device failure times was not observed in either manufacturer's devices, and the estimated activation energies were similar. However, the estimated activation energies (0.84 eV for T.I. and 0.93 eV for RCA) were considerably higher than the estimated activation energy for the LED contained in the Texas Instruments opto-coupler. This is not unexpected since the discrete LEDs are fabricated using Liquid Phase Epitaxy (LPE) and the T.I. opto-coupler LED is of planar construction.

Since Freak populations were not observed in the discrete LED test population, burn-in would be of no value in improving failure rates related to output power degradation.

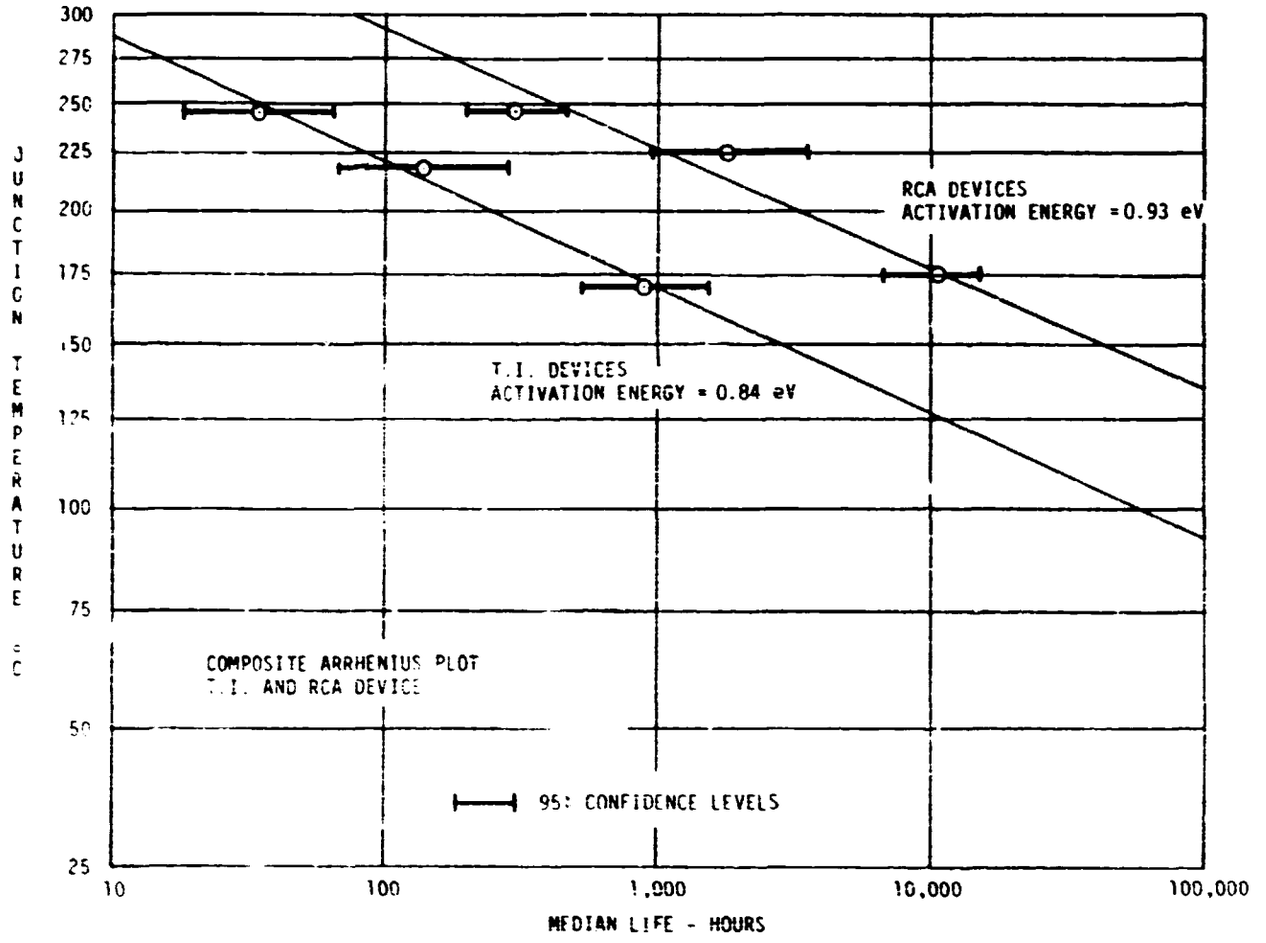

FIGURE 21. LED ARRHENIUS PLOTS - OUTPUT POWER DEGRADATION

10.4 FAILURE RATES

Calculation of use-temperature failure rates was accomplished using the values shown in Table 39 for Arrhenius model parameters (constant "A" and activation energy "E_A"), average value of lognormal distribution standard deviation, and percent Freak and Main populations. Details of the techniques employed generally followed published techniques [5], and are described in Appendix F. Use of these techniques resulted in the instantaneous failure rates for Texas Instruments opto-couplers shown in Figure 22. Failure rates are shown for average phototransistor/LED junction temperatures of 125°C and 50°C, and are a composite of phototransistor and LED failures. However, the failure rates do not include failures due to open bonds. Prior to using these failure rates for equipment MTBF calculations, a factor should be included to account for open bonds. Note that the maximum instantaneous value of the failure rate shown in the previous Figure 22 is 9.41×10^{-4} failures per hour and occurs at 415 hours of use-time. This peak is due to the Freak LED population of failures, and a 782 hour burn-in at a 175°C junction temperature is sufficient to eliminate 99.9% of the Freak population. Burn-in at junction temperatures above 175°C will result in failures due to open bonds, and is not recommended. Removal of 99.9% of the Freak population can be assumed to constitute removal of all Freak devices, and results in a maximum instantaneous failure rate of 1.8×10^{-4} failures per hour that would be observed during the first 10^5 hours of use-time at 125°C. However, due to the overlap of the Freak and Main distributions, the burn-in will also result in removing approximately 32% of the Main population. Thus, a 782 hour, 175°C burn-in of the Texas Instruments opto-couplers to achieve an 80% improvement in failure rate may not be cost effective.

A plot of the Optron opto-coupler instantaneous failure rates at junction temperatures of 125°C and 50°C is shown in Figure 23. The 125°C maximum instantaneous failure rate of 6.59×10^{-3} failures per hour occurs at a use-time of 8.7 hours, and is due to the Freak distribution of open bond failures. A 373 hour burn-in at a junction temperature 125°C is sufficient to assume complete removal of the Freak population and will result in a maximum 125°C instantaneous failure rate of 4.05×10^{-4} failures per hour during the first 10^5 hours of operation, or approximately a one order-of-magnitude reduction. Since the 373 hour, 125°C burn-in will only remove 12% of the main population, and results in an order-of-magnitude improvement in failure rate, burn-in of the Optron devices is an attractive defect screen.

TABLE 39. SUMMARY OF FAILURE RATE CALCULATION PARAMETERS

PART TYPE	FAILURE MODE	AVG. % FREAK	AVG. % MAIN	FREAK			MAIN		
				EA (ev)	A	σ AVG.	EA (ev)	A	σ AVG.
OPTO-COUPLERS, TYPE A									
TEXAS INSTRUMENTS	LED OUTPUT POWER	4	79	0.36	4.85×10^{-3}	0.33	0.40	5.55×10^{-2}	1.15
	PHOTOTRANSISTOR SURFACE INSTABILITY	3	14	0.64	6.06×10^{-7}	1.39	0.45	7.05×10^{-3}	0.62
UPTRON	OPEN BONDS	11	89	0.43	5.51×10^{-5}	1.00	0.70	2.72×10^{-6}	1.48
OPTO-COUPLERS, TYPE B									
HEWLETT PACKARD	———	---	--	INSUFFICIENT DATA					
LEDs									
TEXAS INSTRUMENTS	OUTPUT POWER	---	---	---	---	---	0.84	2.21×10^{-7}	1.80
RCA	OUTPUT POWER	---	---	---	---	---	0.93	3.68×10^{-7}	1.37

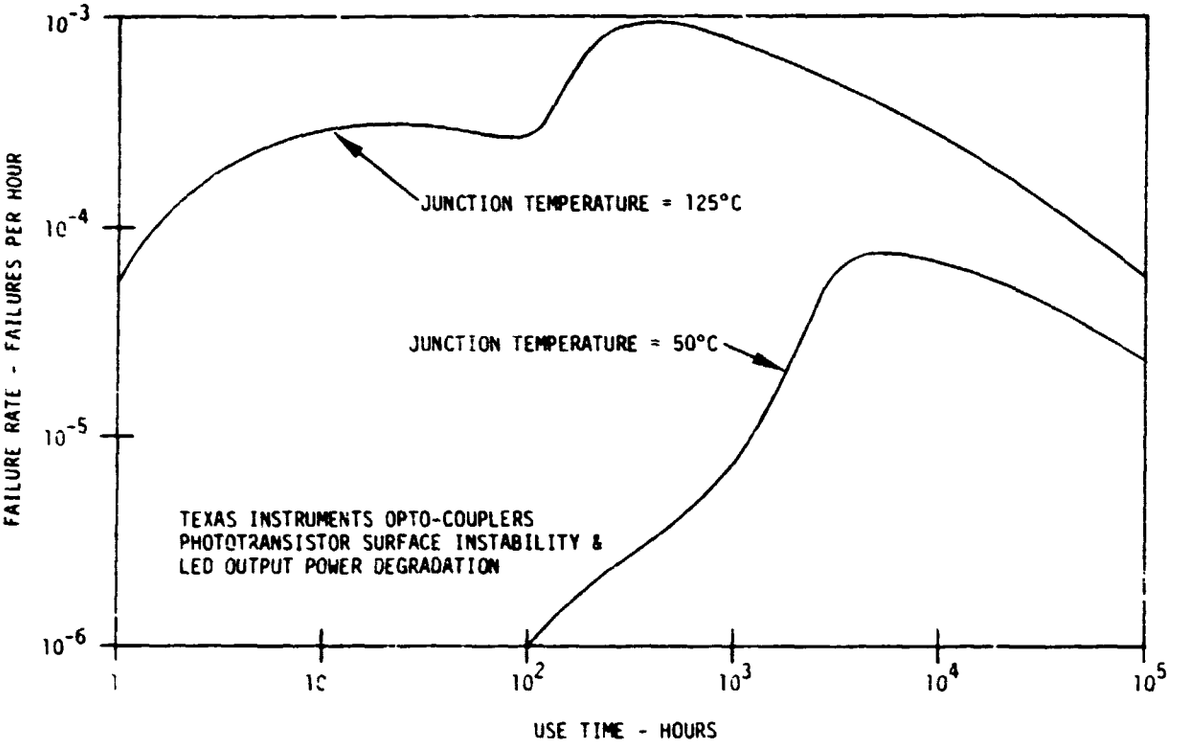

FIGURE 22. INSTANTANEOUS FAILURE RATE - TEXAS INSTRUMENTS TYPE A OPTO-COUPLER

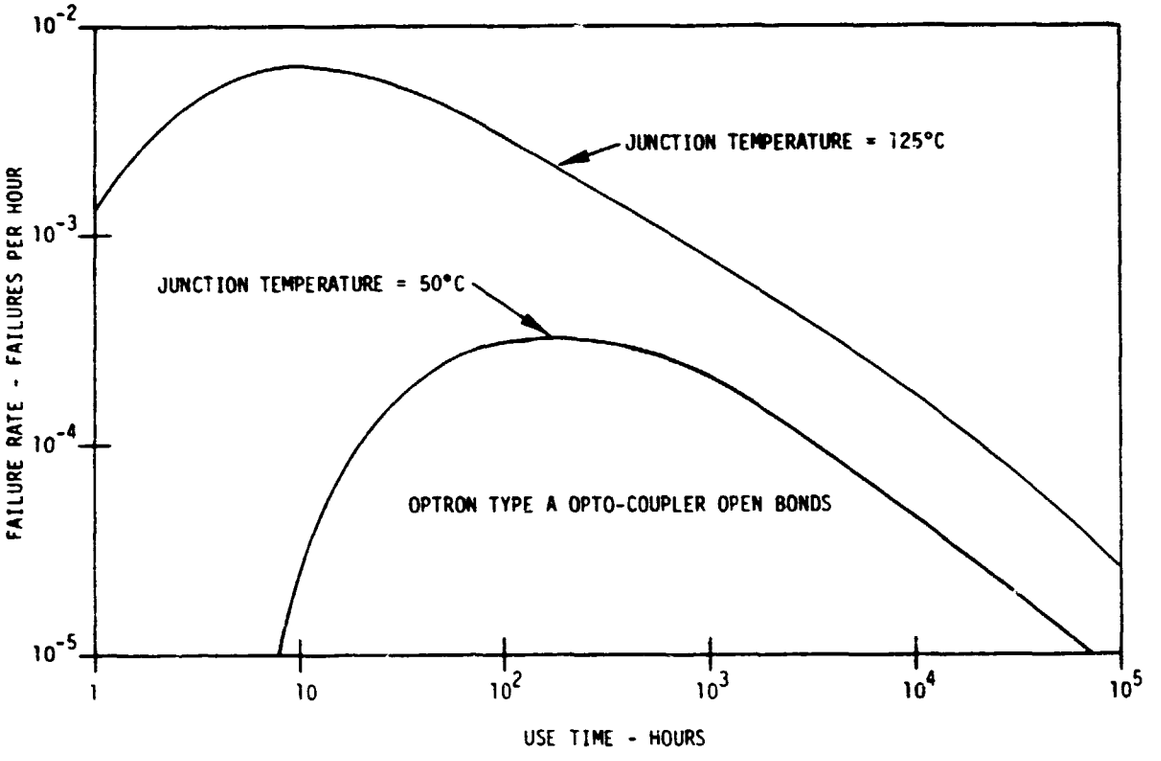

FIGURE 23. INSTANTANEOUS FAILURE RATE - OPTRON TYPE A OPTO-COUPLER

A summary of opto-coupler and discrete LED maximum instantaneous failure rates is shown in Table 40. Comparisons of the 125°C and 50°C failure rates illustrate the value of junction temperature derating to achieve improved failure rates for the predominant failure modes. As previously mentioned, additional factors for secondary failure modes must be included in the total device failure rate prior to using the failure rates for equipment reliability estimates.

TABLE 40. FAILURE RATE SUMMARY

DEVICE TYPE	MAXIMUM INSTANTANEOUS FAILURE RATE IN 10^5 HOURS OF USE-TIME				BURN-IN CONDITIONS	
	WITHOUT BURN-IN		WITH BURN-IN			
	125°C	50°C	125°C	50°C	TIME	T_J
OPTO-COUPLERS TYPE A						
TEXAS INSTRUMENTS	9.41×10^{-4}	7.48×10^{-5}	1.81×10^{-4}	4.44×10^{-5}	782 HRS	175°C
OPTRON	6.59×10^{-3}	3.65×10^{-4}	4.05×10^{-4}	3.48×10^{-6}	373 HRS	125°C
OPTO-COUPLERS TYPE B						
HEWLETT PACKARD	INSUFFICIENT DATA					
LEDs						
RCA	3.30×10^{-6}	7.00×10^{-9}	---	---		
TEXAS INSTRUMENTS	6.98×10^{-5}	2.28×10^{-7}	---	---		

11.0 CONCLUSIONS

This reliability study revealed a variety of different failure mechanisms related to the materials and processes used in the fabrication of opto-couplers and LEDs. The identified modes/mechanisms included: a) phototransistor degradation due to surface effects, b) LED output power degradation due to at least two different mechanisms, c) opto-coupler open circuits due to expansion of the silastic overcoat and multiple contributory defects, and d) opens, shorts and excessive leakage currents due to the use of epoxy die attach material. Some of the failure mechanisms were accelerated by temperature cycling, but most appeared to be accelerated primarily by thermal effects. Activation energies for the time-temperature dependent mechanisms were generally low, and ranged between 0.35 eV and 0.91 eV. Calculated maximum instantaneous 50°C use-temperature failure rates for the discrete LEDs were in the range of 10^{-7} to 10^{-9} failures per hour, and are considered acceptable for most military and space applications. Calculated maximum instantaneous 50°C use-temperature failure rates for the Type A opto-coupler were in the range of 10^{-4} to 10^{-5} failures per hour. These failure rates are considered excessive for most high reliability applications. A high temperature burn-in to remove the Freak population of devices will result in improved failure rates, but at the expense of removing some of the Main population devices. The single manufacturer's Type B opto-coupler evaluated exhibited high reliability during accelerated life testing, but an excessive number of failures were experienced during temperature cycling. The manufacturer has since taken corrective action to minimize the temperature cycling problem. Electrical stability problems were also experienced with the Type B opto-coupler, and although no failures were attributed to oscillation, corrective action to internally stabilize the high gain photo-amplifiers is recommended.

Two serious reliability problems related to workmanship and materials were identified in the opto-coupler devices. A workmanship problem, excessive build-up of silver epoxy during die bonding, was the primary cause of the Spectronics opto-coupler failures during power cycling, and screening and preconditioning tests. The excessive number of failures during screening and preconditioning resulted in deleting this manufacturer's opto-coupler from the evaluation program. Use of the Dow Corning R6104 silastic as a light coupling/dielectric isolation medium, caused

failures in all manufacturer's opto-couplers. The specific contributing causes related to these failures varied, but elimination of the silastic overcoat would minimize the impact of the other failure contributing causes. If the silastic can not be eliminated, special controls should be added into the manufacturing process to ensure high quality wire bonds.

Phototransistor failures (Type A opto-couplers), due to surface related effects could be minimized by additional manufacturing process controls. High temperature burn-in could also be employed as a defect screening technique for these types of process related problems. However, the predominance of Type A opto-coupler failures due to LED degradation minimizes the effectiveness of a high temperature burn-in. The exact cause(s) of LED output power degradation are not well understood, and further work to identify these causes is recommended.

The Type B opto-coupler, which uses a high gain photoamplifier in place of a single phototransistor, did not exhibit surface related problems, and no failures were attributed to LED degradation. However, it is strongly suspected, based on the results of discrete LED and Type A opto-coupler testing, that the Type B opto-coupler LEDs were degrading during accelerated life testing.

12.0 REFERENCES

[1] D. S. Peck and C. H. Zierdt, Jr., "The Reliability of Semiconductor Devices In the Bell System", Proceedings of the IEEE, Vol. 62, pp. 185-211, February, 1974.

[2] D. S. Peck, "The Analysis of Data from Accelerated Stress Tests", Proceedings 9th Annual Reliability Physics Symp., pp. 68-83, 1971.

[3] F. H. Reynolds, "Thermally Accelerated Aging of Semiconductor Components", Proceedings of the IEEE, Vol. 62, pp. 212-222, February, 1974.

[4] S. Glasstone, K. J. Laidler, H. Eyring, "The Theory of Rate Processes", pp. 1-2, McGraw-Hill Book Co., Inc., N.Y., 1941.

[5] Lynn R. Goldthwaite, "Failure Rate Study for the Log Normal Lifetime Model", IRE (NSRQCE) Conference, pp. 208-213, 1961.

C - 2

APPENDIX A

DEVICE CONSTRUCTION ANALYSES

TABLE OF CONTENTS

APPENDIX A1

CONSTRUCTION ANALYSIS

TEXAS INSTRUMENTS 4N22 (L-TI511)

OPTO COUPLER

S/N's 21 & 22

CONSTRUCTION DETAILS
TEXAS INSTRUMENTS 4N22 (L-TI511) OPTO-COUPLER
S/N's 21 & 22

A. PACKAGE

1. Type: Modified (6-Pin) TO-5 type can - Figure A1
2. Dimensions: Conforms to Figure A2
3. Weight: 0.81 gram
4. Materials:
   a) Can: Kovar
   b) Header: Gold-Plated Kovar
   c) Leads: Gold-Plated Kovar (External and Internal)
5. Seal: Hermetic Weld + Glass

B. INTERNAL GEOMETRY - Figure A3

1. Interconnections:
   a) Type: Gold Wire
   b) Diameter: 1 mil
   c) Bonds:
      - Au/Al Thermocompression ball at the transistor chip - Figure A4
      - Au/AuGe Thermocompression ball at the LED chip - Figure A5
      - Au/Au Thermocompression wedge at the posts and header - Figure A6
2. Chips - Figures A7 and A8

	LED - Figure A9	PHOTOTRANSISTOR - Figure A10
Type:	GaAs Planar	Silicon Planar
Dimensions:	24X24X5 mils	46X28X5.6 mils
Scribe Type:	Laser	Laser
Chip Attach:	(see Coupling Medium)	Au-Si Eutectic
Passivation:	SiO_2	SiO_2/Si_3N_4
Metallization:	AuGe	Aluminum (~13,500 Å)
Glassivation:	None	Silicon Nitride
Coupling Medium:	R6104 Cement/3 mil Glass/R6104 Cement	
Overcoating:	Dow Corning R6104 Silicone Resin	

3. Quality of Workmanship and Processing: Fair

   a) The glass light pipe of S/N 22 was misaligned (Figure A7).

   b) Two-thirds of the LED anode contact metal and some of the cathode contact metal of S/N 22 had been scratched away (Figure A9).

   c) The phototransistor of both devices contained numerous crystallographic defects as shown in Figures A11 and A12. The defects in S/N 21 appeared to have been caused by gold-colored inclusions as shown in Figure A13.

4X

(a) TOP VIEW

4X

(b) BOTTOM VIEW

FIGURE A1 - TEXAS INSTRUMENTS 4N22 PACKAGE

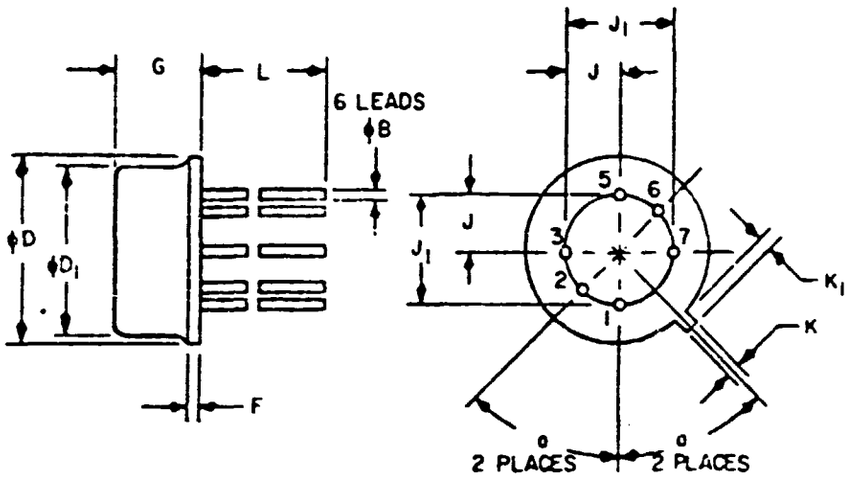

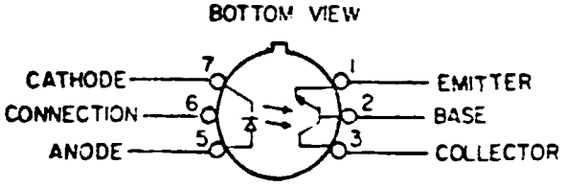

(Collector connected internally to case)

DIM	INCHES		MILLIMETERS		NOTES
	Min	Max	Min	Max	
øD	.335	.370	8.51	9.40	
$øD_1$	.305	.335	7.75	8.51	
øB	.016	.019	.406	.483	
α	45° T.P.		.45° T.P.		1
F	---	.040	---	1.02	
G	.155	.185	3.94	4.70	
J	.100T.P.		2.54T.P.		1
J_1	.200T.P.		5.08T.P.		1
K	.028	.034	.71	.86	
K_1	.029	.045	.74	1.14	
L	.500	.600	12.70	15.40	

NOTES:
1. T.P. designates true position. Leads having maximum diameter (.019") measured in gaging plane .054" +.001" -.000" below the seating plane of the device shall be within .007" of their true position relative to a maximum width tab.

FIGURE A2 - PACKAGE DIMENSIONS

ORIGINAL PAGE IS
OF POOR QUALITY

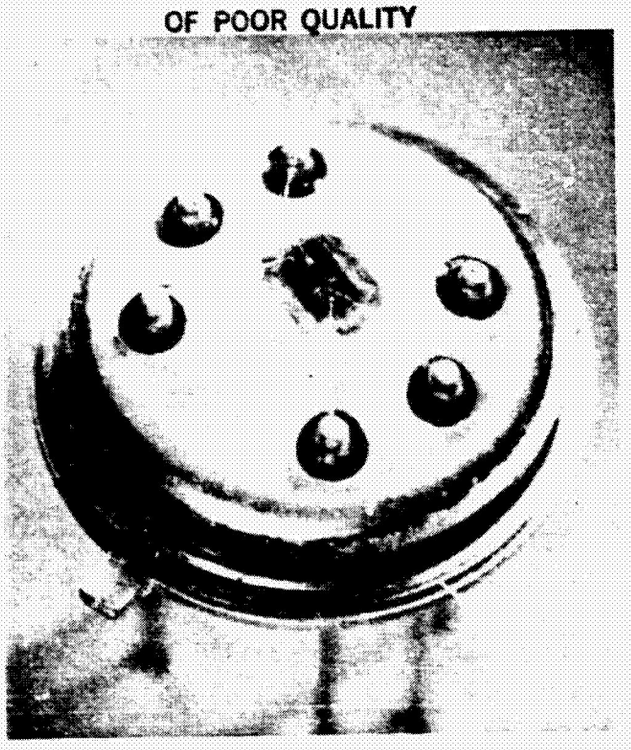

10X

FIGURE A3 - INTERNAL GEOMETRY

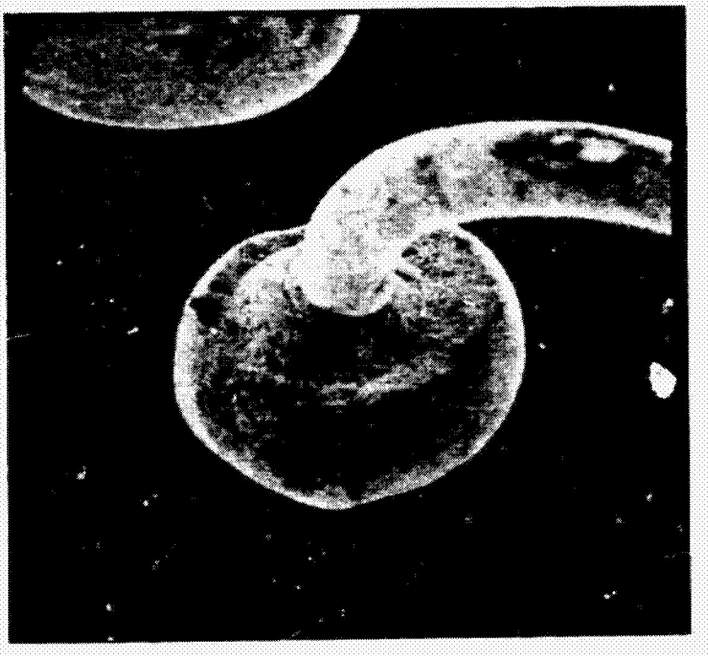

475X

FIGURE A4 - SEM PHOTO OF THE TRANSISTOR BASE BOND

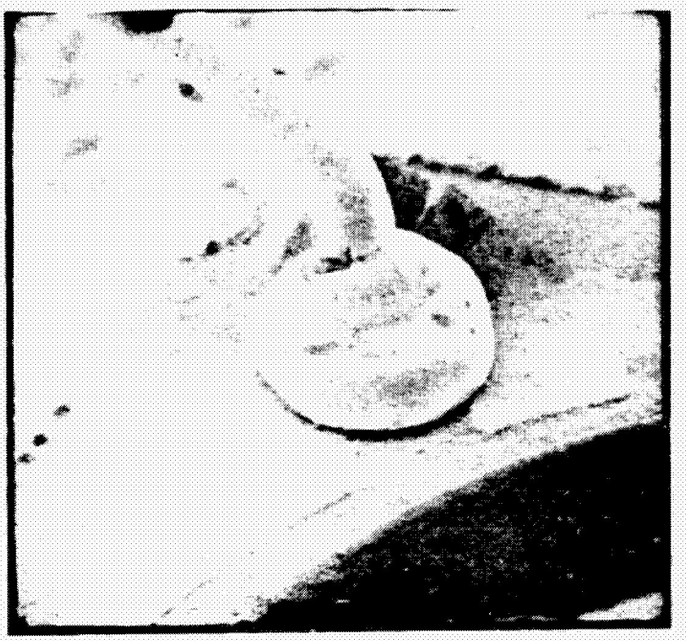

475X

FIGURE A5 - SEM PHOTO OF THE LED CATHODE BOND

550X

FIGURE A6 - SEM PHOTO OF A POST BOND

ORIGINAL PAGE IS
OF POOR QUALITY

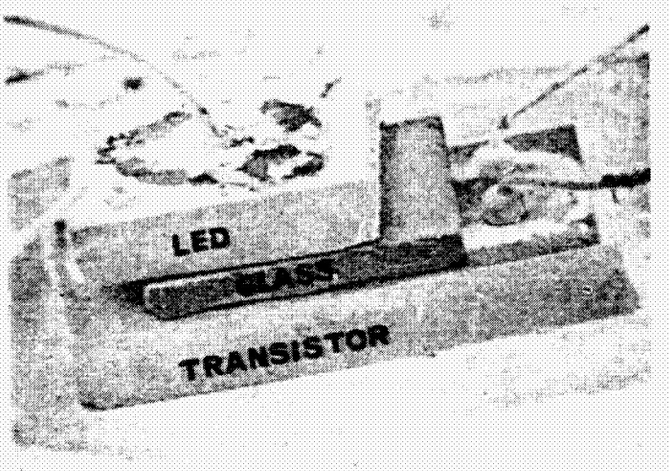

75X

FIGURE A7 - SEM PHOTO OF THE CHIP LAYOUT

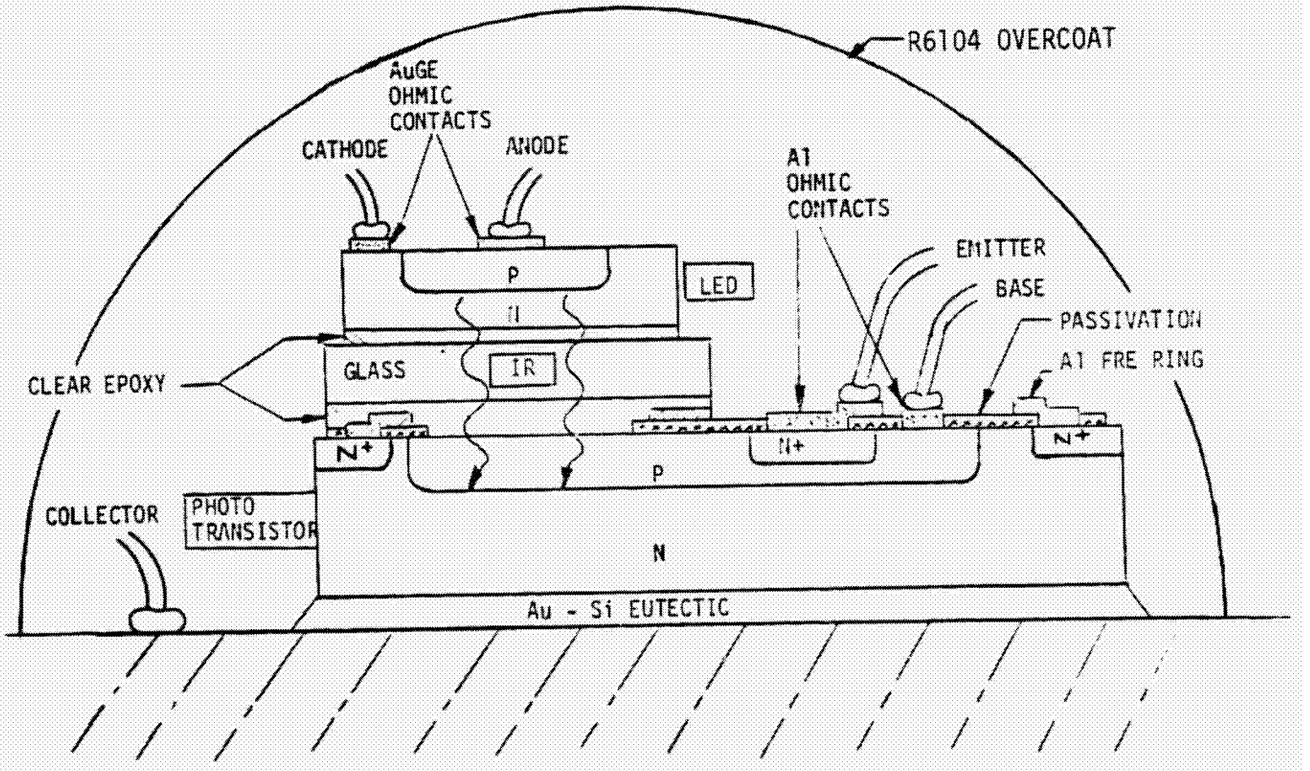

FIGURE A8 - CROSS-SECTIONAL SKETCH (NOT TO SCALE) OF THE CHIPS

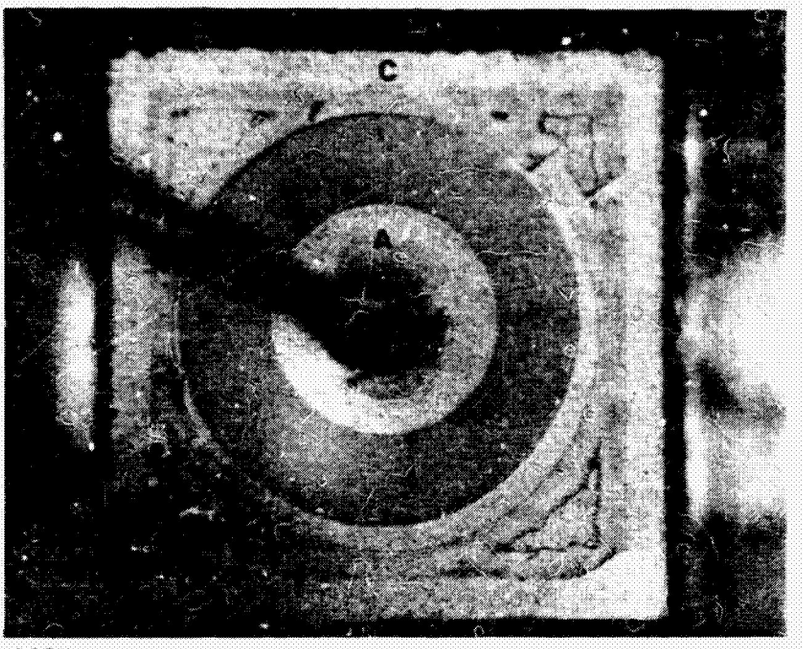

132X

FIGURE A9 - LED CHIP

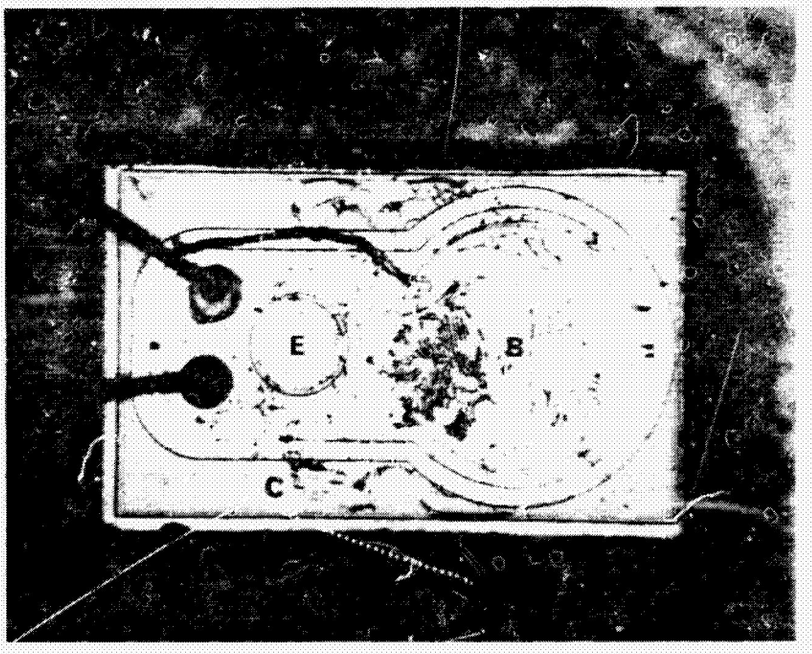

70X

FIGURE A10 - PHOTOTRANSISTOR CHIP

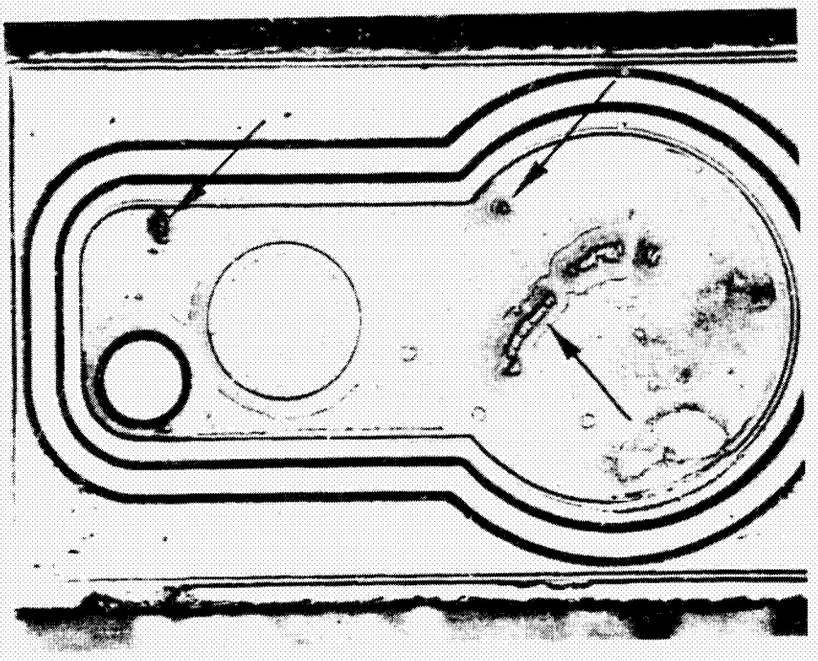

105X

FIGURE A11 - PHOTOTRANSISTOR CHIP OF S/N 22 AFTER SILICON ETCH (SIRTL) SHOWING CRYSTALLOGRAPHIC DEFECTS (ARROWS).

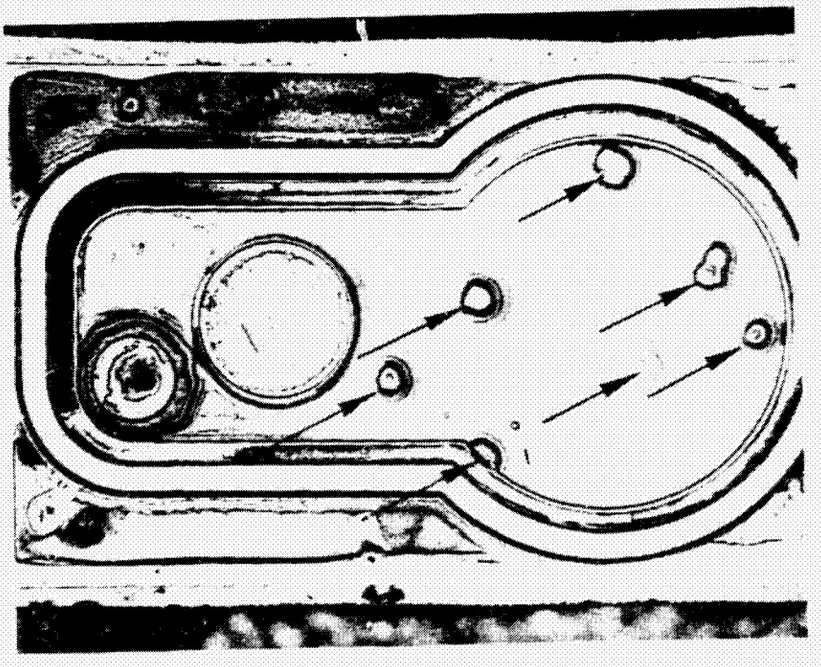

105X

FIGURE A12 - PHOTOTRANSISTOR CHIP OF S/N 21 AFTER SILICON ETCH (SIRTL) SHOWNING CRYSTALLOGRAPHIC DEFECTS (ARROWS).

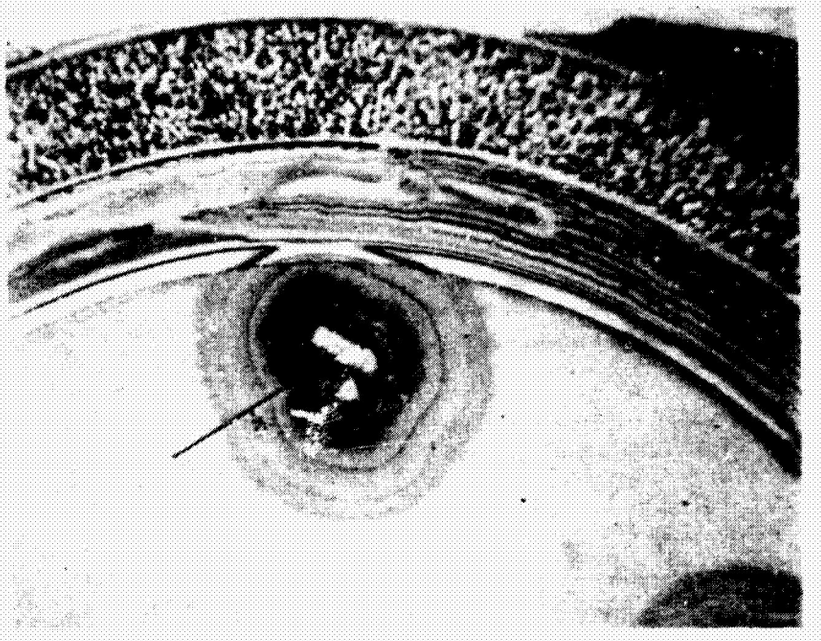

395X

FIGURE A13 - PHOTOTRANSISTOR CHIP OF S/N 21 PRIOR TO SILICON ETCH (AFTER SiO2 REMOVAL) SHOWING CLOSE-UP OF GOLD COLORED INCLUSIONS IN THE DEFECT SITES.

APPENDIX A2

CONSTRUCTION ANALYSIS

SPECTRONICS - SPX-1830

OPTICAL COUPLER

S/N's 14, 15 & 24

CONSTRUCTION DETAILS
SPECTRONICS SPX-1830 OPTICAL COUPLER
S/Ns 14, 15 & 34

A. PACKAGE

1. Type: Modified (6 Pin) TO-5 type can - Figure A14
2. Dimensions: Conforms to Figure A15
3. Weight: 0.9 gram
4. Materials:
   a) Can: Kovar
   b) Header: Gold-plated Kovar
   c) Leads: Gold-plated Kovar (Internal & External)
5. Seal: Hermetic Weld + Glass

B. INTERNAL GEOMETRY - Figure A16

1. Interconnections:
   a) Type: Gold Wire
   b) Diameter: 1-mil
   c) Bonds:
      - Au/Al Thermocompression ball at the chips - Figures A17 and A18
      - Au/Au Thermocompression ball at the gold pad
      - Au/Au Thermocompression wedge at the posts - Figure A19
2. Chips - Figure A20

	LED - Figure A21	Phototransistor - Figure A22
Type:	GaAs, Liquid Phase Epi	Silicon, Planar
Dimensions:	20 X 19 X 4 mils	25 X 25 X 3.1 mils
Scribe Type:	Mechanical	Mechanical
Chip Attach:	Silver epoxy to a deposited gold pad on a header mounted 52 X 52 mil ceramic pedestal.	Silver Epoxy to header
Passivation:	None	SiO_2
Metallization:	Aluminum	Aluminum
Glassivation:	None	None
Coupling Medium:	Dow Corning R6104 Silicone Resin	

3. Quality of Workmanship: Poor

   a) During special curve tracer tests, the LED of several units exhibited intermittent short-circuits or erractic characteristics. This was traced to excessive build-up of silver epoxy which had overlapped the p-n junction as illustrated in Figure A23.

   b) The phototransistor contained numerous crystallographic defects as shown in Figure A24.

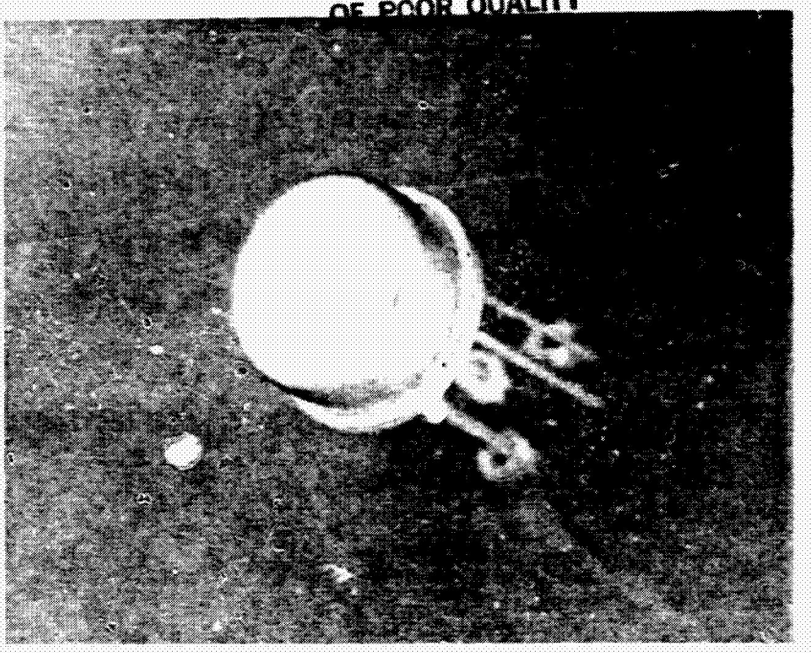

4X

(a) TOP VIEW

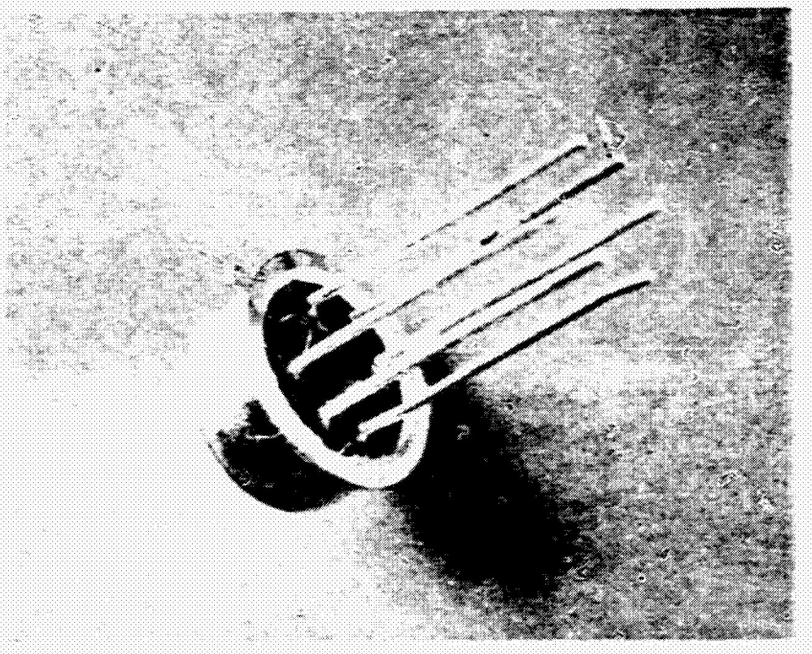

4X

(b) BOTTOM VIEW

FIGURE A14 - SPA-1830 PACKAGE

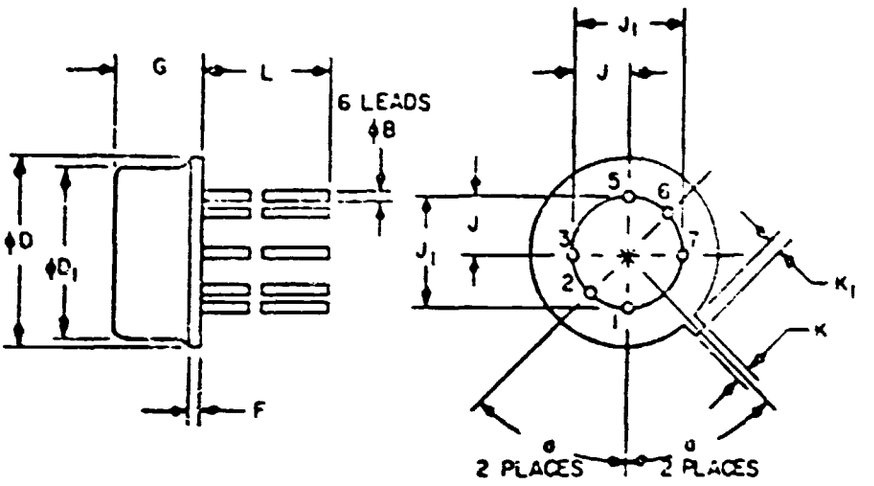

BOTTOM VIEW

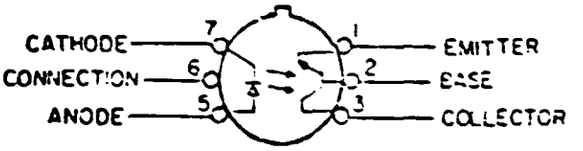

(Collector connected internally to case)

DIM	INCHES		MILLIMETERS		NOTES
	Min	Max	Min	Max	
ØD	.335	.370	8.51	9.40	
ØD1	.305	.335	7.75	8.51	
ØB	.016	.019	.406	.483	
α	45° T.P.		45° T.P.		1
F	---	.040	---	1.02	
G	.155	.185	3.94	4.70	
J	.100T.P.		2.54T.P.		1
J1	.200T.P.		5.08T.P.		1
K	.028	.034	.71	.86	
K1	.029	.045	.74	1.14	
L	.500	.600	12.70	15.40	

NOTES:
1. T.P. designates true position. Leads having maximum diameter (.019") measured in gaging plane .054" +.001" -.000" below the seating plane of the device shall be within .007" of their true position relative to a maximum width tab.

FIGURE A15 - PACKAGE DIMENSIONS

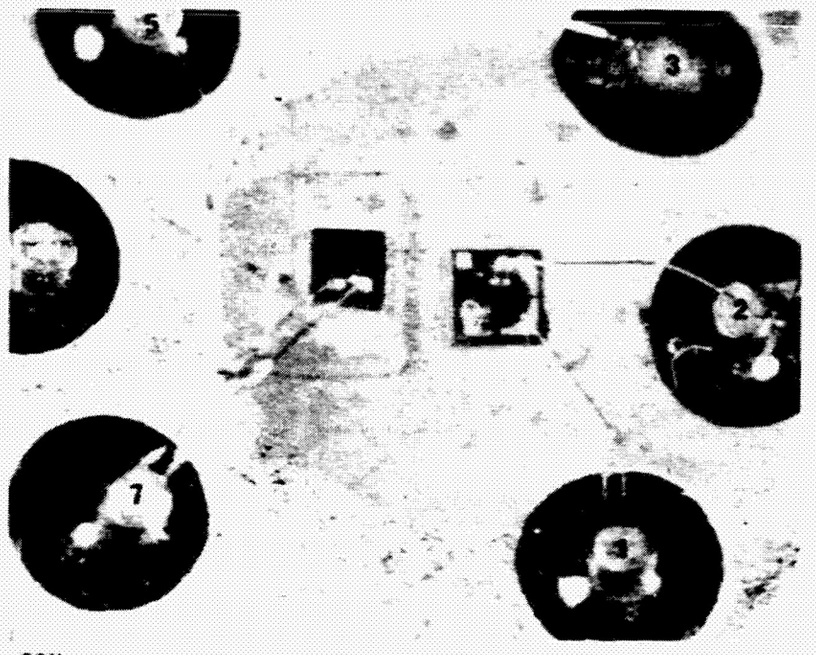

20X

FIGURE A16 - INTERNAL GEOMETRY

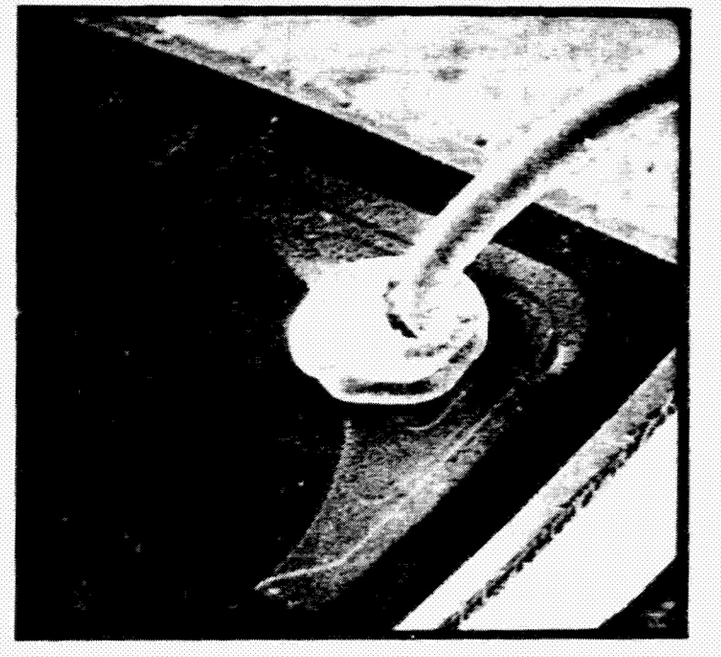

475X

FIGURE A17 - SEM PHOTO OF THE TRANSISTOR EMITTER BOND

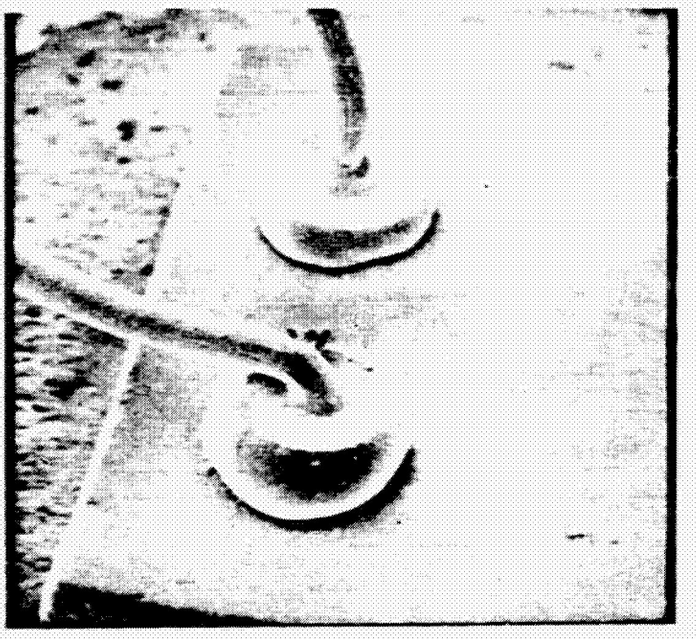

475X

FIGURE A18 - SEM PHOTO OF THE LED CATHODE BONDS

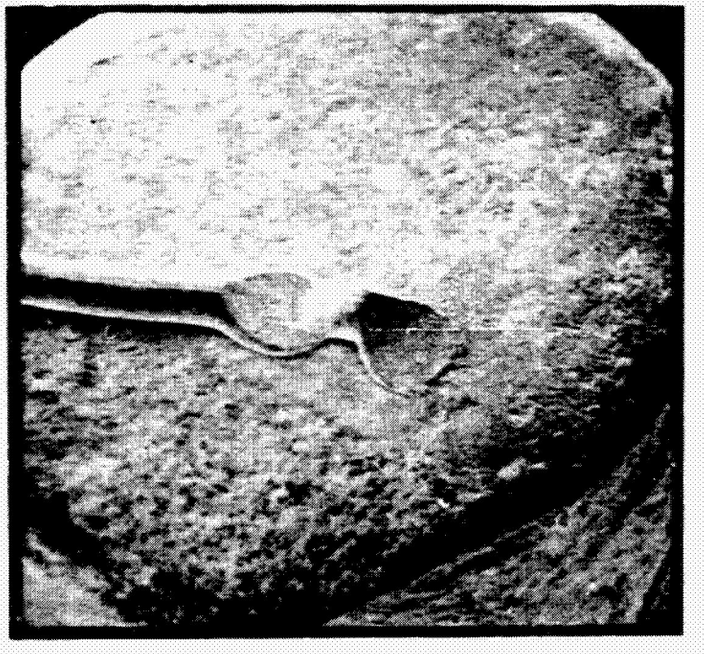

475X

FIGURE A19 - SEM PHOTO OF A POST BOND

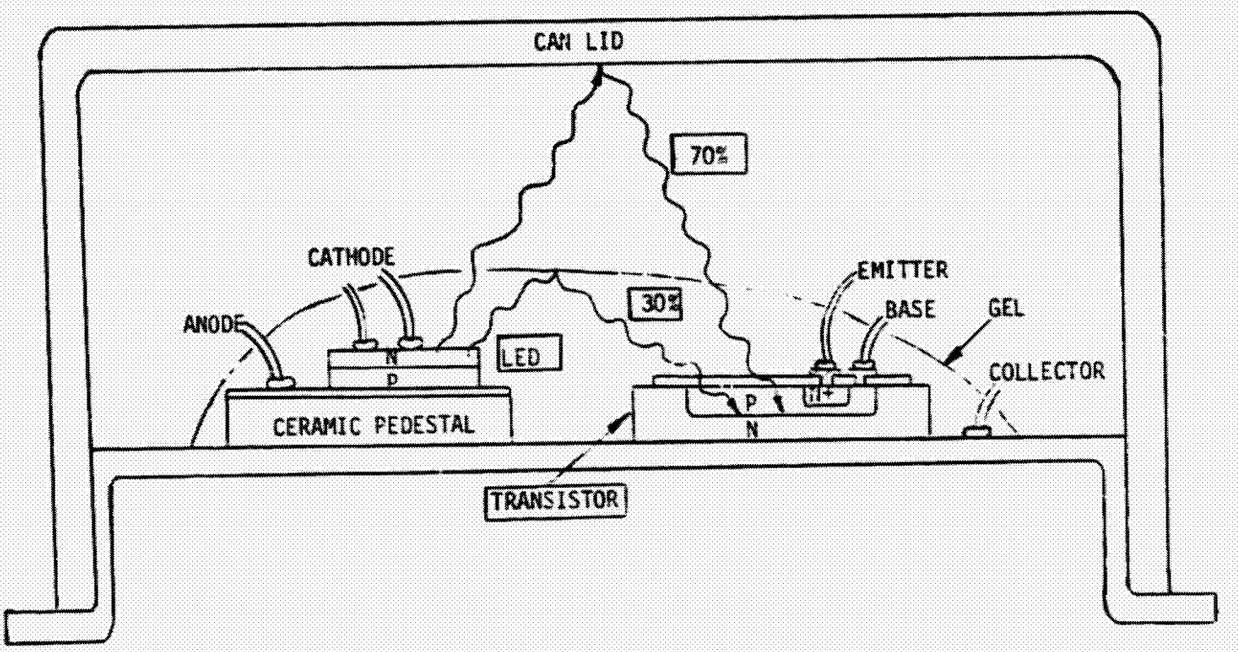

FIGURE A20 - CROSS-SECTIONAL SKETCH (NOT TO SCALE) OF THE DEVICE

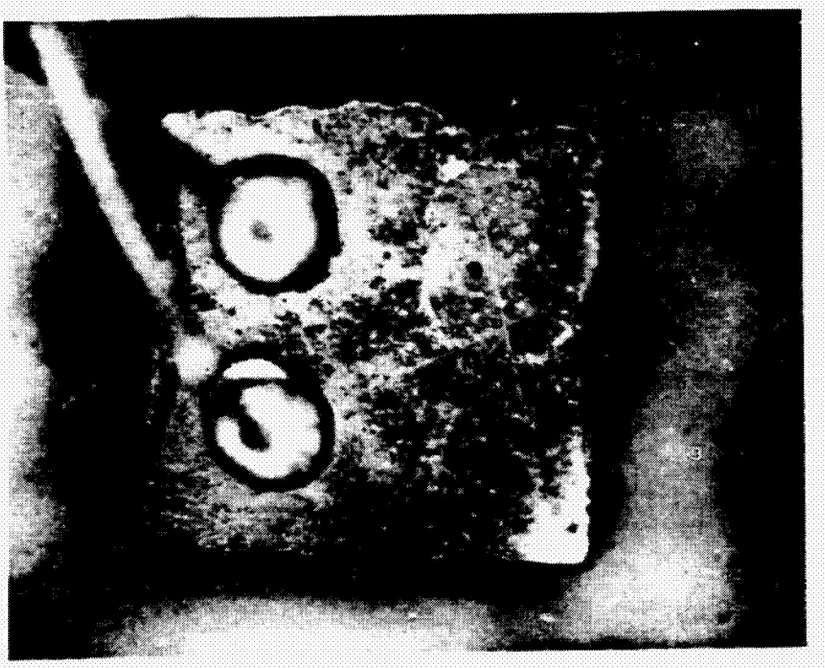

132X

FIGURE A21 - LED CHIP

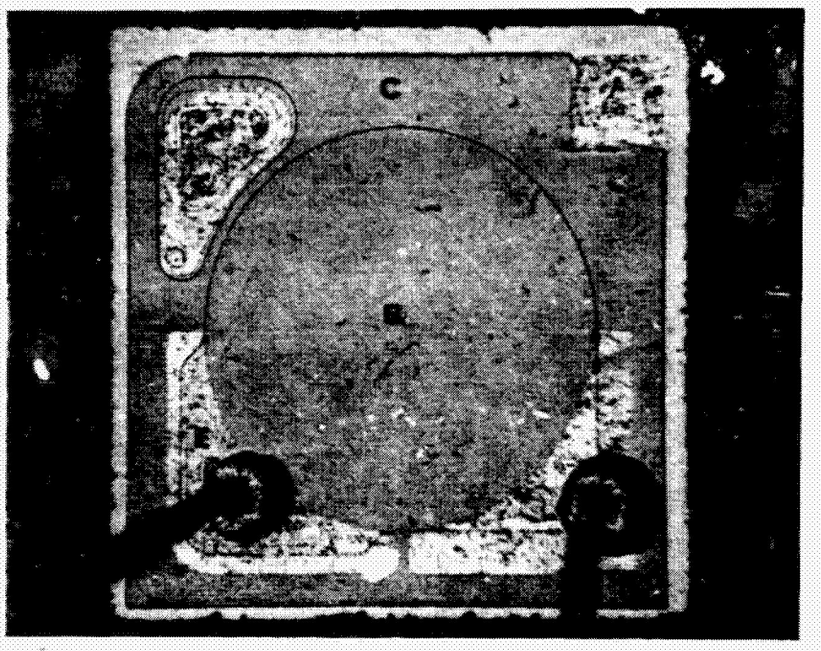

132X

FIGURE A22 - PHOTOTRANSISTOR CHIP

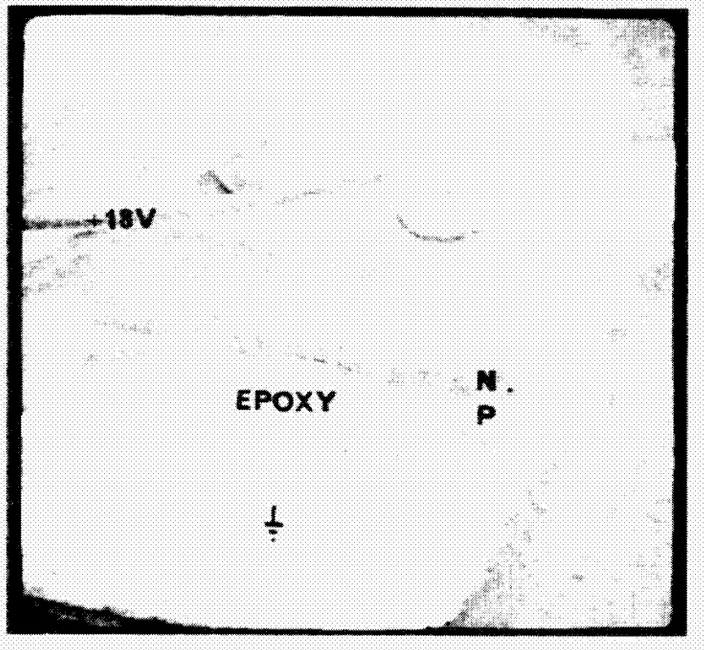

95X

FIGURE A23 - SEM VOLTAGE CONTRAST (TO IDENTIFY THE LOCATION OF THE P-N JUNCTION) PHOTO OF THE INTERMITTENT LED OF S/N 14 SHOWING THAT THE SILVER EPOXY OVERLAPS THE JUNCTION.

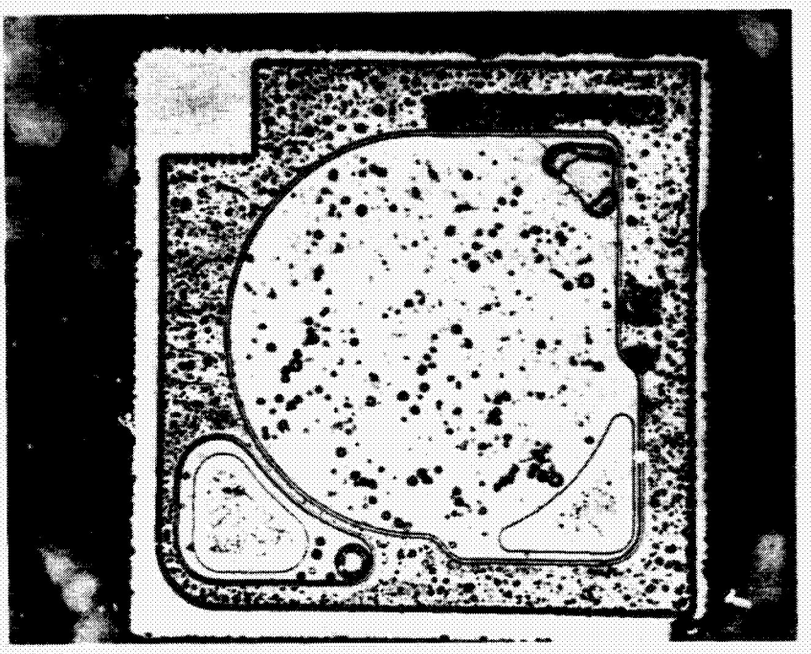

132X

FIGURE A24 - PHOTOTRANSISTOR CHIP OF S/N 34 AFTER SILICONE ETCH (SIRTL) SHOWING CRYSTALLOGRAPHIC DEFECTS

APPENDIX A3

CONSTRUCTION ANALYSIS

OPTRON - OPI 1123

OPTICAL COUPLER

S/N's 982 AND 983

CONSTRUCTION DETAILS
OPTRON OPI 1123 OPTICAL COUPLER
S/N's 982 AND 983 DATE CODE 7502

A. PACKAGE

1. Type: Modified (6 Pin) TO-5 Type can - Figure A25
2. Dimensions: Conforms to Figure A26
3. Weight: 0.87 gram
4. Materials:
   a) Can: Kovar
   b) Header: Gold-Plated Kovar
   c) Leads: Gold-Plated Kovar (Internal & External)
5. Seal: Hermetic Weld + Glass

B. INTERNAL GEOMETRY - Figure A27

1. Interconnections:
   a) Type: Gold Wire
   b) Diameter: 1 mil
   c) Bonds:
      - Au/Al Thermocompression ball at the transistor chip - Figure A28
      - Au/Au Thermocompression ball at the LED chip - Figure A29
      - Au/Au Thermocompression ball at the gold pads
      - Au/Au Thermocompression wedge at the posts - Figure A30
2. Chips - Figures A31 and A32

	LED - Figure A33	Phototransistor - Figure A34
Type:	GaAs, Liquid Phase Epi	Silicon Planar
Dimensions:	11.4 X 9.5 X 5.8 mils	40 X 40 X 6.5 mils
Scribe Type:	Mechanical	Mechanical
Chip Attach:	Gold-Ge Eutectic (chips are attached to deposited gold mil ceramic pedestal)	Silver Epoxy pads on a header mounted 79 X 73
Passivation:	None	SiO_2/Silicon Nitride
Metallization	Au Alloy	Aluminum
Glassivation:	None	None
Coupling Medium:	Dow Corning R6104 Silicone Resin	

3. Quality of Workmanship: Fair

   a) The LED of S/N 982 contained a bond on top of an aborted bond as shown in Figure A35.

   b) The LED gold bonding pad of both units is smaller than the thermocompression ball (no sign of a pad is visible in the optical on SEM photos). Thus the pads may be too small for adequate bond strength.

ORIGINAL PAGE IS
OF POOR QUALITY

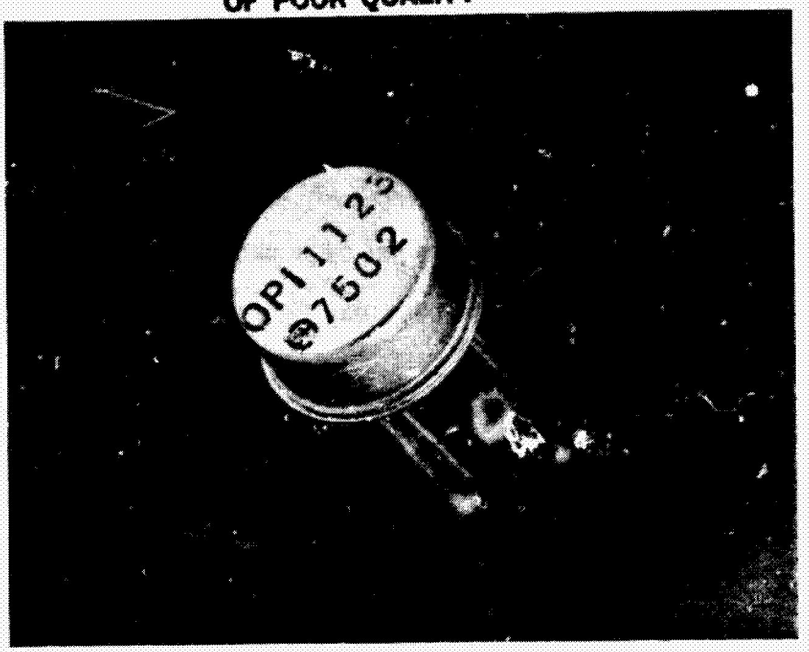

4X

(a) TCP VIEW

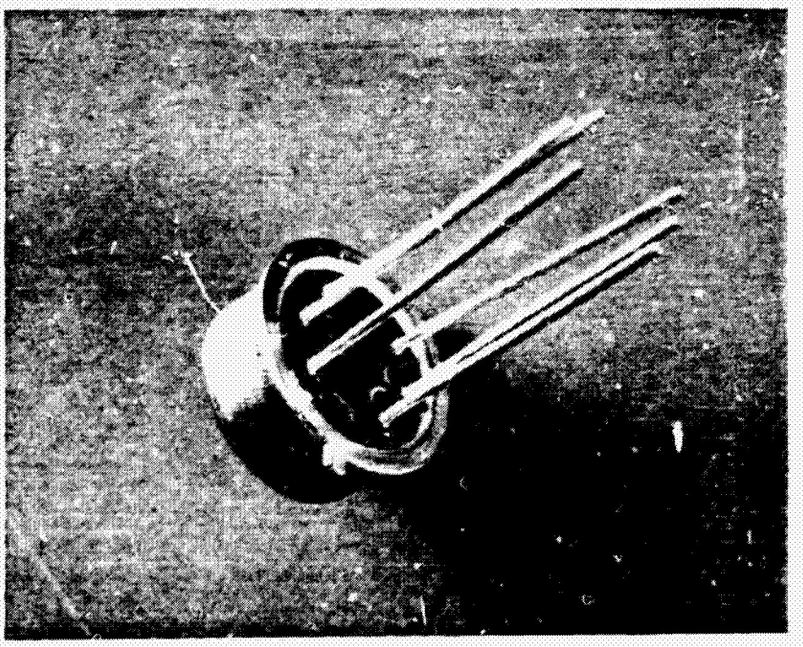

4X

(b) BOTTOM VIEW

FIGURE A25 - OPI 1123 PACKAGE

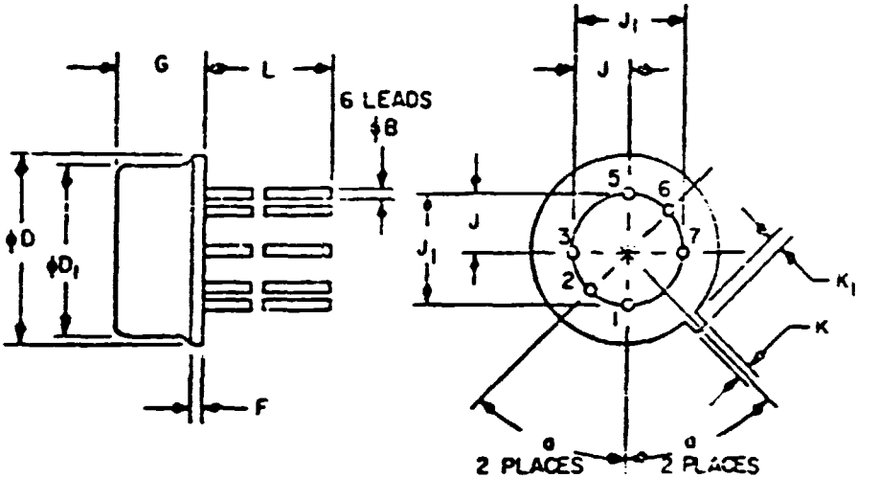

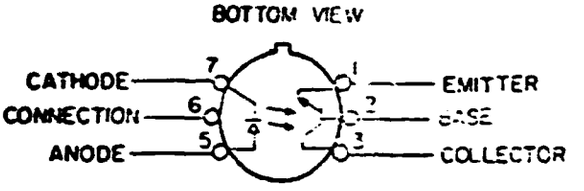

(Collector connected internally to case)

DIM	INCHES		MILLIMETERS		NOTES
	Min	Max	Min	Max	
ϕD	.335	.370	8.51	9.40	
ϕD_1	.305	.335	7.75	8.51	
ϕB	.016	.019	.406	.483	
a	45° T.P.		45° T.P.		1
F	---	.040	---	1.02	
G	.155	.185	3.94	4.70	
J	.100T.P.		2.54T.P.		1
J_1	.200T.P.		5.08T.P.		1
K	.028	.034	.71	.86	
K_1	.029	.045	.74	1.14	
L	.500	.600	12.70	15.40	

NOTES:
1. T.P. designates true position. Leads having maximum diameter (.019") measured in gaging plane .054" -.001" -.000" below the seating plane of the device shall be within .007" of their true position relative to a maximum width tab.

FIGURE A26 - PACKAGE DIMENSIONS

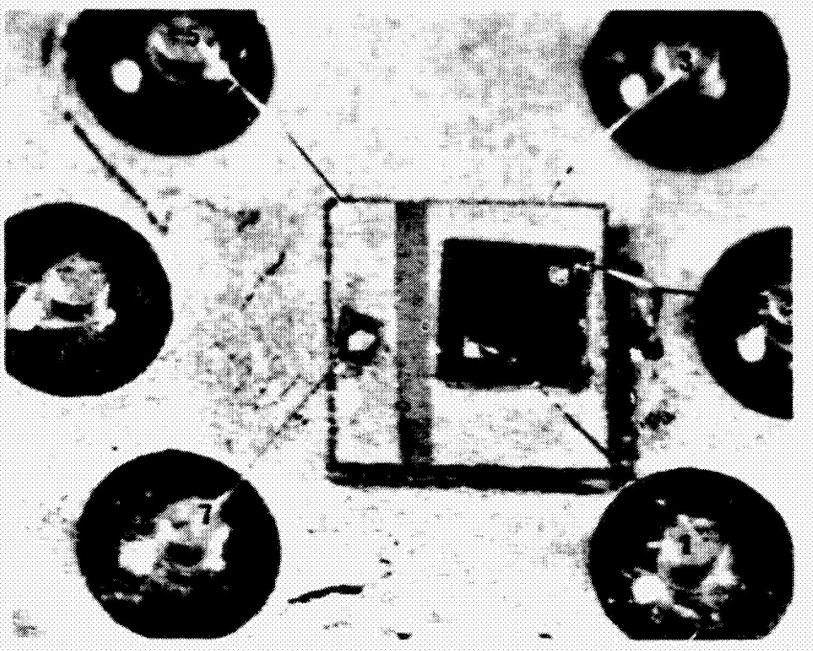

20X

FIGURE A27 - INTERNAL GEOMETRY

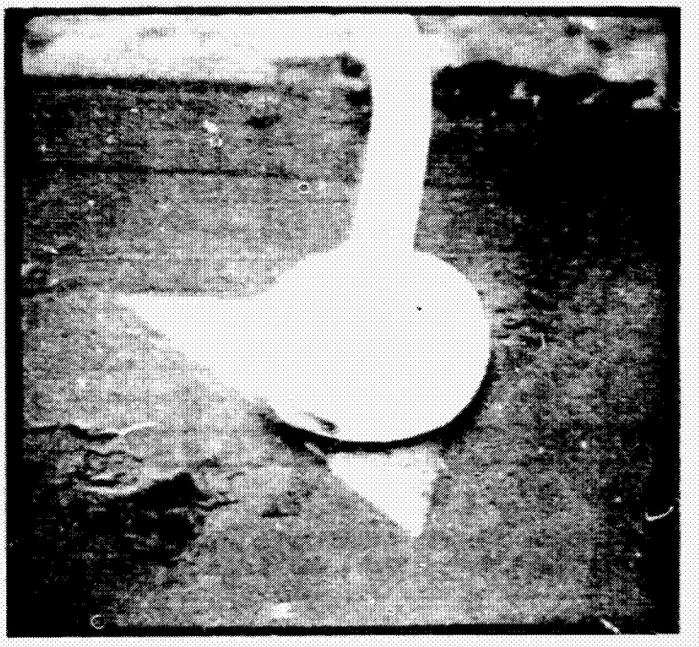

475X

FIGURE A28 - SEM PHOTO OF THE TRANSISTOR EMITTER BOND

475X

FIGURE A29 - SEM PHOTO OF THE LED CATHODE BOND

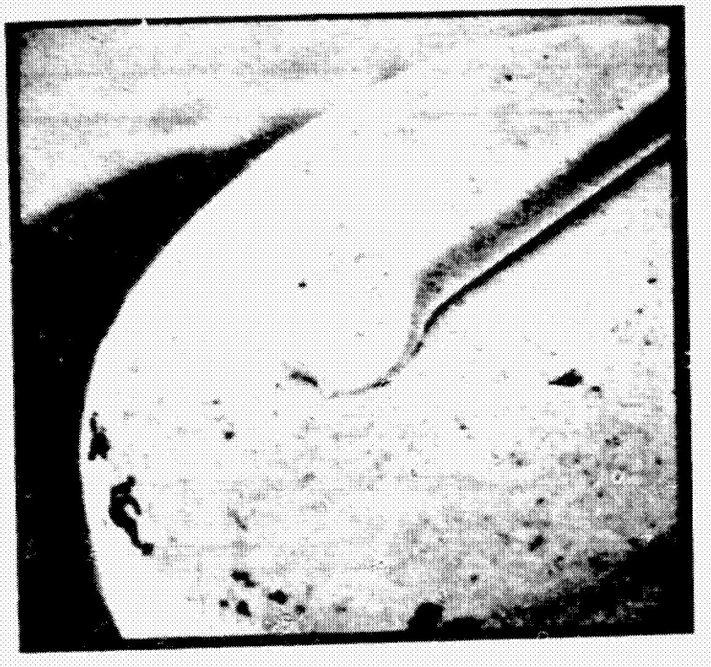

475X

FIGURE A30 - SEM PHOTO OF A POST BOND

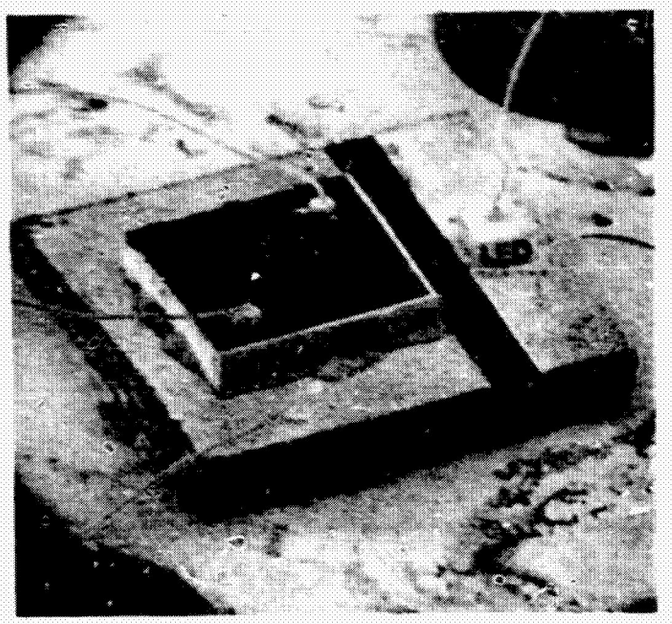

40X

FIGURE A31 - SEM PHOTO OF THE CHIP LAYOUT

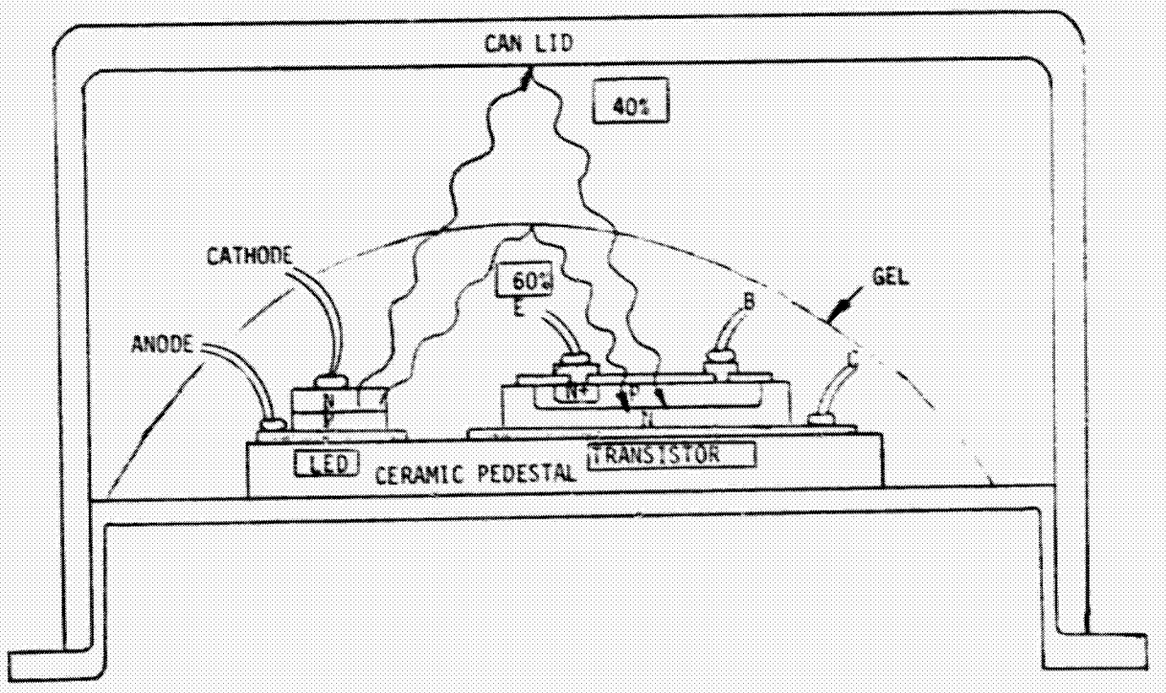

FIGURE A32 - CROSS-SECTIONAL SKETCH (NOT TO SCALE) OF THE DEVICE

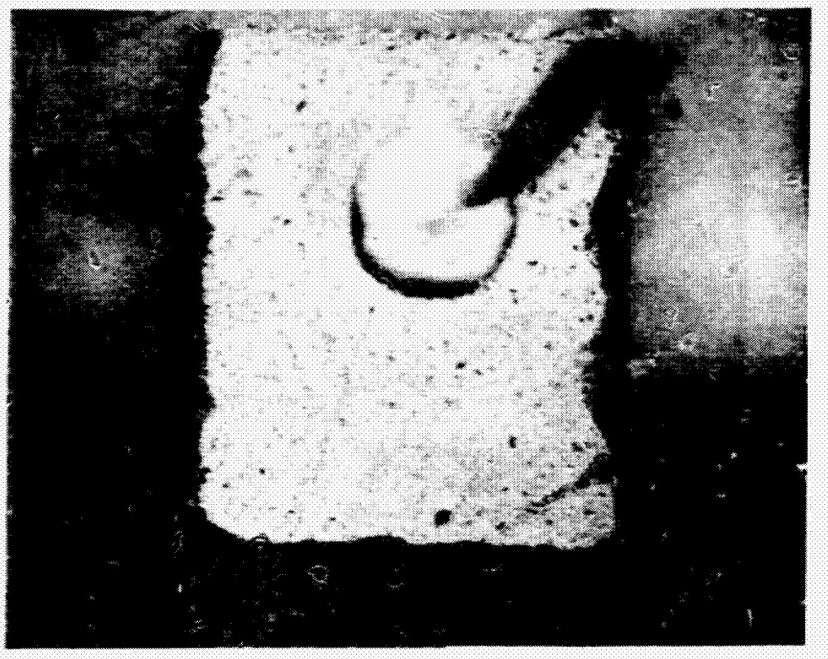

132X

FIGURE A33 - LED CHIP

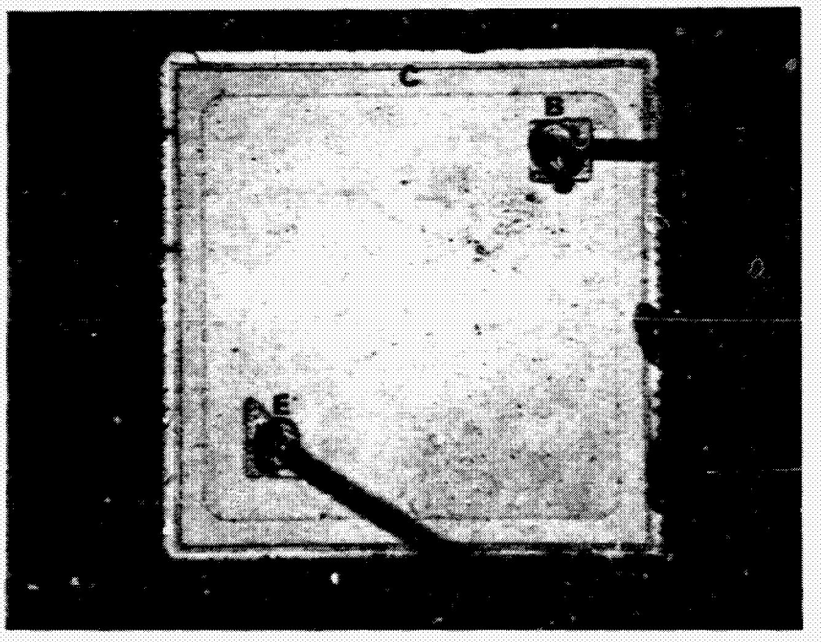

70X

FIGURE A34 - PHOTOTRANSISTOR CHIP

475X

FIGURE A35 - SEM PHOTO OF THE DOUBLE BOND ON THE LED OF S/N 982.

APPENDIX A4

CONSTRUCTION ANALYSIS

HEWLETT PACKARD 4365

DUAL CHANNEL OPTICALLY COUPLED ISOLATOR

S/N's 11 & 12

CONSTRUCTION DETAILS
HEWLETT PACKARD 4365 DUAL CHANNEL OPTICALLY COUPLED ISOLATOR
S/N's 11 AND 12 DATE CODE 605

A. PACKAGE

1. Type: 16-Pin Dual In-Line Ceramic - Figure A36
2. Weight: 1.28 grams
3. Materials:
   a) Case: Ceramic
   b) Lid: Gold-Plated Kovar
   c) Leads: Gold-Plated Kovar (external)
      Gold-Plated Deposited Refractory Metal (Internal)
4. Seal: Hermetic Solder Seal

B. INTERNAL GEOMETRY - Figures A37 & A38

1. Interconnections:
   a) Type: Gold Wire
   b) Diameter: 1 mil
   c) Bonds:
      - o Au/Al Thermocompression ball at the chips - Figure A39
      - o Au/Au Thermocompression wedge at the lead frame and header - Figure A40
2. Chips - Figures A41, A42 and A43

	LED - FIGURE A44	PHOTON DETECTOR - FIGURE A45
Type:	GaAs Planar	Silicon Planar
Dimensions:	15 X 28 mils	36 X 43 mils
Scribe Type:	Mechanical	Laser
Chip Attach:	Au Eutectic	Au Eutectic
Passivation:	SiO_2	SiO_2
Metallization:	Aluminum	Aluminum
Glassivation:	None	SiO_2
Coupling Medium and Overcoating:	Dow Corning R6104 Silicone Resin	

3. Quality of Workmanship and Processing: Good

One unusual anomaly was noted: Both of the pin 10 (ground) ball bonds of S/N 11 were collapsed as illustrated in Figure A46. It appeared that the bonds slid across the pad during cool-down, dragging gold out of the then molten interior of the ball.

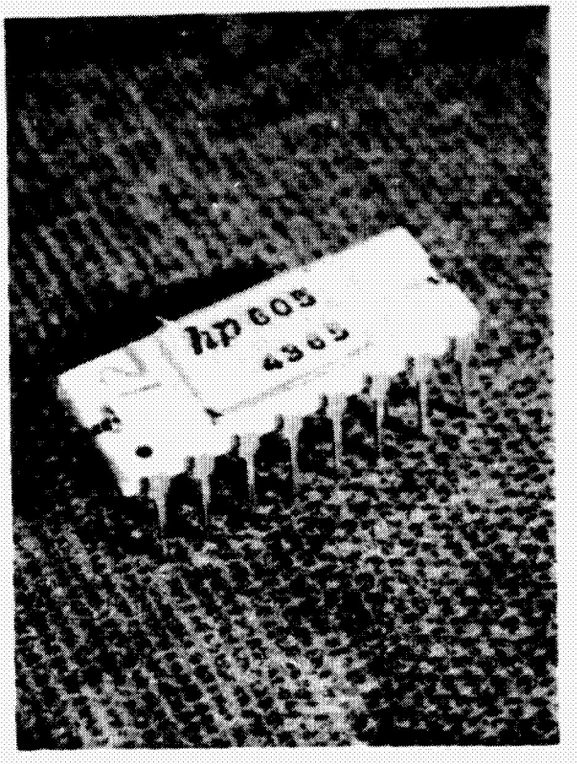

2.5X

FIGURE A36 - HEWLETT PACKARD 4365 PACKAGE

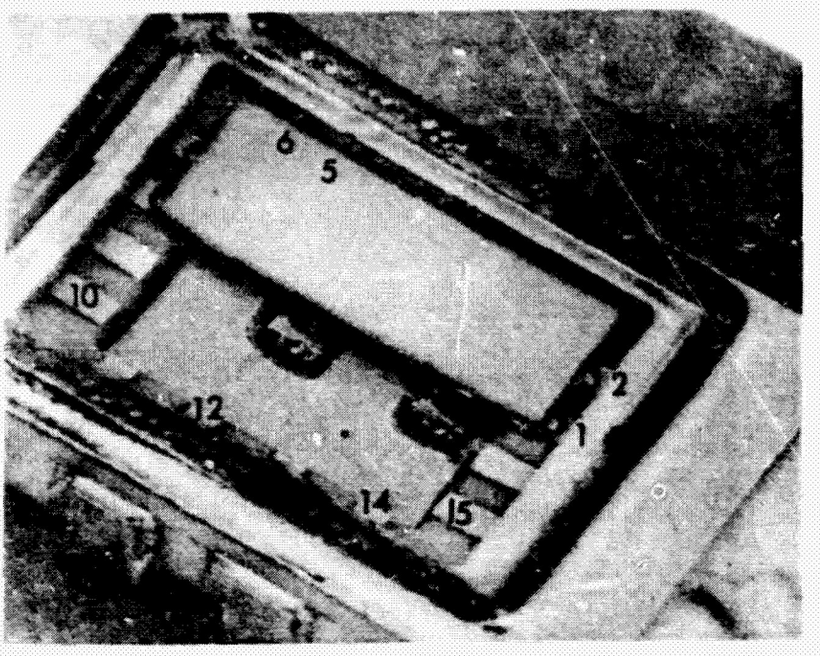

10X

FIGURE A37 - INTERNAL GEOMETRY

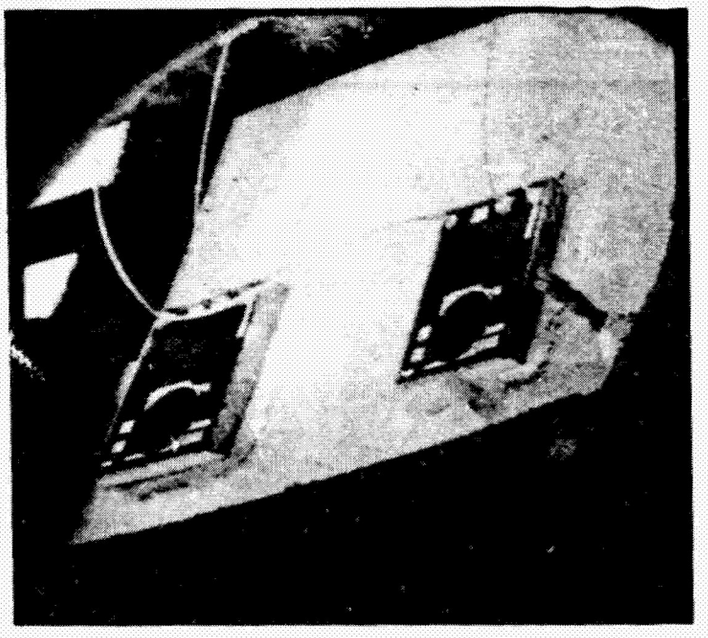

20X

FIGURE A38 - SEM PHOTO OF INTERNAL GEOMETRY AFTER REMOVAL OF THE R6104 AND THE LED SUBSTRATE

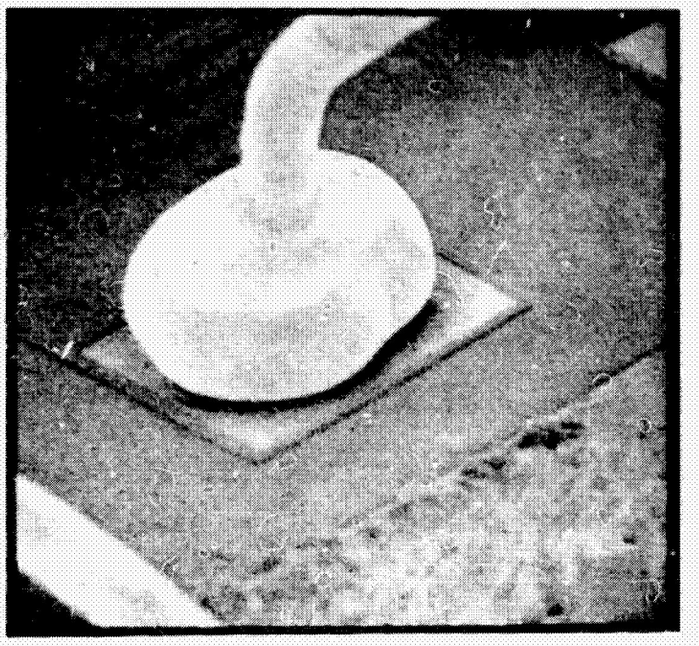

300X

FIGURE A39 - SEM PHOTO OF A WIRE BOND AT THE DIE

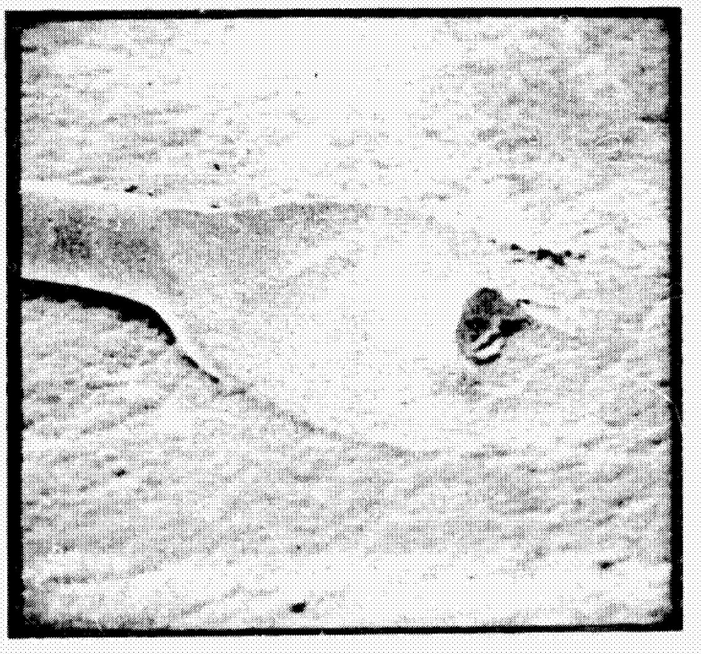

400X

FIGURE A40 - SEM PHOTO OF A WIRE BOND AT THE LEAD FRAME

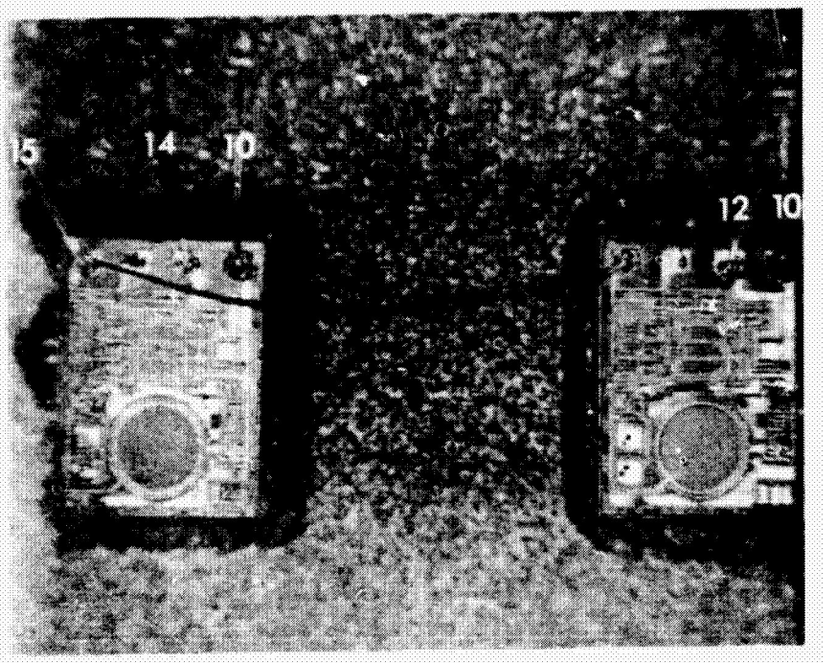

30X

FIGURE A41 - PHOTON DETECTOR CHIPS

30X

FIGURE A42 - LED CHIPS ON CERAMIC SUBSTRATE

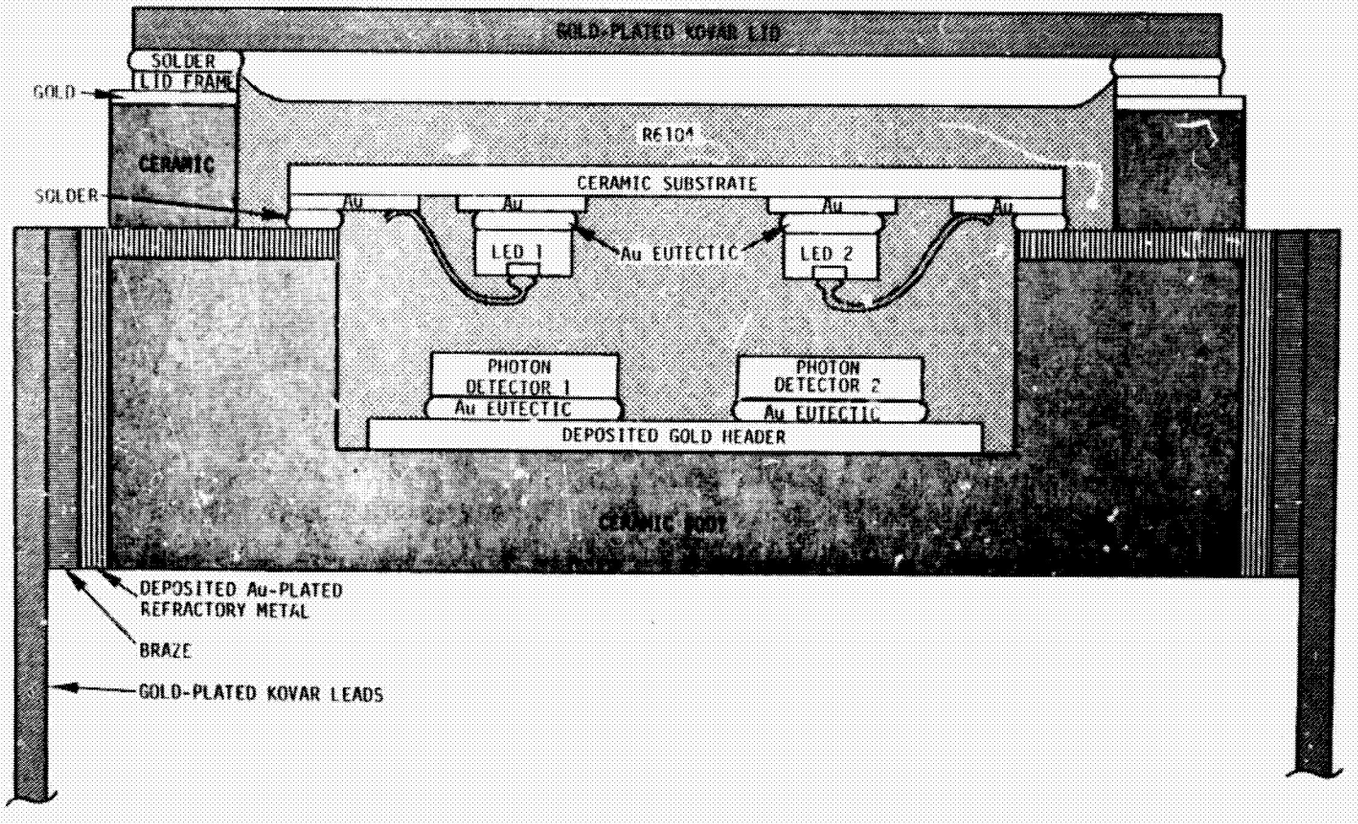

FIGURE A43 - CROSS-SECTIONAL SKETCH (NOT TO SCALE) OF THE HP 4365

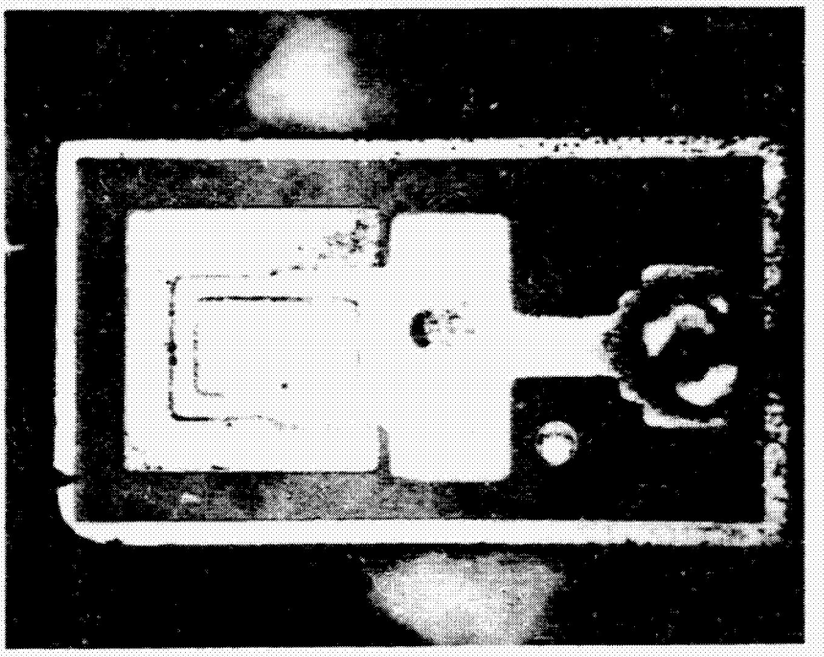

130X

FIGURE A44 - LED CHIP

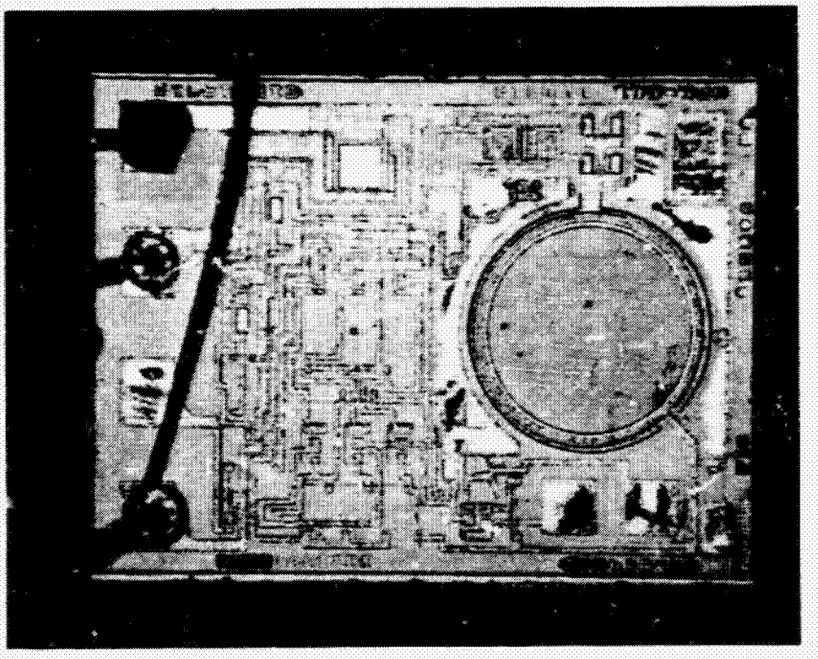

70X

FIGURE A45 - PHOTON DETECTOR CHIP

500X

FIGURE A46 - SEM PHOTO OF ONE OF THE PIN 10 BALL BONDS OF S/N 11

APPENDIX A5

CONSTRUCTION ANALYSIS

RCA SG1009A LED

S/Ns 1732 AND 1651

CONSTRUCTION DETAILS
RCA SG1C09A LED
S/Ns 1732 AND 1651

A. PACKAGE

1. Type: RCA OP-17 Figure A47
   (modified TO-18, 2 leads with window)
2. Weight: 0.27 gram
3. Materials:
   a) Can: Gold Plated Kovar
   b) Header: Gold Plated Steel
   c) Leads: Gold Plated Kovar
   d) Lens: Corning 7052 glass or equivalent
4. Seal: Hermetically sealed welded case

B. INTERNAL GEOMETRY - Figure A48

1. Interconnections:
   a) Type: Gold Wire
   b) Diameter: 0.9 mil
   c) Bonds:
      - o Au/Au Thermocompression Ball At The Chip - Figure A49
      - o Au/Au Thermocompression Stitch At The Post - Figure A50
      - o Pull Strenth - 3.7 gms
2. Chip - Figure A51

   Type: GaAs, Liquid Phase Epi
   Dimensions: 16 x 16 x 9 mils
   Scribe Type: Mechanical
   Chip Attach: Silver Epoxy
   Passivation: Silicon Oxide
   Metallization: Au
   Glassivation: None
   Overcoating: None
3. Quality of Workmanship and Processing: Poor
   a) The ball bonds at the chip were excessively deformed, particularly that of S/N 1732 as shown in Figure A52. This was caused by the formation of an undersized ball during flame-off and can result in low bond strength.

b) The stitch bond at the post of S/N 1732 was torn, as shown in Figure A53, during tool lift-off or pigtail removal. Also the bond had overlapped into the rough, unpolished area of the top of the post. These factors would tend to reduce the bond strength.

c) Incorsistencies in chip surface treatments or preparation were evident. The top and sides of the chip of S/N 1732 were smooth, as can be seen in Figure A51, whereas the surfaces of the chip of S/N 1651 were rough and irregular as shown in Figure A54. The surface of S/N 1732 may have been etched smooth as indicated by the undercutting of the metallization evident in Figure A51.

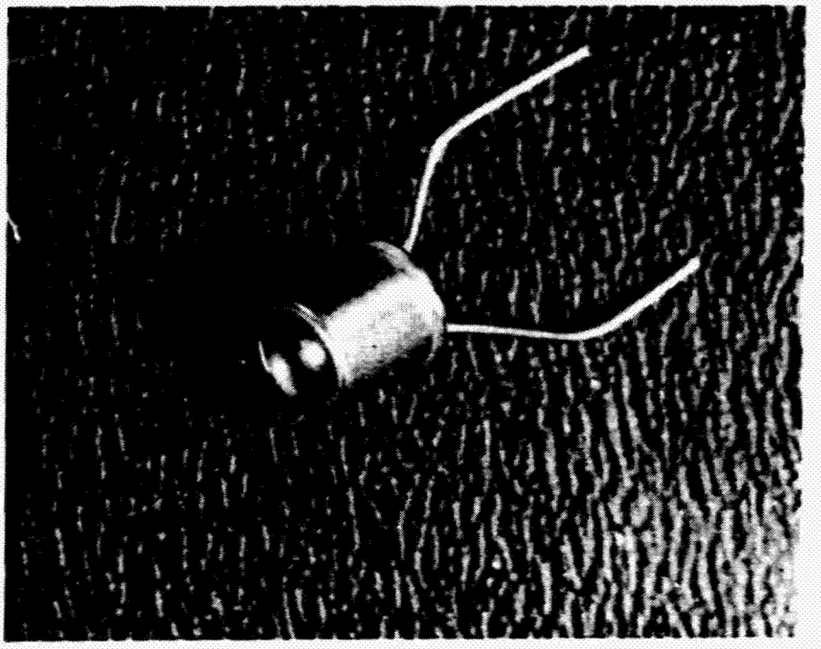

4X

(a) TOP VIEW

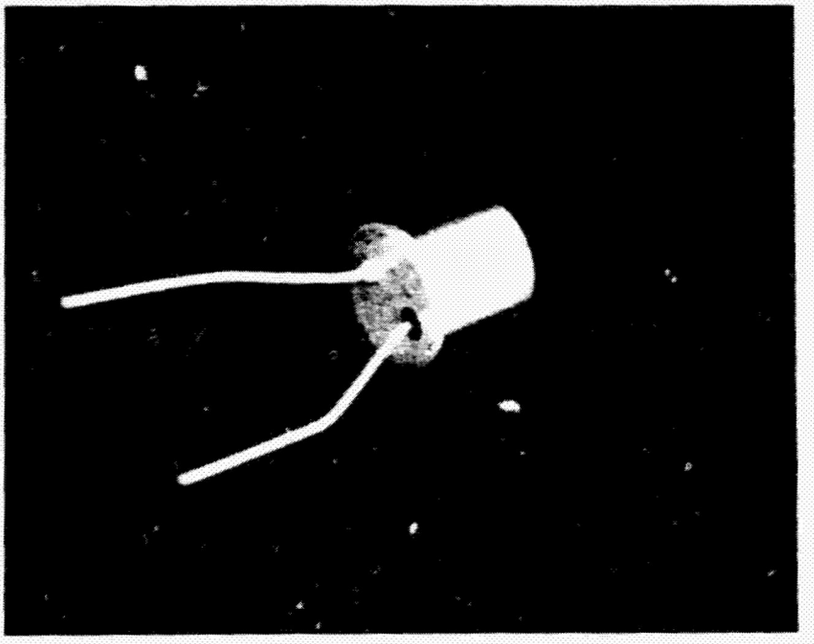

4X

(b) BOTTOM VIEW

FIGURE A47 - RCA SG1009A PACKAGE

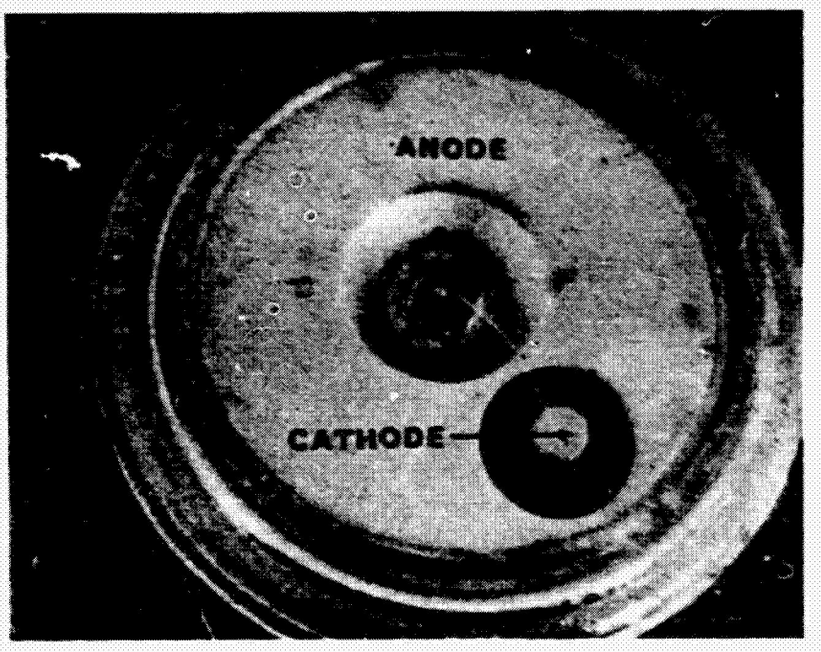

18X

FIGURE A48 - INTERNAL GEOMETRY

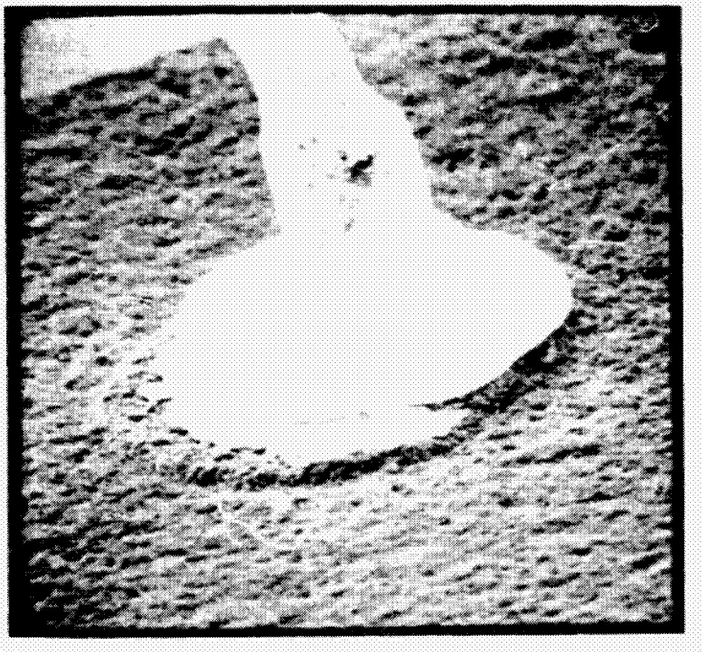

625X S/N 1651

FIGURE A49 - SEM PHOTO OF THE WIRE BOND AT THE CHIP

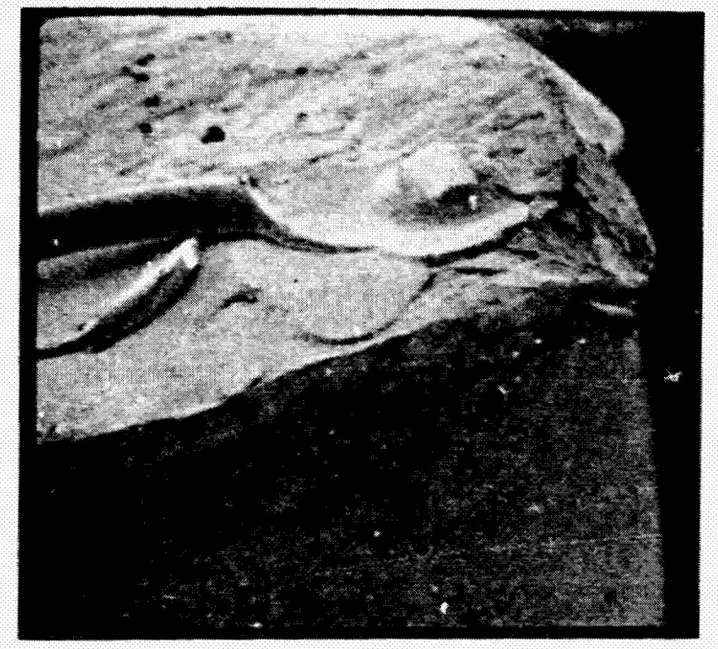

475X S/N 1651

FIGURE A50 - SEM PHOTO OF THE WIRE BOND AT THE POST

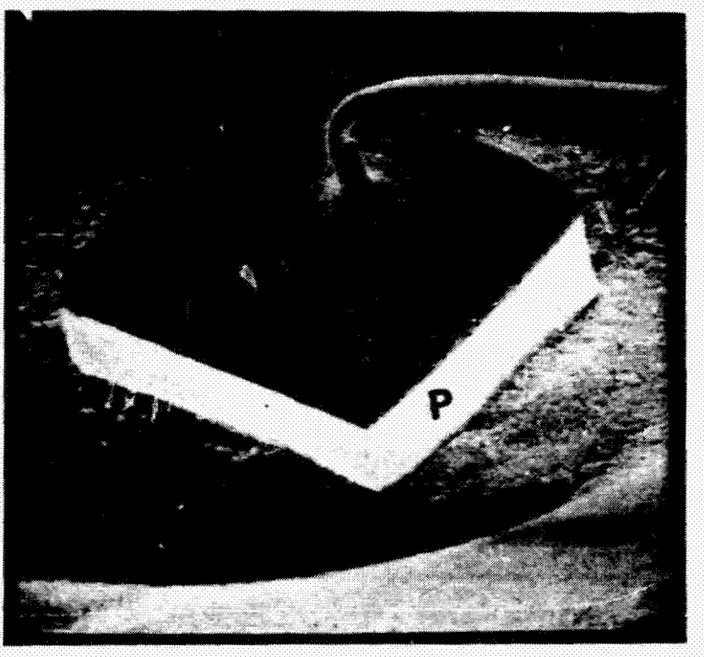

125X S/N 1732

FIGURE A51 - SEM VOLTAGE CONTRAST (TO SHOW THE LOCATION OF THE JUNCTION) PHOTO OF THE LED CHIP.

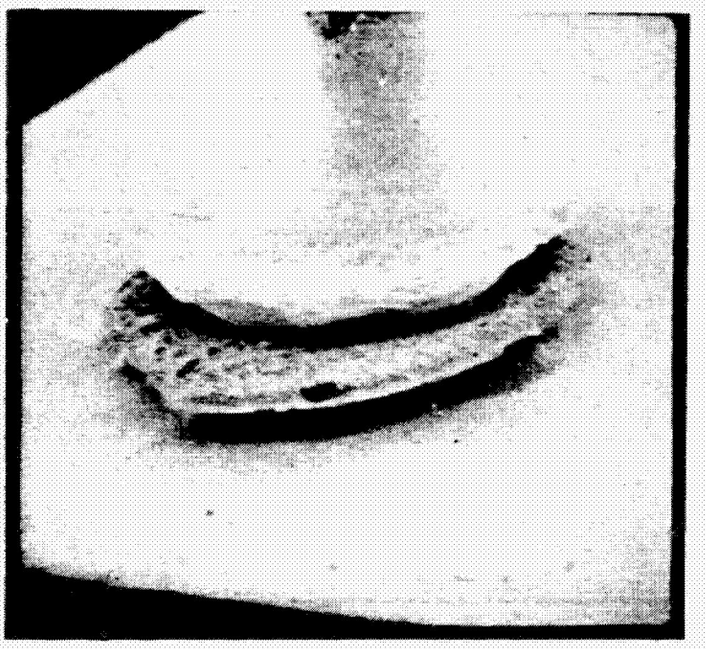

700X S/N 1732

FIGURE A52 - SEM PHOTO OF UNDERSIZED BALL BOND AT THE CHIP

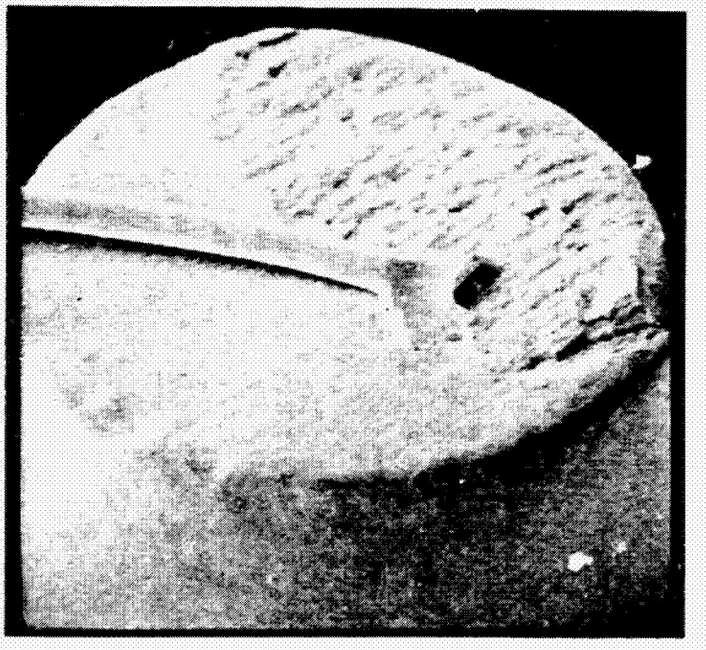

250X S/N 1732

FIGURE A53 - SEM PHOTO OF THE POOR STITCH BOND AT THE POST

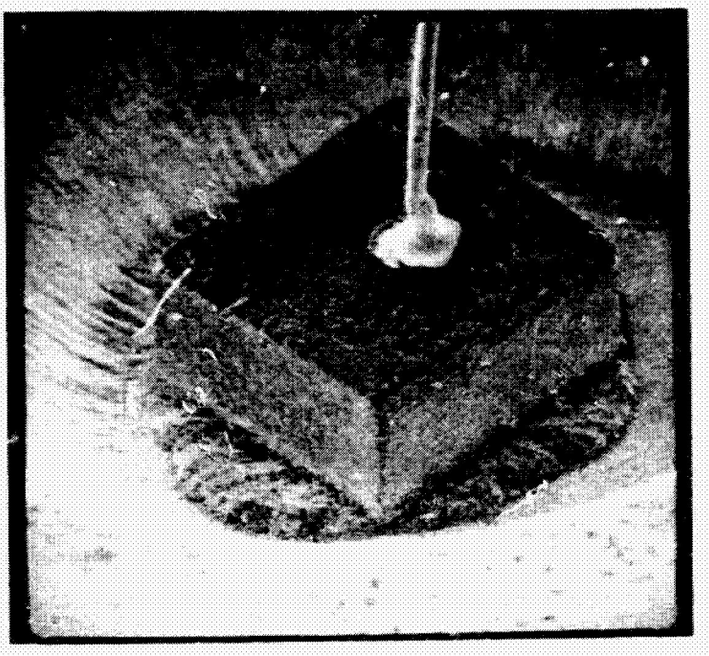

100X S/N 1651

FIGURE A54 - LED CHIP OF S/N 1651

APPENDIX A6

CONSTRUCTION ANALYSIS

TEXAS INSTRUMENTS SL1466 LED

S/N 1731 & 1732

CONSTRUCTION DETAILS
TEXAS INSTRUMENTS SL1466 LED
S/Ns 1731 & 1732

A. PACKAGE

1. Type: JEDEC TO-18 with window. Figure A55.
2. Weight: 0.3 gram
3. Materials:
   a) Can: Gold-Plated Kovar
   b) Header: Gold-Plated Kovar
   c) Leads: Gold-Plated Kovar (External & Internal)
   d) Lens: Corning 7052 glass or equivalent
4. Seal: Hermetically sealed welded case

B. INTERNAL GEOMETRY - Figure A56

1. Interconnections:
   a) Type: Gold Wire
   b) Diameter: 0.9 mil
   c) Bonds:
      - o Au/Au Thermocompression ball at the chip - Figure A57
      - o Au/Au Thermocompression wedge at the post - Figure A58
      - o Pull Strength - 5.0 gms
2. Chip - Figure A59

   Type: GaAs, Liquid Phase Epi
   Dimensions: 15 x 15 x 15 mils
   Scribe Type: Mechanical
   Chip Attach: Gold-bearing Eutectic to Au Deposited Backside.
   Passivation: Proprietary
   Metallization: AuSn
   Glassivation: None
   Overcoating: None
3. Quality of Workmanship & Processing: Fair
   - o The surface of the chip of S/N 1731 was contaminated with splotches of residue as shown in Figure A60. (The residue also appears in Figure A57.)

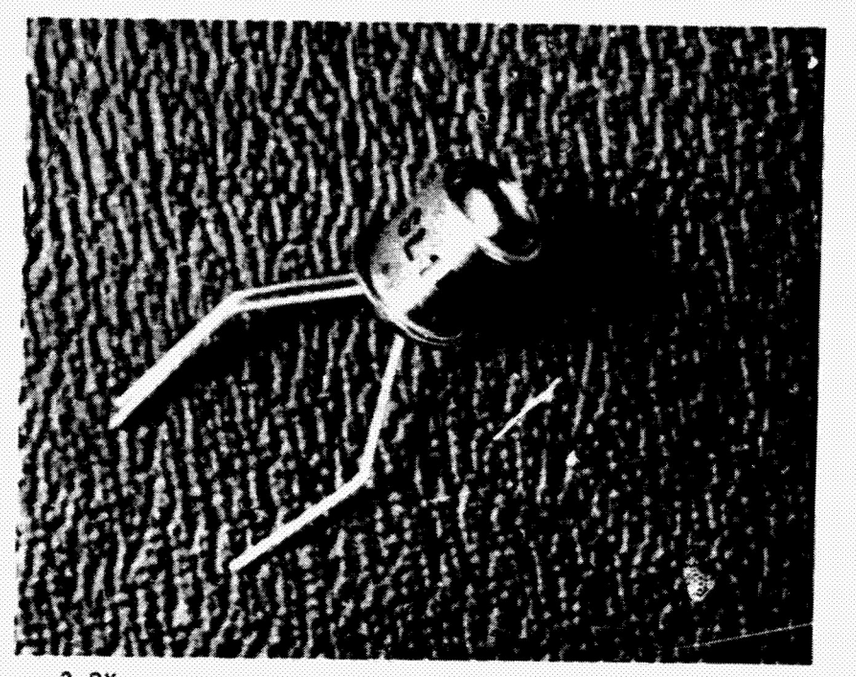

3.8X

(a) TOP VIEW

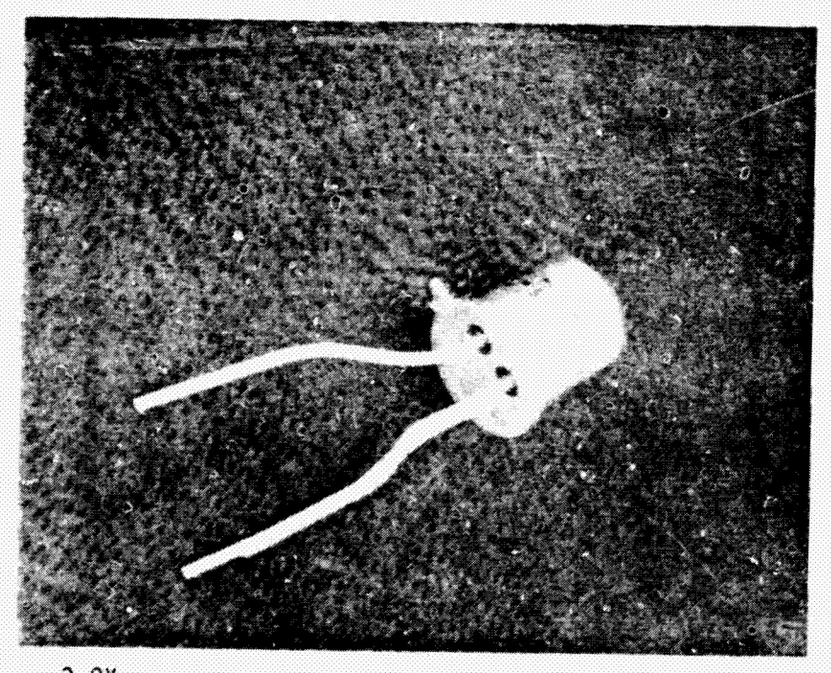

3.8X

(b) BOTTOM VIEW

FIGURE A55 - TEXAS INSTRUMENTS SL1466 PACKAGE

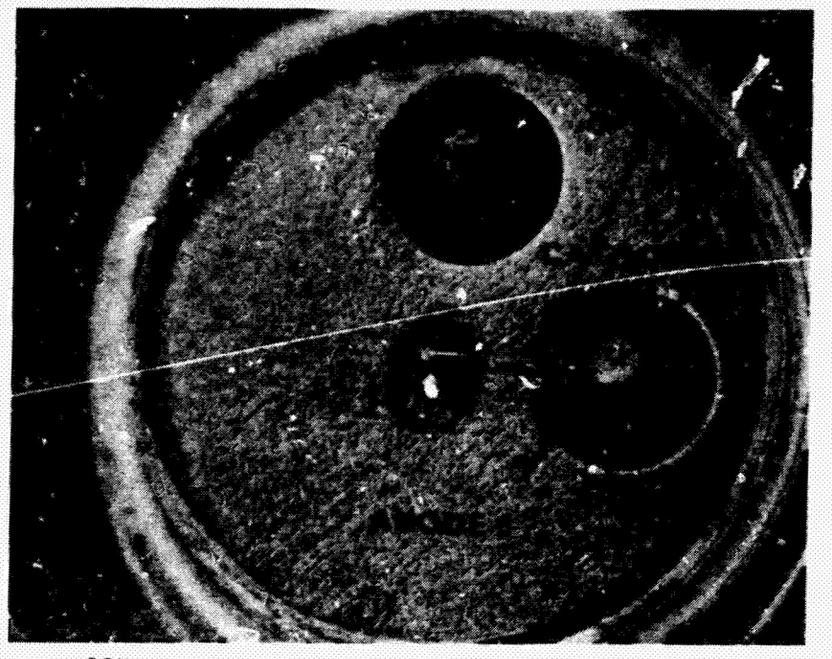

18X

FIGURE A56 - INTERNAL GEOMETRY

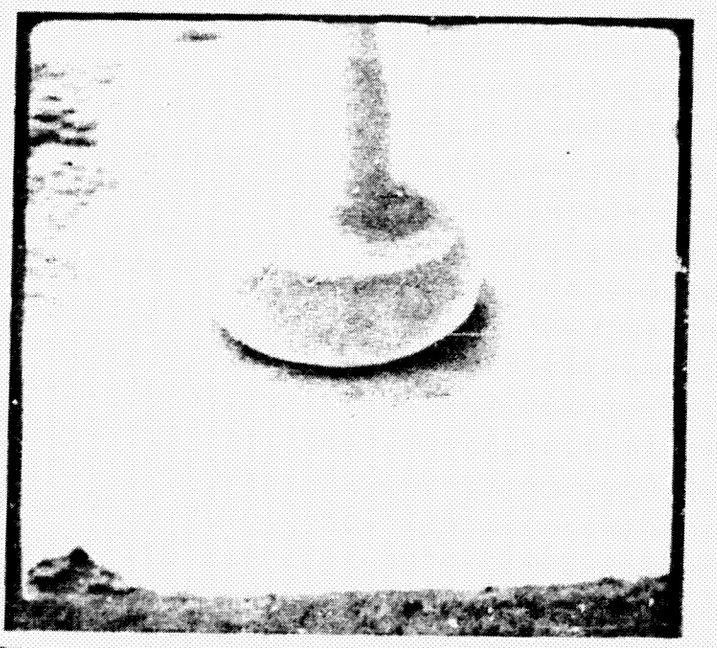

475X

FIGURE A57 - SEM PHOTO OF THE WIRE BOND AT THE CHIP

ORIGINAL PAGE IS
OF POOR QUALITY

457X

FIGURE A58 - SEM PHOTO OF THE WIRE BOND AT THE POST

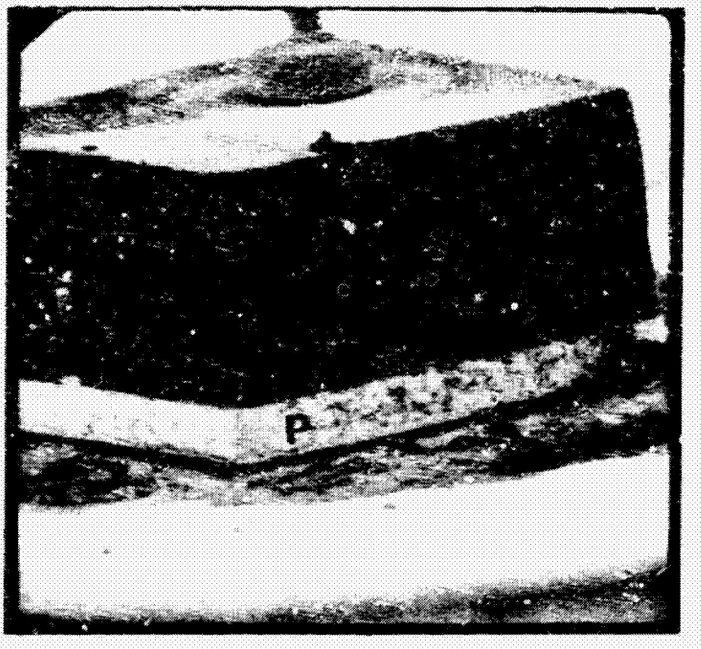

325X

FIGURE A59 - SEM VOLTAGE CONTRAST (TO SHOW THE LOCATION OF THE JUNCTION) PHOTO OF THE LED CHIP.

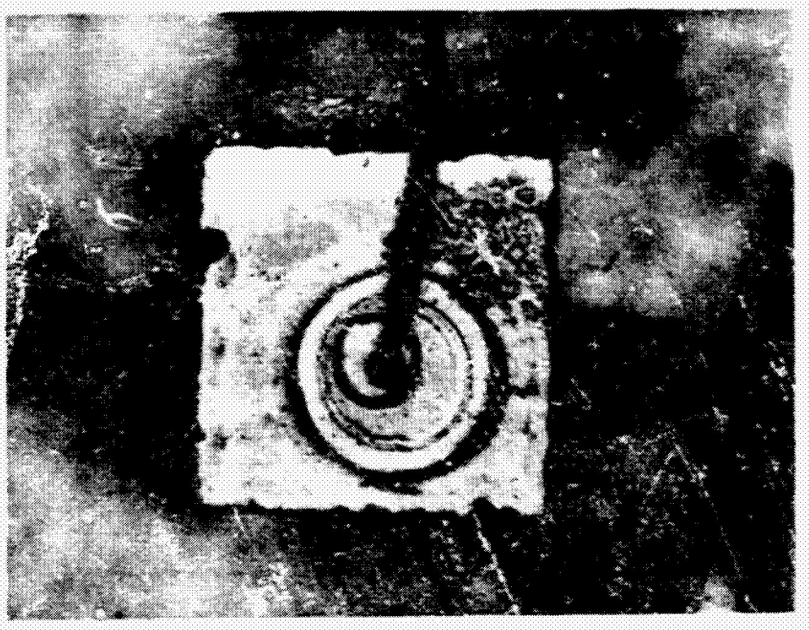

FIGURE A60 - CONTAMINATED CHIP OF S/N 1731

APPENDIX B

ELECTRICAL TEST CONDITIONS

APPENDIX B

ELECTRICAL TEST CONDITIONS

This appendix provides the electrical tests, the test conditions and end-point limits for all the devices used in the program. In addition, the electrical test groups, EM_a, EM_b, and EM_c, utilized during the program are defined.

The Type A opto-coupler tests, test conditions and end-point limits are provided in Table B1, while Figure B1 illustrates the test circuit used to measure switching times. Both the MIL-S-19500/486 limits and the NASA 85M03638 limits are included in Table 1 with the MIL-S-19500/486 limits being used as the pass/fail criteria.

The Type B opto-coupler tests, test conditions and end-point limits and the switching time test circuit are provided in Table B2 and Figure B2, respectively. The manufacturer's specification limits were used for all parameters except output rise and fall time and the various capacitances that were measured. These limits were established following an evaluation of the initial electrical test data.

Table B3 contains a list of the electrical tests, test conditions and limits used for the LEDs. The end-point limits were established either from one of the manufacturers' specification sheets or from evaluation of the initial data.

At various times during the program, different groups of these tests were performed on the devices. The EM_a electrical test group was comprised of dc parametric tests performed at 25°C, the EM_b group contained the same dc parametric tests performed at 125°C (100°C for Type A opto-couplers) and -55°C, and the EM_c group was the dynamic electrical tests performed at 25°C. Tables B4, B5 and B6 are cross references for the electrical test groups for Type A opto-couplers, Type B opto-couplers and the LEDs.

TABLE B1. OPTO-COUPLER TEST CONDITIONS - TYPE A

SYMBOL	TEST NO.	PINS					MEASURE TERMINAL	MIL-STD-LIMITS						NASA LIMITS						UNITS	COMMENTS
								25°C		100°C		-55°C		25°C		100°C		-55°C			
		1	2	3	5	7		MIN	MAX	MIN	MAX	MIN	MAX	MIN	MAX	MIN	MAX	MIN	MAX		
V_F	1				10ma	GND	5	0.8	1.3	0.7	1.2	1.0	1.5	---	1.3	---	1.2	---	1.4	VDC	
R_D	2				15ma	GND	5	---	---	---	---	---	---	---	5.0	---	---	---	---	Ω	$RD = \frac{(V_V @ 20ma) - (V_F @ 15ma)}{5ma}$
					20ma	GND	5														
I_R	3				-2Vdc	GND	5	---	100.0	---	---	---	---	---	10.0	---	100.0	---	---	μA	
BV_{CBO}	4		GND	100μa			3	35.0	---	---	---	---	---	35	---	---	---	---	---	VDC	
BV_{CEO}	5	GND		1.0ma			3	35.0	---	---	---	---	---	35	---	---	---	---	---	VDC	
BV_{EBO}	6	100μa	GND				3	4.0	---	---	---	---	---	4	---	---	---	---	---	VDC	
I_D	7	GND		20V			3	---	100.0	---	1.0E5	---	---	---	100.0	---	12000	---	---	na	
H_{FE}	8	GND	10μa	5Vdc				---	---	---	---	---	---	100.0	500.0	150.0	600.0	20.0	100.0	---	
T_R	9	GND		5V	10ma	GND	3	0.25	---	---	---	---	---	0.25	1.00	0.15	1.00	0.15	1.00	---	$TR = \frac{I}{10ma}$
V_{CES}	10	GND		2.5ma	20ma	GND	3	---	0.3	---	---	---	---	---	0.3	---	---	---	---	VDC	
C_{IN}	11							---	---	---	---	---	---	---	150.0	---	---	---	---	pf	See Note 2
C_{COUP}	12							---	5.0	---	---	---	---	---	3.0	---	---	---	---	pf	See Note 3
t_r	13							---	15.0	---	---	---	---	---	3.0	---	---	---	---	μs	See Note 4
t_f	14							---	15.0	---	---	---	---	---	3.0	---	---	---	---	μs	See Note 4
V_{ISO}	15							1000	---	---	---	---	---	1000.0	---	---	---	---	---	VDC	See Note 3
R_{ISO}	16							10"	---	---	---	---	---	10"	---	---	---	---	---	OHMS	See Note 3

Note 1. Pins not specified are left open.

Note 2. Input capacitance is measured with output terminals open.

Note 3. Isolation voltage, isolation resistance, and common mode coupling capacitance tests are made with the input terminals shorted together and the output terminals shorted together.

Note 4. For switching time test use circuit in Figure B1. The input waveform had the following characteristics: Z out = 50Ω, $t_r \leq 15$ ns, duty cycle ≤ 22, P_W = 100 μsec.

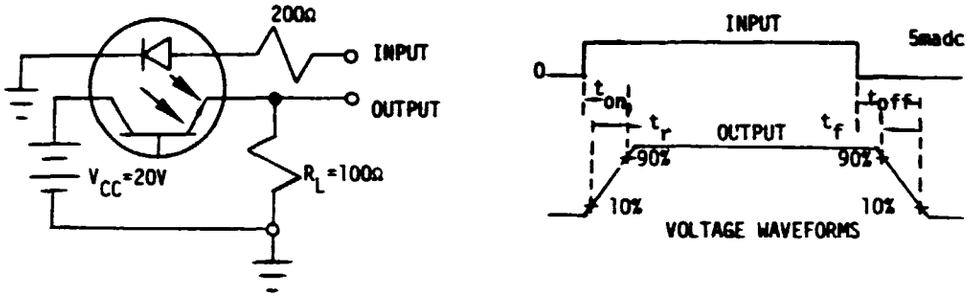

1. The input pulse was supplied with a pulse generator with the following characteristics:

   Z_{OUT}=50 ohms, $t_r \leq$15ns, duty cycle $\leq$ 2%, PW=100µsec.

FIGURE B1. OPTO-COUPLER TYPE A DYNAMIC TEST FIGURE

TABLE B2. OPTO-COUPLER TEST CONDITIONS - TYPE B

SYMBOL	TEST NO.	PINS								MEAS PIN	LIMITS		UNITS
		1	2	5	6	10	12	14	15		MIN	MAX	
I_{OH} 14	1	GND	250uA			GND		5.5V	5.5V	14		250	uAdc
I_{OH} 12	2			GND	250uA		5.5V			12		250	uAdc
V_{OL} 14	3	GND	10mA					10mA		14		0.6	Vdc
V_{OL} 12	4			GND	10mA		10mA			12		0.6	Vdc
I_{CCH}	5									15		20	mAdc
I_{CCL}	6	GND	20mA	GND	20mA					15		36	mAdc
V_F 2	7	GND	20mA							2		1.75	Vdc
V_F 6	8			GND	20mA					6		1.75	Vdc
BV_R 2	9	GND	-10uA							2	5.0		Vdc
BV_R 6	10			GND	-10uA					6	5.0		Vdc
t_{PLH}	11									⚠		90	ns
t_{PHL}	12											90	ns
t_r	13											90	ns
t_f	14											90	ns
C_{in} 1-2	15	V_F=0; f=1 MHz								1 to 2	0	150	pF
C_{in} 5-6	16	V_F=0; f=1 MHz.								5 to 6	0	3	pF
C_{IO} 1-9	17	f=1 MHz. (Pins 1 and 2 common; Pins 9, 10, 11, 12, 13, 14, 15 and 16 common)								1 to 3	0	3	pF
C_{IO} 5-9	18	f=1 MHz. (Pins 5 and 6 common; Pins 9, 10, 11, 12, 13, 14, 15 and 16 common)								5 to 9	0	2	pF
C_{II} 1-5	19	f=1 MHz. (Pins 1 and 2 common; Pins 5 and 6 common)								1 to 5	0	2	pF

Notes:

1. Pins not specified are left open.
2. Parameters and limits for tests 1 through 10 are applicable for T_A=25°C, 125°C and -55°C. Parameters and limits for tests 11 through 19 are applicable for 25°C only.

⚠ For dynamic tests (te. 11-14) use Figure B2. Conditions: R_L=510 Ω, C_L=15pf, I_F=13mAdc.

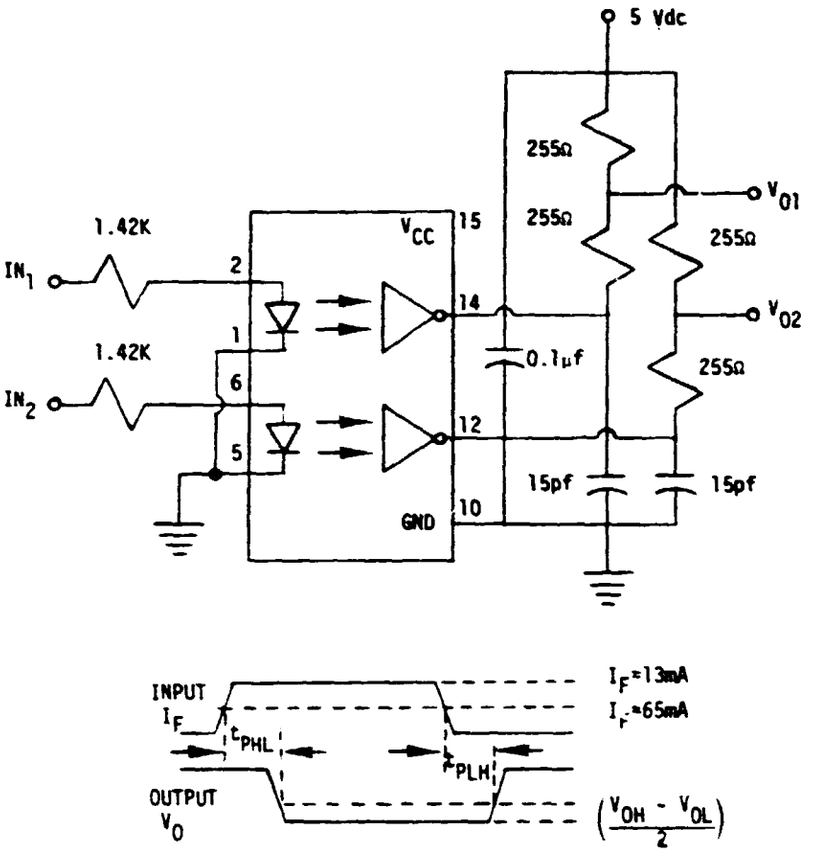

Notes:

1. Input conditions: Z_0=50Ω, t_R=5ns

FIGURE B2. OPTO-COUPLER TYPE B DYNAMIC TEST FIGURE

TABLE B3. LED TEST CONDITIONS

PARAMETER	TEST NO.	CONDITIONS	MIN	MAX	UNITS
IR	1	V_R=2 VDC	---	.050	μadc
BVR	2	I_R=100μAdc	5.0	----	VDC
VF_2	3	I_F=2mAdc	---	1.10	VDC
VF_{20}	4	I_F=20mAdc	---	1.30	VDC
VF_{50}	5	I_F=50mAdc	---	1.40	VDC
VF_{100}	6	I_F=100mAdc	---	1.60	VDC
PO_2	7	I_F=2mAdc	0.005	----	MW
PO_{20}	8	I_F=20mAdc	0.200	----	MW
PO_{50}	9	I_F=50mAdc	0.700	----	MW
PO_{100}	10	I_F=100mAdc	1.600	----	MW
CO	11	V_F=0, f=1MHz	---	----	pf
λ_p	12	I_F=100ma	---	----	nm
B	13	I_F=100ma	---	----	nm

1. Power output was measured with a VDT Model IIA photometer.
2. Peak emission wavelength (λ_p) and half power bandwidth (B) were measured using a Jarral Ash Fisher Model 20 monochrometer and the UDT Model IIA photometer connected to an x-y plotter.
3. Electrical end-point limits only apply to 25°C measurements. Measurements at 125°C and -55°C were made for information only.

TABLE B4. TYPE A OPTO-COUPLER TEST GROUP DEFINITION

PARAMETER	TEST CONDITIONS	EM_B T_A = 25°C	EM_D T_A = -55°C & 100°C	EM_C T_A = 25°C
V_F	I_F = 10 mAdc	X	X	
R_D	I_F = 15 to 20 mAdc	X	X	
I_R	V_R = 2 Vdc	X	X	
BV_{CBO}	I_C = 100 µAdc	X	X	
	I_E = 0, I_F = 0			
BV_{CEO}	I_C = 1.0 mAdc	X	X	
	I_B = 0, I_F = 0			
BV_{EBO}	I_E = 100 mAdc	X	X	
	I_C = 0, I_F = 0			
I_D	V_{CE} = 20 Vdc	X	X	
	I_B = 0, I_F = 0			
h_{FE}	V_{CE} = 5 Vdc	X	X	
	I_C = 10 mAdc			
T_R	I_F = 10 mAdc	X	X	
	V_{CE} = 5 Vdc			
$V_{CE(sat)}$	I_F = 20 mAdc	X	X	
	I_{CE} = 2.5 mAdc			
	I_B = 0			
V_{ISO}	1000 Vdc			X
R_{ISO}	100 Vdc			X
C_{in}	V_F = 0, f = 1 MHz			X
C_{COUP}	f = 1 MHz			X
t_r & t_f	Fig. 2 of MIL-S-19500/486, I_F = 10 mAdc V_{CC} = 10 Vdc			X

TABLE B5. TYPE B OPTO-COUPLER TEST GROUP DEFINITION

PARAMETER	CONDITIONS	EM_A T_A = 25°C	EM_B T_A = -55°C & 125°C	EM_C T_A = 25°C
I_{OH}	V_{CC} = 5.5, VO = 5.5V IF = 250 µa	X	X	
V_{OL}	V_{CC} = 5.5, IF = 10 ma I_{OL} = 10 ma	X	X	
I_{CCH}	V_{CC} = 5.5, IF = 0	X	X	
I_{CCL}	V_{CC} = 5.5 IF = 20 ma EACH CHANNEL	X	X	
V_F	IF = 20 ma	X	X	
B_{VR}	IR = 10 µa	X	X	
C_{in}	V_F = 0, f = 1 MHz			X
C_{IO}	f = 1 MHz			X
C_{II}	f = 1 MHz			X
V_{ISO}	NO FLASHOVER AT 1500 Vdc			X
R_{ISO}	V = 500 Vdc			X
TPLH/TPHL	RL = 510Ω, CL = 15 pf, IF = 13 ma			X
tr/tf	RL = 510Ω, CL = 15 pf, IF = 13 ma			X

TABLE B6. LED TEST GROUP DEFINITION

PARAMETER	CONDITIONS	EM_a T_A = 25°C	EM_b T_A = -55°C & 125°C	EM_c T_A = 25°C
IR	V_R = 2 Vdc	X	X	
BVR	I_R = 100 µAdc	X	X	
VF_2	I_F = 2 mAdc	X	X	
VF_{20}	I_F = 20 mAdc	X	X	
VF_{50}	I_F = 50 mAdc	X	X	
VF_{100}	I_F = 100 mAdc	X	X	
PO_2	I_F = 2 mAdc	X	X	
PO_{20}	I_F = 20 mAdc	X	X	
PO_{50}	I_F = 50 mAdc	X	X	
PO_{100}	I_F = 100 mAdc	X	X	
CO	V_F = 0, f = 1 MHz			X
λ_p	I_F = 100 ma			X
B	I_F = 100 ma			X

APPENDIX C

PARAMETER CHARACTERIZATION

APPENDIX C

PARAMETER CHARACTERIZATION

Electrical parameter measurements were performed initially on all devices, and before and after the burn-in during the screening and preconditioning of the opto-couplers as shown in Table C1. The results of these tests are summarized in Tables C2 through C14.

Examination of the Type A opto-coupler initial data for the three manufacturers reveals a marked difference in several parameter values. The Optron devices exhibit the highest average value of transfer ratio (TR), the lowest H_{FE} and the highest dark current (I_D) of the three manufacturers' devices. In contrast, the Spectronics devices exhibit the lowest TR and the highest H_{FE}. It follows that the Optron LEDs have the highest output power and the Spectronics LEDs have the lowest output power.

Examination of the Type B, Hewlett Packard opto-coupler initial data indicated that the manufacturer's limits were not too tight or loose, and were used for the remainder of the program. In addition, this data was used to establish limits for parameters which did not have manufacturer's limits.

The initial LED parametric data indicates that the RCA and Texas Instruments devices are similar, although the RCA LED does have a slightly higher output power than the Texas Instruments LED.

None of the opto-coupler devices demonstrated major parametric changes following the screening/preconditioning burn-in.

TABLE C1. ELECTRICAL PARAMETER MEASUREMENT SCHEDULE

DEVICE	INITIAL	PRE BURN-IN	POST BURN-IN
OPTO COUPLER	EM_A - 100% EM_B - 50 devices EM_C - 100%	EM_A - 100%	EM_A - 100% EM_B - 100% EM_C - 100%
LED	EM_A - 100% EM_B - 25 devices EM_C - 25 devices	N/A	N/A

TABLE C2. TYPE A OPTO-COUPLER PARAMETER CHARACTERIZATION-TEXAS INSTRUMENTS 25°C

PARAMETER	MIL STD LIMITS		NASA LIMITS		INITIAL		PRE BURN-IN		POST BURN-IN		UNITS
	MIN	MAX	MIN	MAX	MEAN	SIGMA	MEAN	SIGMA	MEAN	SIGMA	
V_F	0.8	1.3	---	1.3	1.161	0.014	1.178	0.013	1.173	0.014	Vdc
R_D	---	---	---	5.0	2.853	0.993	3.171	1.908	3.055	1.074	Ω
I_R	---	100	---	10.0	0.016	0.274	0.017	0.291	0.024	0.303	µAdc
BV_{CBO} ⚠1	35	---	35	---	62.834	5.707	61.551	4.200	63.581	0.785	Vdc
BV_{CEO} ⚠1	35	---	35	---	57.243	10.713	59.033	6.663	61 037	6.369	Vdc
BV_{EBO}	4	---	4	---	10.337	1.806	10.494	0.210	10.539	1.130	Vdc
I_D	---	100	---	100	0.463	3.850	3.758	10.335	3.521	13.463	nAdc
HFE	---	---	100	500	1067	1127	975	216	884	220	---
TR	.25	---	.25	---	0.731	0.229	0.806	0.166	0.651	0.161	---
V_{CES}	---	0.3	---	0.3	0.104	0.020	0.110	0.012	0.117	0.013	Vdc
C_{IN}	---	---	---	50	32.449	5.137	---	--- ⚠2	31.297	5.098	pf
C_{COUP}	---	5.0	---	3.0	1.819	0.061	---	---	1.419	-.077	pf
t_R	---	15.0	---	3.0	6.795	17.035	---	---	6.232	1.429	µS
t_F	---	15.0	---	3.0	8.492	2.197	---	---	8.421	2.491	µS

⚠1 MAXIMUM LIMIT OF ≥ 63.0Vdc IMPOSED BY TEST HARDWARE CONSTRAINTS.

⚠2 TESTS NOT PERFORMED.

TABLE C3. TYPE A OPTO-COUPLER PARAMETER CHARACTERIZATION-TEXAS INSTRUMENTS 100°C

PARAMETER	MIL-STD LIMITS		NASA LIMITS		INITIAL		POST-BURN (2)		UNITS
	MIN	MAX	MIN	MAX	MEAN	SIGMA	MEAN	SIGMA	
V_F	0.7	1.2	---	1.2	1.041	0.016	1.047	0.016	Vdc
R_D	---	---	---	---	3.526	0.886	1.102	3.526	Ω
I_R	---	---	---	100.0	0.056	0.565	0.008	0.007	μAdc
BV_{CBO} (1)	---	---	---	---	63.073	1.191	59.917	0.415	Vdc
BV_{CEO} (1)	---	---	---	---	55.209	6.373	52.939	4.956	Vdc
BV_{EBO}	---	---	---	---	11.043	0.235	11.039	0.127	Vdc
I_D	---	1.0 E5	---	12,000	11,157.383	7,651.406	7,938.737	5,921.227	nAdc
HFE	---	---	150.0	600.0	1,402.560	279.686	1,438.313	172.626	---
TR	---	---	0.15	1.0	0.519	0.111	0.520	0.132	---
V_{CES}	---	---	---	---	0.163	0.033	0.162	0.021	Vdc

(1) Maximum limit of ≥63.0 Vdc imposed by test hardware constraints.

(2) Based on twenty-five devices.

TABLE C4. TYPE A OPTO-COUPLER PARAMETER CHARACTERIZATION-TEXAS INSTRUMENTS -55°C

PARAMETER	MIL-STD LIMITS		NASA LIMITS		INITIAL		POST-BURN		UNITS
	MIN	MAX	MIN	MAX	MEAN	SIGMA	MEAN	SIGMA	
V_F	1.0	1.5	---	1.4	1.262	0.024	1.300	0.018	Vdc
R_D	---	---	---	---	2.146	0.861	3.403	1.267	Ω
I_R	---	---	---	---	0.001	0.004	0.006	0.103	μAdc
BV_{CBO} (1)	---	---	---	---	63.377	0.669	63.584	0.607	Vdc
BV_{CEO} (1)	---	---	---	---	58.384	10.097	53.596	6.953	Vdc
BV_{EBO}	---	---	---	---	10.041	0.110	10.137	2.044	Vdc
I_D	---	---	---	---	0.030	0.095	1.354	15.353	nAdc
HFE	---	---	20.0	100.0	606.384	198.158	551.433	430.647	---
TR	---	---	0.15	1.00	0.967	1.577	0.767	0.305	---
V_{CES}	---	---	---	---	0.082	0.167	0.075	0.019	Vdc

(1) Maximum limit of ≥63.0 Vdc imposed by test hardware constraints.

TABLE C5. TYPE A OPTO-COUPLER PARAMETER CHARACTERIZATION-SPECTRONICS 25°C

PARAMETERS	MIL-STD LIMITS		NASA LIMITS		INITIAL		PRE BURN-IN		POST BURN-IN		UNITS
	MIN	MAX	MIN	MAX	MEAN	SIGMA	MEAN	SIGMA	MEAN	SIGMA	
V_F	0.8	1.3	---	1.3	1.095	0.015	1.105	0.013	1.103	0.012	Vdc
R_D	---	---	---	5.0	3.447	0.761	4.140	8.922	3.624	0.835	Ω
I_R	---	100	---	10.0	14.399	24.463	18.239	23.273	33.564	36.453	μAdc
BV_{CBO}	35	---	35	---	61.740	5.527	61.971	5.568	61.151	6.519	Vdc
BV_{CEO}	35	---	35	---	57.700	7.086	60.482	6.836	60.394	7.195	Vdc
BV_{EBO}	4	---	4	---	8.083	2.641	8.069	2.526	9.143	5.653	Vdc
I_D	---	100	---	100	0.191	1.775	2.856	12.293	0.716	4.891	nAdc
HFE	---	---	100	500	14.710	71.901	13.748	41.510	34.008	85.150	---
TR	.25	---	.25	1.0	0.513	0.197	0.548	0.188	0.530	0.211	---
V_{CES}	---	0.3	---	0.3	0.317	0.036	0.319	0.032	0.315	0.039	Vdc
C_{IN}	---	---	---	150	60.923	9.663	---	---	59.272	8.588	pf
C_{COUP}	---	5.0	---	3.0	1.864	0.074	---	---	1.567	0.060	pf
t_R	---	15.0	---	3.0	3.229	0.524	---	---	2.923	0.800	nS
t_F	---	15.0	---	3.0	5.901	1.360	---	---	72.568	783.300	nS

TABLE C6. TYPE A OPTO-COUPLER PARAMETER CHARACTERIZATION-SPECTRONICS 100°C

PARAMETER	MIL-STD LIMITS		NASA LIMITS		INITIAL		POST-BURN (2)		UNITS
	MIN	MAX	MIN	MAX	MEAN	SIGMA	MEAN	SIGMA	
V_F	0.7	1.2	---	1.2	0.980	0.015	0.968	0.012	Vdc
R_D	---	---	---	---	3.900	0.668	3.624	0.413	Ω
I_R	---	---	---	100.0	42.215	56.016	40.815	53.044	μAdc
BV_{CBO} (1)	---	---	---	---	62.097	4.924	56.598	7.254	Vdc
BV_{CEO} (1)	---	---	---	---	57.443	6.434	53.080	6.691	Vdc
BV_{EBO}	---	---	---	---	8.231	2.071	8.716	0.033	Vdc
I_D	---	1.0E5	---	12,000	6,488.973	6,360.328	3,158.274	1,389.309	nAdc
HFE	---	---	150.0	600.0	860.977	1,729.457	806.086	186.745	---
TR	---	---	0.15	1.00	0.314	0.177	0.237	0.074	---
V_{CES}	---	---	---	---	0.717	1.361	0.570	0.087	Vdc

(1) Maximum limit of ±63.0 Vdc imposed by test hardware constraints.

(2) Based on twenty-five devices.

TABLE C7. TYPE A OPTO-COUPLER PARAMETER CHARACTERIZATION-SPECTRONICS -55°C

PARAMETER	MIL-STD LIMITS		NASA LIMITS		INITIAL		POST-BURN (2)		UNITS
	MIN	MAX	MIN	MAX	MEAN	SIGMA	MEAN	SIGMA	
V_F	1.0	1.5	---	1.4	1.195	0.023	1.183	0.015	Vdc
R_D	---	---	---	---	4.001	1.781	3.514	0.931	Ω
I_R	---	---	---	---	32.160	52.930	26.752	49.248	µAdc
BV_{CBO} (1)	---	---	---	---	56.864	11.027	44.973	11.263	Vdc
BV_{CEO} (1)	---	---	---	---	55.255	9.780	44.598	10.636	Vdc
BV_{EBO}	---	---	---	---	7.572	2.090	7.555	0.032	Vdc
I_D	---	---	---	---	4.983	62.900	0.004	0.142	nAdc
HFE	---	---	20.0	100.0	400.639	1,362.464	373.666	37.385	---
TR	---	---	0.15	1.00	0.387	0.542	0.237	0.090	---
V_{CES}	---	---	---	---	0.256	0.719	0.710	2.529	Vdc

(1) Maximum limit of ≥63.0 Vdc imposed by test hardware constraints.

(2) Based on twenty-five devices.

TABLE C8. TYPE A OPTO-COUPLER PARAMETER CHARACTERIZATION-OPTRON 25°C

PARAMETERS	MIL-STD LIMITS		NASA LIMITS		INITIAL		PRE BURN-IN		POST BURN-IN		UNITS
	MIN	MAX	MIN	MAX	MEAN	SIGMA	MEAN	SIGMA	MEAN	SIGMA	
V_F	0.8	1.3	---	1.3	1.152	0.014	1.168	0.015	1.165	0.014	Vdc
R_D	---	---	---	5.0	3.790	0.895	4.020	1.217	4.028	0.897	Ω
I_R	---	100	---	10.0	0.296	4.243	0.272	2.742	1.341	5.607	µAdc
BV_{CBO}	35	---	35	---	63.043	1.995	63.428	1.792	62.995	2.243	Vdc
BV_{CEO}	35	---	35	---	61.498	4.675	62.805	3.698	62.448	3.826	Vdc
BV_{EBO}	4	---	4	---	7.355	0.217	7.876	3.733	8.596	5.691	Vdc
I_D	---	100	---	100	4.807	9.384	3.697	9.015	5.924	12.670	nAdc
HFE	---	---	100	500	499.900	142.700	35.928	99.800	12,736	26.143	---
TR	.25	---	.25	1.0	0.834	0.615	0.383	0.491	0.728	0.443	---
V_{CES}	---	0.3	---	0.3	0.146	0.023	0.149	0.021	0.155	0.020	Vdc
C_{IN}	---	---	---	15	22.166	8.394	---	---	21.765	7.913	pf
C_{COUP}	---	5.0	---	3.0	1.147	0.045	---	---	0.811	0.446	pf
t_R	---	15	---	3.0			---	---	3.415	1.074	nS
t_F	---	15	---	3.0			---	---	4.735	2.041	nS

TABLE C9. TYPE A OPTO-COUPLER PARAMETER CHARACTERIZATION-OPTRON 100°C

PARAMETER	MIL-STD LIMITS		NASA LIMITS		INITIAL		POST-BURN		UNITS
	MIN	MAX	MIN	MAX	MEAN	SIGMA	MEAN	SIGMA	
V_F	0.7	1.2	---	1.2	1.052	0.017	1.051	0.018	Vdc
R_D	---	---	---	---	4.161	0.748	4.967	0.857	Ω
I_R	---	---	---	100.0	0.576	5.351	2.212	7.974	µAdc
BV_{CBO} (1)	---	---	---	000	63.056	1.800	63.315	1.757	Vdc
BV_{CEO} (1)	---	---	---	---	60.755	4.415	61.073	4.666	Vdc
BV_{EBO}	---	---	---	---	7.603	0.236	8.107	3.634	Vdc
I_D	---	1.0 E5	---	---	8,225.695	10,756.492	19,557.000	17,791.000	nAdc
HFE	---	---	150.0	600.0	494.423	191.570	818.255	1,839.157	---
TR	---	---	0.15	1.00	0.629	0.376	0.515	0.515	---
V_{CES}	---	---	---	---	0.205	0.033	0.226	0.226	Vdc

(1) Maximum limit of ≥63.0 Vdc imposed by test hardware constraints.

TABLE C10. TYPE A OPTO-COUPLER PARAMETER CHARACTERIZATION-OPTRON -55°C

PARAMETER	MIL-STD LIMITS		NASA LIMITS		INITIAL		POST-BURN		UNITS
	MIN	MAX	MIN	MAX	MEAN	SIGMA	MEAN	SIGMA	
V_F	1.0	1.5	---	1.4	1.264	0.011	1.280	0.009	Vdc
R_D	---	---	---	---	3.681	1.092	4.280	0.758	Ω
I_R	---	---	---	---	1.271	11.085	0.021	0.040	µAdc
BV_{CBO} (1)	---	---	---	---	62.472	3.922	73.408	0.613	Vdc
BV_{CEO} (1)	---	---	---	---	60.834	5.316	61.570	4.744	Vdc
BV_{EBO}	---	---	---	---	7.046	0.194	7.132	0.151	Vdc
I_D	---	---	---	---	0.060	0.060	0.039	0.031	nAdc
HFE	---	---	20.0	100.0	245.903	80.762	219.510	41.858	---
TR	---	---	0.15	1.00	0.701	0.425	0.614	0.206	---
V_{CES}	---	---	---	---	0.101	0.016	0.117	0.012	Vdc

(1) Maximum limit of ≥63.0 Vdc imposed by test hardware constraints.

TABLE C11. TYPE B OPTO-COUPLER PARAMETER CHARACTERIZATION
HEWLETT PACKARD 25°C

	PARAMETER	LIMITS		INITIAL		PRE-BURN-IN		POST BURN-IN		UNITS
		MIN	MAX	MEAN	SIGMA	MEAN	SIGMA	MEAN	SIGMA	
STATIC TESTS	I_{OH}	---	250	5.089	5.509	5.209	6.137	5.652	10.780	Adc
	V_{OL}	---	0.6	0.377	0.048	0.739	0.045	0.372	0.048	Vdc
	I_{CCH}	---	20	15.934	1.321	15.844	1.320	15.959	1.359	mAdc
	I_{CCL}	---	36	25.736	3.109	25.529	3.003	25.666	3.060	mAdc
	V_F	---	1.75	1.536	0.015	1.545	0.015	1.544	0.016	Vdc
	BV_R	5.0	---	9.873	1.697	10.129	1.476	10.179	1.443	Vdc
DYNAMIC TESTS	C_{IN}	0	150	76.773	5.847	--- ⚠	---	76.778	6.731	pF
	C_{IO}	0	3	1.853	0.245	---	---	1.351	0.245	pF
	C_{II}	0	2	0.218	0.007	---	---	0.231	0.019	pF
	T_{PLN}	30	90	34.622	2.900	---	---	33.370	3.122	nS
	T_{PNL}	0	90	35.897	5.540	---	---	36.200	5.498	nS
	t_r	0	90	60.813	8.097	---	---	59.494	7.290	nS
	t_f	0	90	37.402	6.194	---	---	38.000	6.010	nS

⚠ DYNAMIC TESTS NOT PERFORMED.

TABLE C12. TYPE B OPTO-COUPLER PARAMETER CHARACTERIZATION
HEWLETT PACKARD 125°C

PARAMETERS	LIMITS		INITIAL		POST BURN-IN		UNITS
	MIN	MAX	MEAN	SIGMA	MEAN	SIGMA	
I_{OH}	---	250	1.999	4.356	2.311	10.710	mAdc
I_{OL}	---	0.6	0.311	0.038	0.317	0.036	Vdc
I_{CCH}	---	20	14.312	1.294	14.090	1.264	mAdc
I_{CCL}	---	36	26.228	2.686	25.954	2.635	mAdc
V_F	---	1.75	1.419	0.020	1.406	0.015	Vdc
BV_R	5.0	---	10.077	1.892	10.448	1.646	Vdc

TABLE C13. TYPE B OPTO-COUPLER PARAMETER CHARACTERIZATION
HEWLETT PACKARD -55°C

PARAMETERS	LIMITS		INITIAL		POST BURN-IN		UNITS
	MIN	MAX	MEAN	SIGMA	MEAN	SIGMA	
I_{OH}	---	250	23.705	15.840	28.825	15.370	mAdc
V_{OL}	---	0.6	0.412	0.044	0.445	0.041	Vdc
I_{LCH}	---	20	16.862	1.422	16.392	1.732	mAdc
I_{CCL}	---	36	22.309	2.593	20.901	2.592	mAdc
V_F	---	1.75	1.618	0.020	1.642	0.017	Vdc
BV_R	5.0	---	9.596	1.602	9.853	1.331	Vdc

TABLE C14. LED INITIAL PARAMETER CHARACTERIZATION

PARAMETER	LIMITS		RCA						T.I.						UNITS
			25°C		125°C		-55°C		25°C		125°C		-55°C		
	MIN	MAX	MEAN	SIGMA	MEAN	SIGMA	MEAN	SIGMA	MEAN	SIGMA	MEAN	SIGMA	MEAN	SIGMA	
IR	---	0.050	0.016	0.013	0.425	0.322	0.003	0.004	0.002	0.005	0.272	1.132	0.054	0.257	uAdc
BVR	5.0	---	31.410	2.742	29.881	0.383	29.082	2.006	26.620	8.832	26.270	7.418	25.020	7.225	Vdc
VF1	---	1.10	1.060	0.007	0.904	0.009	1.162	0.009	1.057	0.009	0.888	0.013	1.180	0.082	Vdc
VF20	---	1.30	1.193	0.013	1.055	0.017	1.282	0.022	1.165	0.017	1.030	0.010	1.254	0.012	Vdc
VF50	---	1.40	1.299	0.028	1.154	0.038	1.388	0.050	1.234	0.029	1.115	0.019	1.323	0.021	Vdc
VF100	---	1.60	1.432	0.051	1.272	0.071	1.481	0.235	1.314	0.040	1.213	0.035	1.408	0.034	Vdc
PO2	0.005	---	0.044	0.008	0.001	0.005	0.020	0.004	0.024	0.009	0.003	0.001	0.011	0.003	mW
PO20	0.200	---	0.807	0.143	0.094	0.112	0.269	0.077	0.522	0.146	0.080	0.014	0.169	0.036	mW
PO50	0.700	---	2.162	0.378	0.267	0.028	0.726	0.153	1.495	0.411	0.245	0.038	0.449	0.093	mW
PO100	1.600	---	4.187	0.676	0.519	0.045	1.398	0.282	3.039	0.661	0.522	0.082	0.887	0.184	mW
CO	---	---	29.33	7.34	---	---	---	---	34.03	4.50	---	---	---	---	pF
λ_p	---	---	944.6	6.06	---	---	---	---	938.2	3.35	---	---	---	---	nm
δ	---	---	42 60	1.83	---	---	---	---	48.92	2.93	---	---	---	---	nm

NOTE: OUTPUT POWER MEASUREMENTS AT 125°C AND -55°C MUST BE MULTIPLIED BY 3.050 FOR RCA AND 2.400 FOR TEXAS INSTRUMENTS DUE TO LIGHT PIPE ATTENUATION.

APPENDIX D

BIAS CIRCUIT EVALUATION

TABLE OF CONTENTS

APPENDIX D

BIAS CIRCUIT EVALUATIONS

1.0 GENERAL

The selection of bias circuits evolved from a study of device operation, and the biasing requirements for each particular test. Bias circuits were required for each of the tests shown in Table D1. The candidate bias circuits were evaluated for each test to ascertain proper device operation at the required conditions, and to determine maximum life test temperatures. The plots in this appendix are based on an average of three devices for the Type A opto-couplers and LEDs and on one device for the Type B opto-coupler.

2.0 OPTO-COUPLER CIRCUIT EVALUATION

2.1 Burn-In and Operating/Accelerated Life Circuit Evaluation

Burn-in circuit requirements were that maximum rated power be dissipated in the phototransistor and that maximum rated current be maintained through the LED. The same requirements were established for the Type A opto-coupler Operating/Accelerated Life test circuit. The Operating/Accelerated Life test circuit requirements for the dual-channel Type B opto-coupler were that one channel be maintained in the Burn-in configuration and that the other channel be maintained in the HTRB configuration (LED current equal zero).

The circuit first selected for the Type A opto-couplers placed the phototransistor in a constant current configuration, with this current source used to bias the LED at the maximum rated current of 40 mAdc. Maximum rated power dissipation of 300 milliwatts was achieved by adjusting the positive power supply. The LED was placed in the emitter branch of the phototransistor to bias the LED negative with respect to the transistor. This was done to accelerate a suspected charge migration problem in the glass or R6104 gel of the T.I. devices. The circuit operated satisfactorily as shown in Figures D1 and D2 up to 150°C. Above this temperature, the devices exhibited open circuits. It was decided that the circuit would be acceptable if the maximum ambient temperature was maintained at or below 150°C. Later it was learned that the T.I. opto-couplers supplied for this program were not susceptible to the initially reported charge migration problem, but may be susceptible to charge migration failures resulting from biasing the LED

TABLE D1. BIAS CIRCUIT REQUIREMENTS

TEST CIRCUIT	TYPE A OPTO-COUPLER	TYPE B OPTO-COUPLER	LED
BURN-IN	X	X	
OPERATING LIFE	X	X	
ACCELERATED LIFE	X	X	X
HIGH TEMPERATURE REVERSE BIAS (HTRB)	X	X	
MONITORED TEMPERATURE CYCLING/ VIBRATION/SHOCK	X	X	X
POWER CYCLING	X	X	X

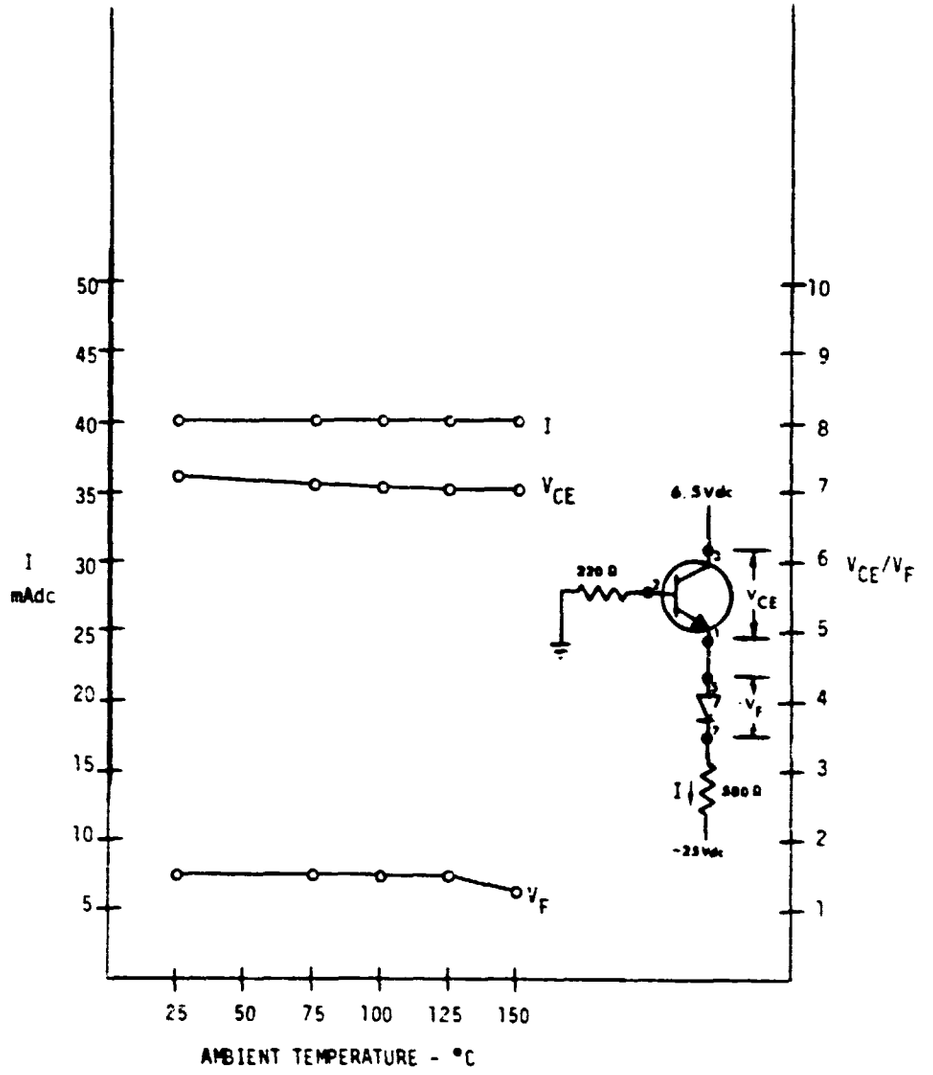

FIGURE D1. TYPE A OPTO-COUPLER BURN-IN/OPERATING LIFE/ACCELERATED LIFE TEST CIRCUIT EVALUATION - TEXAS INSTRUMENTS

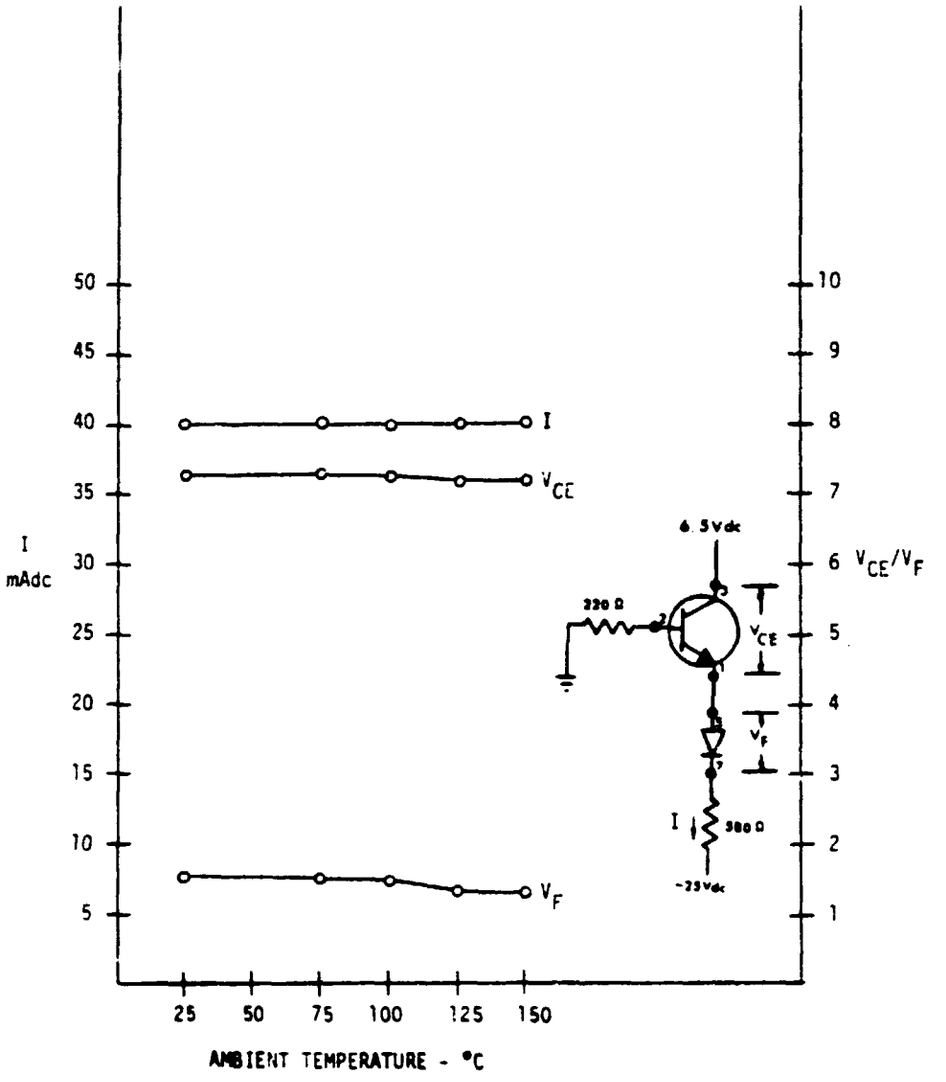

FIGURE D2. TYPE A OPTO-COUPLER BURN-IN/OPERATING LIFE/ACCELERATED LIFE TEST CIRCUIT EVALUATION - OPTRON

positive with respect to the phototransistor. Thus, the final circuit configuration placed the LED in the phototransistor collector circuit, as shown in Figure D3. No additional circuit evaluation was performed on this circuit, but the preliminary and formal step stress results indicated no major deviation in operating characteristics from the circuit evaluation results obtained with the LED biased negative with respect to the transistor.

Due to the nature of the Type B opto-coupler photodetector, there was little flexibility in bias circuit design. Thus, the devices were biased with the maixmum rated current of 20 mAdc in the LEDs and 25 mAdc in the output transistors. The burn-in circuit, as shown in Figure D4, has both of the channels in the "on" condition. The operating/accelerated life circuit placed one of the channels in the "on" condition and the other channel in the "off" condition (LED current=0), and is shown in Figure D5. As shown in Figures D4 and D5, device operation was satisfactory at ambient temperatures up to approximately 200°C. However, in the operating/accelerated life test circuit, the open circuits were observed at 200°C. Thus, it was decided to maintain ambient life test temperatures below 200°C.

2.2 Power Cycling Circuit Evaluation

The primary requirement for the power cycling test was to achieve a phototransistor junction temperature rise of 100°C. The first step in the design of this circuit was to calculate the thermal resistance between junction and ambient (θ_{JA}) of the phototransistor. This was done using a technique similar to MIL-STD-883, Method 1012 which uses a diode forward voltage as a temperature sensitive parameter. θ_{JA}'s of 236°C/W, 255°C/W and 149°C/W were established for the Texas Instruments, Optron, and Hewlett Packard opto-couplers, respectively. Based on these values of θ_{JA}, the power dissipated in each device was adjusted to achieve the required 100°C temperature rise. For the Type A opto-couplers this involved adjusting the positive and negative supply voltages, as shown in Figure D6, to obtain approximately 400 mW power dissipation in the phototransistor. Due to the nature of the Type B opto-coupler, power dissipation could not be increased in the photoamplifier or the output transistor. Thus, the devices were cycled between the "off" condition and the maximum rated current of 25 mAdc in the output transistor. This achieved a temperature rise of approximately 25°C in the output transistor. The circuit used is shown in Figure D7.

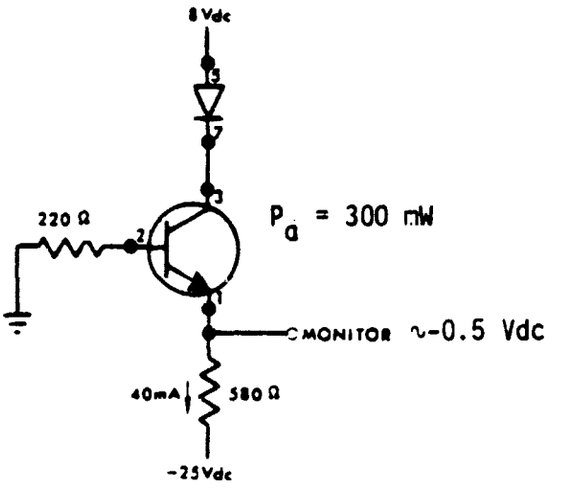

FIGURE D3. FINAL TYPE A OPTO-COUPLER BURN-IN/LIFE TEST CIRCUIT

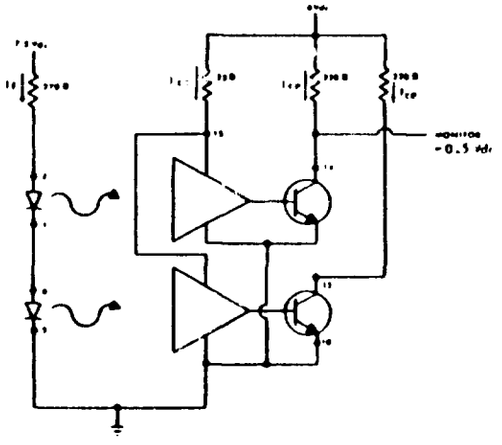

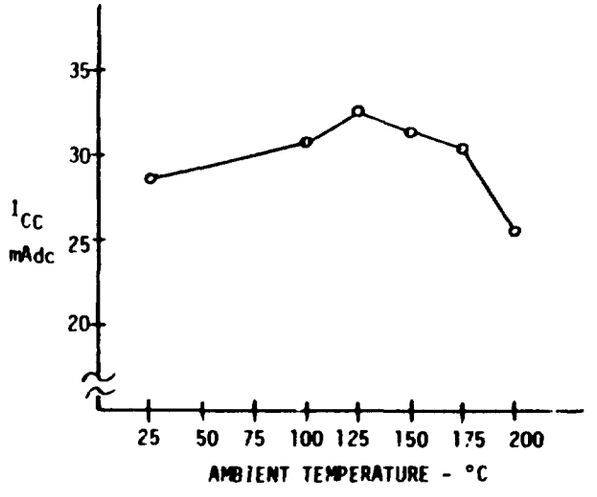

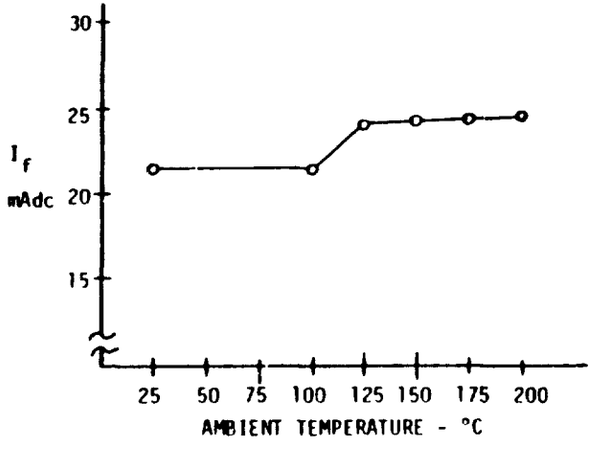

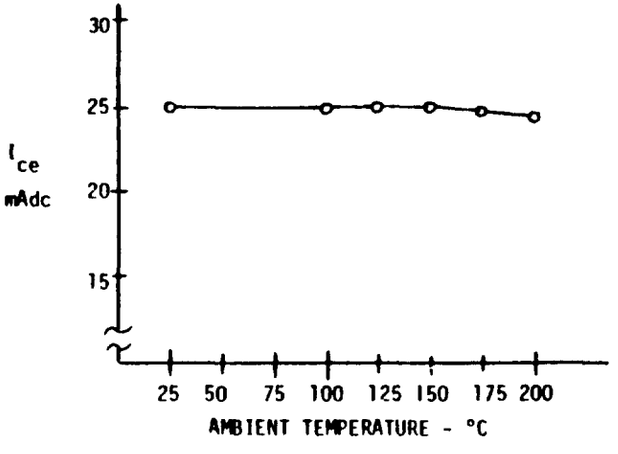

FIGURE D4. TYPE B OPTO-COUPLER BURN-IN TEST CIRCUIT EVALUATION - HEWLETT PACKARD

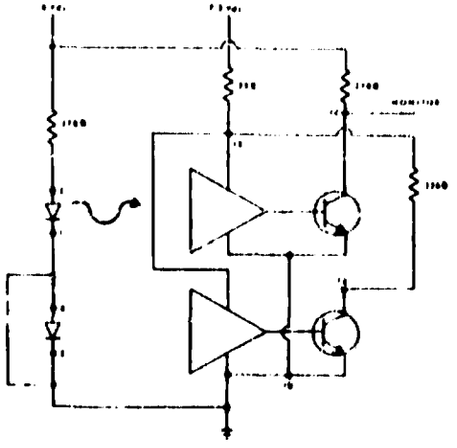

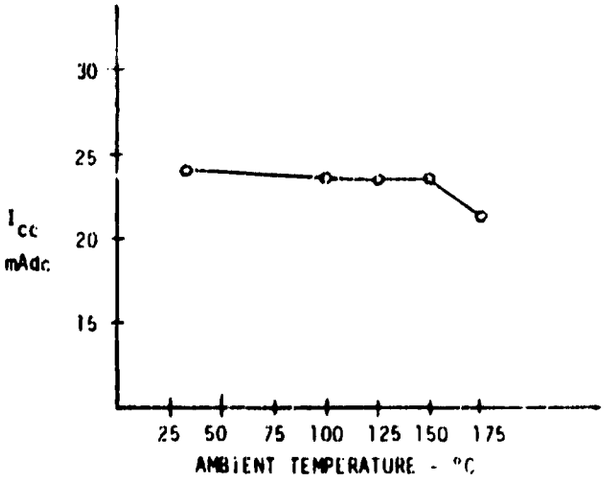

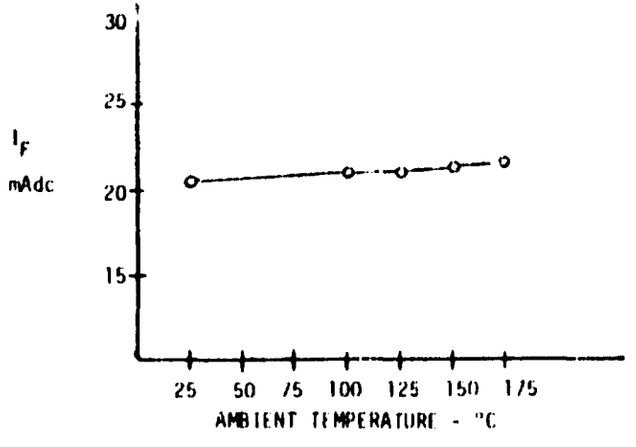

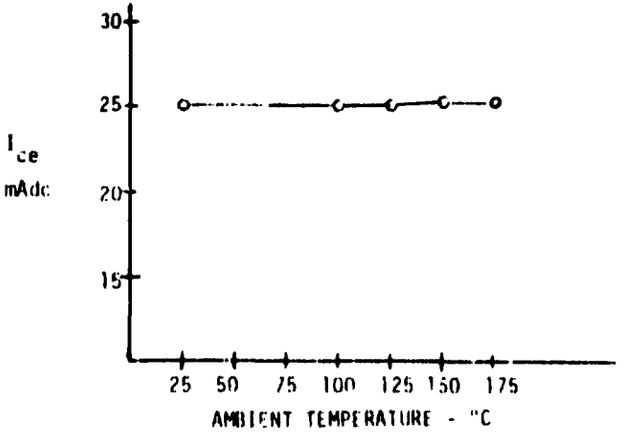

FIGURE D5. TYPE B OPTO-COUPLER OPERATING/ACCELERATED LIFE TEST CIRCUIT EVALUATION - HEWLETT PACKARD

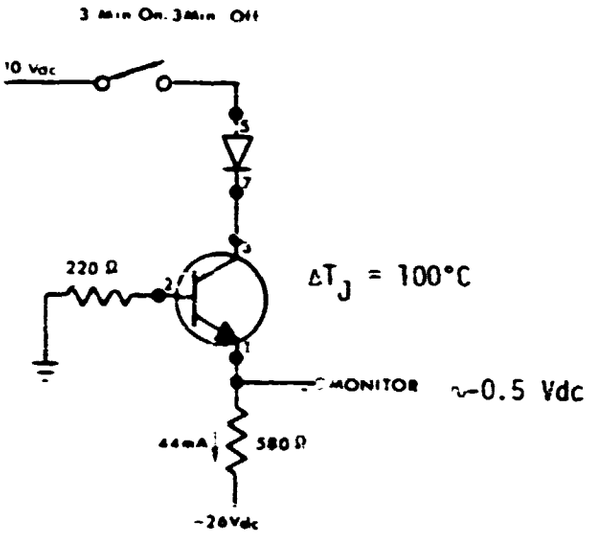

FIGURE D6. TYPE A OPTO-COUPLER POWER CYCLING TEST CIRCUIT

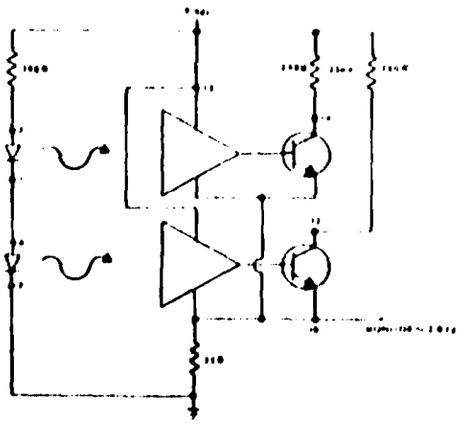

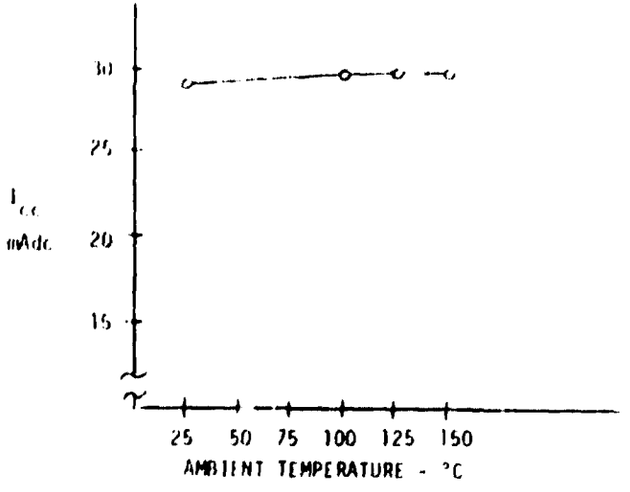

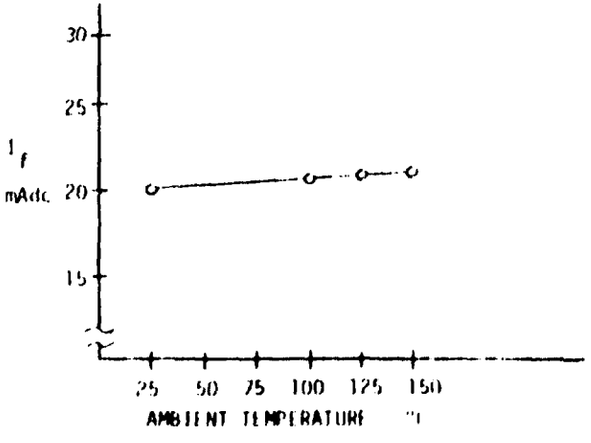

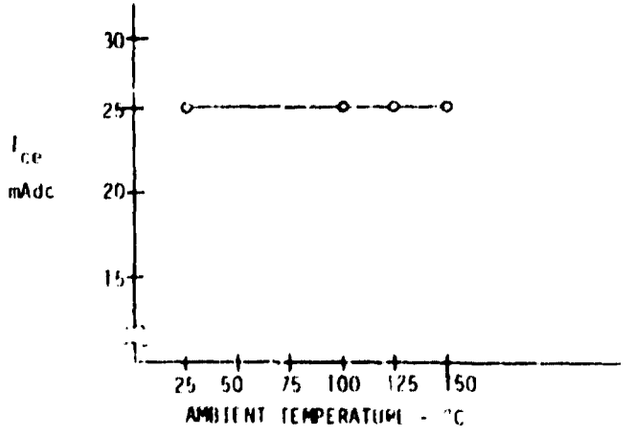

FIGURE D7. TYPE B OPTO-COUPLER POWER CYCLING/TEMPERATURE CYCLING/VIBRATION/SHOCK TEST CIRCUIT EVALUATION

2.3 Monitored Temperature Cycling/Vibration/Shock Test Circuit Evaluation

The primary requirement for the monitored Temperature Cycling/Vibration/Shock test circuits was to detect any open or shorted conditions when the devices were undergoing the specific tests. The circuit selected for the Type A opto-couplers was stable over the required temperature range and was capable of detecting any opens or adjacent pin shorts. The circuit and the temperature evaluation are shown in Figure D8. For the Type B opto-coupler the power cycling test circuit, which was previously evaluated, provided the desired capabilities and was used for the Monitored Temperature Cycling, Vibration, and Shock tests. The operation of this circuit over the required temperature range is shown in Figure D7. A list of the expected monitor voltages for normal, open pin, and shorted pin conditions for both the Type A and Type B opto-couplers is provided in Table D2. Due to the R6104 gel overcoat, the shorting of two bond wires is highly improbable, nevertheless, the monitoring was such that adjacent pins shorting would be detected.

2.4 HTRB Test Circuit Evaluation

The criteria for the HTRB test circuit required the LED current to be zero and a specified voltage be maintained across the phototransistor or photoamplifier. The Type A opto-coupler circuits, as shown in Figure D9 and D10, operated satisfactorily up to 175°C. The Optron devices exhibited open circuits above 175°C. The T.I. devices operated satisfactorily up to 200°C, above which device current was excessive. Thus, Type A opto-coupler HTRB test temperatures of 125°C and 150°C were selected.

The Hewlett Packard Type B opto-coupler was operated satisfactorily at 7.5 Vdc at ambient temperatures up to 200°C as shown in Figure B11. Thus, the Type B opto-couplers were operated in the HTRB test at ambient temperatures up to 200°C.

3.0 LED CIRCUIT EVALUATION

All LED tests were performed with the devices forward biased at the maximum rated current of 100 mAdc. This circuit, shown in Figure D12, operated satisfactorily up to 250°C. However, during the power "on" portion of the power cycling test the maximum temperature rise achievable was only 20°C in the T.I. devices and 30°C in the RCA devices. This circuit was also acceptable for the monitored temperature cycling test, monitored vibration/shock test and the accelerated life tests.

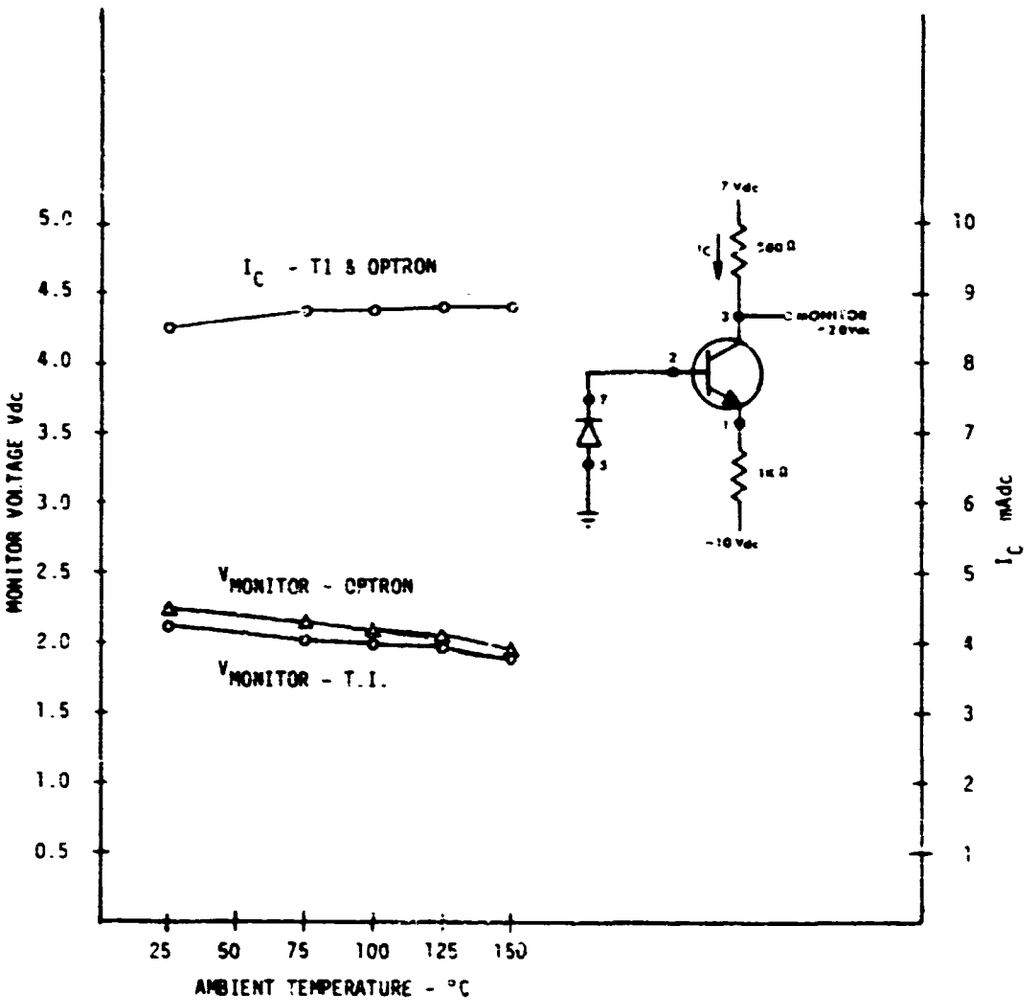

FIGURE D8. TYPE A OPTO-COUPLER MONITORED VIBRATION/ SHOCK/TEMPERATURE CIRCUIT EVALUATION

TABLE D2. OPTO-COUPLER MONITOR CONDITIONS

TYPE A OPTO-COUPLER	
CONDITION	MONITOR VOLTAGE (VDC)
NORMAL	2.0
OPEN PIN	
1	7.00
2	7.00
3	7.00
5	7.00
7	7.00
SHORTED PINS	
1-2	7.00
2-3	1.22

TYPE B OPTO-COUPLER	
CONDITION	MONITOR VOLTAGE (VDC)
NORMAL	2.0
OPEN PIN	
1	0.75
2	0.75
5	0.75
6	0.75
10	0.00
12	1.38
14	1.38
15	0.00
SHORTED PINS	
1-2	1.20
5-6	1.38
14-15	1.75

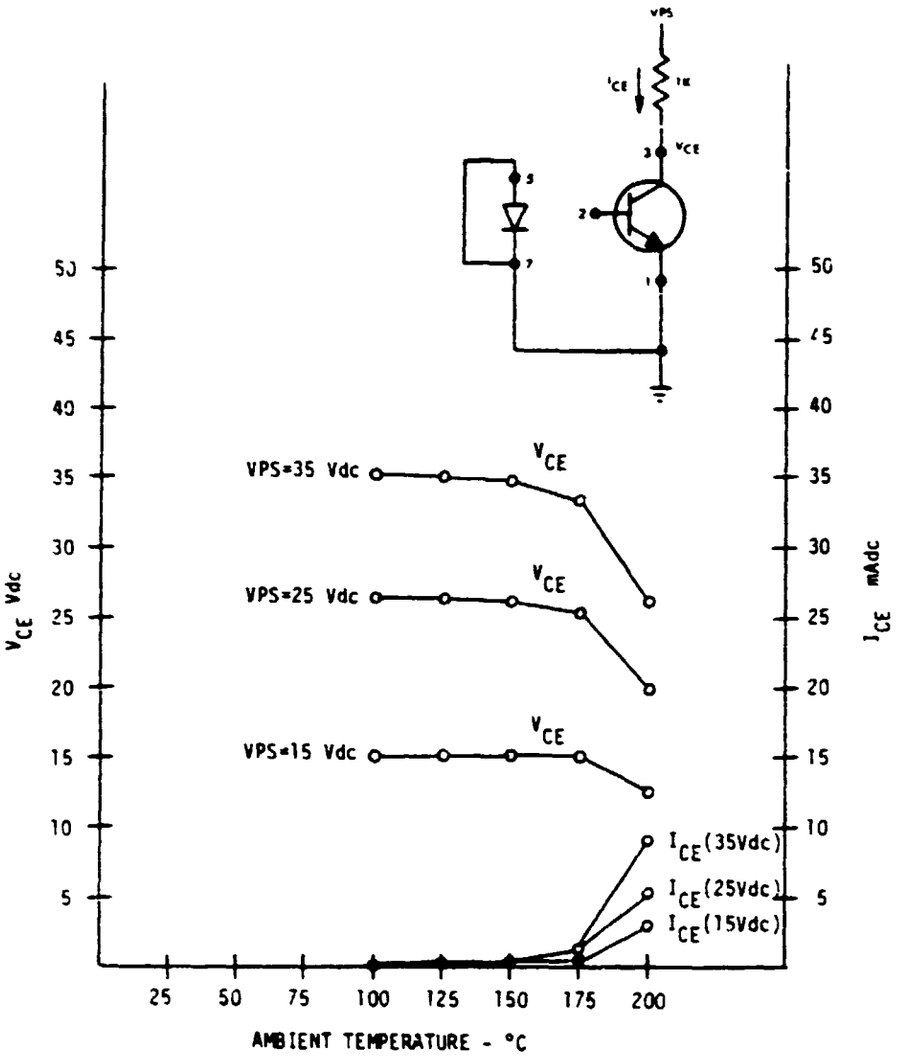

FIGURE D9. TYPE A OPTO-COUPLER HTRB CIRCUIT EVALUATION - T.I.

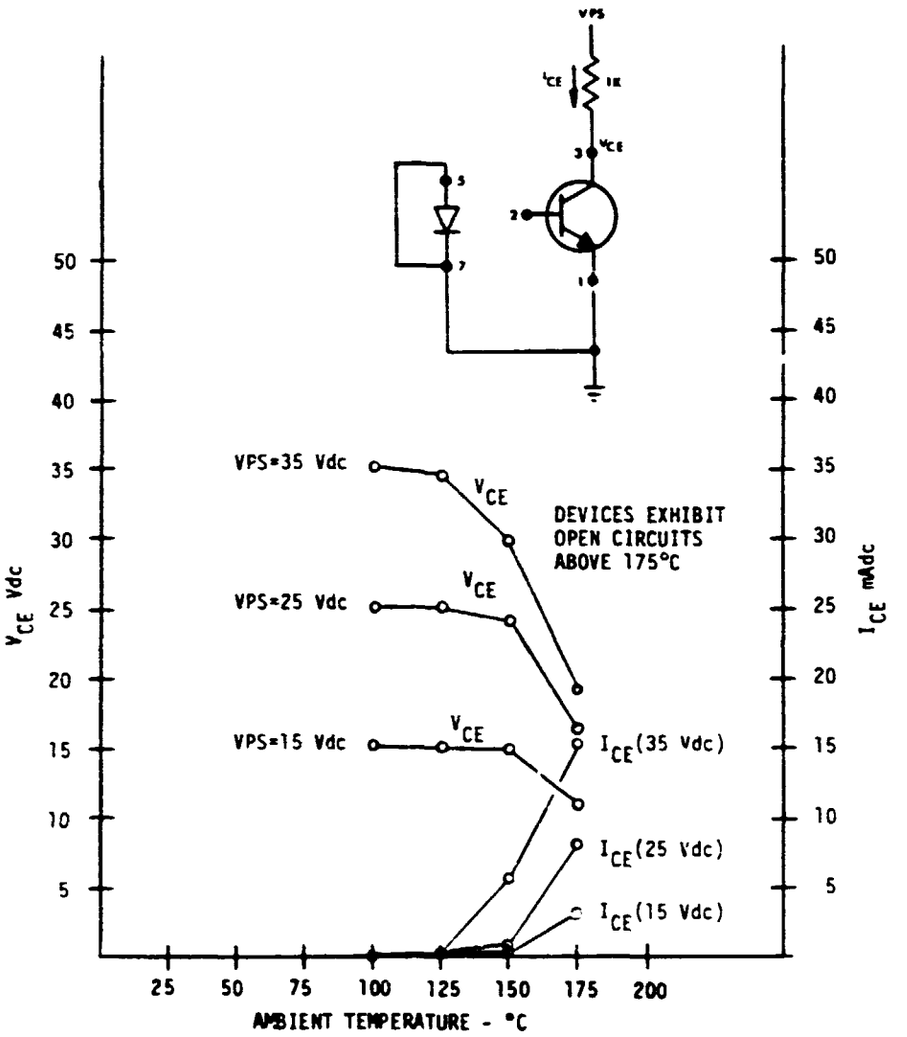

FIGURE D10. TYPE A OPTO-COUPLER HTRB CIRCUIT EVALUATION - OPTRON

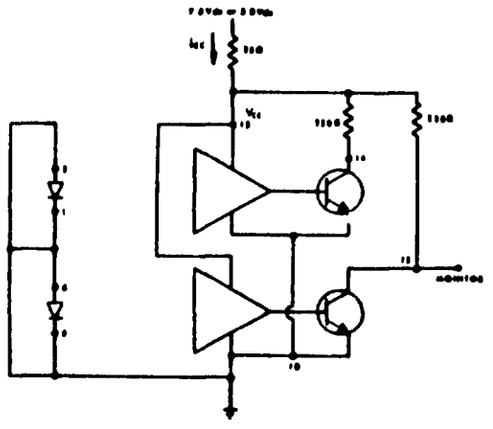

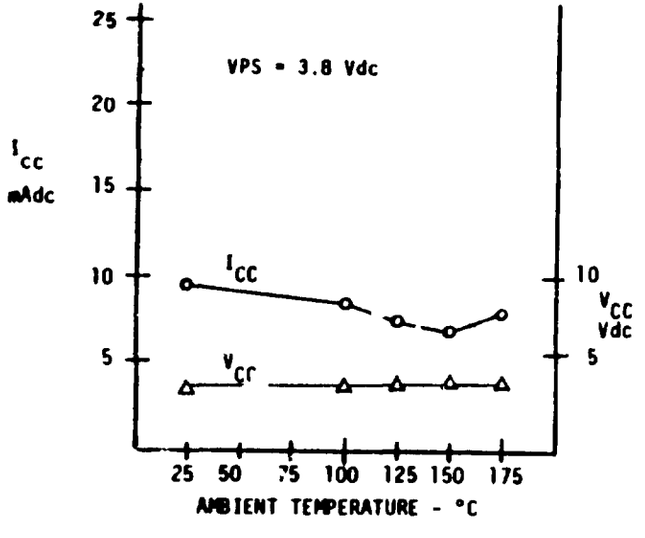

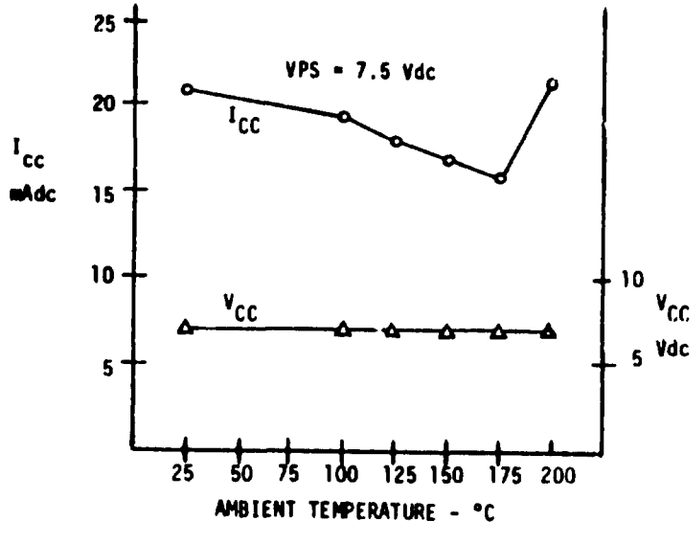

FIGURE D11. TYPE B OPTO-COUPLER HTRB TEST CIRCUIT EVALUATION - HEWLETT PACKARD

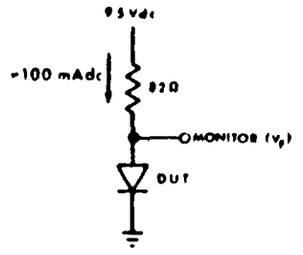

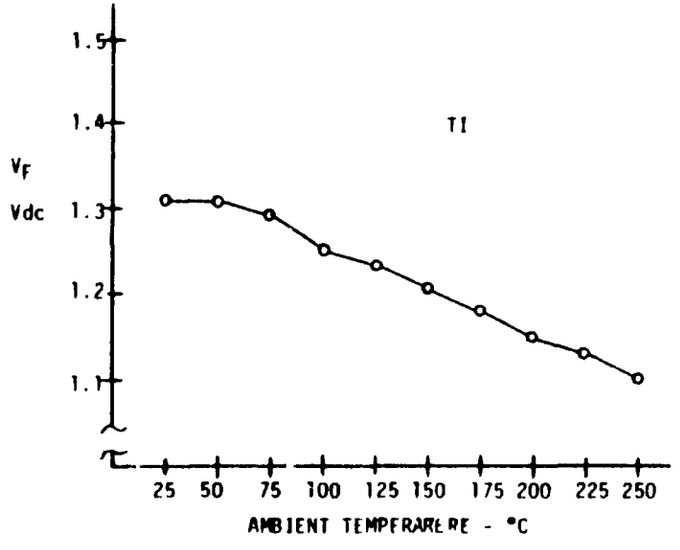

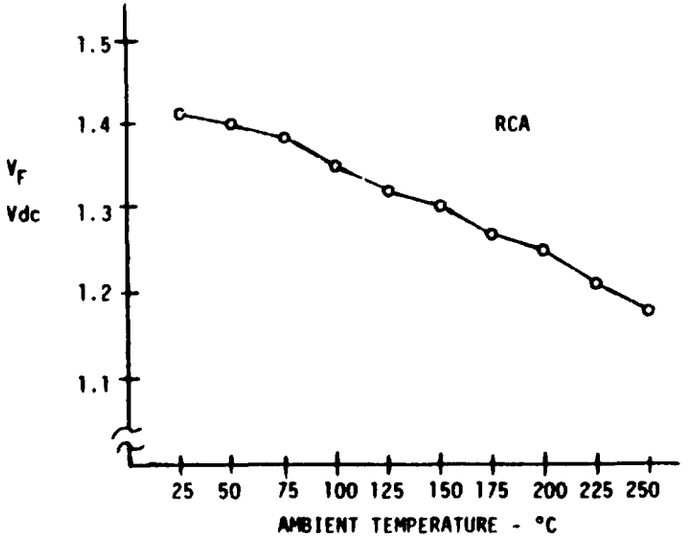

FIGURE D12. LED TEST CIRCUIT EVALUATION

APPENDIX E

FAILURE ANALYSIS

APPENDIX E

FAILURE ANALYSIS

TABLE OF CONTENTS

Appendix E
FAILURE ANALYSIS

1.0 INTRODUCTION

This appendix presents a condensation of the comprehensive failure analyses performed during this program. To facilitate reader use of this appendix the detailed failure analysis data is subdivided into three (3) sections: TI and Optron opto-couplers, Hewlett Packard opto-couplers, and TI and RCA LEDs. In addition a comprehensive summary overview of the complete failure analysis history is presented in section 3.0.

2.0 FAILURE ANALYSIS PROCEDURE

All parts that failed an electrical test during Step Stress, Group I Tests, HTRB, or Life Tests were analyzed to determine the particular failure mode, failure mechanism, and probable cause of failure. The general analysis procedure was as follows:

1) All failures were retested separately on the automatic test set to verify the failures.
2) All failed parameters were confirmed using a curve tracer, or if necessary, a bench test set.
3) The failure was isolated to a specific junction or element to the extent possible via external pin-pin curve tracer measurements.
4) The failures were classified into subgroups, on the basis of the analysis findings to this point.
5) A representative sample of parts from each subgroup was subjected to detailed analysis including external optical examination, unpowered bakes, leak testing, delidding, internal optical and SEM examination, die level probing, and chemical or metallurgical dissectioning.

3.0 FAILURE ANALYSIS SUMMARIES

The results of the detailed failure analyses of the test program are summarized in Tables E1 through E5. The tables contain a brief description of the different symptoms, failure modes, failure mechanisms, and cause of failure displayed by each part type and vendor. The detailed analyses reports are presented in sections 4 through 6 and the specific sub-section associated with each brief description is referenced on the tables.

The failures were also categorized into the Defect and Cause Categories shown in the last two columns of the tables. The abbreviations used for both categories and definitions of the cause categories are explained below. The categorizations were made on the basis of the analysis findings. However, in many instances, the absolute cause of failure could not be positively determined within the scope of this program. Consequently, in the case of many of the failures identified as process-related, the failure may also ultimately or indirectly involve the design or materials of the part.

ABBREVIATIONS

DEFECT CATEGORIES

(S) = Surface Related
(BK) = Bulk Related
(W) = Wire Related
(BD) = Wire Bond Related
(DA) = Die Attach Related
(R) = R6104 Related
(EO) = Electrical Overstress
(U) = Undefined
(N) = None

CAUSE CATEGORIES

(P) = Process Related (Caused by a variation or anomaly in one of the steps of fabrication such as masking, oxidation, diffusion, metallization or bonding).
(D) = Design Related (Caused by improper layout or selection of the process steps or the materials)
(M) = Material Related (Caused by an abnormality in the composition of a material or by the presence of material that could not withstand the test program environment).
(W) = Workmanship Related (Caused by an obvious operator mistake during assembly)
(T) = Test Related (Caused by an anomaly in the test conditions or method)
(U) = Undetermined

TABLE E1. TEXAS INSTRUMENTS OPTO-COUPLER FAILURE ANALYSIS SUMMARY

FAILED PARAMETER(S) OR SYMPTOMS	FAILURE MODE	FAILURE MECHANISM	CAUSE OF FAILURE	QUANTITY OF FAILURES BY TEST TYPE	F/A REFERENCE		DEFECT CATEGORY	CAUSE CATEGORY
					SECTION	FIGURES		
SURFACE INSTABILITY FAILURES								
HIGH DARK CURRENT (I_D)	DEGRADED C-B OR C-E JUNCTION	INVERSION OF THE BASE	PROBABLY IONIC CONTAMINATION	11 LIFE 5 HTRB 11 EXT. HTRB 2 STEP-STRESS	4.1	E1	S	P
LOW TRANSFER RATIO (T_R)	DEGRADED B-E JUNCTION	INVERSION OF THE BASE	PROBABLY IONIC CONTAMINATION	11 LIFE 2 HTRB 5 EXT. HTRB	4.2 & 4.2.2	E2-E6	S	P
BOTH HIGH ID AND LOW TR	DEGRADED JUNCTION	INVERSION OF THE BASE	PROBABLY IONIC CONTAMINATION	13 LIFE 7 EXT. HTRB	4.1 & 4.2.2	E1-E6	S	P
BULK RELATED FAILURES								
LOW TRANSFER RATIO	DEGRADED LED	OUTPUT POWER DECREASE	PROBABLY BULK DEFECTS	88 LIFE 1 STEP-STRESS	4.2 & 4.2.1	E2	BK	P
WIRE AND BOND FAILURES								
OPEN EMITTER	LIFTED Au-Al BALL BOND	KIRKENDALL VOIDING	INTERMETALLIC GROWTH DURING BONDING AND R6104 EXPANSION	4 LIFE	4.5	E13-E14	R + BD	P OR M + D
OPEN LED	LIFTED Au-Au	NONE	UNDERBOND AND EXPANSION OF THE R6104	6 LIFE 5 STEP-STRESS	4.6	E15	R + BD	P OR M + D
OPEN EMITTER OR LED	BROKEN WIRES	METAL FATIGUE OR CREEP RUPTURE	EXPANSION OF THE R6104	4 TEMP CYCLE	4.7	E17-E21	R + W	D
TEST ERROR								
OPEN EMITTER	MELTED STRIPE	SHORTED JUNCTION	ELECTRICAL OVERSTRESS	1 STEP-STRESS	4.9	---	EO	T
NONE	---	---	INADVERTENTLY REMOVED FROM TEST	1 LIFE	4.9	---	N	T

TABLE E2. OPTRON OPTO-COUPLER FAILURE ANALYSIS SUMMARY

FAILED PARAMETER(S) OR SYMPTOMS	FAILURE MODE	FAILURE MECHANISM	CAUSE OF FAILURE	QUANTITY OF FAILURES BY TEST TYPE	F/A REFERENCE		DEFECT CATEGORY	CAUSE CATEGORY
					SECTION	FIGURES		
SURFACE INSTABILITY FAILURES								
HIGH DARK CURRENT	DEGRADED C-B OR C-E JUNCTION	INVERSION OF THE BASE	IONIC CONTAMINATION	5 LIFE 3 EXT. HTRB 1 TEMP CYCLE	4.1	E1	S	P
LOW TRANSFER RATIO	DEGRADED B-E JUNCTION	INVERSION OF THE BASE	IONIC CONTAMINATION	2 EXT. HTRB	4.2 & 4.2.2	E2-E6	S	P
BULK RELATED FAILURES								
LOW TRANSFER RATIO	DEGRADED LED	OUTPUT POWER DECREASE	PROBABLY BULK DEFECTS	15 LIFE 1 EXT. HTRB 2 PWR. CYC.	4.2 & 4.2.1	E2	BK	P
LOW TR, LOW BVEBO, HIGH ID	DEGRADED E-B JUNCTION	METAL PENETRATION	CRYSTALLOGRAPHIC FLAWS - AND EXCESSIVE TEMP.	5 LIFE	4.3	E7-E9	BK	P
WIRE AND BOND FAILURES								
OPEN EMITTER OR BASE	LIFTED Au-Al BALL BOND	KIRKENDALL VOIDING AND UNDERBONDING	MARGINAL BONDS AND EXPANSION OF THE R6104	109 LIFE 19 STEP-STRESS 5 EXT. HTRB 6 PWR. CYC.	4.4	E10-E12	R + BD	P + B
OPEN LED	LIFTED Au-Au BALL BOND	NONE	UNDERBONDED BALL AND EXPANSION OF THE R6104	1 LIFE	4.6	E15	R + BD	W
OPEN COLLECTOR	BROKEN BOND	METAL FATIGUE OR FRACTURE	POOR BOND	1 TEMP. CYC.	4.7	E16	BD	W
OPEN LED	BROKEN WIRE	CREEP RUPTURE	EXPANSION OF THE R6104	1 TEMP. CYCLE	4.7	E21	R+W	O
MULTIPLE OPENS	BROKEN WIRES	METAL FRACTURE	R6104 EXPANSION UNDER ACCELERATION	11 ACCEL.	4.8	E22-E23	R + W	O
TEST ERRORS								
OPEN EMITTER	MELTED WIRE	SHORTED JUNCTION	ELECTRICAL OVERSTRESS	2 LIFE	4.9	---	EO	T
SHORTED LED	DEGRADED JUNCTION	BULK DAMAGE	ELECTRICAL OVERSTRESS	1 LIFE	4.9	---	EO	T
NONE	---	---	INADVERTENTLY REMOVED FROM TEST	1 LIFE	4.9	---	N	T

TABLE E3. HEWLETT PACKARD OPTO-COUPLER FAILURE ANALYSIS SUMMARY

FAILED PARAMETER(S) OR SYMPTOMS	FAILURE MODE	FAILURE MECHANISM	CAUSE OF FAILURE	QTY OF FAILURES BY TEST TYPE	F/A SUMMARY		DEFECT CATEGORY	CAUSE CATEGORY
					SECTION	FIGURES		
WIRE AND BOND FAILURES								
OPEN PIN	BROKEN Au WIRE	CREEP RUPTURE AND/OR FATIGUE	EXPANSION OF THE R6104	2 PREL. STEP-STRESS 3 FORM. STEP-STRESS 6 EXT HTRB 24 TEMP. CYC.	5.1	E24-E27	R+W	D
OPEN LED	LIFTED Au-Al BOND	KIRKENDALL VOIDING	INTERMETALLIC GROWTH DURING BONDING AND R6104 EXPANSION	4 EXT. HTRB 4 LIFE	5.2	E28	R&BD	P&D
BULK RELATED FAILURES								
PIN 14 SHORTED	SHORTED JUNCTION	MELT-OVER	JUNCTION IRREGULARITY AND TRANSIENT	1 EXT. HTRB	5.3	E29	BK	P
LOW BVR (LED)	DEGRADED JUNCTION	BULK DEGRADATION	NOT DETERMINED	1 FORM. STEP-STRESS 1 LIFE	5.3	---	BK	U
SURFACE RELATED FAILURES								
HIGH V_{OL}	NOT DETERMINED	NOT DETERMINED	IONIC CONTAMINATION	2 LIFE	5.4	---	S	P
HIGH I_{OH}	NOT DETERMINED	NOT DETERMINED	IONIC CONTAMINATION	1 EXT. HTRB	5.4	---	S	P

TABLE E4. TEXAS INSTRUMENTS LED FAILURE ANALYSIS SUMMARY

FAILED PARAMETER(S) OR SYMPTOMS	FAILURE MODE	FAILURE MECHANISM	CAUSE OF FAILURE	QTY OF FAILURES BY TEST TYPE	F/A REFERENCE		DEFECT CATEGORY	CAUSE CATEGORY
					SECTION	FIGURES		
BULK RELATED FAILURES								
LOW OUTPUT POWER	DEGRADED LED	DISLOCATION CLIMB	CRYSTALLINE IMPURITIES	82 LIFE 7 STEP-STRESS	6.1	E30-E31	BK	P
HIGH REVERSE LEAKAGE CURRENT	DEGRADED JUNCTION	NOT DETERMINED	NOT DETERMINED	20 LIFE 3 POWER CYC. 3 STEP-STRESS	6 2	E32	U	U
TEST ERRORS								
CATASTROPHIC	OPEN WIRE	MELTED WIRE	ELECTRICAL OVERSTRESS	4 STEP-STRESS	6.7	---	EO	T

TABLE E5. RCA LED FAILURE ANALYSIS SUMMARY

FAILED PARAMETER(S) OR SYMPTOMS	FAILURE MODE	FAILURE MECHANISM	CAUSE OF FAILURE	QTY OF FAILURES BY TEST TYPE	F/A REFERENCE		DEFECT CATEGORY	CAUSE CATEGORY
					SECTION	FIGURES		
BULK RELATED FAILURES								
LOW OUTPUT POWER	DEGRADED LED	DISLOCATION CLIMB	CRYSTALLINE IMPURITIES	26 LIFE	6.1	E30-E31	BK	P
SILVER EPOXY RELATED FAILURES								
CATASTROPHIC	SHORTED OR OPEN LED	MIGRATION OF Ag	DECOMPOSITION OF THE Ag EPOXY	10 LIFE 1 STEP STRESS	6.3	E33-E34	DA	M
HIGH REVERSE LEAKAGE CURRENT	INTERNAL MOISTURE	OUTGASSING	DECOMPOSITION OF THE Ag EPOXY	27 LIFE 12 STEP STRESS	6.4	E35	DA	M
HIGH FORWARD VOLTAGE	RESISTIVE DIE BOND	OUTGASSING	DECOMPOSITION OF THE Ag EPOXY	15 LIFE	6.5	---	DA	M
BOND RELATED FAILURES								
CATASTROPHIC	OPEN BOND	SEPARATION UNDER ACCEL.	BONDING ERROR	2 ACCELERATION	6.6	E36	BD	M
TEST ERRORS								
OPEN-CIRCUIT	OPEN WIRE	MELTED WIRE	ELECTRICAL OVERSTRESS	1 LIFE 3 STEP STRESS	6.7	---	EO	T

4.0 FAILURE ANALYSIS REPORTS - TI AND OPTRON OPTO-COUPLERS

4.1 DARK CURRENT FAILURES - SURFACE INSTABILITY

Forty-nine (49) TI parts and nine (9) Optron parts exhibited excessive dark current (I_D). The failed values ranged from 131 nanoamperes to 10 milliamperes (specified limit is 100 nanoamperes maximum at V_{CE}=20 volts). Since the LED is not conducting during measurement of I_D, the dark current is simply I_{CEO} of the phototransistor. In some cases, the excessive I_{CEO} was caused by collector-base leakage. The collector-base junction exhibited a channeled reverse characteristic, as illustrated in Figure E1, and I_{CEO} was equal to h_{FE} I_{CBO}. In other cases, the excessive I_{CEO} was caused by leakage from the collector to the emitter. The transistor displayed a channeled characteristic from collector to emitter and I_{CEO} was equal to I_{CES} indicating that the leakage was due to unamplified current flow across the base region. I_D would completely recover if the part was subjected to an unpowered bake. These findings indicated that the p-type base region of the phototransistor had inverted due to the accumulation of a net positive charge in or above the passivation over the base (surface instability). The charge accumulation most likely was caused by drift of contamination in the passivation or the R6104 under the influence of the applied bias and elevated temperature.

4.2 TRANSFER RATIO FAILURES - DEGRADED LED (I_P DECREASE) AND DEGRADED E-B JUNCTION (GAIN DECREASE)

One hundred twenty-seven TI parts and twenty Optron parts failed due to low transfer ratio (TR). The failed values ranged from .000 to .248 (specified limit is .25 minimum). TR is the ratio of the phototransistor collector current to the LED forward current (I_C/I_F) at V_{CE}=5 volts and I_F=10 mA. $\frac{IC}{IF}$ is dependent on the gain of the phototransistor (β), the transistor flux responsitivity (R_ϕ), the transmission coefficient of the coupling medium (Tm), and the conversion efficiency of the LED (nc) as shown in Figure E2. To determine whether the TR degradation was due to degradation of the phototransistor gain or due to a decrease in the collector-base junction photocurrent, the photocurrent (I_P) was measured at each test point during the life tests and extended HTRB (only). I_P was measured at V_{CB}=5 volts and I_F=10 mA. Each time a failure of TR occurred, the data was examined and the ratio of I_P at the time of failure to I_P prior to stress (I_{PF}/I_{PO}) was determined. If I_{PF}/I_{PO} was equal to or approximately equal to TR_F/TR_O, the failure

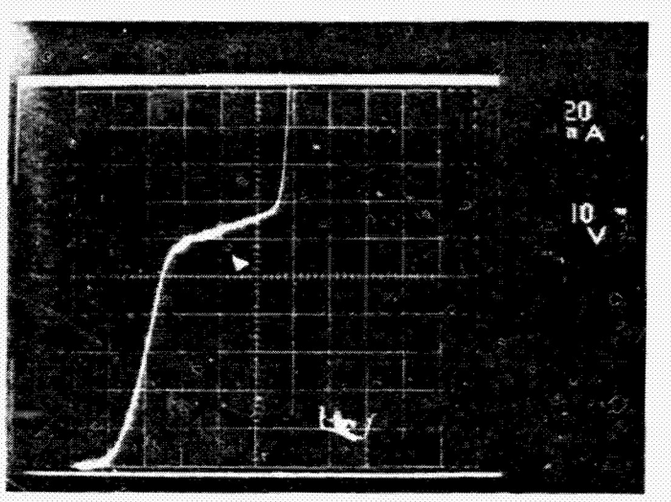

TI S/N 464 (48 HRS/HTRB)

FIGURE E1 - I_{CBO} VS V_{CB} OF THE PHOTOTRANSISTOR OF A PART THAT FAILED I_D AFTER 48 HOURS OF HTRB (I_D = 73 μA)

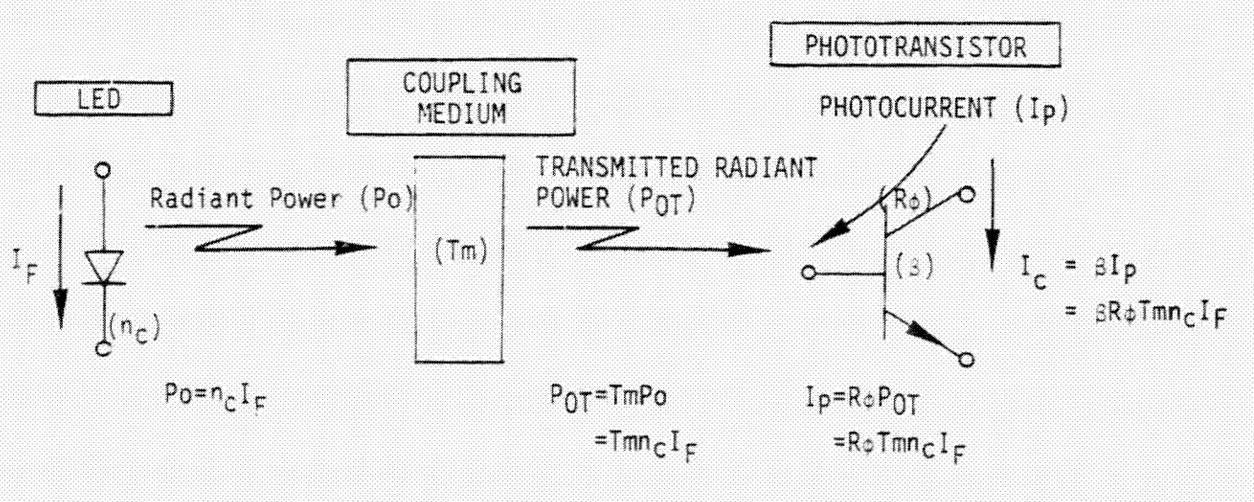

FIGURE E2 - MODEL OF THE OPTICALLY COUPLED ISOLATOR

was classified as an I_p decrease failure; if not, it was classified as a gain decrease failure. (The phototransistor gain decrease could, of course, also be identified by examining the parameter h_{FE} since phototransistor degradation was always accompanied by a decrease in h_{FE}. However, h_{FE} was measured at a fixed collector current (10 mA) which was higher than that developed during measurement of TR. Therefore, h_{FE} did not decrease in proportion to TR, as will be shown later.) In a few instances the TR failure was due to the combined effect of an I_p decrease and a gain decrease. In these instances the failure was classified according to which parameter showed the greatest decrease. In general, all of the parts on test showed a gradual decrease in I_p with time.

4.2.1 I_p DECREASE

Eighty-nine (89) TI parts and eighteen (18) Optron parts exhibited low TR caused by a decrease in I_p. The degradation was non-bake reversible. The behavior of I_p vs. time of the failed parts resembled that displayed by P_0 vs. time of the discrete IRLEDs tested in this program. The discrete IRLED, failed due to gradual, non-reversible P_0 degradation. Therefore, it was suspected that the I_p decrease probably was due to a decrease in P_0 of the opto-coupler LED. To ascertain this, the LED P_0 of representative failed T.I. parts was measured and compared to the P_0 of unfailed parts. Five failed parts were selected from the lowest temperature cell (25°C Life) and four failed parts were selected from the highest temperature cell (150°C Life). No unstressed parts were available since all parts were subjected to screening and preconditioning and exhibited TR decrease to some degree after the powered burn-in. Therefore, four parts that were not used after screening and preconditioning and that did not exhibit any serious shift in TR after burn-in were selected as comparison samples. Each part was delidded and the R6104 resin was removed chemically. The P_0 of the LED at I_F=10 mA was measured using a UDT Model 11A-11B Microphotometer System with the detector focused at the same point on the top surface of the junction of each LED. These test results are presented in column A of Table E6. Next, the constant of proportion, TM · Rϕ, was calculated for each part by dividing I_p by P_0 (I_p = Rϕ · Tm · Po). The values of Tm · Rϕ are given in column B of Table E6. Statistical tests of significance showed no difference between the TM · Rϕ values of the failed parts and the Tm · Rϕ values of the sample parts at the 5% level of significance. This indicated that Tm · Rϕ had not degraded during life testing and that the decrease in I_p during life was due to degradation of the LED P_0. The P_0 decrease was probably caused by a

TABLE E6. LED P_O TEST RESULTS

SAMPLE GROUP	S/N	t_F	I_P (μA) HISTORY PRIOR TO LIFE (POST BURN-IN)	@t_F	(COLUMN A) LED P_O (MICROWATTS)	(COLUMN B) $T_M \cdot R_\phi$
Ref. Samples	962	---	5.90	---	.067	88
	963	---	3.25	---	.031	105
	964	---	6.35	---	.054	117
	965	---	8.95	---	.085	105
25°C Life	941	3000 Hrs	7.44	3.34	.044	76
	433	↓	3.89	2.66	.022	121
	955	4000 Hrs	5.56	2.21	.022	100
	473	|	5.94	3.08	.041	75
	952	↓	5.92	2.25	.032	70
150°C Life	761	168 Hrs.	4.05	2.69	.035	77
	793	1000 Hrs.	5.81	2.19	.026	84
	805	2000 Hrs	5.08	1.58	.024	66
	763	3000 Hrs	7.36	2.60	.026	100

Notes

1. t_F = time of failure
2. I_P and P_O were measured at I_F = 10 mA

mechanism similar to that responsible for the degradation of the discrete IRLEDs. This mechanism is discussed in detail in the IRLED analysis section.

4.2.2 GAIN DECREASE

Thirty-eight (38) TI parts and two (2) Optron parts exhibited low TR caused by a decrease in the gain of the phototransistor. Many of the parts in addition failed $V_{CE(SAT)}$ which is also affected by the TR. The degradation was bake reversible. The TR decrease was shown to be due to a decrease in gain by plotting gain curves of parts before and after baking as illustrated in Figure E3. I_C (and therefore TR) is a function of I_P and the gain ($I_C=\beta I_P$) and the gain in turn varies with I_C ($\beta=fI_C$). The operating point is determined by the point of intersection of the two equations. The curves of β vs I_C were obtained by measuring β at V_{CE}=5 volts and at I_C=1, 10, 12^2, 10^3 and 10^4 microamperes on a curve tracer before and after baking. The photocurrent, I_P, was essentially constant (seven microamperes in the example) before and after baking and a single curve of $I_C=\beta I_P$ μA was plotted by inserting β values of 1, 10, 10^2, 10^3 and 10^4 into the equation. In the example, TR improved from .03 to .80 after baking and this was accompanied by an increase in β at the operating point from 45 to 1100.

As indicated by the β vs I_C curves obtained at the time of failure, the gain degradation was greatest at low collector currents. This suggested that the gain decrease was caused by degradation of the base-emitter junction. Examination of I_B vs V_{BE} of the parts disclosed that the forward characteristic was degraded at the time of failure, as illustrated in Figure E4, and would return to normal after baking, as illustrated in Figure E5. In many instances, the emitter junction also exhibited a channeled reverse characteristic at the time of failure as illustrated in Figure E6. Bake reversible degradation of gain due to degradation of the emitter junction is caused by depletion or inversion of the base side of the emitter junction due to the accumulation of a net positive charge in or on the passivation over the base (surface instability). Thus, these TR failures were probably caused by the same (or similar) mechanism responsible for the bake reversible dark current failures. This is further indicated by the fact that twenty of the TI parts failed both I_D and TR simultaneously. Furthermore, many parts which had failed only one of the parameters were left on test and most of these parts eventually failed both I_D and TR.

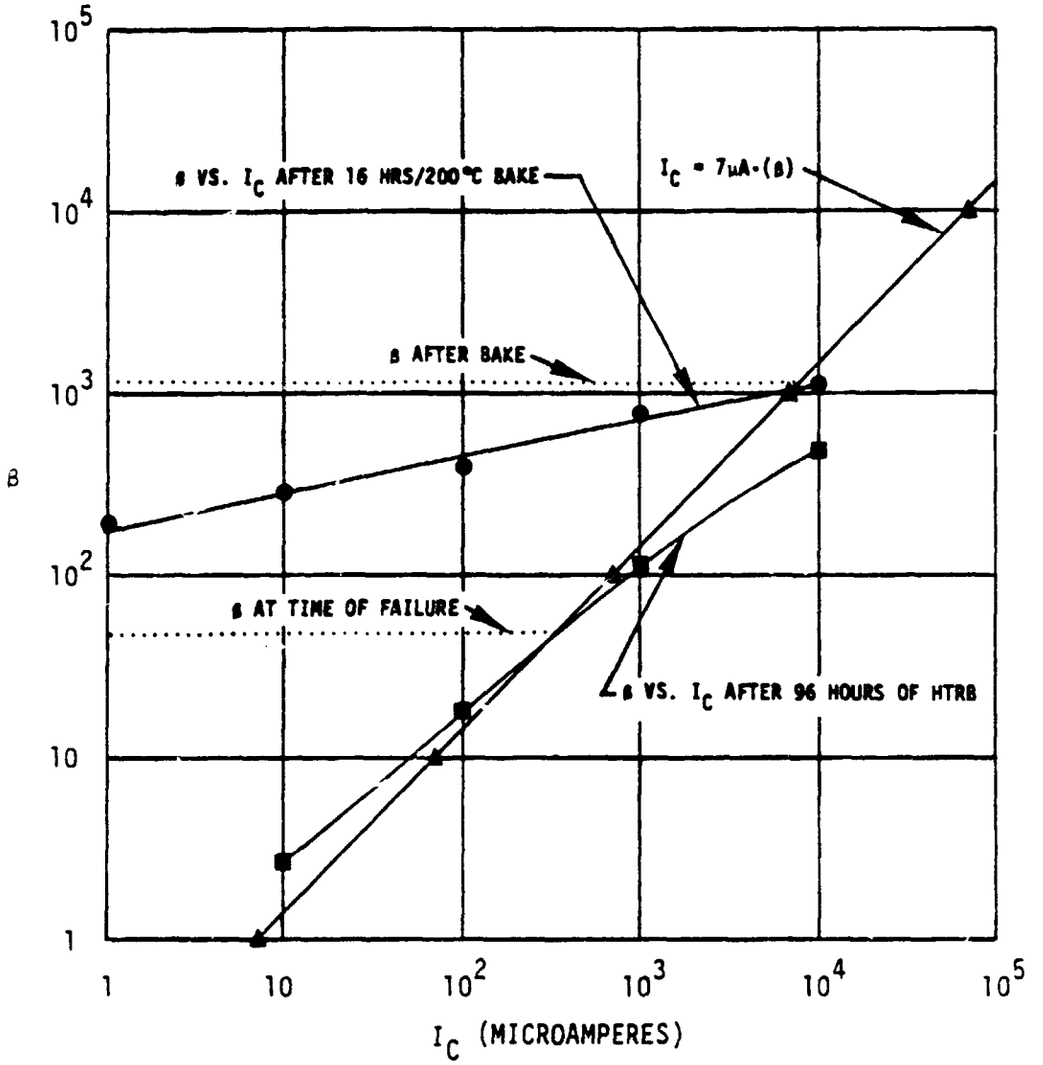

FIGURE E3. β VS. I_C OF S/N 415 (20V, 150°C HTRB FAILURE AT 96 HOURS) BEFORE AND AFTER BAKING

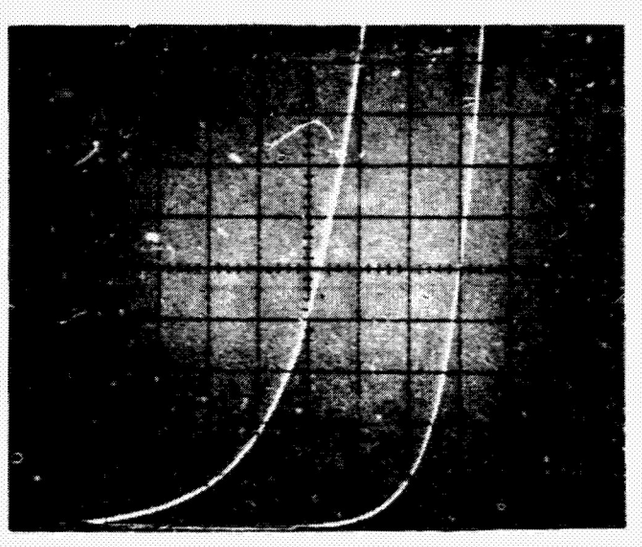

I_B = 50 nA/Div

V_{BE} = 50 mV/Div

FIGURE E4 - FORWARD B-E CHARACTERISTIC OF A PART, TI S/N 743, WITH LOW TR (.004) AFTER 2000 HOURS IN 150°C ACCELERATED LIFE TEST (L/H TRACE) COMPARED TO THAT OF A NORMAL UNSTRESSED PART (TR=.58) (R/H TRACE)

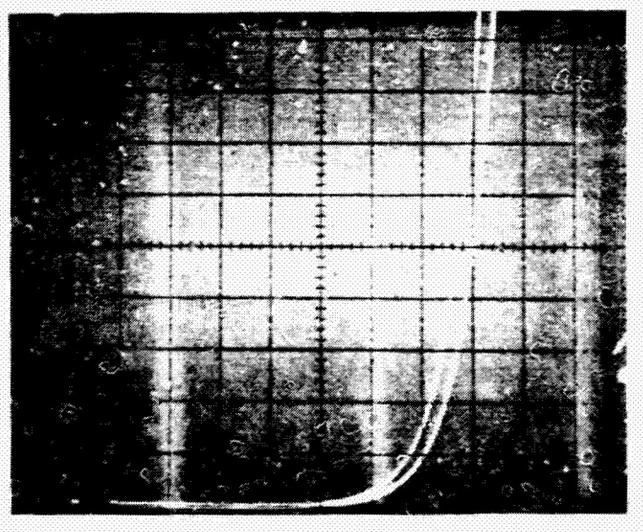

I_B = 50 nA/Div

V_{BE} = 50 mV/Div

FIGURE E5 - B-E CHARACTERISTIC OF S/N 743 (L/H TRACE) AFTER BAKING COMPARED TO THAT OF A NORMAL, UNSTRESSED PART

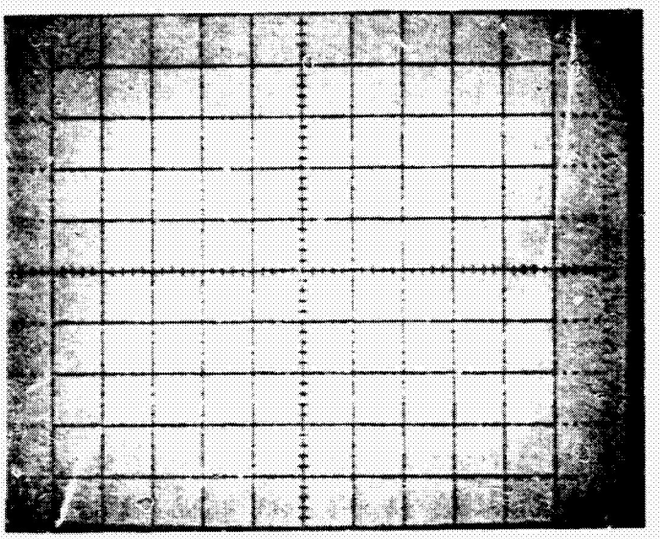

FIGURE E6 - REVERSE E-B CHARACTERISTIC OF A PART (TI S/N 702) WITH LOW TR (.009) AFTER 2000 HOURS IN 125°C ACCELERATED LIFE TEST

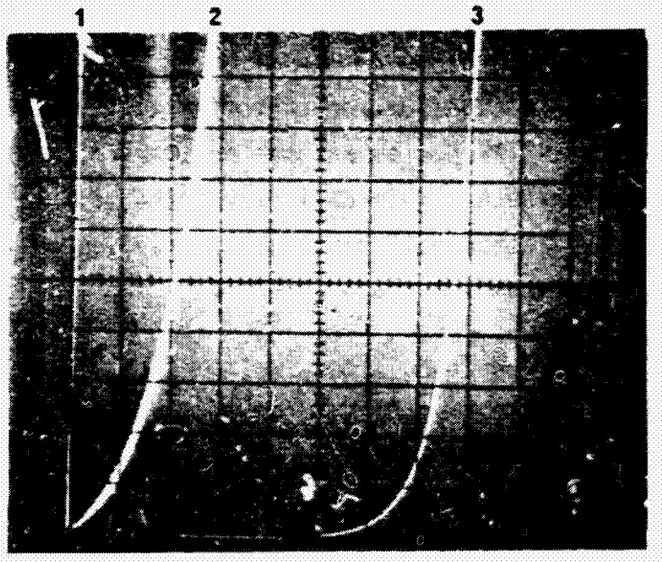

FIGURE E7 - FORWARD CHARACTERISTICS OF THE BASE-EMITTER JUNCTION OF TWO FAILED PARTS (TRACES 1 & 2) AND, FOR COMPARISON, A NORMAL UNSTRESSED PART (TRACE 3).

4.3 TR/ID FAILURES - METAL PENETRATION (OPTRON)

Five Optron parts in the 150°C accelerated life test exhibited low TR and low BV_{EBO} due to degradation of the emitter-base junction that was not bake reversible. Two of these parts also exhibited excessive I_D due to excessive I_{CEO} that was not bake reversible. The forward base-emitter characteristics of the phototransistors were severly degraded as illustrated in Figure E7.

The gold ball bond and the aluminum contact metal were etched from the phototransistor emitters. This revealed a large, deep crater in the ohmic contact region of the parts which exhibited both a degraded emitter and excessive I_{CEO}. An example of such a crater is shown in Figure E8. The parts which exhibited only a degraded emitter were found to contain smaller, shallower pits as illustrated in Figure E9. From these findings it was concluded that aluminum or gold from the bond migrated into the silicon and penetrated the emitter junction causing it to degrade. In the case of the two parts that also displayed excessive I_{CEO}, the metal also penetrated into the collector region. The migration was probably caused by crystallographic damage or flaws in the emitter silicon and the high time/temperature product of the test (all five failures occurred after 1000 hours in the test cell having the highest junction temperature).

4.4 OPEN Au-Al BONDS (OPTRON)

One hundred thirty-nine (139) Optron parts failed during step-stress, power cycling, life testing, and HTRB due to an open emitter. One part failed during step-stress due to an open base. In each instance the open was traced to a lifted gold wire-aluminum metallization ball bond. Every failed bond examined had separated at the gold-aluminum interface.

During the step-stress test, the output of each part was checked after reaching temperature. Any part that exhibited an open circuit at temperature that could be confirmed with a bench test was considered a failed part. Nineteen parts exhibited an open base-emitter junction at elevated temperature. Of these 19 parts, only four failed the post-step 25°C parametric testing. $V_{CE(SAT)}$ was in excess of 33 volts and TR was .000 indicating that the parts contained an open emitter. The failure of the remaining 15 parts was confirmed either by repeating the parametric tests at the step temperature at which the part exhibited the open or by testing the part on a curve tracer and warming it with a heat gun. Analysis of these 19

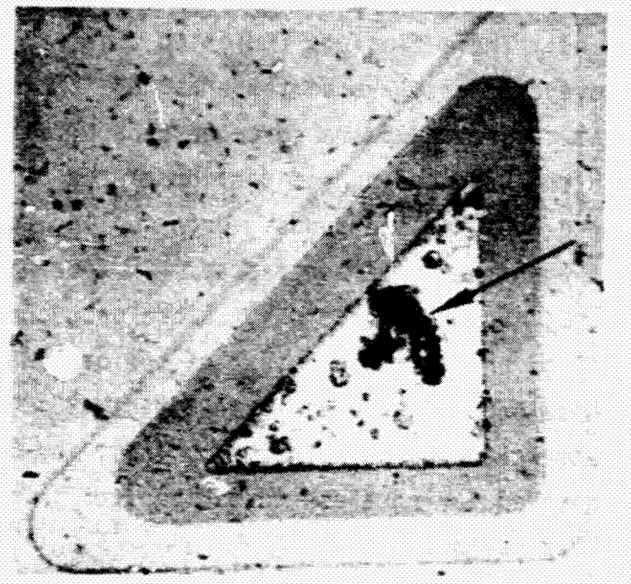

491X OPTRON S/N 955 (4000 HRS/150°C ACCEL. LIFE)

FIGURE E8 - CRATER (ARROW) IN THE EMITTER OHMIC CONTACT

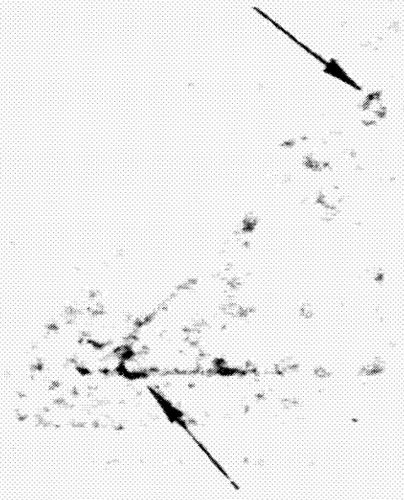

491X S/N 924 (3000 HRS/150°C ACCEL. LIFE)

FIGURE E9 - PITS (APROWS) IN THE EMITTER OHMIC CONTACT

parts established that 18 contained a separated emitter ball bond and one contained a separated base ball bond. These findings indicated that the opens resulted from expansion of the R6104 overcoat at elevated temperature. It is believed that expansion of the overcoat causes an upward force to be applied to the ball due to wedging of R6104 between the unbonded curved portion of the ball and the metallization and that this force ruptured the bonds. Upon cooling to room temperature, most of the bonds closed when the R6104 contracted. In four parts, the R6104 must have intruded into the gap, and the bond did not close upon cool-down. During power cycling, life testing, and HTRB the output of the part was checked at elevated temperature, but only those parts which failed an interim 25°C parametric test or the final parametric tests were considered failed. Thus, the 121 failures due to open emitter bonds encountered during these tests involved intrusion of the R6104 into the gap after bond separation.

Examination of the failure mode of the bonds disclosed two contributing factors. In each instance, the bond had separated in the Au-Al intermetallic region. The amount of intermetallics on the aluminum bond pads ranged from covering as little as 10 percent of the ball diameter as illustrated in Figures E10 and E11 to as much as almost 100 percent of the ball diameter as illustrated in Figure E12. No relationship between the amount of intermetallics present and test temperature or time to failure was evident. The bonds with a low percentage of intermetallics were underbonded, probably due to insufficient time/temperature product during the bonding operation, and consequently were initially weak. In the case of the bonds with a high percentage of intermetallics, the bonds broke cleanly in the intermetallics with no sign of torn gold or aluminum. This indicates that they were weakened by Kirkendall voiding in the Au-Al intermetallics. The voiding probably was initiated by the bonding operation and accelerated to failure by the test temperatures. Thus, the 140 open Au-Al ball bonds encountered during the tests were attributed to a combination of expansion of the R6104 overcoat and bonds that were weak or marginal due to either underbonding or Kirkendall voiding.

During all but the step-stress test, a part was rejected only if it contained an open emitter. A part containing only an open base would exhibit only high BV_{EBO}, BV_{CBO}, and h_{FE} and would not be rejected because these parameters do not have a specified upper MIL-STD-19500/486 limit. Curve tracer tests and examination of the parametric data of the parts containing an open emitter disclosed that only

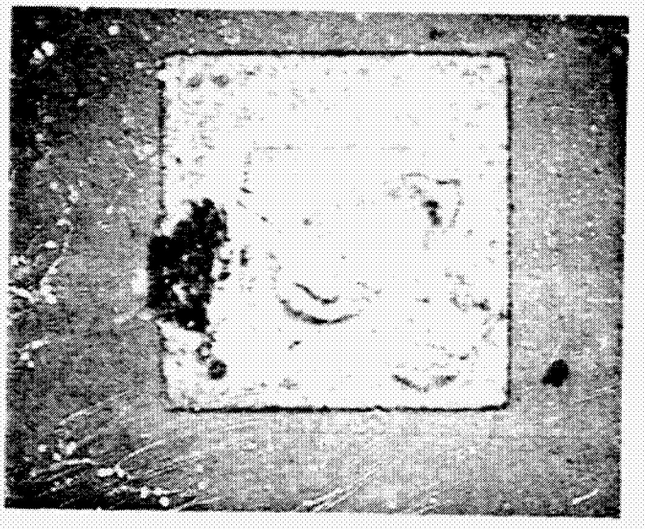

395X OPTRON S/N 153 (96 HR/100°C STEP)

FIGURE E10 - EXAMPLE OF BOND PAD (BASE) WITH VERY LITTLE Au-Al INTERMETALLIC GROWTH

395X OPTRON S/N 305 (504 HRS/POWER CYCLING)

FIGURE E11 - EXAMPLE OF BOND PAD (EMITTER) WITH VERY LITTLE Au-Al INTERMETALLIC GROWTH

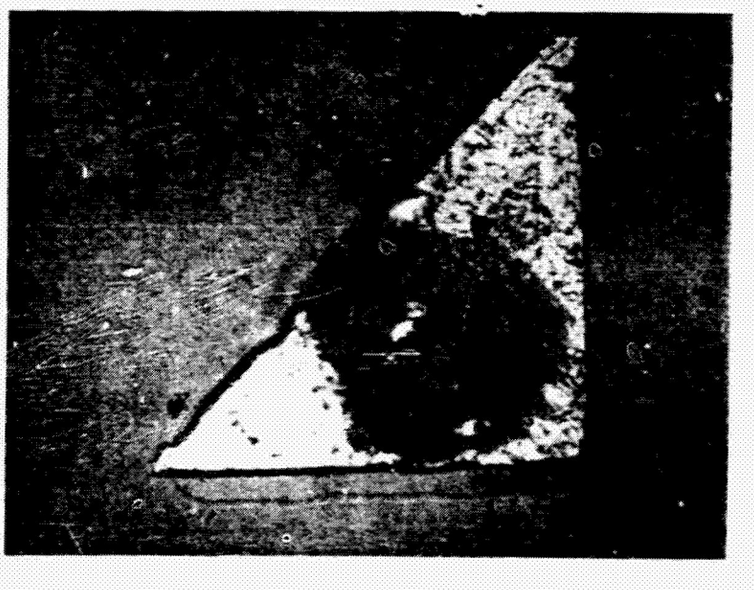

395X OPTRON S/N 505 (168 HRS/150°C ACCEL. LIFE)

FIGURE E12 - EXAMPLE OF BOND PAD WITH Au-Al INTERMETALLICS COVERING ALMOST 100% OF THE BOND SITE

two parts alsc contained an open base. To determine the quality of the base bonds, 28 life test parts that failed due to an open emitter were selected at random and the base wire was pulled with a hooked probe until a visible open occurred. In eleven instances, the ball lifted from the pad with minimal force applied to the wire. In eight instances, the ball broke from the pad before the wire broke and in nine instances the wire broke and the ball bond remained intact. This indicated that the base bond was also affected by the mechanisms identified for the emitter bond, but the low percentage of electrically open base bonds compared to open emitter bonds is not fully understood.

4.5 OPEN Au-Al BONDS (TI)

Four TI parts failed in the 125°C and the 150°C accelerated life tests due to an open emitter. In each instance the open was traced to a lifted Au-Al ball bond and separation occurred in the Au-Al intermetallics. In each case, the aluminum bond pad was completely covered with intermetallics as illustrated in Figure E13. Similar intermetallic growth was evident on the base bond as illustrated in Figure E14. Thus, these four failures were attributed to a combination of expansion of the R6104 overcoat at elevated temperature and Kirkendall voiding in the Au-Al intermetallics.

4.6 OPEN Au-Au BONDS

Eleven TI parts and one Optron part failed during step stress and the life tests due to an open LED. Analysis of these parts established that they contained an open gold wire-gold metallization ball bond at either the anode contact or the cathode contact. Examination of the contact metal in each instance disclosed only a faint impression of the ball and little or no sign of torn metal, as illustrated in Figure E15, indicating that very little bonding had occurred. This condition coupled with the expansion of the R6104 and elevated temperature resulted in the bond failures.

4.7 OPEN WIRES - TEMP CYCLING

Two Optron and four TI parts failed due to open-circuits after temperature cycling. In each instance, the open was traced to a broken gold interconnect wire.

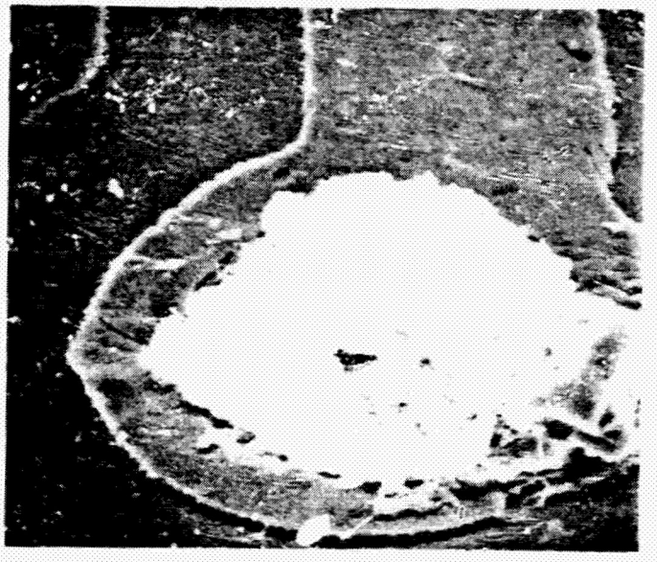

1000X T.I. S/N 455 (4000 HRS/150°C ACCEL. LIFE)

FIGURE E13 - SEM PHOTO OF THE INTERMETALLICS ON AN EMITTER BOND PAD

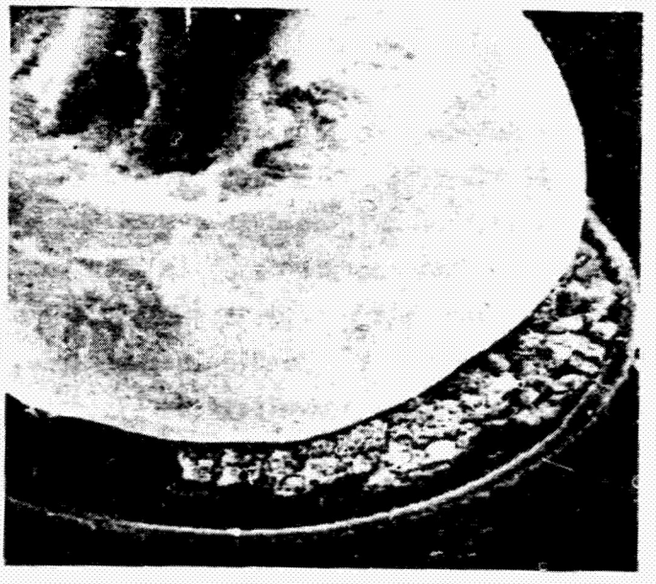

1100X T.I. S/N 455 (4000 HRS/150°C ACCEL. LIFE)

FIGURE E14 - SEM PHOTO OF INTERMETALLICS ON THE BASE WIRE BALL BOND

491X T.I. S/N 243 (144 HR/125°C STEP)

FIGURE E15 - LED CATHODE BOND SITE SHOWING THE FAINT OUTLINE OF THE BALL IMPRINT (A) AND THE MINIMAL JOINT THAT FORMED (B)

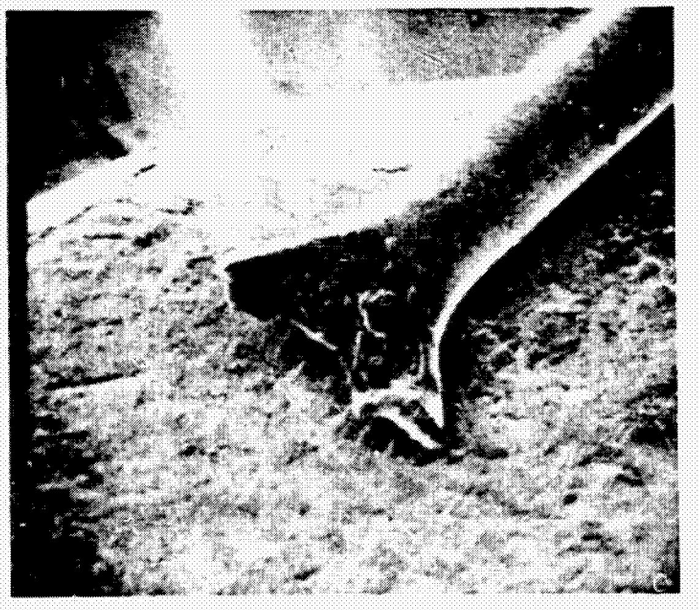

775X OPTRON S/N 31 (TEMP. CYCLE)

FIGURE E16 - SEM PHOTO OF THE OPEN COLLECTOR WIRE BOND AT THE POST

One Optron part contained a break in the collector wire at the heel of the bond at the post as shown in Figure E16. The entire foot of the bond was missing (it probably was torn off during the bonding operation). Thus, the wire was, at best, only marginally attached and probably required only a few cycles of stress to open.

Two TI parts contained an open wire which broke at the edge of the post as shown in Figures E17 and E18. One TI part contained a cathode wire that was badly kinked, as shown in Figure E19, and had broken at one of the kinks as shown in Figure E20. In all three cases, the wire was twisted and striated from flexure at the point of failure as noted in Figure E20. These conditions indicate that the three wires had failed due to fatigue caused by expansions and contractions of the R6104 overcoat during cycling.

One Optron part and one TI part contained a break in the wire above the anode ball and the cathode ball, respectively as illustrated in Figure E21. In both cases, the gold wire exhibited signs of excessive grain growth and slip plane development at the point of failure. This indicated that both of these wires had probably failed as a result of creep rupture [1,2] caused by a combination of time, temperature, and tensile stress in the wire from expansion of the R6104 overcoat.

4.8 OPEN WIRES - ACCELERATION (OPTRON)

Eleven Optron parts failed due to multiple open circuits after acceleration. The opens were traced to a broken gold wire at the post. Nine parts contained a broken emitter wire, two contained a broken base wire, three contained a broken collector wire, and nine contained a broken cathode wire. The wires were torn off at the post, breaking at the heel of the bond or breaking in the wire where it passed over the edge of the post as illustrated in Figure E22. In every failed part, the R6104 completely covered the header and the top of the posts. The R6104 contained a shallow tear at each wire failure site as illustrated in Figure E23. This indicated that the wire breaks were caused by stretching of the R6104 under the forces of acceleration.

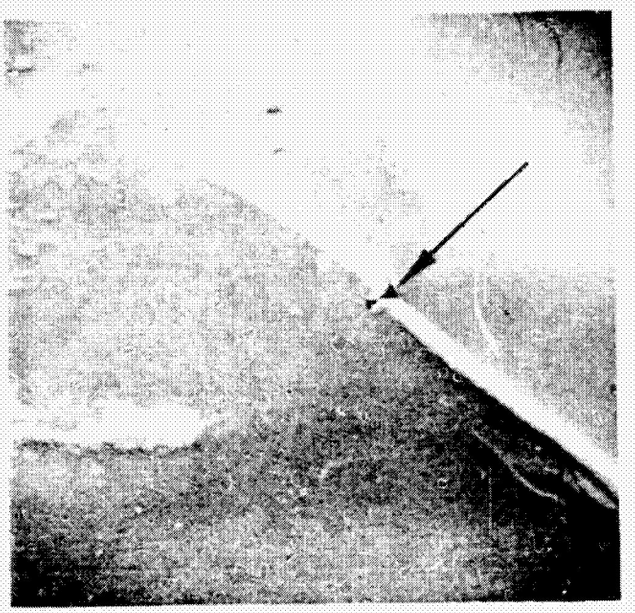

250X T.I. S/N 53 (TEMP. CYCLE)

FIGURE E17 - SEM PHOTO OF THE BREAK (ARROW) IN THE CATHODE WIRE AT THE EDGE OF THE POST

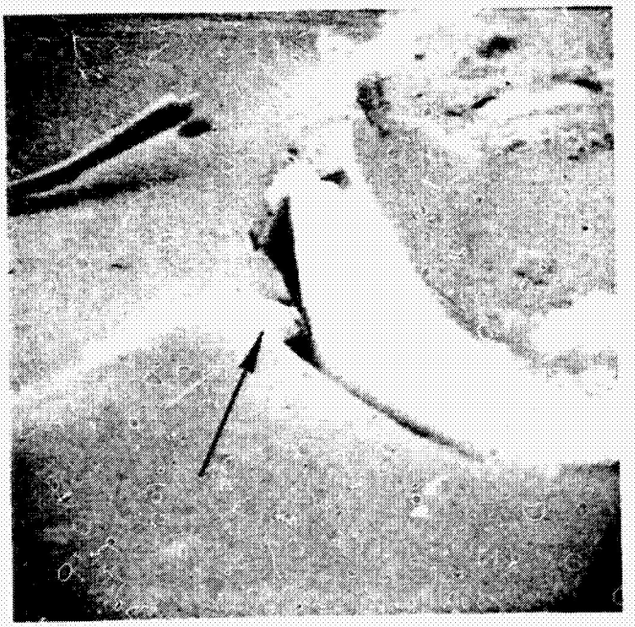

250X T.I. S/N 105 (TEMP. CYCLE)

FIGURE E18 - SEM PHOTO OF THE BROKEN EMITTER WIRE (ARROW) AT THE EDGE OF THE POST

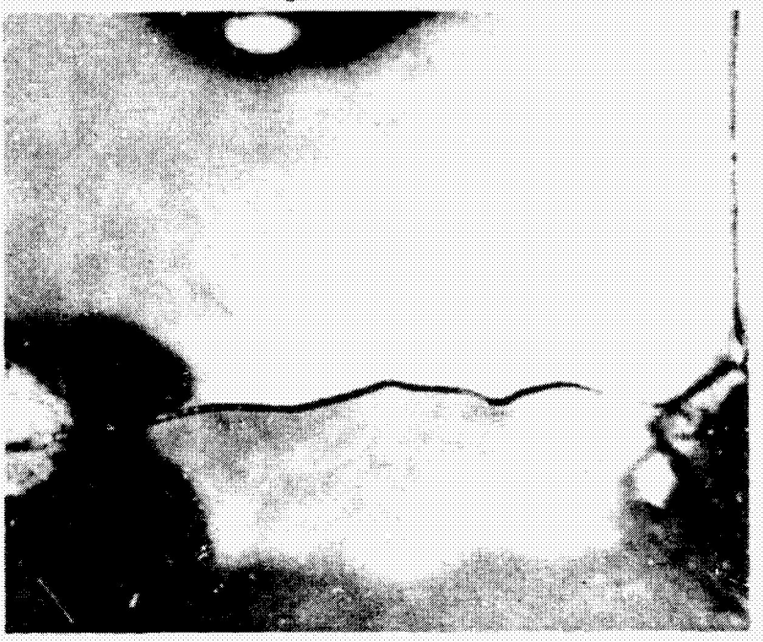

50X T.I. S/N 82 (TEMP. CYCLE)

FIGURE E19 - OPTICAL PHOTO OF THE KINKED CATHODE WIRE

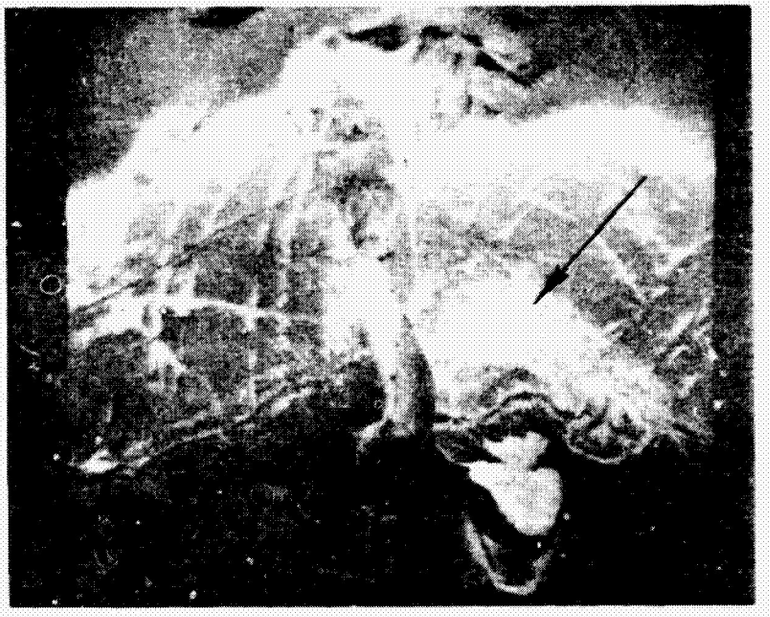

2500X T.I. S/N 84 (TEMP. CYCLE)

FIGURE E20 - SEM PHOTO OF THE BREAK IN THE CATHODE WIRE AT A KINK SHOWING THE FATIGUE STRIATIONS (ARROW).

700X OPTRON S/N 34 (TEMP. CYCLE)

FIGURE E21 - SEM PHOTO OF A WIRE BREAK ABOVE THE ANODE BALL BOND

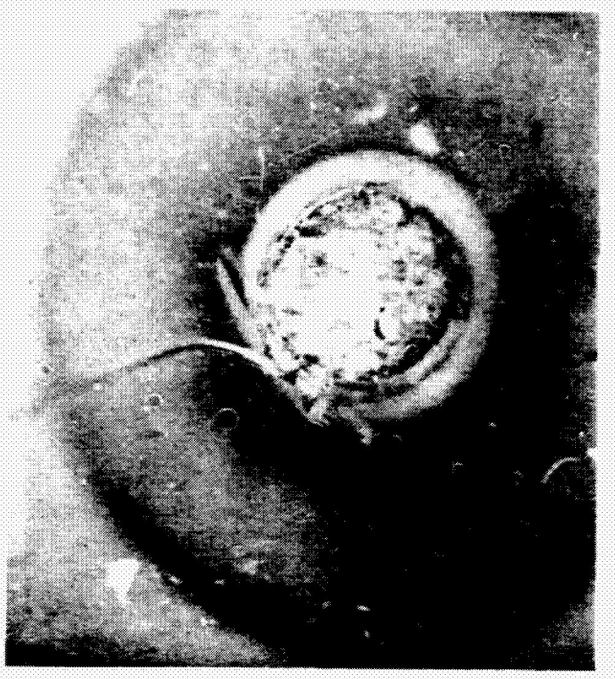

70X OPTRON S/N 551 (ACCELERATION)

FIGURE E22 - EXAMPLE OF A WIRE BREAK AT THE POST AFTER ACCELERATION. THE ARROW INDICATES THE LOCATION OF THE BROKEN END OF THIS WIRE.

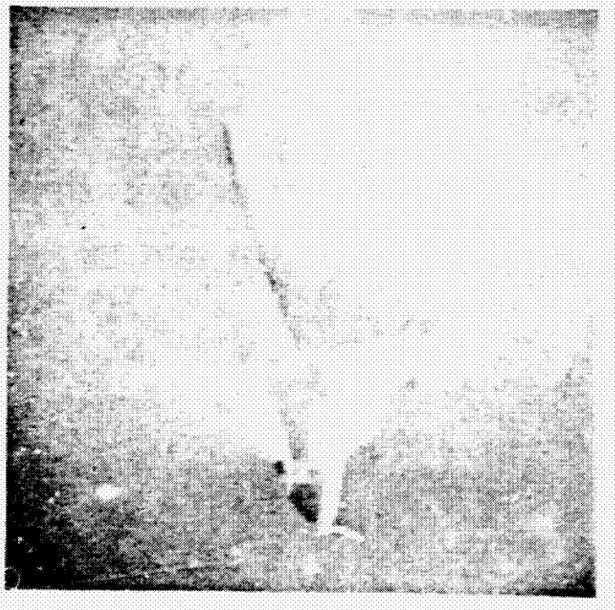

90X OPTRON S/N 551 (ACCELERATION)

FIGURE E23 - SEM PHOTO OF THE TEAR IN THE R6104 AT THE WIRE BREAK SHOWN IN FIGURE E22

4.9 TEST ERRORS

One TI part and two Optron parts failed due to an open emitter that was traced to either a melted open emitter wire or a melted open emitter stripe. In each case the emitter junction contained an associated flash-over short. Consequently, these failures were attributed to accidental electrical overstress of the emitter base junction.

One Optron part failed due to a shorted (4K ohms) LED. Examination of the LED disclosed no sign of any mechanical short, thus it was suspected that the p-n junction of the LED had been electrically overstressed.

One unfailed Optron part and one unfailed TI part were inadvertently removed from test after the 2000 hour parametric tests. The error was discovered too late return the parts to test.

5.0 FAILURE ANALYSES REPORTS - HEWLETT PACKARD OPTO-COUPLERS

5.1 OPEN PINS - BROKEN GOLD WIRE

Thirty-five parts failed during step stress, temperature cycling, and extended HTRB due to an open or resistive pin traced to a broken gold interconnect wire. Five step stress parts contained an open pin 15 (V_{CC}). Four extended HTRB parts contained an open pin 15, one contained an open pin 10 (ground), and one contained an open pin 12 (output). Of the 24 parts that failed temp cycle, seventeen contained an open pin 15, two contained an open pin 12, two contained an open pin 14 (output), five contained an open pin 2 (LED anode), and five contained an open pin 6 (LED anode). (Seven parts contained two open pins.) In every instance the wire broke in a brittle mode at the bend in the wire above the ball bond as illustrated in Figures E24 and E25. In each case, the wire exhibited signs of excessive grain growth and slip plane development at and above the rupture as illustrated in Figures E26 and E27. This indicated that the wires had failed as a result of creep rupture. It is believed that the grain growth and slippage was caused by the combined effect of the elevated temperature and tensile stress in the wire due to expansion of the R6104 at elevated temperature. Most of the wires in each part were dressed with a relatively sharp bend just above the ball bond and this combined with the long horizontal span of the wire probably increased the susceptibility of the wire to the expansion of the R6104. In the temperature cycle test, because the R6104 would expand and contract during the cycling, the failures probably were predominately due to fatigue.

5.2 OPEN LED - LIFTED (Au-Al) BOND

Eight parts failed during life test and extended HTRB due to an open LED traced to a lifted gold wire-aluminum ball bond at an anode contact (pin 6 or pin 2). In each instance, separation occurred at the Au-Al interface and examination of the bond pad disclosed that the entire bond site was covered with gold-rich intermetallics as illustrated in Figure E28. This indicates that the failures were caused by Kirkendall voiding in the intermetallics. The voiding probably was initiated during the bonding operation and accelerated to failure by the test-temperatures and expansion of the R6104.

5.3 MISCELLANEOUS BULK-RELATED FAILURES

One part failed during extended HTRB due to a 6K ohm short between pin 14 (output) and ground. The output transistor contained a melt-over short from its collector (pin 12) to the substrate (ground) as shown in Figure E29. The melt-over

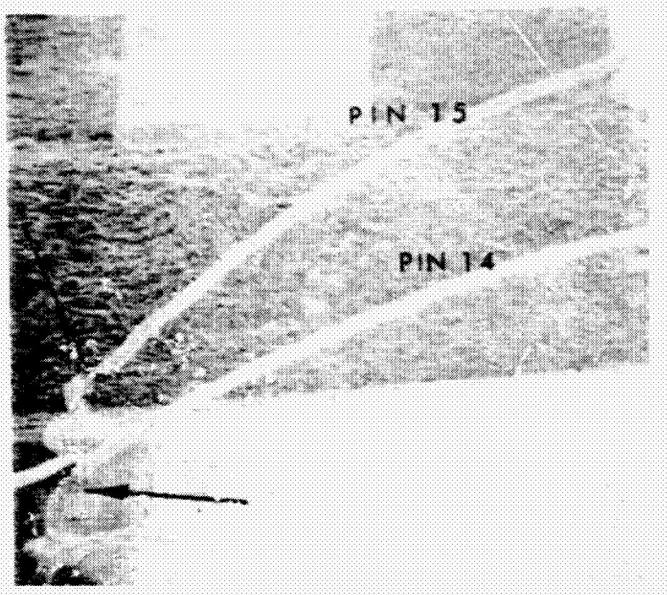

20X H/P S/N 243 (TEMP CYCLE)

FIGURE E24 - EXAMPLE OF TWO WIRE BREAKS (ARROWS) THAT OCCURRED IN TEMP CYCLING. (SEM PHOTO)

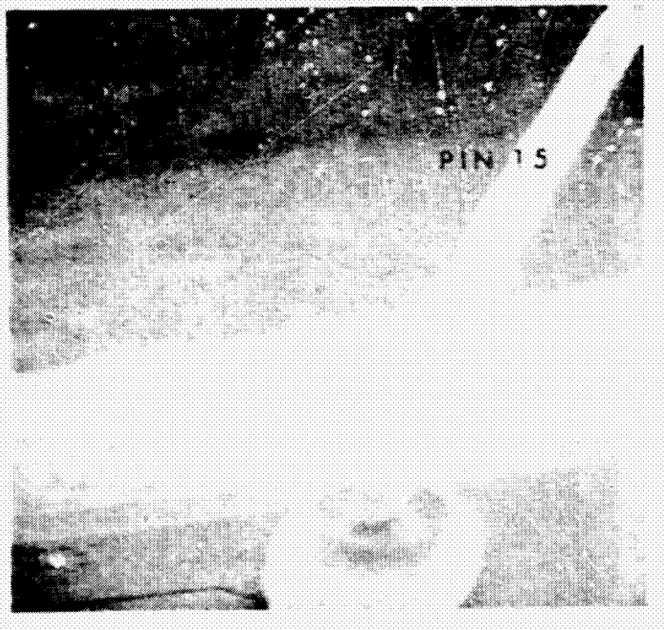

175X H/P S/N 392 (504 HRS/EXT HTRB)

FIGURE E25 - EXAMPLE OF A WIRE BREAK THAT OCCURRED IN EXTENDED HTRB. (SEM PHOTO)

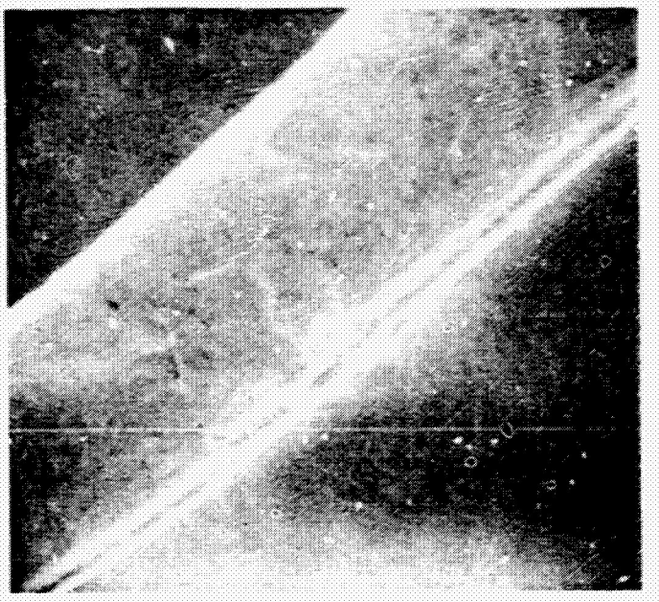

1800X H/P S/N 392 (504 HR/EXT HTRB)

FIGURE E26 - GRAIN GROWTH IN THE GOLD WIRE ABOVE THE BREAK (SEM PHOTO)

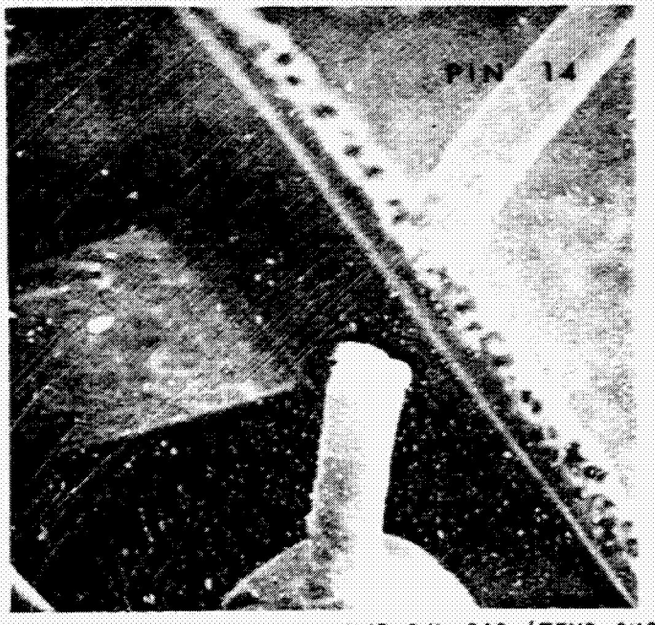

500X H/P S/N 243 (TEMP CYCLE)

FIGURE E27 - CLOSE-UP OF THE PIN 14 BREAK SHOWN IN FIGURE E24 (SEM PHOTO)

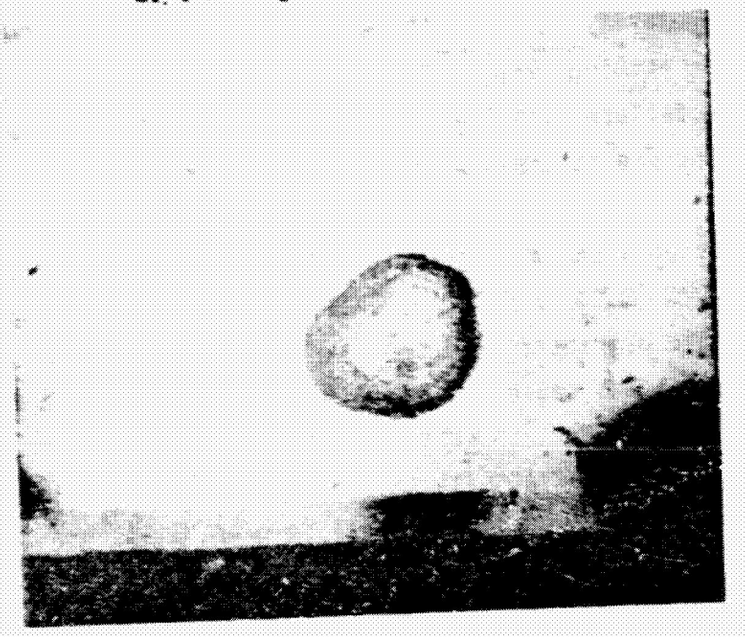

250X H/P S/N 324 (3000 HR/175°C ACCEL. LIFE)

FIGURE E28 - EXAMPLE OF INTERMETALLIC GROWTH ON THE ANODE BOND PAD

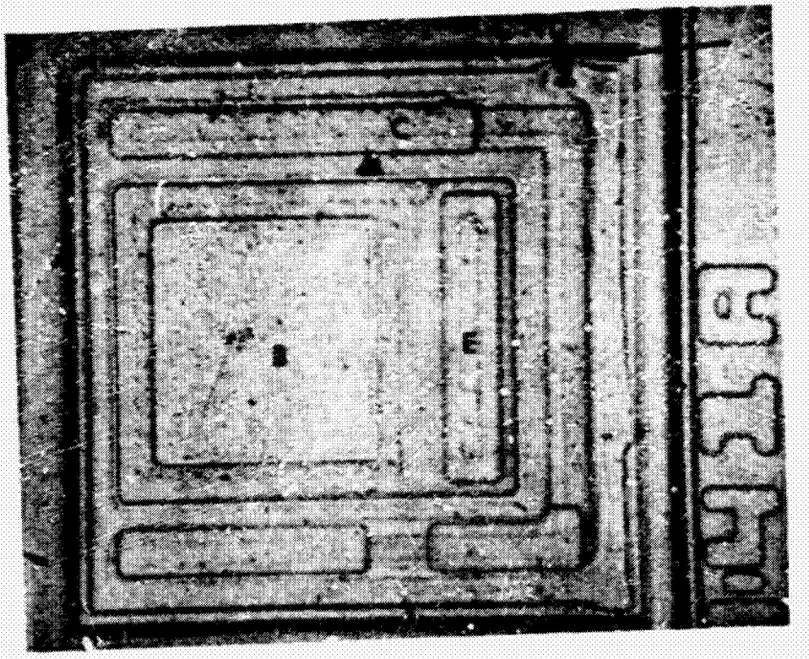

490X H/P S/N 403 (504 HR/EXT HTRB)

FIGURE E29 - PIN 14 OUTPUT TRANSISTOR AFTER REMOVING THE METAL AND PASSIVATION AND ETCHING THE SILICON TO DELINEATE THE JUNCTIONS. THE ARROW DENOTES THE MELT-OVER SHORT THROUGH THE COLLECTOR ISOLATION JUNCTION.

occurred at an irregularity in the collector-to-substrate junction caused by a photolithographic or etching error. The irregularity probably was only a contributing factor. The failure most likely was the result of an electrical transient which caused the junction to break down at the weakest point.

One step stress part and one operating life part failed due to low BVR/2 (3.18 volts) and BVR/6 (2.03 volts), respectively. The low breakdown was isolated to non-bake reversible degradation of the p-n junction but it was not determined whether the degradation was caused by a defect or by an overstress condition.

5.4 MISCELLANEOUS SURFACE INSTABILITY FAILURES

One part failed due to excessive I_{OH}[14] (3.0 mA) after 3000 hours of extended HTRB. Two parts failed due to excessive V_{OL} [14] and V_{OL} [12] after 504 hours in the 125°C accelerated life test. In each case, the failed parameter returned to within specification after subjecting the part to an unpowered bake. This indicated that the failures were due to surface instability caused by contaminant ions or charges in the passivation of the photodetectors. The specific failure mode or mechanism was not determined for these isolated failures.

6.0 FAILURE ANALYSES REPORTS - TI AND RCA LED'S

6.1 LOW OUTPUT POWER

Eighty-nine TI parts and 26 RCA parts failed due to low output power (P_0). Data analysis of the behavior of P_0 with time and temperature indicated that the activation energies of the degradation mechanism were 0.85 eV for the TI parts and 0.91 eV for the RCA parts. To determine the nature of the degradation a series of experiments were conducted which included unpowered baking, infrared spectroscopy, capacitance-voltage plotting, infrared microscopy, microsectioning, dislocation etching, and optical rise/fall time measurements. From the results of these tests, in conjunction with the activation energy estimates for the failure mechanism, the degradation was attributed to the formation of non-radiative acceptor sites within the p-type, diffusion current recombination region. The formation of the acceptor sites was believed to be the result of an increase in the number of incompletely bonded arsenic atoms along dislocation lines due to nonconservative climb of edge character dislocations. Much of the effort leading to these conclusions was conducted as part of a MDAC-St. Louis in-house related study. Because of the magnitude of the experimental results and the complex development of the degradation model, only a summary of the experimental results and conclusions are presented in this report.

6.1.1 Experimental Test Results

Unpowered bakes of representative degraded parts and unstressed parts were performed at a temperature of 250°C for a period of 815 hours. Typical results are shown in Table E7. Output power generally degraded upon baking. Data analysis indicated that the output power of the TI device exhibited the same log time degradation rate at temperature with or without applied bias.

Room temperature measurement of the spectral response of degraded parts using IR Spectroscopy disclosed no extraneous emission peaks in the range from 0.93 to 1.86 μm and no change in the shape of the primary emission peak. C-V plots of degraded parts established that the deep-level states in the space charge region of the p-n junction were either non-existent or very small compared to the shallow-level doping.

TABLE E7 - EFFECTS OF THE 250°C BAKE

VENDOR	S/N	TEST PARAMETER*	PARAMETRIC EFFECTS			
			INITIAL	POST 1000 HRS @ T_A LIFETEST	POST 815 HRS @ 250°C BAKE	REMARKS
RCA	851			(T_A = 150°C)		
		I_R	0.001	170	0.000	
		BV_R	30	35.2	34.9	LIFE
		$V_{F(2)}$	1.070	1.059	1.061	DEGRADED
		$P_{O(100)}$	5.130	3.792	3.98	
				N/A		
RCA	351	I_R	0.001	-	0.017	
		BV_R	36.5	-	36.0	UNSTRESSED
		$V_{F(2)}$	1.060	-	1.063	DEVICE
		$P_{O(100)}$	5.085	-	3.14	
TI	1142			(T_A = 200°C)		
		I_R	0.001	2.00	0.78	
		BV_R	8.717	8.65	8.65	LIFE
		$V_{F(2)}$	1.037	0.989	0.986	DEGRADED
		$P_{O(100)}$	2.215	0.602	0.255	
				N/A		
TI	123	I_R	0.000	-	0.006	
		BV_R	29.9	-	29.9	UNSTRESSED
		$V_{F(2)}$	1.063	-	1.061	DEVICE
		$P_{O(100)}$	3.379	-	2.27	

*PARAMETER UNITS

I_R(A), BV_R(V), $V_{F(2)}$(V), $P_{O(100)}$ (mw)

Measurement of the radiative rise (t_r) and fall (t_f) times and the diode reverse recovery time (t_{rr}) showed that the output power degradation was accompanied by a decrease in the minority carrier lifetime (τ). The values of t_r, t_f, and t_{rr} of representative degraded and unstressed parts were measured and are shown in Table E8. Then, the effective minority carrier lifetime (τ_{eff}) was calculated from the radiative fall time assuming an exp ($-t/\tau$) decay. From this, the diffusion length of the minority electrons in the p-region (L_e) and the minority holes in the n-region (L_h) were estimated and are given in Table E8. The results showed that the degradation was predominately due to a decrease in the diffusion length for electrons in the p-region. This is significant because IR microscopy established that the p-region is the emitting source of the device.

Infrared microscopy also disclosed dark spot defects in degraded parts as illustrated in Figures E30 and E31. These were initially thought to be a possible cause of the degradation. However, using focus height measurements, the location of the defects were placed at 53 μm (RCA) and 143 μm (TI) below the top surface of the die. Microsectioning and etching of the die established that the p-n junction was located 130 μm below the surface in the RCA part and 180 μm below the surface in the TI part. This meant that in each instance the dark spot defects were located well above the junction in the neutral n-type substrate material (in the RCA part) or n-type LPE material (in the TI part) and could not have been responsible for the decrease in the diffusion length for electrons in the p-region.

The dice of degraded parts were sequentially etched to follow the existing dislocation structure into the crystal. This dislocated no perceptible changes in the dislocation structure indicating an absence of any significant density of misfit dislocation near the p-n junction. The parts contained relatively high etch pit densities of $5 \times 10^5/cm^2$ for the TI part and $1 \times 10^5/cm^2$ for the RCA part. Also, the RCA part contained evidence of stacking faults.

6.1.2 Discussion and Conclusions

The tests showed that the degradation in output power was due primarily to a decrease in the diffusion length for minority carrier electrons in the p-type LPE layer bordering the junction. This can only be due to the introduction of non-radiative acceptor sites within the diffusion current recombination region on the p-side. The observed 0.85 and 0.91 eV activation energies, eliminated the

TABLE E8 - RESULTS OF THE RECOMBINATION LIFETIME TESTS

	MEASURED AND CALCULATED VALUES			
	RCA		T.I.	
	S/N 721 (UNSTRESSED)	S/N 1143 (FAILED)	S/N 721 (UNSTRESSED)	S/N 1253 (FAILED)
MEASURED PARAMETERS				
t_r (n Sec)	1450	730	580	380
t_f (n Sec)	1500	440	600	350
t_{rr} (n Sec)	260	108	123	51
CALCULATED PARAMETERS				
τ_{eff} (nS)	660	200	273	159
L_e (μM)	81	44	52	40
L_h (μM)	18	10	12	10

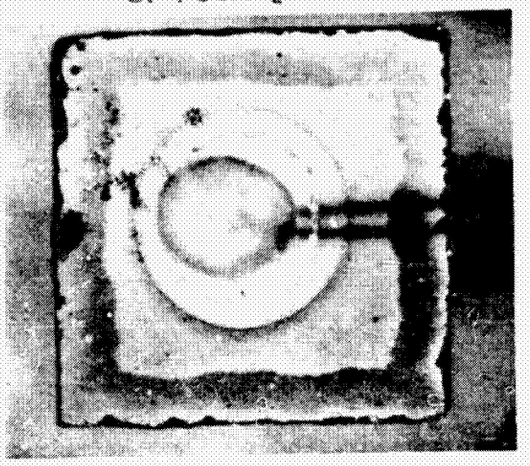

199X

a) OPTICAL PHOTO

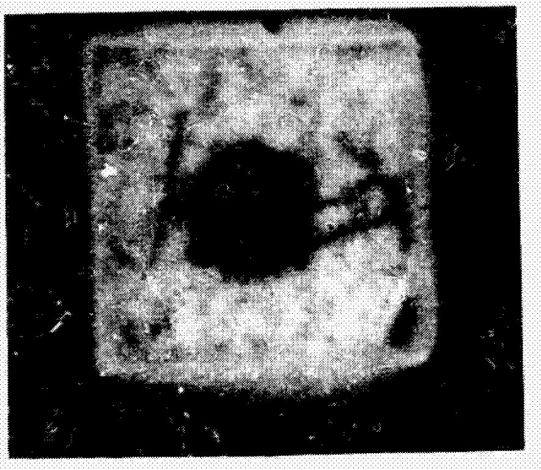

210X

b) INFRARED PHOTO (MIRROR IMAGE WITH RESPECT TO THE OPTICAL PHOTO) AT I_F = 100 mA

FIGURE E30 - OPTICAL AND INFRARED PHOTOS OF A DEGRADED TI LED (S/N 1113, 64 HRS/200°C LIFE).

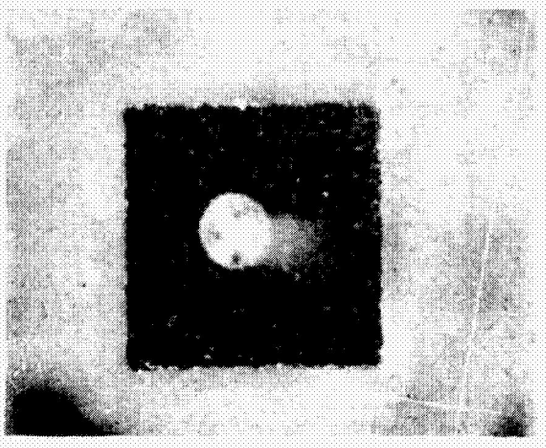

132X

a) OPTICAL PHOTO

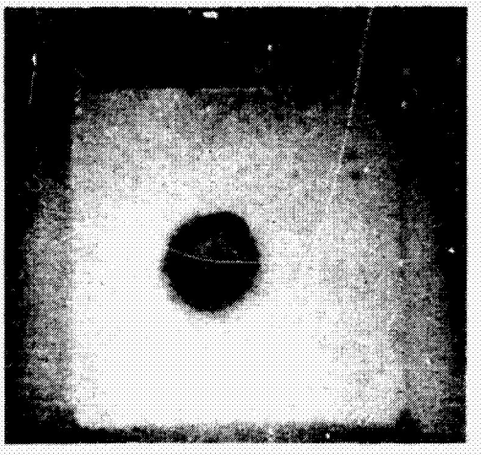

210X

b) INFRARED PHOTO (MIRROR IMAGE WITH RESPECT TO THE OPTICAL PHOTO) AT I_F = 50 mA

FIGURE E31 - OPTICAL AND INFRARED PHOTOS OF A DEGRADED RCA LED (S/N 1223, 512 HRS/200°C LIFE)

majority of published mechanisms, including the Longini-type mechanisms [3,4], as possible causes of the increase in the acceptor sites. The observed activation energies, however, did appear to support a dislocation climb mechanism. Dangling bonds bordering edge character dislocation lines constitute acceptor sites and the number of dangling bonds can increase by non-conservative climb of the edge character dislocations. Climb can be initiated by an excess concentration of vacancies or interstitials in the vicinity of the dislocation line. The rate limiting process retarding this type of climb in the p-region is expected to be migration of arsenic vacancies from the vicinity of the dislocation line. The activation energy for the migration of arsenic vacancies is reported to be about 1 Ev [7].

6.2 EXCESSIVE REVERSE LEAKAGE CURRENT (TEXAS INSTRUMENTS)

Twenty-six TI parts failed during accelerated life, step stress and power cycling due to excessive reverse leakage current (IR). The failed values ranged from 54 to 437 nanoamperes. In each instance, the part exhibited a quasi-exponential reverse characteristic as illustrated in Figure E32. IR would improve somewhat when the parts were baked, but usually IR would not return to specification even after baking the parts for as long as 24 hours at 250°C. This indicated that the failure mechanism most probably involved both a bulk-related mechanism and a surface-related mechanism (such as surface-state density increases). However, dissection and examination of failed parts did not disclose the specific cause of the degradation.

6.3 SHORTED LED (RCA)

Eleven RCA parts failed catastrophically; ten due to a shorted or badly degraded junction and one due to an open-circuit. The shorts and degradation were traced to migration of the conductive silver die-attach epoxy up the sides of the die. As shown in Figure E33, silver has flowed up the side of the die, across the top surface of the chip, and over to the gold ball bond causing a low resistance short from the header to the ball. In the case of the parts that were only degraded, the silver overlapped the p-n junction, but did not flow across the surface to the ball. The silver also migrated out from the die bond, across the gold header plating, and up the sides of the wall. In the open part, all of the silver migrated out from under the die and the die lifted from the header supported only by the interconnect wire as shown in Figure E34.

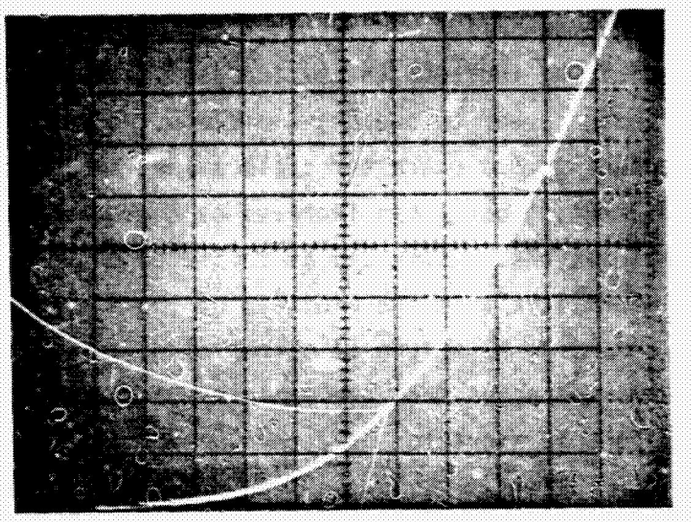

V_F = 0.2 Volt/Div

TI S/N 1212 (64 HRS/200°C ACCEL. LIFE)

FIGURE E32 - EXAMPLE OF THE REVERSE I-V CHARACTERISTIC OF A TI PART WITH HIGH IR.

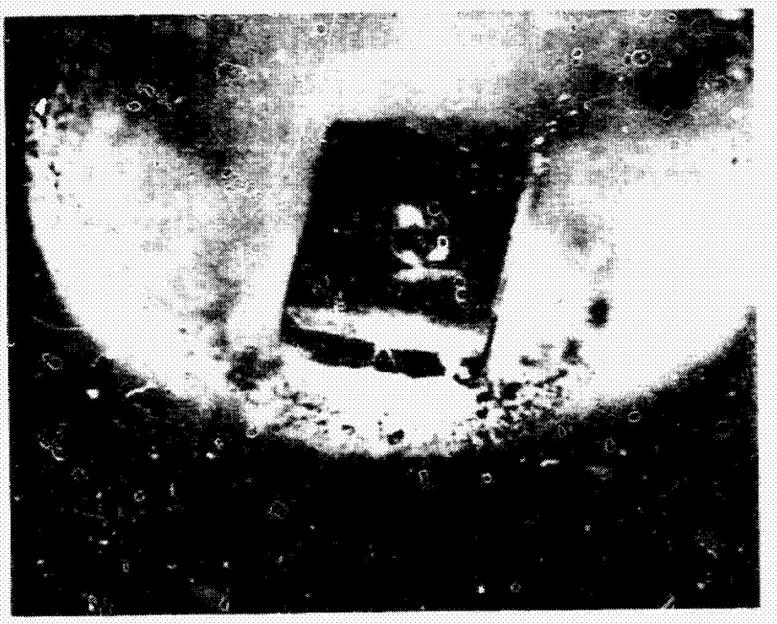

70X RCA S/N 451 (250°C/STEP STRESS)

FIGURE E33 - EXAMPLE OF MIGRATION OF THE SILVER EPOXY.
(A) = Ag DIE BOND
(B) = Ag MIGRATION ALONG THE SIDE OF THE DIE.
(C) = Ag MIGRATION ACROSS THE SURFACE OF THE DIE.
(D) = GOLD BALL BOND.

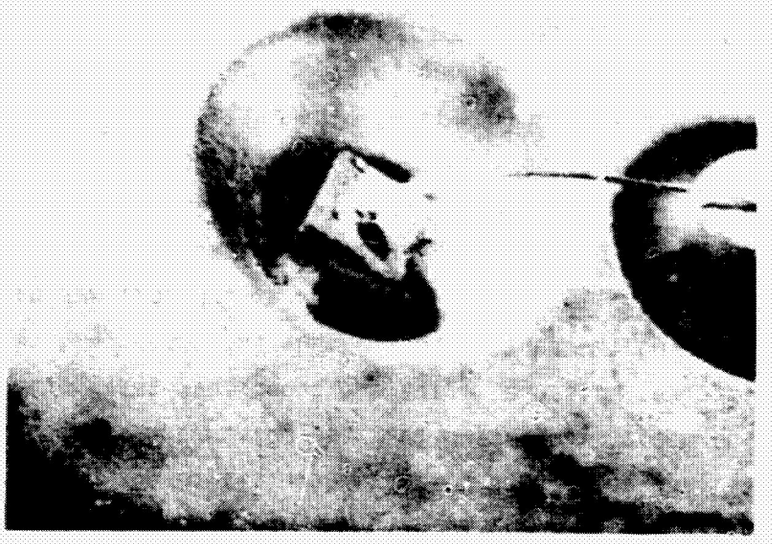

70X RCA S/N 323 (168 HRS/225°C ACCEL. LIFE)

FIGURE E34 - LOOSE DIE THAT RESULTED FROM MIGRATION OF THE SILVER EPOXY.

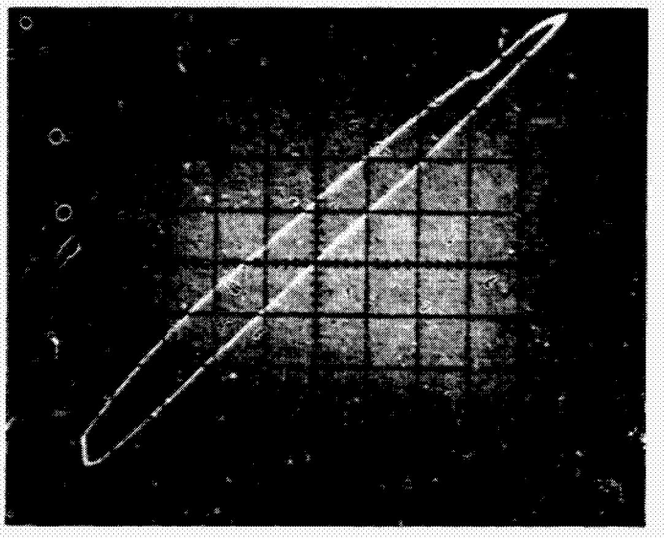

V_R = 0.2 V/Div

RCA S/N 1033 (168 HRS/225 °C ACCEL. LIFE)

FIGURE E35 - EXAMPLE OF THE REVERSE I-V CHARACTERISTIC OF AN RCA PART WITH HIGH IR.

6.4 EXCESSIVE REVERSE LEAKAGE CURRENT (RCA)

Thirty-nine RCA parts failed due to excessive reverse leakage current (IR) during step stress and accelerated life. The failed values ranged from 51 to 452 nanoamperes. When examined on a curve tracer, the reverse characteristic of these parts exhibited a looped trace with inductive and capacitive components, as illustrated in Figure E35. Also, the reverse leakage decayed slowly with time. The reverse leakage usually would not recover if the part was baked, but would recover upon delidding the part. The findings indicated that the high leakage was caused by internal moisture. Fine and gross leak tests of the parts disclosed that they were hermetic, indicating that the moisture was liberated from package material. The silver epoxy used to attach the die to the header is the most likely source of the moisture.

6.5 HIGH FORWARD VOLTAGE (RCA)

Fifteen RCA parts exhibited high forward voltage at I_F=100 mA (VF_{100}) during accelerated life. Most of these parts also exhibited high V_F at I_F=50 mA. VF_{100} of these parts ranged from 1.60 to 2.52 volts. The high V_F was traced to excessive IR drop from the die to the header. This indicated that the silver die attach epoxy had deteriorated and become resistive. When the die was nudged with a probe, it separated from the header relatively easily. The epoxy appeared porous, but no sign of silver migration was evident, indicating that migration was not the principle mechanism. In view of the findings involving the RCA high IR failures, it is probable that the epoxy resistance increase was caused by outgassing of the epoxy binder materials at elevated temperature.

6.6 OPEN BONDS (RCA)

Two RCA parts failed due to an open-circuit after the acceleration test. One open was traced to a broken gold ball bond at the cathode contact. No actual ball existed because it was undersized and had been smashed flat during the bonding operation as shown in Figure E36. The other open was traced to a broken gold stitch-bond at the cathode post. The wire had broken at the heel of the bond and the entire foot of the bond was missing indicating that the wire had been only marginally attached to the post. The appearance of the bond was identical to that of the bond examined in the initial construction analysis part as shown in Figure A53. Thus both of these failures were attributed to defective bonds that broke under the force of acceleration.

550X RCA S/N 753 (ACCELERATION)

FIGURE E36 - SEM PHOTO OF THE OPEN CATHODE BALL BOND.

6.7 TEST ERRORS

Four TI parts and four RCA parts failed due to an open-circuit. In each case, the open was traced to a melted open gold cathode interconnect wire (25 to 90 percent of the wire vaporized). By probing the die, it was determined that in every instance the die had not sustained any electrical damage or degradation. Consequently, these failures were attributed to excessive forward current caused by an accidental overvoltage or overload.

REFERENCES

1. E. Cohn, "Effects of Wire Quality and Capillary Maintenance on Bonding Reliability", Solid State Technology, September, 1975.
2. C. N. Adams, "A Bonding-Wire Failure Mode in Plastic Encapsulated Integrated Circuits", 11th Annual Proceedings, Reliability Physics 1973, IEEE Catalog No. 73CH0775-9PHY.
3. L. R. Weisberg, "Electroluminescent Diode Degradation Models", 8th Annual Proceedings, Reliability Physics, IEEE Cat. No. 70C59-Phy, 43, (1970).
4. A. S. Jordon and J. M. Ralston, "A Diffusion Model for GaP Red LED Degradation", Journal of Applied Physics, 47, 4518, (1976).
5. P. M. Petroff and L. C. Kimerling, "Dislocation Climb Model in Compound Semiconductors with Zinc Blende Structure", Applied Physics Letters, 29, 461, (1976).
6. P. M. Petroff, O. G. Lorimor, and J. M. Ralston, "Defect Structure Induced During Forward-Bias Degradation of GaP Green-Light-Emitting Diodes", Journal of Applied Physics, 47, 1583, (1976).
7. H. R. Potts and G. L. Pearson, "Annealing and Arsenic Overpressure Experiments on Defects in Gallium Arsenide", Journal of Applied Physics, 37, 2098, (1966).

APPENDIX F

DATA ANALYSIS TECHNIQUES

Table of Contents

1.0 INTRODUCTION

The evaluation of the opto-coupled device/LED test data generally followed published techniques [F1][F2][F3]. A general discussion of the analytical approach is provided in section 10 of the main text. The purpose of this appendix is to describe in greater detail the analytical methods applied to the data. For ease of discussion, the analytical methods are separated into two sections: 1) Analysis, which deals with the analysis of the test data obtained from the individual tests, and 2) Synthesis, where the individual test results are synthesized into Arrhenius equations and failure rate equations.

2.0 ANALYSIS

2.1 Failure Time Interpolation

The reported device failures exhibited parameter values that were outside the prescribed limits and, in some cases, catastrophic failures. In the case of a failure due to a degraded parameter value, the failed parameter value and previous non-failed values of the parameter were obtained from the test records. Then the failed and non-failed values, along with the corresponding measurement time, were used to generate an empirical equation relating time to the parameter value. Solving the empirical equation, using the parameter failure limit, provides an interpolated estimate [F4] of the actual failure time of the device (Figure F1). When a failure exhibited more than one failed parameter, each failed parameter was interpolated and the earliest failure time used for the device. Using this procedure to estimate the failed time for each failed device, allowed the number of data points to reflect the number of device failures.

In the case of non bond related catastrophic failures, and in cases where there was a dramatic shift in the parameter value, a straight line interpolation method was used. Failure times for open circuits due to bond related failures were plotted as the time the open circuit was first detected. Open circuits were detected while monitoring devices in situ at the life test temperatures and while performing 25°C electrical measurements.

2.2 Failure Distribution Evaluation

Initially, all test cell data was fitted to a single lognormal distribution [F5]. However, the results of some of the single distribution analysis indicated that a single distribution did not provide a good representation of the observed data. Therefore, a bimodal distribution (consisting of two lognormal distributions) was evaluated. This bimodal failure distribution is:

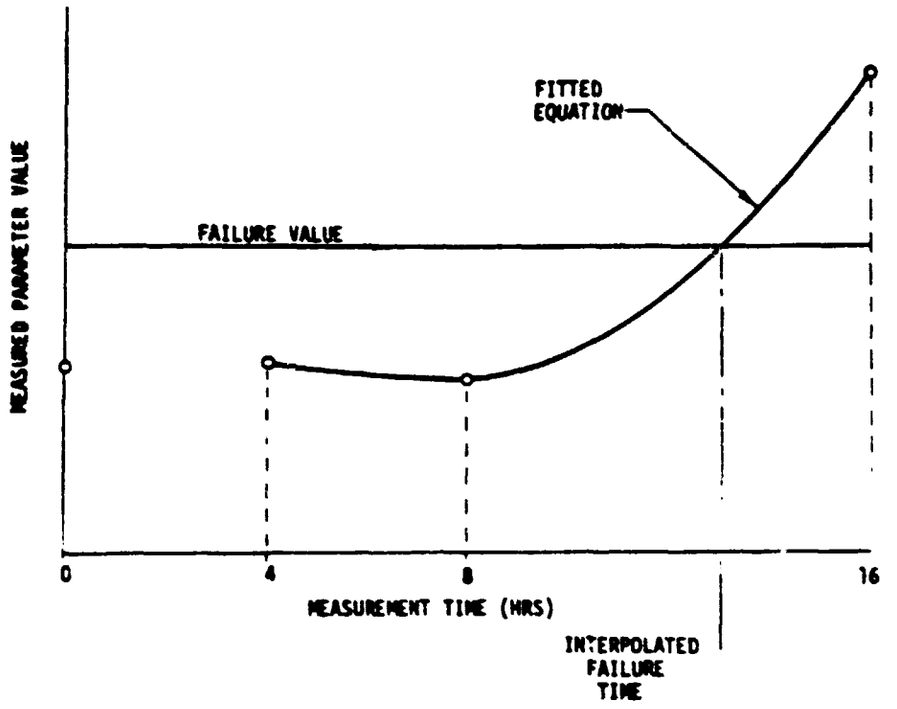

FIGURE F1. INTERPOLATED FAILURE TIMES

$$\text{Cdf life}_{\text{TOTAL}} = \left\{ \frac{1}{\sigma_F \sqrt{2\pi}} \int_0^t \frac{1}{t'} \left\{ \exp - \frac{(\ln t' - \mu_F)^2}{2\sigma_F^2} \right\} dt' \right\} \quad (\%F)$$

$$+ \left\{ \frac{1}{\sigma_M \sqrt{2\pi}} \int_0^t \frac{1}{t'} \left\{ \exp - \frac{(\ln t' - \mu_M)^2}{2\sigma_M^2} \right\} dt' \right\} \quad (\%M) \qquad (2)$$

where:

μ_F = ln (median life of the freak distribution)

σ_F = standard deviation of the freak distribution

μ_M = ln (median life of the main distribution)

σ_M = standard deviation of the main distribution

$\%_F$ = the percentage of the total population that is described by the freak distribution

$\%_M$ = the percentage of the total population that is described by the main distribution

t = use time, or cycles in the case of cyclic related failure data

The bimodal distribution was fitted using a graphical method [F2], [F3]. Then the graphical result was used with equation (1) and the calculated probability was compared to the test probability at each failure time. From this starting point, the values of the unknowns in equation (1) were iterated and the probabilities compared until plots of the resulting equation appeared to provide a good representation of the observed data. Plots of the resulting bimodal distribution, the test data, and the corresponding freak and main distributions are shown in Section 10.

3.0 SYNTHESIS

3.1 Arrhenius Equation

The Arrhenius equation, as defined in Section 10, is:

$$t_{50\%} = A \exp\left[\frac{E_A}{k\,T}\right]$$

The linear transform of this equation is:

$$\ln t_{50\%} = \ln A + \frac{E_A}{k}\left[\frac{1}{T}\right]$$

The transformed Arrhenius equation was evaluated using a linear regression analysis that assumes the junction temperature is a known value and $\ln t_{50\%}$ is the only variable [F6][F7]. The results of this evaluation is shown in Section 10.

3.2 Failure Rates

The failure rate for a single distribution is defined as [F8]:

$$\lambda(t) = \frac{f(t)}{R(t)}$$

where:

$\lambda(t)$ = the instantaneous failure rate at time t.

$f(t)$ = the failure density at time t.

$R(t)$ = the reliability at time t.

Also, a lognormal failure rate for a single distribution is defined as [F9]:

$$\lambda(t) = \frac{\frac{1}{t\,\sigma\sqrt{2\pi}} \exp - \frac{(\ln t - \mu)^2}{2\sigma^2}}{\frac{1}{\sigma\sqrt{2\pi}} \int_t^{\infty} \frac{1}{t'} \left\{\exp - \frac{(\ln t - \mu)^2}{2\sigma^2}\right\} dt'}$$

Where:

μ = ln (median life)

σ = the standard deviation

Assuming that an Arrhenius equation defines the median life at a junction temperature provides the following temperature dependent, lognormal failure rate:

$$\lambda(t) = \frac{\frac{1}{t\,\sigma\sqrt{2\pi}} \exp - \frac{[\ln t - (\ln A + E_A/k\,T)]^2}{2\sigma^2}}{\frac{1}{\sigma\sqrt{2\pi}} \int_t^\infty \frac{1}{t'} \left\{ \exp - \frac{[\ln t' - (\ln A + E_A/k\,T)]^2}{2\sigma^2} \right\} dt'}$$

For a bimodal distribution consisting of two lognormal failure rates, the total failure rates is defined as:

$$\lambda(t)_{Total} = \left\{\lambda(t)_{Freak}\right\} \text{ (\% Freak)} + \left\{\lambda(t)_{Main}\right\} \text{ (\% Main)}$$

4.0 REFERENCES

[F1] D. S. Peck & C. H. Zierdt, Jr., "The Reliability of Semiconductor Devices in the Bell System", Proceedings of the IEEE, Vol. 62, 00.185 - 211, February 1974.

[F2] D. S. Peck, "The Analysis of Data from Accelerated Stress Tests", Proceedings 9th Annual Reliability Physics Symp., pp. 68-83, 1971.

[F3] F. H. Reynolds, "Thermally Accelerated Aging of Semiconductor Components", Proceedings of IEEE, Vol. 62, pp. 212-222, February 1974.

[F4] P. J. Davis, "Interpolation and Approximation", Dover Publications Inc., N.Y., 1975.

[F5] J. Aitchison and H. A. C. Brown, "The Lognormal Distribution", Cambridge University Press, N.Y., 1969.

[F6] M. G. Natrella, "Experimental Statistics", National Bureau of Standards Handbook 91, 1963.

[F7] F.S. Acton, "Analysis of Straight Line Data", Dover Publications, Inc., N.Y., 1966.

[F8] I. Bazovsky, "Reliability Theory and Practice", Prentice-Hall, Inc., Englewood Cliffs, New Jersey, 1961.

[F9] I. R. Goldthwaite, "Failure Rate Study for the Log Normal Lifetime Model", IRE (NSRQCE) Conference, pp. 208-213, 1961.

APPENDIX G

TEMPERATURE CYCLE STRESS PERFORMANCE OF THE DUAL HERMETIC OPTICAL ISOLATOR (6N134)

PREPARED BY

HEWLETT PACKARD

TEMPERATURE CYCLE STRESS PERFORMANCE OF THE DUAL HERMETIC OPTICAL ISOLATOR (6N134)

The purpose of this report is to present the test results characterizing the cycle stress performance of the 6N134 Opto Isolator to the McDonnell Douglas Tests.

A problem was indicated by the temperature cycle results of an evaluation that McDonnell Douglas was conducting for NASA (1) on a number of optical isolator products.

The McDonnell Douglas test showed a rather high failure rate beginning in the early cycles of the stress. Although the stress imposed was above the rating of the device, it was a legitimate acceleration of stress for the purpose of generating failures in a reasonable time period used in their comparative life study. Unfortunately, the results did not compare with the history and experience HP Reliability Engineering has had with this product. HP's data history was based on a different stress profile that was also accelerated, however, did not match the stress used by McDonnell Douglas' test, i.e., power plus temperature cycle.

HP Reliability Engineering took on a task to more nearly match the stress level used by McDonnell Douglas. Two differences may be worth mentioning. The temperature chamber was a small one. The cabling and circuit boards remained physically stationary during temperature excursions to reduce possible intermittent contact problems. The monitor circuits may be different (HP didn't receive a schematic of the monitor circuits used), however, the stress circuit itself was the same. Particular attention was taken to design a monitor circuit that would not false trigger.

The temperature cycle was from -55°C to 125°C with fifteen minutes dwell at each temperature extreme and the transfer set at the fastest rate (10 minutes). The monitor circuit was active for each device under stress. The combined power, 376 mW plus the upper 125°C chamber temperature brought the hot spot temperature between 164°C to 182°C.

Initially two samples of twenty units each were tested. One sample was of the same date code as was tested by McDonnell Douglas (605). This means 1976, week number 5. The second sample was from the current production. It should be pointed out that the present product is an upgraded design since date code 605.

The test results were plotted on Weibull Probability paper. The McDonnell Douglas results were included on the same paper. The coordinates are the accumulated percent of device failures versus the cycle of failures. The mean cycle life (63% failure) and β were as follows:

McDonnell Douglas Test Results.....4[illegible] cycles, β= 1

HP Test of similar date code (605)..215 cycles, β= 2.8

HP Test of current packages design..370 cycles, β= 2.8

The key revelation is in the slope β this data traces. The β parameter of the Weilbull Transformation can be interpreted for the life cycle characteristics as follows:

Less than 1	-decreasing failure rate, associated with infant mortality.
Equal to 1	-a constant failure rate, associated with normal use period.
Greater than 1	-an increasing failure rate, associated with a wear-out mode.

The analysis of the date code 605 T.C. failures conducted by McDonnell Douglas and HP have established a bond wire fatiguing mechanism as the cause of failure. The β of 2.8 on the HP tests fits the wear-out model. The β of one on the McDonnell Douglas tests does not match the determined failure mechanism. The devices on these tests were run out to 500 cycles. A possible explanation could be that the cycle-time failures were prematurely indicated by false triggering of the monitor circuits. This sort of triggering would be of a random nature which in turn would plot with a β equal to one.

An improvement was expected in the number of cycles to a given percent failed in the current design over the earlier design used in the 605 date code. The upgrading to the current design dealt with reducing the wire bond lengths in the wire bond lay-out. Reduced lead lengths effects a lower fatiguing rate. The 605 date code had a projected 99.5% failure rate at 400 cycles. Although significantly improved, the current design has projected 74% failures at 400 cycles. Please note that all devices exhibited in Graph 1 were built with 1 mil gold bond wire.

Stress analysis of the isolator design with the 1.0 mil gold bonding wire showed that the maximum strength for the wire was being reached (2). In order to improve the fatigue boundary without compromising the performance characteristics of the 6N134, it was decided to build several samples using 1.5 mil wire.

Forty 1.5 mil wired devices were temp cycled with the same conditions and equipment used in the previous tests.

The results were six failures out of forty by 594 cycles. These results plotted show a projected mean life 3,500 cycles. See Graph 2.

Failure analysis of the six devices had only one device that failed as a result of a combination of a necked down wire and fatiguing of the wire. The other five did not fail because of wire fatiguing.

Conclusion:

HP 6N134 made with one and one half mil gold wire bond can easily exceed passing the 400 temperature cycles stress goal that was set by McDonnell Douglas Tests for NASA. Therefore, we intend to incorporate this change into the 6N134.

References:

(1) Identification of Failure Mechanisms and Activation Energies of Opto Devices, by Leon Hamiter and Felminio Villella, NASA/Marshall Space Flight Center.

(2) A Bonding - Wire Failure Mode In Plastic Encapsulated Integrated Circuits, by Clark N. Adams, Honeywell Bull.

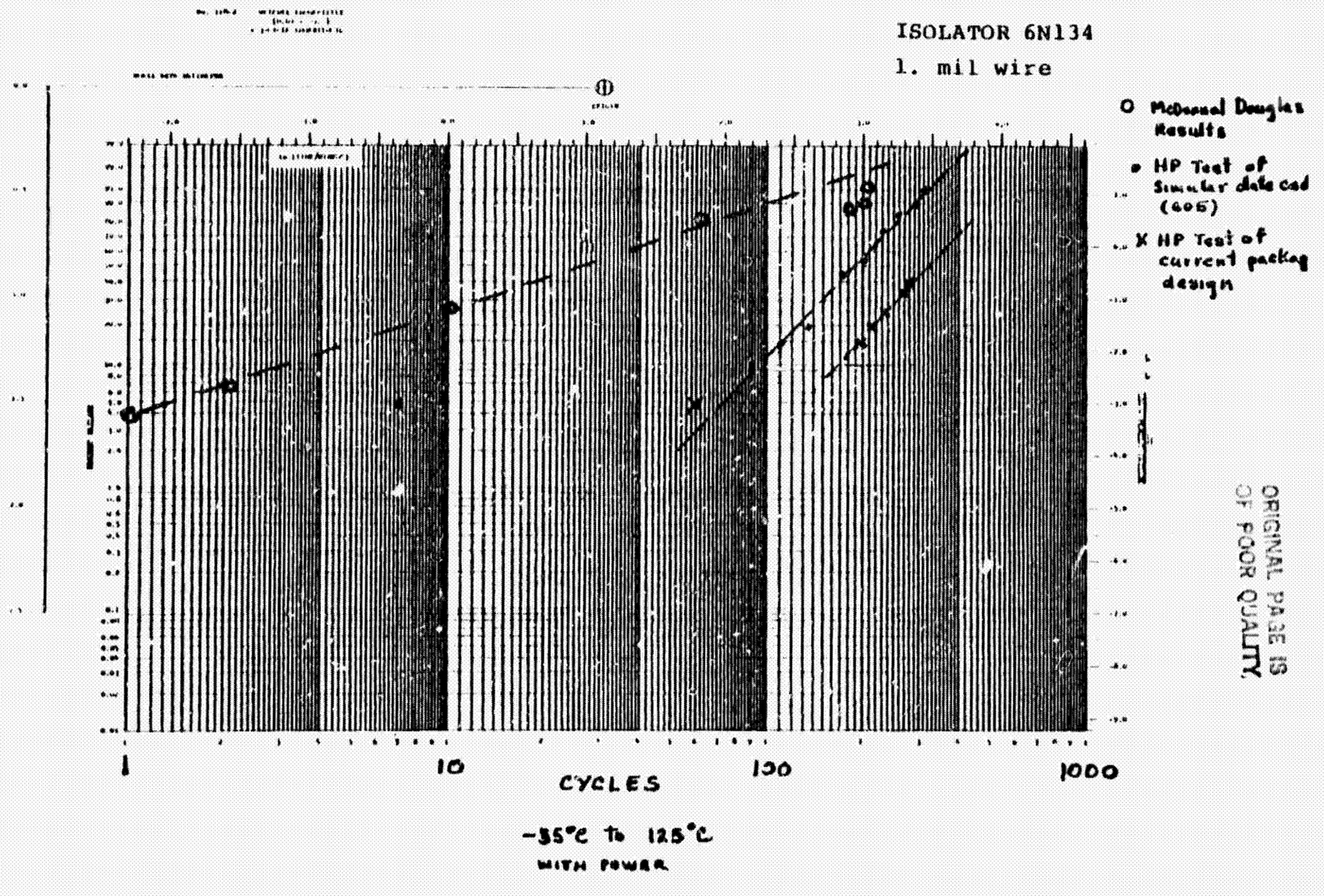

GRAPH 1

WKH 6/7/77 TEST LOG 7601

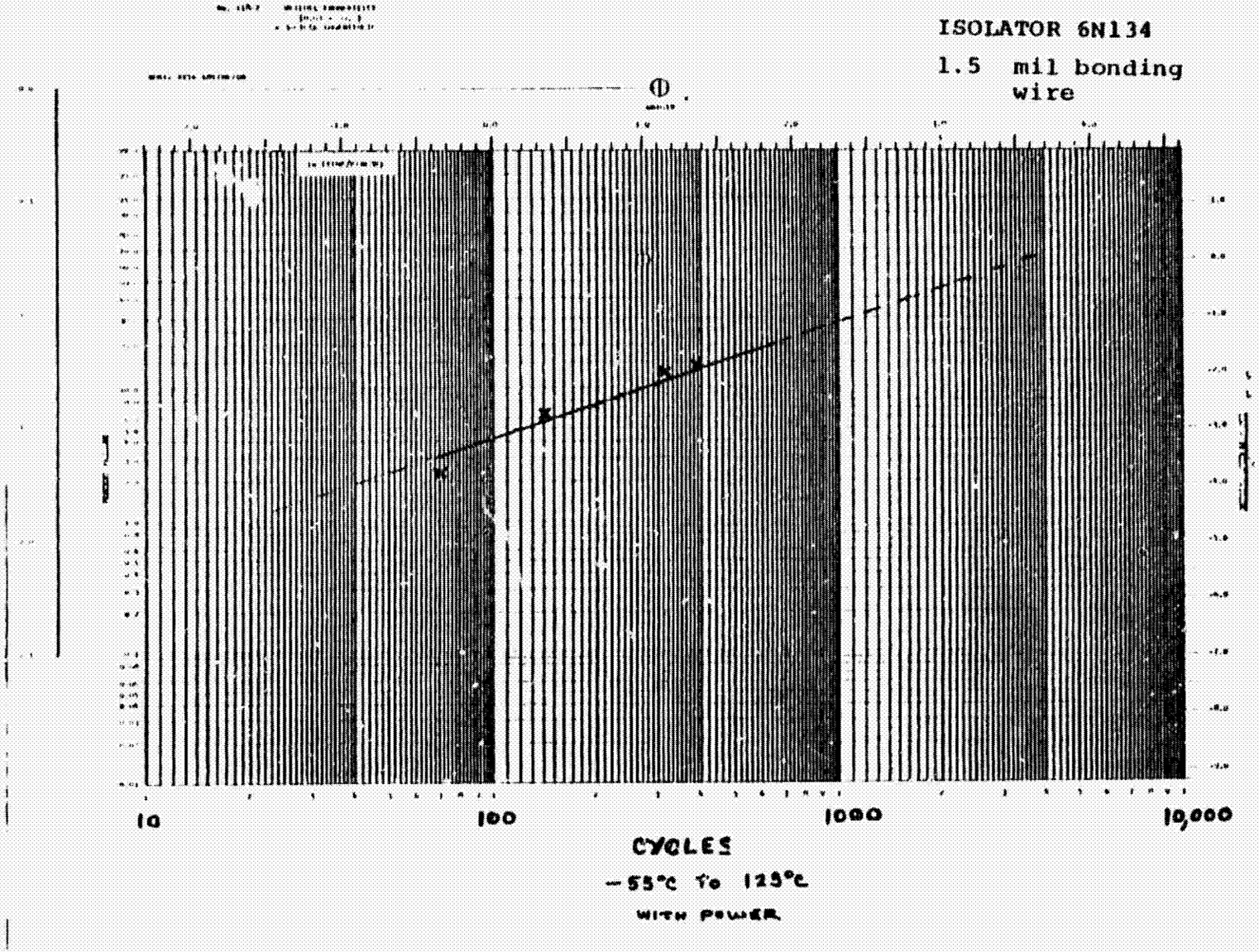

ORIGINAL PAGE IS
OF POOR QUALITY

GRAPH 2

WKH TEST LOG 7601